Dipl.-Ing. Patrick Ofner, BSc.

Evaluation of low-frequency EEG signals as an intuitive movement control signal for BCIs

DOCTORAL THESIS

to achieve the university degree of

Doktor der technischen Wissenschaften

submitted to

Graz University of Technology

Supervisor

Univ.-Prof. Dipl.-Ing. Dr.techn. Gernot R. Müller-Putz

Institute of Neural Engineering

Faculty of Computer Science and Biomedical Engineering

Graz, September 2019

Affidavit

I declare that I have authored this thesis independently, that I have not used other than the declared sources/resources, and that I have explicitly indicated all material which has been quoted either literally or by content from the sources used. The text document uploaded to TUGRAZonline is identical to the present doctoral thesis.

Date	Signature

Acknowledgments

Pursuing a PhD is a demanding and challenging journey where one is rewarded with new experiences, knowledge, and skills – and much more if you are lucky. I would like to thank at this point the persons who have guided, supported, challenged, and entertained me.

Gernot, thank you for your supervision, the necessary guidance, for insights on how to handle various matters in science, and also for the hard work of collecting the funding which allowed me to conduct my research for my PhD.

Reini, for always having a productive critical view in discussions, having an inspirational pragmatic approach on scientific and technical challenges, and most of all for spreading good vibes around the institute.

Rüdiger, for very interesting and funny talks, and sharing your vast knowledge about the nervous system.

Joana and **Andi**, I think we had our moments, and I'm very grateful for that! Besides, thank you for the cooperation, for pointing out different ways to solve problems, for seeing things I would have missed, very often for thinking beyond not just ahead, for being a sparring partner in discussions, and for always questioning things.

I would also like to thank **all** my other colleagues which I have met during my time at the institute, from whom I learned a lot, who offered me their help, or who made it fun and interesting, like Clemens, Alex, Breidi, Josef, David, Maria, and many, many more.

All the people from the **MoreGRASP** project, it was an interesting time, sometimes funny, sometimes challenging, but always worthwhile.

My family, who always kept my back free and supported me in every imaginable way.

My PhD, thank you for bringing me the love of my life, Joana.

Joana, the love of my life. You helped me in so many ways for this PhD! Also, you proofread my thesis. Thank you for all that, and simply, for being by my side!

This thesis was supported by the European ICT programme projects FP7-224631 TOBI and H2020-643955 MoreGrasp, and SGM-UAV.

Abstract

A device generating control signals from the information encoded in brain signals is called a brain-computer interface (BCI). One particular type of BCI is based on electroencephalography (EEG) signals. An EEG-based BCI can decode movement information from the brain and use it to control end effectors like motor neuroprostheses or robotic arms. Such a BCI is usually controlled via motor imaginations of different limbs. So far, an EEG-based BCI can detect which limb is involved in the movement imagination but not how the limb is moved. This PhD thesis researches low-frequency EEG signals for decoding information how a limb is moved. This additional movement information should enable a natural and intuitive control of end effectors. This thesis focuses in the first part on the decoding of trajectories of executed and imagined continuous arm movements, and shifts its focus in the second part on the decoding of different discrete movements of the arm or hand. The decoding of discrete movements was then successfully translated from non-disabled persons to persons with spinal-cord injury (SCI). A proof-of-concept BCI was eventually implemented and tested on a person with complete SCI and without residual hand function. This thesis shows that low-frequency EEG signals encode movement information highly relevant for a natural and intuitive movement control. However, the performance and reliability of the developed BCI needs to be further improved to allow for an effective movement control of end effectors.

Kurzfassung

Eine Gehirn-Computer-Schnittstelle (auf Englisch BCI) erzeugt Steuersignale aus den in Gehirnsignalen enthaltenen Informationen. Eine bestimmte Art von BCI basiert dabei auf Elektroenzephalographie (EEG) Signalen. Ein EEG-basiertes BCI kann Bewegungsinformationen aus Gehirnsignalen extrahieren und zur Steuerung von Endeffektoren wie motorischen Neuroprothesen oder robotischen Armen verwenden. Es wird in der Regel über Bewegungsvorstellungen von verschiedenen Körperteilen gesteuert, wobei das BCI in der Regel nur erkennt auf welches Körperteil sich eine Bewegungsvorstellung bezieht, nicht aber wie es in der Vorstellung bewegt wird. Diese Dissertation beschäftigt sich mit niederfrequenten EEG-Signalen zur Dekodierung von Informationen wie diese Bewegung erfolgt. Diese zusätzlichen Informationen über die Bewegung könnten eine natürliche und intuitive Kontrolle von Endeffektoren ermöglichen. Diese Arbeit konzentriert sich im ersten Teil auf die Dekodierung von Trajektorien ausgeführter und vorgestellter kontinuierlicher Armbewegungen, und verschiebt den Fokus im zweiten Teil auf die Dekodierung von unterschiedlichen diskreten Bewegungen des Arms oder der Hand. Die Dekodierung von diskreten Bewegungen wurde dann erfolgreich von gesunden Menschen auf Personen mit Querschnittlähmung übertragen. Schlussendlich wurde ein Proof-of-Concept BCI implementiert und an einer Person mit Querschnittlähmung und ohne residualer Handfunktion getestet. Diese Arbeit zeigt, dass niederfrequente EEG-Signale Bewegungsinformationen beinhalten, die für eine natürliche und intuitive motorische Kontrolle relevant sind. Die Performance und Zuverlässigkeit des entwickelten BCI muss jedoch weiter verbessert werden, um eine effektive Bewegungskontrolle von Endeffektoren zu ermöglichen.

Contents

Acronyms

AHP	afterhyperpolarization
ANN	artificial neural network
BCI	brain computer interface
BMI	brain machine interface
CAR	common average reference
CSP	common spatial pattern
ECoG	electrocorticography
EEG	electroencephalography
EMG	electromyography
EPSP	excitatory postsynaptic potential
ErrP	error-related potential
FBCSP	filter bank common spatial pattern
FES	functional electrical stimulation
fMRI	functional magnetic resonance imaging
fNIRS	functional near-infrared spectroscopy
GAM	generalized additive models
ICA	independent component analysis
IPSP	inhibitory postsynaptic potential
LDA	linear discriminant analysis
LFP	local field potential
LFTD	low-frequency time-domain
LSTM	long-short term memory
ME	movement execution
MEG	magnetoencephalography
MI	movement imagination
MRCPs	movement-related cortical potentials
MUA	multiunit activity
PCA	principal component analysis
PLS	partial least squares
SCI	spinal cord injury
SCP	slow cortical potentials
sLDA	shrinkage linear discriminant analysis
SMA	supplementary motor area
SNR	signal-to-noise ratio
SQUID	superconducting quantum interference device
SSEP	steady-state evoked potentials
SSAEP	steady-state auditory evoked potentials
SSSEP	steady-state somatosensory evoked potentials
SSVEP	steady-state visual evoked potentials
SUA	single-unit activity

1 Introduction

Clinical and biomedical research has seen enormous progress in the last centuries, being accompanied with tremendous benefits for society and individuals. Humanity has developed anesthesia, antibiotics, vaccines, genetic screening, and imaging techniques, to name a few [9]. This progress was one of the essential drives behind the increase of life expectancy, and it has allowed us to fight illnesses as never before in the history of humankind. However, like previously in history, there are limits in our understanding of the human physiology and the available technologies. One limit is that we are still incapable of repairing or reconnecting nerves in persons who sustained a chronic spinal cord injury (SCI), potentially leaving the affected persons with impairments or even loss of their motor, sensory and autonomic functions.

The prevalence of SCI is reported to range from 250 per million (Rhone-Alps region in France) to 906 per million (USA), and annual incidence rates of SCI range from 9.2 per million (Denmark) to 49.1 per million (New Zealand) [10]. Most studies found falls in the elderly population and traffic accidents as the two most common causes of SCI [10, 11]. This is also a reason why traumatic SCI incidences show a bimodal age distribution with one peak between 15 and 29 years and another peak in older adults (50 years and above), whereas non-traumatic SCIs show a steadily increasing incidence rate with increasing age [11]. Depending on the level and completeness of the lesion in the spinal cord, persons with SCI can be paralyzed on the lower extremities, called paraplegia, or even on all four limbs, called tetraplegia. Studies reported the proportion of paraplegic and tetraplegic persons between 19 % to 68 %, and 32 % to 75 %, respectively, while there is evidence that older adults are more prone to SCI in the cervical area which could cause tetraplegia [11]. Particularly tetraplegic persons have a substantially decreased movement function and are dependent on full-time care. They also require substantial health care resources, imposing financial costs on individuals and society [12]. Tetraplegic persons report that the main priority is therefore the restoration of a missing grasping and reaching function (other important priorities are bowel, bladder, and sexual functions) [13–15].

Surgical procedures, like muscle and tendon transfers or tenodeses can be applied to restore grasp function [16, 17]. However, these procedures require a sufficient number of voluntary controllable muscles distal to the elbow and an individual willing to undergo surgery. If these requirements are not met, upper limb motor neuroprostheses based on functional electrical stimulation (FES) can be an alternative in order to restore grasping and reaching functions [18–20]. FES-based motor neuroprostheses repetitively inject short current impulses into peripheral efferent nerves and generate physiological action potentials. These action potentials are transmitted via nerves to muscles and cause their contraction resulting in a movement. To elicit meaningful grasp patterns and not just random movements, it is necessary that FES electrodes are placed or even implanted on

specific points on the extremity. Furthermore, the paralyzed targeted muscles must be still innervated so that the action potentials can propagate along the nerves. However, this is not always the case as peripheral nerves around the level of the spinal cord lesion degenerate when the lower motor neuron is damaged [21, 22].

In case a person with SCI fulfills all requirements to be equipped with a motor neuroprosthesis, the question remains how the person controls the neuroprosthesis. A standard method is a shoulder joystick control where a joystick is placed on the contralateral shoulder. Up/down or forward/backward movements of the shoulder are then used to control, e.g., grasp function [20]. As a joystick is a low-tech device, this is a relatively robust solution from a technical point of view. However, persons with SCI are often restricted in their shoulder movements which makes it impossible for them to control a shoulder joystick with full degree-of-freedom and high precision. Furthermore, a shoulder joystick imposes additional movement restrictions to an already paralyzed person when both arms have to be used simultaneously to interact with an object. An interesting alternative is a motor neuroprosthesis control via selective contraction of ear muscles [23]. Ear muscle contractions do not interfere with a grasp action and can be easily measured using electromyography (EMG) signals [24]. Other control inputs have been proposed but are not practicable for a neuroprosthesis control (e.g., speech control, tongue control) [20, 25, 26]. The common principle of all these control options is to use a remaining movement function as a control signal, but this principle has a downside. The control is not natural and intuitive because neuroprosthesis users are forced to use non-grasping muscles as a control proxy. Although in some cases, it may be possible to record EMG signals from grasp-related muscles (e.g., extensor carpi radialis longus) [27] that are innervated but too weak to provide a function. But not every tetraplegic person has grasp-related weak muscles, nor is the EMG easy to measure as the FES electrodes are very close and interfere [20].

An intuitive and natural control for motor neuroprostheses is still missing. It is the objective of this thesis to further advance the current state of the art towards a more natural control for motor neuroprostheses or robotic arms in general. The idea behind this thesis is to bypass the lesioned spinal cord by acquiring brain signals, extracting the movement intention from the brain signals, and forwarding the movement intention to the motor neuroprosthesis [28, 29]. Thus, every time a person with SCI intends to perform a movement, this intention is detected and transformed into a real movement with a neuroprosthesis. This idea itself, however, is not new. So-called brain-computer interfaces (BCIs), sometimes also called brain-machine interfaces, exist now for a while and allow to read brain signals and exploit them as a control signal for various devices [30–34]. These BCIs can be used to control motor neuroprostheses in persons with SCI as the pioneering work of the Graz BCI lab showed. The Graz BCI lab restored grasp function in persons with SCI and used for that purpose a non-invasive BCI based on electroencephalography (EEG) [28, 35, 36]. EEG is a non-invasive recording technique which measures the electrical activity of the brain with electrodes placed on the scalp. The underlying principle of a common type of EEG-based BCIs is that some of the brain processes generating EEG oscillations (brain rhythms), can be intentionally altered. These changes can be measured in the EEG and used as a control signal. For example,

in the EEG it can be detected from oscillation changes whether a person imagines a left hand or a right hand movement, and these movement imaginations can then be used to control the grasp state of a motor neuroprosthesis [28, 36].

Despite that thoughts about movements are detected, the resulting control is not yet natural enough. The general state of a movement imagination (MI) is detected but not the detailed movement: it is detected if a hand movement *is* imagined, but not *how* the hand is moved in the imagination. To facilitate a more natural control for existing upper limb motor neuroprostheses it would be necessary (1) to detect how a body part is moved, and (2) to increase the spatial resolution with which body part movements are detected. Current EEG-based BCIs can differentiate MIs of *different limbs*. However, for an improved upper limb motor neuroprosthesis control, it would be necessary to differentiate individual movements within the *same limb* (e.g., hand movements, elbow movements). A detailed differentiation would then allow a more natural control of upper limb motor neuroprostheses, as a person with SCI would attempt a movement, and the same movement is then executed via FES. Unfortunately, this is not yet possible with current BCIs based on EEG and further research is required. It is therefore the objective of this dissertation to analyze and exploit the encoded movement information in the EEG to eventually provide a more intuitive and natural control signal for an end effector like a motor neuroprosthesis or a robotic arm.

The next sections will explain the types of measurable brain signals and the principles of BCIs. The subsequent sections describe then the current state of the art of BCIs with a focus on movement control and explain the aim of this thesis in detail.

1.1 Types of Brain Signals

The brain is a complex organ, and we are far from a complete understanding of its function. We do not know, for example, how higher-order brain functions like human intelligence, emotions, or consciousness emerge out of a biological signal processing system. In this biological system, information is integrated, processed and transported via dendrites, neurons, and axons [37], and one may even compare aspects of this system with human-made information processing systems like computer chips. Both technical and biological systems process and distribute information, and if information is the fundamental currency of our brain, technical systems may one day be able to reproduce, not only partly simulate, the higher-order functions mentioned before. So far, we do not yet adequately understand how the brain interacts with itself simultaneously on different scales (e.g., neurons, neuronal ensembles, networks), and between different building elements on the same scale (e.g., different types of neurons or brain structures). Thus, we lack a *holistic* understanding of the information processing in the human brain. However, we can partly observe the brain during its operation and find sometimes reoccurring patterns associated with behavior or sensation. These patterns are called neural correlates and can be detected by BCIs and translated into a control signal for various devices. This section gives a short overview which brain signals can be measured, and in particular how the electrical signals relevant for EEG are generated and form

neural correlates. Basic knowledge about neurons and information transfer via synaptic transmission is assumed here and can be found somewhere else [37].

1.1.1 Types of Electrical Brain Signals

Electrical brain signals relevant for BCIs can be measured on various spatial scales [29, 38]. The smallest scale refers to neural activities of individual neurons or small ensembles of neurons and is termed microscale. Microscale measurements are conducted with microelectrodes inserted in brain tissue, and measure activity of neural tissue within volumes of $10^{-3}\,\mathrm{mm}^3$ to $1\,\mathrm{mm}^3$. The microelectrodes are usually embedded in a grid which is inserted in the cortex. By high-pass filtering the measured voltage signals ($> 300\,\mathrm{Hz}$), one can separate action potentials or neuronal spikes (voltage changes of $100\,\mathrm{mV}$ in the order of $1\,\mathrm{ms}$). However, due to volume conduction, a grid electrode receives neuronal spikes from multiple neurons. One refers to this signal mix as multiunit activity (MUA) [39]. A spike sorting algorithm can be used to separate the overlaying spikes [40]. A neuronal spiking signal isolated in such a way is then referred to as single-unit activity (SUA). MUA and SUA are then usually transformed into neuronal firing rates before further processing in a BCI. Local field potentials (LFPs) are also measured with grid electrodes, just like SUA/MUA, but are low-pass filtered (ca. $<300\,\mathrm{Hz}$) to separate synaptic currents from action potentials.

The next larger spatial scale is referred to as mesoscale. Mesoscale voltage signals can be recorded with electrocorticography (ECoG) electrodes placed on the cortical, pia, arachnoid, or dura surface [41]. The mesoscale corresponds to a volume of $1\,\mathrm{mm}^3$ to $20\,\mathrm{mm}^3$, which corresponds to one or more cortical columns [38].

The largest spatial scale is the macroscale covering an area of $10\,\mathrm{cm}^2$ to $40\,\mathrm{cm}^2$, which corresponds to Brodmann areas and even brain lobes. It can be measured with EEG electrodes, where each electrode measures the averaged activity in the order of 100 million neurons [38]. However, the spatial averaging effect can be reduced with spatial filtering techniques or source imaging [38, 42–46]. The amplitude of the EEG signal is in the range of $1\,\mu\mathrm{V}$ to $100\,\mu\mathrm{V}$, and frequencies of interest are often within $1\,\mathrm{Hz}$ to $100\,\mathrm{Hz}$.

Electrical microscale and mesoscale brain signals provide in general a better signal-to-noise ratio than macroscale signals. However, they require invasive recording techniques, whereas macroscale signals can be measured non-invasively with EEG.

1.1.2 Generation of Electrical Signals

Various processes in the brain cause the generation of electrical currents. Due to volume conduction in the brain, these electrical currents propagate, and electrical currents from various sources superimpose in the extracellular medium in the brain. These superimposed electrical currents are associated with a certain electrical potential at a given point. Voltage differences between electrical potentials can then be measured invasively with microelectrodes or ECoG, and non-invasively with EEG.

Synaptic activity is considered as the essential contributor to extracellular electrical fields. In particular, excitatory postsynaptic potentials (EPSPs) in apical dendrites of

pyramidal neurons found in the cortex, cause an influx of cations from the extracellular into the intracellular space. This influx forms an active local extracellular sink. Because of electroneutrality, the additional charges brought into the intracellular space cause a *return current* which forms passive extracellular sources somewhere remote from the sink [47]. The formed sink and sources generate a dipole which gives rise to an electrical field which decays proportionally to $1/r^2$ [48]. The electrical field together with the volume conduction leads then to the electrical currents and electrical potentials which can be measured with electrodes. Beside EPSPs, also inhibitory postsynaptic potentials (IPSP) contribute to the electrical field. IPSPs are often located on the soma and lesser on the dendrites of the postsynaptic neuron. Analogous to EPSPs, the IPSPs cause then an active extracellular source on the soma, and because of electroneutrality, passive extracellular sinks possibly on the dendrites. Therefore, IPSPs and EPSPs can create dipoles with similar orientation and similar electrical potentials in the extracellular space. However, inhibitory neurons comprise only one-fifth of cortical neurons [49], and their effect on the electrical field is therefore thought to be lower than with excitatory neurons.

Two factors have a substantial impact on the measured electrical potentials [48]. The first factor is the spatial configuration of the contributing neurons. Especially, the apical dendrites of pyramidal neurons in the cortex have a parallel arrangement, and the electrical fields generated by their dipoles can easily add up. Furthermore, pyramidal neurons have long apical dendrites, which lead to distinct dipoles arising between them and the soma. The second factor is the temporal synchronicity of the postsynaptic potentials. Postsynaptic potentials of the same type (excitatory or inhibitory) induced simultaneously in a neuron or a group of neurons generate electrical fields with higher amplitude than the same postsynaptic potentials when induced non-simultaneously. Thus, spatial and temporal integration of postsynaptic potentials boosts the amplitude of the generated electrical field.

However, synaptic activities are not the only type of biochemical activity affecting the electrical field [48]. Also, calcium spikes can contribute substantially to the extracellular electrical field. They are long-lasting (10 ms to 100 ms) and large events (10 mV to 50 mV) which can propagate actively within the neuron, and can be triggered by back-propagating somatic action potentials or by EPSPs. Contrarily, fast action potentials ("spikes") do not contribute substantially to EEG and ECoG signals. Because of their short duration (2 ms) they rarely overlap in time. However, synchronous fast action potentials from larger neuron groups can contribute to high-frequency components in the electrical field. Bursts of both calcium spikes and fast action potentials can be followed by a distinct hyperpolarization in neurons, the so-called afterhyperpolarization (AHP). AHPs are comparable in duration to synaptic events and can therefore contribute substantially to the extracellular electrical field. Furthermore, neurons have resonance and oscillation features, and excitation of neurons with a particular frequency can cause self-sustained voltage oscillations in the theta or gamma band. The interested reader can find more information on how the electrical field is generated in the detailed reviews of Buzsáki et al. [48] and Einevoll et al. [49].

1.1.3 Other Types of Brain Signals

Beside electrical brain signals, also other brain signals applicable for BCIs can be detected non-invasively. These brain signals are presented below. However, they do not provide a clear advantage over EEG in BCI applications and are therefore of lesser importance. These brain signals are rather used in neuroscience research or clinical applications in general.

Brain signals can also be recorded with magnetoencephalography (MEG). MEG measures the magnetic field caused by the electrical currents in the brain (ca. 10 fT to 10^3 fT) [50]. MEG employs magnetometers which are usually realized with superconducting quantum interference devices (SQUIDs). Although both MEG and EEG are related to electrical currents in the brain, they are not equivalent but rather complementary. At frequencies occurring in the brain, the electric and magnetic fields can be considered as decoupled. These fields are, however, sensitive to different sources in the brain. Due to the propagation properties of the magnetic field, MEG is insensitive to dipoles with axes perpendicular to the head surface, like the dipoles on cortical gyri. MEG measures therefore preferentially dipoles on sulcal walls on the cortex [51]. Contrarily, EEG is insensitive to the dipole orientation but measures, due to the $1/r^2$ electric field decrease, preferentially sources on cortical gyri.

Moreover, brain signals based on metabolic activities can be measured. When neuronal ensembles increase their neural activity, they also increase their metabolic activity and consume more oxygen. The uptake of oxygen in neuronal cells is reflected in a localized change of the concentration of oxygenated and deoxygenated hemoglobin in the blood, which in turn causes a change of the magnetic susceptibility of the local hemoglobin. This effect is referred to as blood-oxygen-level-dependent (BOLD) effect and can be non-invasively detected with functional magnetic resonance imaging (fMRI) [52]. As the BOLD effect is a result of the slow hemodynamic response, its temporal resolution is usually longer than a second [53]. However, fMRI provides a better spatial resolution than EEG and allows measurements from the mesoscale up to the macroscale [53, 54]. fMRI is an indirect measurement of the neural activity, and it has been shown that the BOLD signal corresponds closer to LFPs than to spiking activity [55].

The concentration change of oxygenated and deoxygenated hemoglobin affects furthermore the spectral absorption properties of hemoglobin. Functional near-infrared spectroscopy (fNIRS) can be used to measure these changes in the cortex via infusing light in the near-infrared spectrum through the skull in the cortex and measuring its absorption [56].

1.2 Introduction to BCIs

1.2.1 Definition

BCIs are sophisticated technical devices which read brain signals and derive control signals for external devices. Before further explanations of the basic components of a BCI are given, it is expedient to give a proper definition of a BCI. A BCI, sometimes

also called brain-machine interface (BMI), needs to fulfill four requirements according to the definition given in [57]:

1. a BCI must rely on signals originating from the brain (i.e., brain signals)
2. the BCI user must intentionally modulate the brain signal(s)
3. the signal processing must occur in (soft) real-time and yield a communication or control signal
4. the BCI user must perceive feedback about the state of the utilized brain signals

The last two points are sometimes emphasized by redundantly calling a BCI an *online* BCI. The online aspect refers in the context of BCIs to the (1) prompt processing of brain-signals, and (2) the output of this processing is observable by the BCI user. However, this definition has been updated in [38]. This newer definition is:

> "A BCI is a system that measures central nervous system (CNS) activity and converts it into artificial output that replaces, restores, enhances, supplements, or improves natural central nervous system output and thereby changes the ongoing interactions between the central nervous system and its external or internal environment."

It suffices now that the BCI interacts with the environment. Thus, the BCI users can perceive the state of the brain signals indirectly through overt changes in the environment. Direct observation of the state of the brain signals is not necessary anymore. Furthermore, intentional control of brain signal is not required. This definition allows the inclusion of so-called passive BCIs, which observe the state of the BCI user and react to it [58]. However, in both definitions, a system which only monitors brain activity is not a BCI.

BCIs are primarily researched and developed to support people with disabilities. They have the potential to provide solutions in the future which are superior to conventional approaches or complement them. BCI applications which have been developed so far can be categorized into the following three application domains:

- *communication and control*

  Communication and control applications include spellers to allow persons who suffer from, e.g., amyotrophic lateral sclerosis (ALS), and entered a locked-in state, to communicate with their environment [59–62]. Also, BCIs could provide a communication channel to persons in a minimally conscious state [63]. Furthermore, BCIs for wheelchair control [64, 65] or computer applications like web browser [66–68], painting programs [69, 70], music composition programs [71], and gaming applications [72, 73] have been implemented.

- *motor restoration*

  Motor restoration applications provide a technical bypass around impaired brain areas or injuries in the spinal cord to restore motor function. More BCI related

information can be found in section 1.3, which describes the state of the art of BCIs related to movement control.

- *motor recovery*

  Motor recovery applications [32, 34, 74–77] support persons during a neurological rehabilitation process after, e.g., stroke. BCIs can help to guide the mental activity to foster brain plasticity and to suppress abnormal brain activity, probably supporting the restoration of normal motor control. Furthermore, BCIs can be used to stimulate muscles or passively move body parts whenever a movement intention is detected (particularly with no residual movements). The resulting sensory input can then engage the recovery process [78], especially if the sensory input is not delayed by more than a few hundred milliseconds [79].

To build a BCI one needs to understand (1) how the different types of brain signals can be modulated, and (2) how these signal modulations can be detected via signal processing and classification methods. The following subsection 1.2.2 and subsection 1.2.3 address these two questions and give an introduction to BCIs.

1.2.2 Modulation of Brain Signals

A BCI transforms brain activity or neural correlates into a control signal. While many different brain signals can be measured, the measurement alone is not sufficient to build a BCI. First and foremost, a BCI user needs to be able to modulate a certain brain activity measure *intentionally*, or a brain activity measure is modulated due to an *interaction* with the environment. Second, the BCI system can detect that modulation to derive a control signal from it. Several modulate-able brain signals have been found, and the most relevant for BCIs are introduced in the following.

Modulation of Neuronal Firing Rates Neuronal firing rates are derived from microscale brain activity with SUA and MUA. It was found that voluntary limb movements affect the spiking activity of neurons in the primary motor cortex, primary somatosensory cortex, supplementary motor area, premotor areas, and posterior parietal cortex in non-human primates [37, 80–82] and that this activity does not solely arise from sensory feedback [80, 81]. In particular, the spiking activity of neurons is affected by, e.g., exerted force, position, or velocity of body parts [83]. Georgopoulos et al. [84] found moreover that the firing rate of individual motor neurons depends on the direction of arm reaches, and that the movement direction is better decodable from a population of cortical motor neurons [82], this became known as the "population vector".

Noteworthy, also movement planning and movement preparation were detected from neuronal activity in studies which employed a delay period before movement execution (ME) in non-human primates [85, 86] and humans [87]. See Synder et al. [88] for a review on the planning-related activity in the posterior parietal cortex. Furthermore, cognitive imagery modulates neuronal activity in the temporal lobe. It was shown that neurons which respond to a particular visual stimulus also respond during recall of this

stimulus [89]. Besides these modulations induced by behavior, subjects can also learn to control the activity of motor neurons by neurofeedback learning. Fetz [90] showed that non-human primates can learn to increase and decrease the activity of motor neurons when they are rewarded. Interestingly, neuronal activity required to get the reward was associated with limb movements, but it was then found that the neuronal activity of motor neurons can be dissociated from movements [91–94], i.e., movements can be suppressed during voluntary control of neural activity. For a review about volitional control of neural activity see Fetz [95].

Modulation of Brain Oscillations Rhythmic activity or brain oscillations are an essential part of brain function and occur on various spatial and temporal scales (microscale to macroscale, and milliseconds to a day) [96]. They become measurable in EEG when large neuronal ensembles engage in a synchronous activity. Brain oscillations were first observed by Hans Berger [97] in macroscale EEG signals on the occipital cortex, and afterward also on other areas like sensorimotor areas. Furthermore, it was found that oscillations on sensorimotor areas can be blocked by movements [98]. Later it was then found that the oscillations can be intentionally modulated by *execution* and *imagination* of movements [99, 100], as well as mental tasks like mental rotation, mental subtraction, or spatial navigation [101]. Motor and mental tasks cause activation of respective areas on the cortex. This increased activation presumably reflects active information processing, and leads to a desynchronization of the involved neural ensembles. This desynchronization manifests as a power decrease relative to a certain baseline in the alpha/mu (8 Hz to 13 Hz) or beta band (around 20 Hz) in LFP, ECoG and EEG signals. This effect is called *event-related desynchronisation* (ERD) [100, 102]. An intensification of the idle state of neuronal ensembles, however, leads to an increase in power relative to a baseline, which is called *event-related synchronization* (ERS). These effects are often confined to the mu band and beta band. However, in the gamma band (around 40 Hz) oscillations are interpreted as active information processing [102]. Thus, the increased computational load due to movement tasks can cause a power increase in the gamma band. Besides the before-mentioned movement and mental tasks, brain oscillations are also modulated by mental states related to, e.g., mental workload, attention level, or fatigue, which is exploited in passive BCIs [103, 104].

Brain oscillations measured on the microscale and mesoscale are particularly interesting because these scales allow access to higher frequencies than at the macroscale. This is due to the low-pass characteristic of the brain [48], which causes a decrease of the signal-to-noise ratio (SNR) with increasing frequency. LFP and ECoG with their increased SNR can partly compensate for that effect. Accordingly, it was found that voluntary limb movements are accompanied by modulations of LFP signals on motor areas up to 300 Hz [105–107]. Furthermore, movement planning modulates LFP signals up to 250 Hz on motor areas and up to 100 Hz on the posterior parietal cortex [108, 109]. Voluntary limb movements also modulate ECoG signal on motor areas up to 180 Hz [110, 111].

An oscillation-based BCI utilizes then these oscillations and typically transforms the

power modulations in one or more frequency bands into a control signal.

SCP Slow cortical potentials (SCP) are changes of the cortical potentials lasting for 300 ms to several seconds [112]. A negative shift of SCPs indicates an excitation increase of underlying neuronal circuits, whereas a positive shift indicates a decrease in excitation. Persons can learn via neurofeedback to shift their cortical potentials and use them as a control signal for BCIs [59, 113].

MRCPs Movement-related cortical potentials (MRCPs) are elicited during self-initiated voluntary movements and are time-locked to the movement onset. They comprise several subcomponents, most notably the readiness potential [114]. The readiness potential can again be divided into an early and a late component. The early readiness potential is a potential with a negative slope which starts around 2 s before movement onset (the movement onset is here defined as the peak of the respective averaged rectified EMG signal). It occurs first on the supplementary motor area (SMA), and then bilaterally on the lateral premotor cortices. It is then replaced by the late readiness potential, which has a steeper negative slope, approximately 0.4 s before movement onset. The late readiness potential appears on the contralateral premotor and primary motor areas. Another subcomponent is the motor potential, which occurs 10 ms before movement onset well-localized on the respective somatotopic area on the primary motor cortex. It most likely represents the activity of pyramidal tract neurons. Beside these pre-movement potentials, also post-movement potentials on frontal and parietal areas exist which are thought to be related to kinaesthetic feedback. The subcomponents of the MRCPs are not consistently defined in the literature, however, and several other names exist for most of the potentials. See Shibasaki and Hallet [115] for a review on MRCPs and the individual subcomponents. MRCPs are elicited in movement tasks, and their detection with a BCI could benefit, for example, motor recovery applications [116–118].

SSEP Periodic external stimulation of sensory neurons induces oscillations on the respective primary sensory areas. These induced oscillations are called steady-state evoked potentials (SSEP). Depending on the stimulated sensory system, they can be further subdivided into steady-state visual evoked potentials (SSVEP), steady-state somatosensory evoked potentials (SSSEP), and steady-state auditory evoked potentials (SSAEP) [119–122]. One can build a BCI by simultaneously stimulating a user with different frequencies, where each frequency is associated with a particular class label. The user can then select a class label by focusing the attention on the associated frequency. This focusing causes oscillations with the fundamental frequency of the stimulation and often its harmonics or subharmonics [123, 124] to appear on the corresponding primary sensory area. A BCI can detect these oscillations and attribute them to a class label. Typical stimulation methods include, for example, visual stimulation via flickering icons on a computer screen or tactile stimulation via vibrations. Especially BCIs operating with visual stimulation combined with EEG recording from the occipital cortex, i.e., SSVEP-based, are reported in the literature [125, 126].

P300 P300 [127] is an event-related potential well measurable in macroscale brain signals and is associated with stimulus evaluation [128]. One way to elicit a P300 is via the *oddball paradigm* [129]. In this paradigm, non-target stimuli are presented frequently to the BCI user. These frequent stimuli are interspersed with less frequent target stimuli. Importantly, the BCI user focuses exclusively on the target stimuli, which usually comprise not more than 25 % of the stimuli. When a target stimulus occurs, a phase-locked potential is elicited. One component of this potential is the P300, which occurs as a positive deflection in EEG signals approximately 300 ms after stimulus presentation. The P300 has been used to build applications such as spellers based on EEG signals [130, 131]. A P300-based BCI speller presents the user a visual matrix of characters, with the characters flashing in a random sequence [130]. The user selects a character and focuses then on this character. This makes each flashing of the selected character a target stimulus. After several flashes of the character – each flash elicits a P300 – the BCI system can detect the selected character, and one can use such a system for spelling. In addition to such a visual paradigm, paradigms based on tactile or auditory stimulation are also researched [132, 133].

ErrP An error-related potential (ErrP) can be measured in macroscale brain signals and is evoked whenever a person becomes aware of an error. Several ErrP types have been identified so far: response ErrP, feedback ErrP, recognition ErrP, and interaction ErrP. Important for the categorization of ErrPs is to determine who committed an error. When an error is committed and recognized by the same person, the evoked ErrP is either a response ErrP or a feedback ErrP. A response ErrP is elicited when the person recognizes the error immediately after committing it, whereas a feedback ErrP is elicited when the person recognizes the error only after feedback is provided by some system. When an error is committed and recognized by different persons, the person recognizing the error elicits a recognition ErrP. Especially interesting for BCIs are interaction ErrPs, which are elicited when the controlled system, i.e., the BCI, makes an error which is then recognized by the BCI user [134]. ErrPs can be exploited for error correction after a wrong BCI output, e.g., in a speller application or robotic arm control, or to learn a BCI classifier with reinforcement learning [135–137].

Haemodynamic Response-Related Signals Neuronal activity causes a local hemodynamic response and changes in the BOLD signal. This can be detected via fMRI [55] and used for neurofeedback [138, 139]. Also, mental tasks can be used as a control strategy in an fMRI-based BCI [140]. The hemodynamic response can further be measured with fNIRS and used as a control signal for BCIs [141, 142].

1.2.3 Components of a BCI

A BCI acquires brain signals and derives a control signal or a communication channel from it. Virtually all BCIs can be split into the following components:

1. signal acquisition
2. feature extraction
3. classification
4. control signal generation
5. feedback

This pipeline is shown in Figure 1.1. Essential is that feedback is provided to the BCI user. Thus, the control signal generated by the BCI or its effects are perceivable by the BCI user and the user can react to the output of the BCI. A BCI is therefore always a *closed-loop system*.

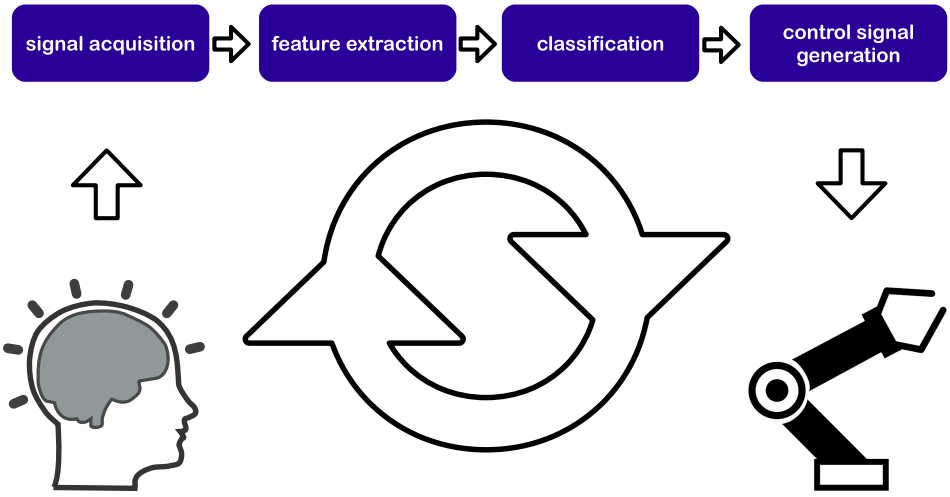

Figure 1.1: Typical processing pipeline of a BCI. The BCI acquires the brain signals of the user and generates a control signal for some device. The user is then given feedback, resulting in a closed-loop system.

This section provides a short overview of the basic building blocks of a typical *EEG-based* BCI system. Technical specifics of BCIs based on other brain signal types, e.g., magnetic brain signals [143], blood oxygen level signals [141], or invasive recording techniques are out of the scope of this thesis. However, their differences are mainly in signal recording, while the concepts in the subsequent steps are similar. For further information about invasive or non-invasive BCIs, one may read the review articles [31, 32, 34, 144].

Signal Acquisition The first step in a BCI pipeline is to acquire and to digitize brain signals [38]. EEG-based BCIs employ electrodes placed on the scalp to measure macroscale brain signals (often on standardized positions [145]). Different types of electrodes exist for this purpose: gel-based, water-based, or dry electrodes. Gel-based electrodes use an electrolyte gel to establish contact between the electrodes and the skin; water-based electrodes employ water-soaked sponges for that purpose. Dry-electrodes use no additional conductive medium, and in general suffer therefore from more noise, voltage offsets and unstable signals than gel or water-based electrodes [146]. The standard for research-grade gel or water-based electrodes are sintered silver/silver chloride (Ag/AgCl) electrodes. For dry electrodes, a comparable clear standard has not yet evolved, and different materials are in use and researched (e.g., gold alloy or electrically conductive polymer).

Moreover, electrodes can be subdivided into active and passive electrodes. Active electrodes have a preamplifier integrated into each electrode and are therefore less prone to interferences on the electrode cables than passive electrodes. However, passive electrodes can be combined with actively shielded electrode cables to reduce interferences on the electrode cables. The acquired brain signals are then transmitted via the electrode cables to a biosignal amplifier.

Biosignal amplifiers are based on so-called instrumentation amplifiers. Instrumentation amplifiers can offer a high input impedance ($>100\,\mathrm{G\Omega}$) and high common-mode rejection ratio ($>10^7$), allowing them to record even small voltages as in EEG with a reasonable SNR. The amplifier digitizes the EEG signals and transmits them wired or wireless to the BCI pipeline. Typically, it suffices to sample EEG signals with no more than 256 Hz to cover all EEG frequency bands relevant for BCIs, as they are usually located below 60 Hz.

Feature Extraction Once signals are acquired and digitized, one needs to preprocess the signals and extract discriminative features from the preprocessed signal. One of the first steps is usually a spatial filtering of the signals. Due to volume conduction, electrodes pick up signals not just from the closest source, but also from many other more distant sources and record therefore a mix of many sources. The further away an electrode is placed from the source of interest, the more severe that effect becomes. Thus, EEG is affected the most by volume conduction and has therefore a lower SNR compared to invasive methods like ECoG. Furthermore, the conduction inhomogeneities caused by the cerebrospinal fluid, skull, and scalp affect and distort the propagation of the electric field [147].

Spatial filtering helps to counteract volume conduction, and various spatial filters can be applied. Simple spatial filters are the bipolar filter or the Laplace filter [38, 148, 149]. A bipolar filter computes the voltage difference between an electrode pair, and a Laplace filter computes the difference between a center electrode and the average of the surrounding electrodes (typically the 4 or 8 closest electrodes). The Laplace filter is therefore a generalization of the bipolar filter with a focus on sources below the center electrode. Another often used spatial filter is the common average reference (CAR)

[149]. A CAR filter calculates the average potential of all electrodes at each time instant and subtracts the average potential from all electrodes. The potential common to all electrodes is therefore removed. Besides these simple filters, unsupervised and supervised *data-driven* spatial filters exist. Typical examples of unsupervised spatial filters are principal component analysis (PCA) and independent component analysis (ICA). Both methods are so-called blind-source separating methods. PCA decorrelates signals [150, 151], whereas ICA finds sources (components) which are statistically independent of each other. Various ICA variants exist to maximize the statistical independence among sources [152, 153]. A prominent supervised spatial filter is the common spatial pattern (CSP) filter [43, 154, 155]. CSP finds sources which have a maximum difference in variance between conditions. It is often used to extract mu and beta rhythms and is usually combined with a subsequent variance computation and log transformation.

Other than enhancing the SNR, a spatial filter can also remove the influence of the reference electrode on the recorded signals. EEG signals are recorded as difference signals to a common reference electrode. As the reference electrode also picks up electrical signals, the placement of the reference electrode affects the time course of the recorded signal. Spatial filters can help here, as they can extract components independent of the reference electrode. Especially, CAR is used for that purpose in source imaging applications [156].

Temporal filtering is beside spatial filtering another standard signal processing technique for brain signals. The brain signals of interest are often contained in specific frequency bands, e.g., mu rhythm. Temporal filtering increases the SNR by reducing the power of brain signals which are not of interest (i.e., noise) as well as by reducing the power of artifacts, e.g., muscle artifacts.

Features are then extracted from the preprocessed EEG signals, and fed in a classifier. Features are often merely the time points of spatially and temporally filtered EEG voltages (c.f. P300 based BCIs [67]), called *time-domain* features in this PhD thesis. Another feature type are *frequency-domain* features, which are used by oscillation based BCIs. These features refer to the power (i.e., variance), amplitude, or phase of EEG oscillations. Frequency-domain features are usually calculated over one or more frequency bands obtained via temporal filters or via a discrete-time Fourier or wavelets transform [157]. One prominent example of a frequency-domain feature is the so-called band power feature. For this, one computes the instantaneous variance in a specific frequency band and smooths it with a moving average filter. Subsequently, a log transformation is applied to reduce the skewness of the data. Another often applied feature extraction algorithm is the filter bank CSP (FBCSP) [158]. With FBCSP, signals are first filtered with a filter bank, followed by a CSP filter for each frequency band. Similar to band power features, the variances of the CSP filtered signals are computed and smoothed, followed usually by a log transformation. Also, connectivity features can be computed in the time or frequency-domain [159–161]. See [162] for a survey of signal processing algorithms applied in BCIs.

Classification Once the signals are acquired and features are extracted, the features are fed into a classifier (see the reviews [163, 164]). Typical BCI classifiers are, e.g., linear discriminant analysis (LDA), support vector machine, or random forest classifier. Most classifiers share a common problem when training the classifier: the limited number of available training trials. The consequence is an adversely low trials to features ratio. Without countermeasures, this can lead to overfitting on the training data, especially when the classifier model has a high degree-of-freedom (e.g., many weights). In the case of overfitting, the classifier performs well on training data but poorly on test data. The high risk of overfitting may be one of the reasons why relatively simple linear classification models are still widely used for BCIs, and why regularization, like shrinkage for LDA [165, 166], is highly advantageous. More complex classifiers like artificial neural networks (ANNs) were also investigated, but their little performance improvement – if any at all – may not justify the attending high computational costs [167] – at least as EEG signals are concerned. The advent of deep learning, as seen in other domains (e.g., speech recognition, object detection) [168], did not yet happen in the BCI domain.

A noteworthy classification concept introduced in BCI are adaptive classifiers [169]. Adaptive classifiers update their classifier model during the operation of the BCI. Thus, they cope with the inherent short and long-term non-stationarities present in brain signals. Furthermore, they can account for the learning progress of BCI users. Particularly the modulation of brain oscillations can be learned and improved by BCI users [170, 171]. In general, the control of a BCI needs to be seen as a skill which has to be learned with time, and the classifier should adapt to the training progress.

Another important concept is transfer learning [172, 173]. Transfer learning in the context of BCI refers to the usage of training data from other users (subject-to-subject transfer) or other sessions of the same user (session-to-session transfer) to train a classifier. Transfer learning can help in cases where little training data are available, or to shorten the training phase. Transfer learning can also be combined with adaptive classification [174]: an initial classifier is built with transfer learning, and then improved via adaptive classification during operation.

Control Signal Generation In a typical BCI processing pipeline, the classifier outputs discrete class labels or continuous class probabilities (or the underlying raw scores). Furthermore, the output can also be any predicted continuous variable, e.g., 3D hand position. In the latter case, the term "classifier" is not accurate and is often replaced by the more general term "decoder" [144, 175] applicable to discrete and continuous outputs. The output of the classifier or decoder is then used as a control signal for various devices or software programs. Examples are neuroprostheses, wheelchairs, telepresence mobile robots, web browsers, spelling programs, or computer games [32].

Feedback The effect of the control signal on the controlled devices or on the environment is perceived by the BCI user, which closes the control loop. The feedback component is of more relevance for BCIs deliberately controlled by the BCI user than for passive BCIs, but all BCIs share this feature.

1.3 State of the Art of Movement Control BCIs

This section summarizes the state of the art of BCIs related to movement control. The state of the art is outlined as it was at the beginning of this thesis. The limitations are then identified in the next section section 1.4, and the research question is formulated in section 1.5. An update of the state of the art – in so far as relevant for this thesis – is then given in section 3.2. Both non-invasive and invasive BCIs used for the control of motor neuroprostheses or other end effectors, like orthoses or robotic arms, are considered in this section. Moreover, BCIs which have the potential to be used for an end effector control are included as well (e.g., cursor control).

invasive BCIs The development of invasive BCIs for movement control applications started in non-human primates, which are thought to provide an appropriate model for the human nervous system. Most of the following studies recorded SUA or MUA from premotor, primary motor or parietal areas, and decoded kinematic parameters from the neuronal firing rates with linear (e.g., multiple linear regression) or non-linear models (e.g., artificial neural networks, Kalman filter).

The group of Nicolelis showed that non-human primates could learn to control a robotic arm [176]. Other research groups showed then the 2D and 3D control of a computer cursor [92, 177–179], and the prediction of discrete targets on a computer screen [180] with non-human primates. Next, the control was extended to reach and grasp movements. Carmena et al. [93] showed the control of a robotic arm equipped with a gripper in monkeys. The monkeys observed the robotic arm state only indirectly via a screen and learned to reach and grasp virtual objects. Based on data from this experiment, Kim et al. [181] proposed to equip the robotic arm with proximity sensors to facilitate reflex-like reactions and augment brain-controlled trajectories. In a renowned demonstration, the group of Schwartz has shown the real-time interaction with physical objects via a prosthetic arm attached to monkeys [182]. The monkeys learned to control the prosthetic arm to feed themselves. Moritz et al. [183] and Pohlmeyer et al. [184] showed a BCI combined with a motor neuroprosthesis in a monkey where forearm muscles were transiently paralyzed. Neural activity was decoded and used to control wrist movements via FES and allowed the subjects to grade the amount of produced force. Moreover, grasp types were also decoded [185]. The aforementioned invasive BCIs decoded from neuronal ensembles. Although single cortical neurons correlate with movement parameters, the correlation varies over time, and neuronal ensembles provide more stable predictions of movement parameters [186].

Invasive BCIs were moreover demonstrated in humans. Hochberg et al. [187] showed the BCI control of a computer cursor in 2D, the opening and closing of a prosthetic hand, and rudimentary actions with a robotic arm. The BCI system was tested on a participant suffering from SCI at level C4 (ASIA A), who had an electrode array implanted onto the surface of the arm/hand region in the primary motor cortex. Kim et al. [188] improved this BCI by decoding velocity instead of position, and by replacing the linear filter by a Kalman filter, and tested the system in two tetraplegic persons.

Also, studies in humans with ECoG-based BCIs were conducted. Leuthardt et al.

[110] demonstrated a one-dimensional control of a computer cursor with different types of imagined and executed motor and speech tasks. However, the strategy for online control was not intuitive, as, e.g., MI of opening and closing the right hand vs. rest was used to control a cursor in 1D. Interestingly, the authors found in an additional offline analysis that joystick movement directions were encoded in the ECoG, namely in the high-gamma band. The online control of a cursor was later then extended to 2D [189].

non-invasive BCIs Movement control applications were also demonstrated with non-invasive BCIs based on EEG. The Graz BCI group showed the restoration of hand grasp function in a tetraplegic person with no residual hand function (SCI at level C4/C5, ASIA A) in Pfurtscheller et al. [35]. For this purpose, an oscillation-based BCI was used to detect right hand MI and foot MI. These MIs were translated into a control signal for a hand orthosis fitted to the left hand. Later, the same tetraplegic person was equipped with an FES-based neuroprosthesis controlled with a BCI [28]. Foot MI was then used to cycle through the different phases of a lateral grasp. Müller-Putz et al. [36] also showed the control of an implanted neuroprosthesis (Freehand system) with a BCI. The study participant, who sustained an SCI at level C5, learned to control his right hand with left hand MI. He was able to cycle through the phases of a lateral grasp. Moreover, Tavella et al. [190] demonstrated the BCI control of an FES-based neuroprosthesis in healthy persons. Notably, the control strategy was more natural than in the studies before as it included MI of the hand equipped with the FES. A hybrid neuroprosthesis consisting of FES and a semi-active orthosis was demonstrated by Rohm et al. [191] to restore hand and elbow function in a tetraplegic person with a complete SCI at level C4. The control was facilitated with a shared control between a shoulder joystick and an oscillation-based BCI. Furthermore, SSVEP-based BCIs were used to control a hand prosthesis and a hand orthosis [192, 193] by non-disabled persons, and a two degrees-of-freedom robotic arm by non-disabled persons and a tetraplegic person (SCI at level C4/C5, ASIA A) [194]. The latter robotic arm was also controlled with a hybrid BCI based on SSVEP and MI [195], and MI combined with temporal coding [196]. Moreover, Gomez-Rodriguez et al. [197] showed the control of a robotic arm with a single degree of freedom using an oscillation-based BCI and MI. Interestingly, haptic feedback improved the classification accuracy.

The BCIs mentioned in the preceding paragraph all provided a discrete control signal, i.e., one out of n classes could be selected by the BCI user. Wolpaw and McFarland [198] demonstrated a BCI based on brain oscillations that also provided a continuous control signal. The authors showed that users could control a computer cursor in 2D. This 2D control was later on then extended to 3D [199]. Both studies showed that BCI users can learn to independently modulate their mu and beta rhythms on different spatial locations and thus provide different continuous control signals.

1.4 Current Limitations

The last section listed BCIs which were used in control applications, in particular, in movement restoration applications. Various BCI research groups have reported success stories with invasive and non-invasive BCIs. Which type will prevail in the future is difficult to predict as both methods have their advantages and disadvantages. Non-invasive BCIs are safe to apply and do not impose any risk to the user as opposed to invasive BCIs. The implantation of electrodes may cause an infection, and particularly long-term usage is an issue because the insertion of electrodes leads to damages of the neural tissue and neurovasculature. These damages cause the formation of fibrous and cellular sheath encapsulating the electrodes [200, 201], which then impedes the recording of neuronal activity [202]. A re-implantation of the electrodes could be the consequence. So far, the lifetime of an electrode grid is months to years instead of decades. On the upside, invasive BCIs can provide a better SNR than non-invasive BCIs.

In the context of movement control applications, there is another fundamental difference between both methods. Invasive BCIs are often trained on executed movements, and a decoder learns a mapping between neuronal activity and movement parameters such as hand trajectory or muscle force level. Subjects can control then the decoder output with executed movements, and can also learn to suppress the motor output and produce the proper neuronal activity without overt movements [93]. Also, imagined movements in humans with SCI had been used as control signals by the time this thesis started [187, 188]. Thus, the decoder control is associated with natural movements, which is sometimes called biomimetic decoding [203]. However, the non-invasive oscillation-based BCIs often employ a decoder or classifier which is based on MIs, but the MIs are not associated with the desired movement of the neuroprosthesis. For example, in Pfurtscheller et al. [28] foot MI was used to control the FES on the left hand. The reason for this non-intuitive control is that the number of MIs which can be detected and classified is limited, and one has to select from the set of available MIs the ones which produce the most reliable control signal. Additionally, the details of how a movement is performed are hardly decodable with oscillation based BCIs, e.g., if a hand is opened or closed. Furthermore, MIs are often repetitive movements instead of single movements.

The non-intuitive control strategies for non-invasive BCIs are a limitation of the current state of the art. It would be desirable to have a control paradigm similar to invasive BCIs as this would allow for a more natural and therefore more intuitive non-invasive BCI control of motor neuroprostheses or robotic arms.

This limitation could perhaps be overcome with *low-frequency time-domain* (LFTD) signals. LFTD signals can be extracted from EEG by low-pass filtering with ca. 3 Hz. In contrast to oscillations, LFTD signals have been recently shown to encode upper limb movement trajectories in EEG [204, 205], MEG [206–208], ECoG [209–212], and LFP signals [213]. Furthermore, upper limb movement directions or movement targets were decoded from EEG [214, 215], MEG [216, 217], ECoG [218], and LFPs LFTD signals [105, 213, 219]. Noteworthy, the EEG signals associated with movement direction decoding may be related to – or are in fact – MRCPs [115], which also occur in the LFTD. MRCPs are evoked during self-paced movements and are modulated by various

factors, including movement speed or movement force [115, 220, 221]. MRCPs were furthermore used to detect movement initiation in single-trial EEG [222, 223]. Thus, hand trajectories decoded from LFTD signals could be used for intuitive and natural control of robotic arms or sophisticated future motor neuroprosthesis. Furthermore, decoded discrete movements like wrist movements, or movement parameters like speed or force could be used as intuitive control signals as well.

1.5 Aim of This Thesis

So far, non-invasive BCIs employ movement control paradigms that are unnatural and not intuitive. The aim of this thesis is hence:

1. to find non-invasive brain signals that can allow a more natural and intuitive movement control

2. and to develop a proof-of-concept online decoder based on those signals.

A more intuitive movement control could potentially be realized by employing LFTD EEG signals (see section 1.4). Whether continuous movements, i.e., hand/arm trajectories, can be decoded from these signals with sufficient accuracy to serve as a control signal for motor neuroprostheses or end effectors had to be researched in this thesis. The decoding of discrete movements was here a conceivable alternative to the decoding of continuous movements. Eventually, a natural and intuitive movement decoder had to be realized, and a proof-of-concept BCI had to be tested on a person with SCI.

1.6 Organization of This Thesis

The next chapter explains the methodology and describes the publications comprising this thesis (chapter 2). Four primary and four secondary publications are included. The first part in the method section is dedicated to the trajectory decoding of executed and imagined *continuous* arm movements. The second part in the method section focuses then on the decoding of executed and imagined *discrete* arm and hand movements of non-disabled persons and attempted movements in persons with SCI. Eventually, a proof-of-concept online decoder is presented. The outcomes of the conducted studies are then discussed and summarized in the third chapter and put in the context of the current state of the art (chapter 3). The third chapter concludes with an outlook for movement decoding. The primary and secondary publications created during this thesis are collected in the appendix.

2 Methods

2.1 Decoding of Continuous Movements

This section describes the studies related to continuous movement decoding from EEG LFTD signals. The primary studies analyze the decoding of executed and imagined hand/arm trajectories, respectively. The secondary studies cover supplemental decoding analyses.

2.1.1 Primary Publication I: Decoding of Velocities and Positions of 3D Arm Movement from EEG

Ofner, P. & Müller-Putz, G. R. *Decoding of Velocities and Positions of 3D Arm Movement from EEG* in *2012 34th Annual International Conference of the IEEE Engineering in Medicine and Biology Society* (IEEE, 2012), 6406–6409. [1]

LFTD signals were shown to encode movement trajectories. For example, they encode the velocity of the hand in 2D and 3D [204, 205]. LFTD signals may therefore be suitable to derive an intuitive control signal for a robotic arm or a future motor neuroprosthesis. In this work [1], hand trajectories were decoded in 3D from LFTD EEG signals with a decoder based on the work of Bradberry et al. [205]. The primary purpose was to gain further understanding of the decoder and to identify issues and possibilities for an online application. The paradigm was adapted from the original center-out reaching task in [205] to a continuous self-chosen movement task that had not yet been studied at the time. In this task, non-disabled study participants moved their right hand continuously in all directions in front of their body. The hand was in a position so that the thumb was always on the upside, see Figure 2.1. The hand trajectory was tracked, and the measured position and velocity were compared with the decoded position and velocity, respectively.

The secondary publication [5] described in subsection 2.1.3 adds to this study, and analyzed in a similar paradigm frontal and lateral arm movements and localized correlated brain sources.

Contribution to the PhD thesis Hand velocities were successfully decoded from the EEG using the velocity decoder initially presented in Bradberry et al. [205], see Figure 2.2 for an example. The obtained Pearson correlation coefficients between the measured and decoded hand movements were on average 0.70/0.77/0.62 (x/y/z) with standard deviations of 0.13/0.11/0.15. The publication showed moreover that it is also possible to

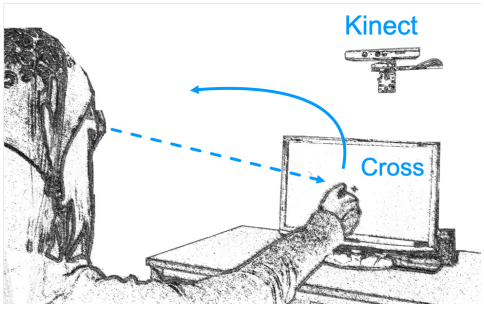

Figure 2.1: Experimental setup. Participants moved their right arm in front of them while simultaneously the hand position and EEG were measured.

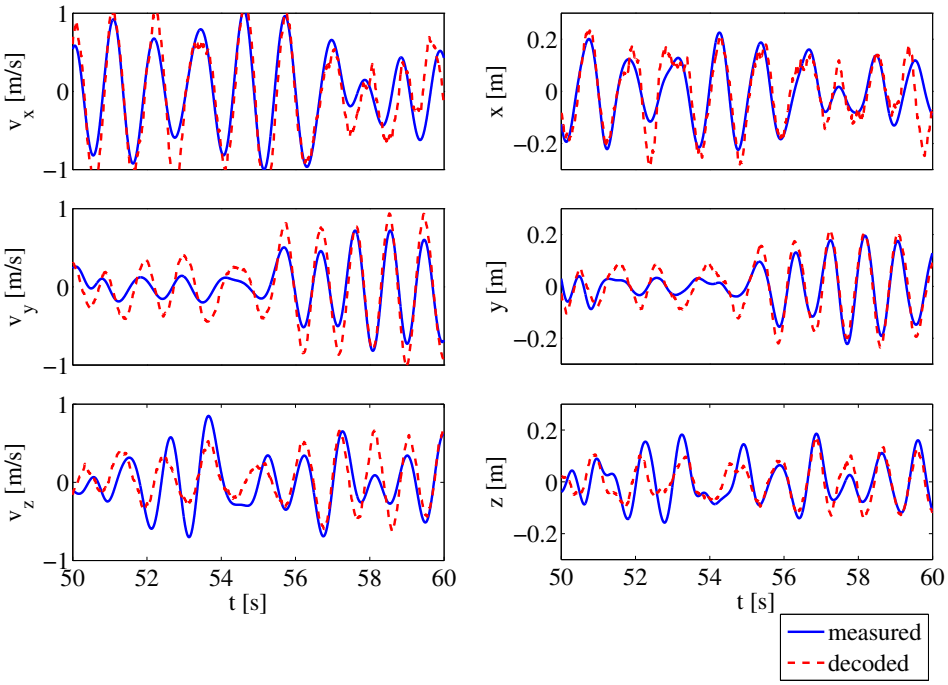

Figure 2.2: An example of measured and decoded trajectories. The left side shows velocities; the right side shows positions.

decode movements during longer self-chosen movements (65 s intervals) without external targets. Especially, self-chosen movements are essential for an eventual free control of a robotic arm. Additionally, in this work, the velocity decoder was modified to a position decoder. The original velocity decoder processing pipeline comprised a low-pass filter at 1 Hz, a difference computation, and three multiple linear regressions (for x/y/z directions) from channels and time lags to decode velocities. The low-pass filter and difference computation were replaced with a band-pass filter to realize a position decoder. Here, on average x/y/z correlation coefficients of 0.70/0.78/0.62 with a standard deviation of 0.12/0.09/0.14 were obtained.

Two important insights were gained in this study. First, eye movements affect the LFTD EEG signals strongly – even on central and parietal electrodes – and therefore had to be controlled. Second, the decoder employs solely linear operations, and can only attenuate or amplify existing frequencies but not shift or add frequencies. Therefore, the decoder can only decode movement frequencies that are also present in the EEG.

2.1.2 Primary Publication II: Using a Non-Invasive Decoding Method to Classify Rhythmic Movement Imaginations of the Arm in Two Planes

Ofner, P. & Müller-Putz, G. R. Using a Noninvasive Decoding Method to Classify Rhythmic Movement Imaginations of the Arm in Two Planes. *IEEE Transactions on Biomedical Engineering* **62,** 972–981 (2015). [2]

Both ME and MI modulate the power of brain oscillations in non-disabled participants [99, 102]. The type of MI, however, is crucial. Kinesthetic MI can activate motor areas similar to ME and lead to classifiable patterns in the EEG. Contrarily, visual MI, i.e., creating a mental video in third-person view of the moving limb, yields less distinctive patterns and causes poor classification accuracies [224]. Persons with SCI who cannot perform ME of a limb can still perform MI. MIs can then be detected with a BCI and used as a control signal [31–33]. For oscillation-based BCIs, it is generally assumed that the BCI performance achieved in non-disabled persons with kinesthetic MI is a proper proxy for performance in persons with SCI. Due to the lack of literature on LFTD-based trajectory decoding in persons with SCI, this assumption was also made in this thesis for movement decoding based on LFTD EEG signals. This work transferred therefore the decoding of executed movements to imagined movements in non-disabled persons [2]. Another motivation to study MI instead of ME was the absence of movement artifacts. If not carefully controlled, executed movements could cause particularly electrode and cable movements, which could interfere with the brain signals at low frequencies. This may cause overly optimistic decoding results partly based on artifacts.

The decoder comprised linear models that had to be trained with EEG and trajectory data. However, the imagined movement trajectory can not be directly measured. An apparent solution is to guide the imagined movement with an external moving target, e.g., a moving ball on a computer screen which is followed by the study participant with imagined arm movements. The problem is that this strategy would inevitably induce

eye movements correlated to the movement trajectory. Correlated eye movements are an immense problem here because the decoder would most likely be trained on the shifts of the electric potentials caused by the eye dipoles instead on brain signals. While eye artifact removal methods exist for EEG [225, 226], these methods attenuate the influence of eye movements on the EEG but do not guarantee their complete removal. A new paradigm was therefore designed to allow the measurement of imagined trajectories without inducing eye movements (c.f. Figure 2.3). For that purpose, the imagined arm movements were (1) restricted to two movement planes (horizontal and vertical), and (2) movements were rhythmic and synchronized with a metronome. In that way, it was possible to infer the imagined position of the right hand. A decoder was then build to decode the imagined horizontal and vertical positions of the right hand, and a subsequent classifier discriminated then between horizontal or vertical MI.

The sources of the brain signals carrying movement information were determined using a partial least squares (PLS) regression. Another study of this thesis presented in subsection 2.1.4 analyzed the same data set and used a correlation analysis instead of PLS regression to find the brain sources [6].

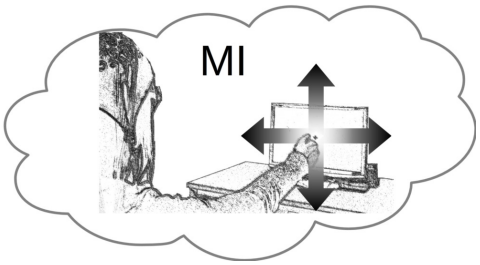

Figure 2.3: Subjects imagined rhythmic movements in the horizontal or vertical plane. The movements were synchronized with a metronome.

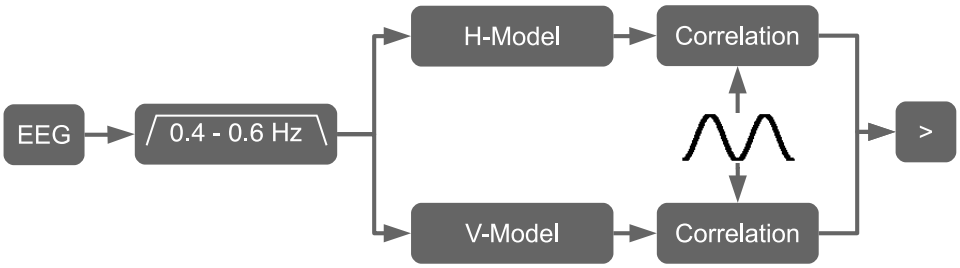

Figure 2.4: The classification method was based on the decoding approach introduced in [1]. The decoded vertical and horizontal positions were correlated with a sinusoidal oscillation, i.e., the assumed imaged trajectory. A trial was then classified as horizontal or vertical MI depending on which decoding model yielded a higher correlation.

Contribution to the PhD thesis The movement plane of imagined movements was successfully classified from LFTD signals with an accuracy of $64\,\% \pm 10\,\%$. As the classi-

fier was based on the position decoder introduced in [1] (c.f. Figure 2.4), it was indirectly shown that the decoding of imagined movement trajectories is possible. Noteworthy, it became evident in this study that the decoder weights should not be interpreted to estimate the sources. Due to volume conduction, EEG channels are correlated. Especially in low-frequency signals, which are more widespread than high-frequency signals [48]. The correlation of prediction variables is also known as multicollinearity and prevents the interpretation of the weights of a multiple linear regression [227]. The regression weights may change erratically due to small changes in the data. This problem was tackled by using PLS regression. PLS regression estimates latent variables which were then interpreted instead. In that way, it was found that the SMA encodes imagined movement trajectories. As the carefully designed paradigm did not provoke artifacts and motor areas were found to encode imagined movement trajectories, it became evident that indeed brain signals provide the discriminative signals for the movement decoder. However, the actual correlations were very low (around 0.3), and were found to be unusable for continuous control applications in persons with SCI. The decoding of movements was therefore not further pursued, and instead, the decoding of discrete movements was studied.

2.1.3 Secondary Publication I: Decoding of Executed Movements and Source Imaging

Ofner, P., Pereira, J. & Müller-Putz, G. R. *Decoding of Executed Movements and Source Imaging* in *Proceedings of the 6th International Brain-Computer Interface Conference 2014* (Graz University of Technology Publishing House, 2014), 026-1–026-4. ISBN: 978-3-85125-378-8. [5]

This study [5] decoded hand movements similar to [1] in subsection 2.1.1 but analyzed three movement conditions, and decoded from single brain sources instead of from all EEG channels. In the first and second movement condition, participants moved their hand frontally and laterally, respectively. In the third movement condition, participants observed a randomly moving ball on the computer screen while executing frontal movements. The correlation with the actual movements, achieved by each single brain source was then plotted in source space.

Contribution to the PhD thesis It was possible to decode movements in all three movement conditions, and the decoder performance was comparable between the movement conditions. Furthermore, sources on the primary motor cortex encoded movement trajectories in LFTD signals, see Figure 2.5. This supports the findings in [1] that hand position can be decoded from LFTD EEG signals. However, also lateral areas showed significant correlations with movement trajectories, which were possibly caused by movement artifacts. This corroborated the decision to analyze the decoding of imagined movement trajectories instead of executed movement trajectories in the follow-up study [2] presented in subsection 2.1.2.

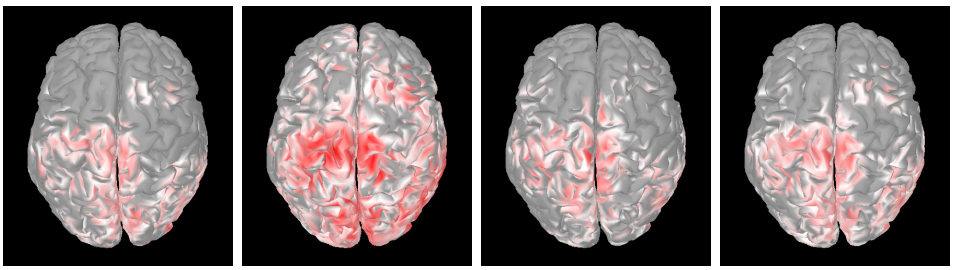

frontal condition lateral condition ball condition condition average

Figure 2.5: Subject averaged correlations on a per voxel basis for all three conditions and the average of them. Red corresponds to the maximum value, white to 50 % of the maximum value. Correlations below 50 % of the maximum are not shown.

2.1.4 Secondary Publication II: Time-Domain Correlations of Imagined Arm Positions with Brain Sources

Ofner, P. & Müller-Putz, G. R. *Time-domain Correlations of Imagined Arm Positions with Brain Sources* in *Proceedings of the BMT 2013* (Walter de Gruyter GmbH, 2013). [6]

This work analyzed the correlation of brain sources, including time lags, with imagined movements [6]. The imagined movements were restricted to up-down or left-right movements and synchronized with a metronome. The same EEG data were used as in the previous work [2] in subsection 2.1.2, however, informative brain sources were found with a canonical correlation analysis instead of a PLS regression.

Contribution to the PhD thesis The correlation analysis of LFTD EEG signals showed for four out of nine participants that the SMA encodes imagined movement trajectories (see Figure 2.6). As no movement artifacts were provoked in the paradigm and plausible brain areas showed higher correlations, one may assume that brain signals encode information about movement trajectories. However, the observed correlations on the SMA could also be caused by the perception of the metronome beats instead of performing MI [228]. Nevertheless, the similar findings in [2] (see subsection 2.1.2) are not affected by the metronome beat as a confounding variable. By considering both publications [2, 6], it is evident that LFTD brain signals encode indeed imagined movement trajectories.

2.2 Decoding of Discrete Movements

Facing the poor trajectory decoder performance for ME and especially for MI in the previous studies [1, 2], two options were conceivable. Either the trajectory decoder performance is improved substantially, or the decoding of less complex and discrete movement

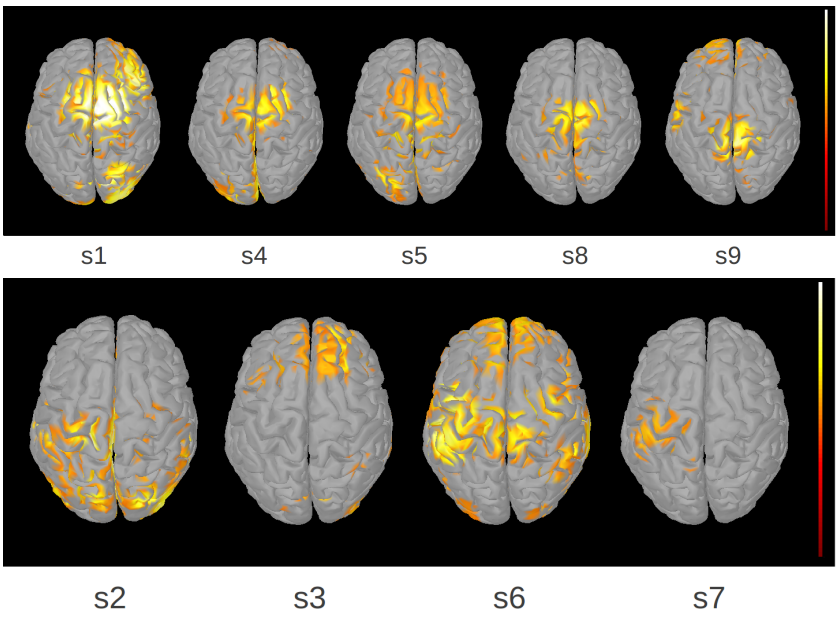

Figure 2.6: This figure shows the absolute canonical correlations for each subject. White corresponds to a canonical correlation of 0.5 for s1, 0.4 for s4 and s9, 0.3 for s8, and 0.2 for all others. The lowest possible value is 0 for all subjects.

parameters is researched. This PhD thesis followed the latter approach and changed the focus from *continuous* trajectory decoding to classification of *discrete* movements of the same upper limb. Single movements like hand open or hand close could then provide new and more intuitive control classes for motor neuroprostheses or robotic arms. Single movements elicit MRCPs, which are modulated by various factors like movement speed or force [115]. MRCPs could make a movement classifier possible and are researched in the two primary studies presented here. The two secondary studies analyzed a movement target decoding paradigm and the influence of visual input during MI.

2.2.1 Primary Publication III: Upper limb movements can be decoded from the time-domain of low-frequency EEG

Ofner, P., Schwarz, A., Pereira, J. & Müller-Putz, G. R. Upper Limb Movements Can Be Decoded from the Time-domain of Low-frequency EEG. *PLoS ONE* **12,** e0182578 (2017). [3]

This study analyzed whether MRCPs, time-locked to the movement onset, encode discriminative information about hand open, hand close, pronation, supination, elbow extension, and elbow flexion for ME and MI in non-disabled persons [3]. The movement classifier was based on a linear model where the weights were found with a shrinkage linear discriminant analysis (sLDA) [166]. Furthermore, the classifier patterns – they show which sources are used by a classifier – were analyzed in the source space.

In persons with SCI, a classifier has to be trained by using MI of discrete movements and some training paradigm. However, various aspects of the employed training paradigm may affect the elicited MRCPs. For this purpose, the influence of the visual input during imagined upper limb movements was studied in [8] (see subsection 2.2.4).

Contribution to the PhD thesis This work shows that various movements of the same upper limb can be classified from LFTD EEG signals. Movements can be discriminated from a rest class with an accuracy of 87 % ± 4 %, and the six movements can be discriminated from each other with an accuracy of 55 % ± 9 %. However, LFTD signals during ME provided significantly more information than during MI. The MI classification accuracies were 73 % ± 7 % and 27 % ± 4 % for movement vs. rest and movement vs. movement, respectively. The sources exploited by the classifier were located on movement associated areas on the cortex, i.e., premotor areas, primary motor cortex, somatosensory cortex, and posterior parietal cortex (see Figure 2.7). Thus, movement discriminative LFTD signals originate from the brain and not from artifacts. Next, it was to be studied if these findings can be translated to persons with SCI.

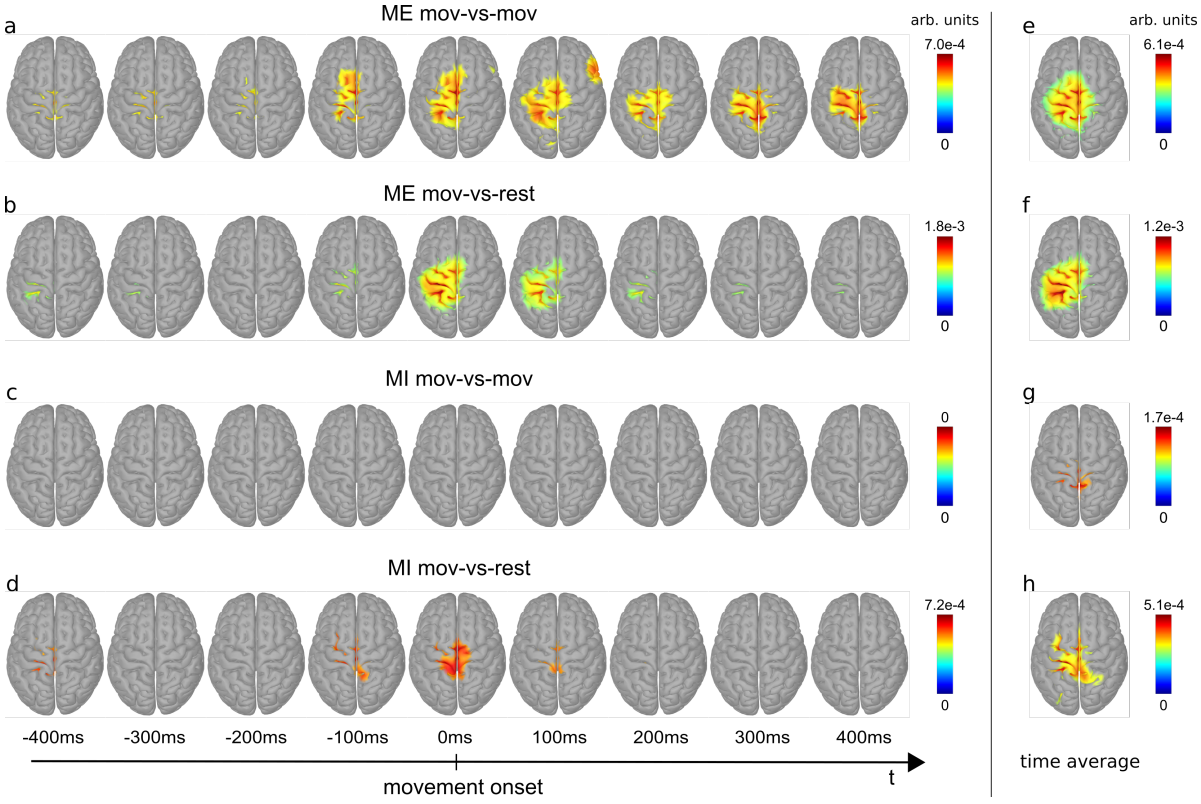

Figure 2.7: Classifier patterns. Shown are patterns between −0.4 s and 0.4 s relative to movement onset (a-d) and averaged over this time period (e-h). **a** and **e:** mov-vs-mov patterns during ME. **b** and **f:** mov-vs-rest patterns during ME. **c** and **g:** mov-vs-mov patterns during MI. **d** and **h:** mov-vs-rest patterns during MI.

2.2.2 Primary Publication IV: Attempted Arm and Hand Movements can be Decoded from Low-Frequency EEG from Persons with Spinal Cord Injury

Ofner, P. *et al.* Attempted Arm and Hand Movements Can Be Decoded from Low-frequency EEG from Persons with Spinal Cord Injury. *Scientific Reports* **9,** 7134 (2019). [4]

This study translated the EEG-based classification of single upper limb movements to persons with SCI [4]. Noteworthy, the assumption that MI in non-disabled persons provides a reasonable estimate for the expected performance in persons with SCI was dropped. Motivated by the findings in Blokland et al. [229], the study participants were instead instructed to perform *attempted movements*. The recruited participants suffered from SCI in the range from level C1 to C7. The participants attempted palmar grasp, lateral grasp, hand open, pronation, and supination in a cue-based paradigm. An offline analysis was then performed to analyze if LFTD EEG signals encode discriminative information, and the underlying sources were located in the channel space.

Furthermore, a proof-of-concept of an sLDA-based online movement classifier was introduced and tested on a participant with complete SCI at level C4. While a cue-based paradigm is suitable for an offline analysis, it is problematic for recording EEG data to train an online classifier. The movement-related potentials generated in a typical cue-based paradigm do not resemble the MRCPs elicited with self-paced movements [230], and are besides contaminated with cue-related potentials. However, EEG data for training a classifier cannot simply be gathered using a self-paced movement paradigm because the attempted movement onsets are unknown, and time-locking to the movement onsets is therefore impossible. Methods based on unsupervised learning can probably provide a solution, but do not yet exist in this context. The initial cue-based paradigm was therefore modified to elicit more MRCPs-like signals (c.f. Figure 2.8), which eventually allowed the training of an online classifier.

Contribution to the PhD thesis This publication concludes the PhD thesis by showing that five attempted single upper limb movements can be classified offline from LFTD EEG signals from persons with SCI. Thus, an intact spinal cord is not a necessity for decoding single upper limb movements from the EEG. The obtained classification accuracies were on average 45 % with a 95 % confidence interval of 40 % to 50 %. Moreover, this publication demonstrates the *online* detection and classification of hand open vs. palmar grasp in a closed-loop with a person with no residual hand function. In two sessions, the two movements were discriminated with an accuracy of 66 % and 71 %, respectively. A movement was detected with a true positive rate of 27 % and 37 %, false positives were detected with a rate of 3.2 and 3.6 per minute. Key to the successful classification was the modification of the initial cue-based paradigm so that MRCPs-like signals were elicited.

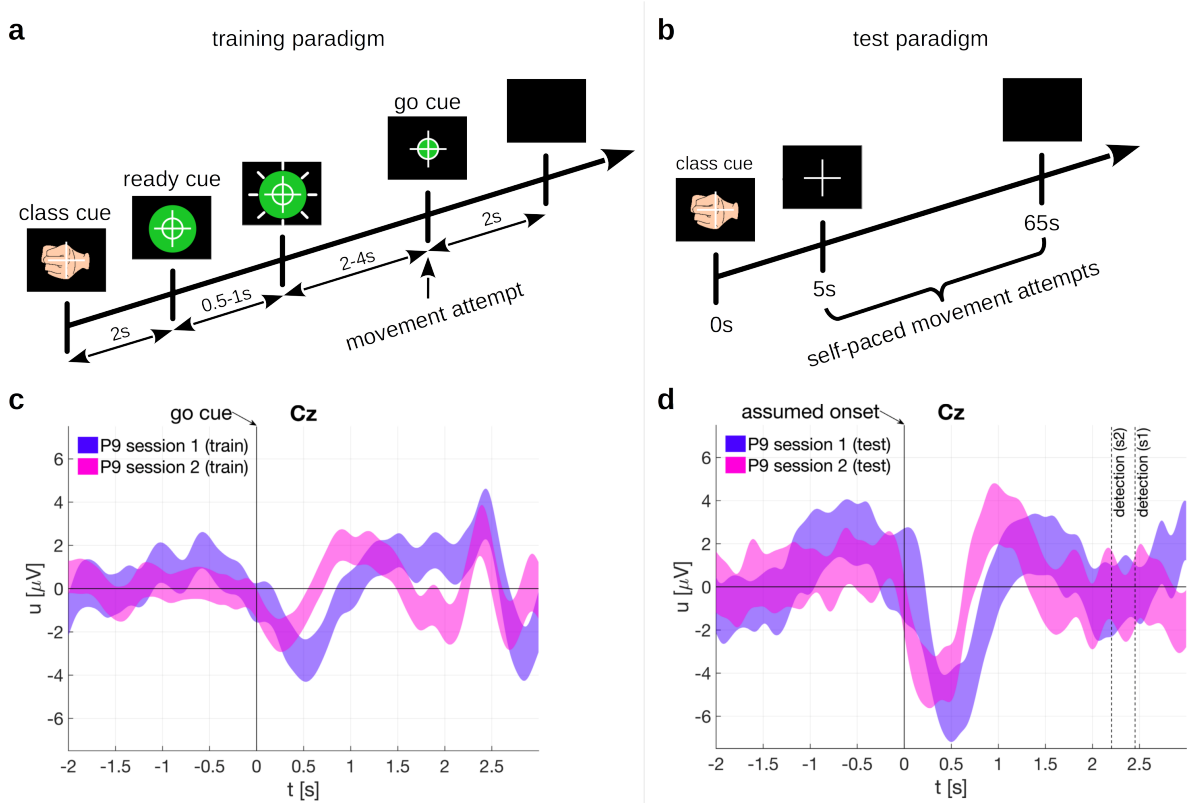

Figure 2.8: Training and test paradigms for online classification and respective electrode potentials. **a:** Training paradigm. A green filled circle shrunk with a random speed. The participant attempted a movement hand (hand open or palmar grasp) when it hit the inner white circle, i.e., the go cue. **b:** Test paradigm. The participant repeatedly attempted self-paced movements. **c:** 95 % confidence intervals of the electrode potentials on Cz time-locked to the go cue. **d:** 95 % confidence interval of the electrode potentials on Cz time-locked to the assumed movement onsets (i.e., corrected by detection delay).

2.2.3 Secondary Publication III: Movement Target Decoding from EEG and the Corresponding Discriminative Sources: a Preliminary Study

Ofner, P. & Müller-Putz, G. R. *Movement Target Decoding from EEG and the Corresponding Discriminative Sources: A Preliminary Study* in *2015 37th Annual International Conference of the IEEE Engineering in Medicine and Biology Society* (IEEE, 2015), 1468–1471. [7]

In addition to movement trajectory decoding and single movement classification, also movement target decoding was studied in this PhD thesis [7]. Movement target decoding could facilitate a high-level discrete control signal for end effectors. Instead of planning movements as in movement trajectory decoding or single movement classification, the user would select the target and initiate a movement attempt. The actual movement trajectory would then be planned by the end effector system instead of the user. A preliminary study with a small participant group was conducted to analyze the potential of LFTD EEG signals for discrete movement target decoding.

Contribution to the PhD thesis Movement targets were successfully classified in one out of three participants before the movement onset in a self-paced movement paradigm with an accuracy of 63 % w.r.t. four targets (see Figure 2.9) . The corresponding classifier pattern shows discriminative sources on contralateral motor areas. As the decoding was possible before the movement onsets, i.e., in the movement planning phase, this approach may also be feasible for persons with SCI. This study adds to the discrete movement paradigm in [3, 4] another possible high-level discrete control paradigm. However, this approach was not pursued any further as the thesis focused eventually on the decoding of discrete movements of the same upper-limb.

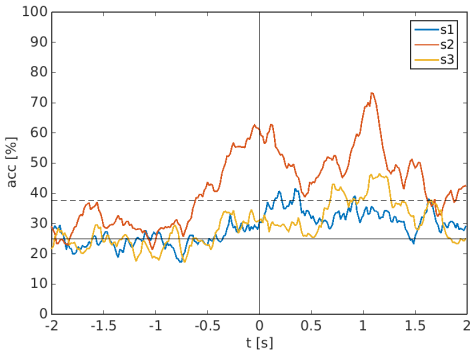

Figure 2.9: Participants' classification accuracies. Timepoint 0 s corresponds to the movement onset. The dashed line depicts the significance level.

2.2.4 Secondary Publication IV: Visual Input Affects the Decoding of Imagined Movements of the Same Limb

Ofner, P., Kersch, P. & Müller-Putz, G. R. *Visual Input Affects the Decoding of Imagined Movements of the Same Limb* in *Proceedings of the 7th Graz Brain-Computer Interface Conference 2017* (Graz University of Technology Publishing House, 2017), 367–372. [8]

The MI classification accuracies in [3] (see subsection 2.2.1) are mediocre and need to be improved to be applicable for a motor neuroprosthesis control. For that, a better understanding of the factors influencing the classification accuracy is necessary. This work studied therefore whether the type of visual input (realistic vs. abstract, see Figure 2.10) influences the classification accuracies of hand open MI vs. supination MI [8].

Contribution to the PhD thesis The study found that MI combined with realistic visual input yields higher classification accuracies than MI combined with abstract visual input (64 % ± 8 % vs. 57 % ± 5 %). Realistic visual input is therefore favorable to train a movement classifier. However, it was also found that the mere observation of realistic visual input leads to a significant classification accuracy of 62 % ± 6 %. This needs to be considered when interpreting classification accuracies as they may not be entirely caused by the actual MI but also by the observation itself.

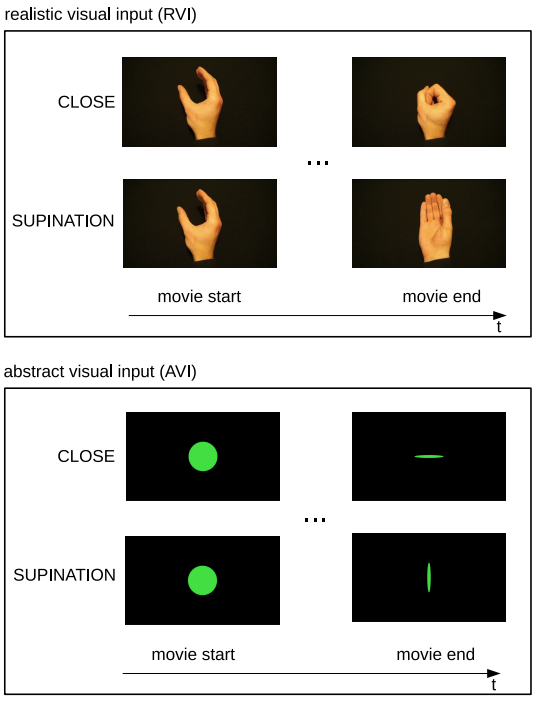

Figure 2.10: Participants observed movements or performed MI while watching realistic visual input or abstract visual input.

3 Discussion

3.1 Overview

The brain encodes various movements parameters. This thesis investigated if movement parameters relevant for movement control applications, e.g., motor neuroprostheses, robotic arms, or exoskeleton, can be decoded non-invasively from LFTD EEG signals. The publications comprising this thesis show that movement trajectories, as well as single upper limb movements, can be decoded from LFTD EEG signals.

Eventually, it could be shown that different *attempted* upper limb movements can not only be decoded from non-disabled persons but also from persons with SCI. The development of a BCI complemented this thesis: a proof-of-concept of an online asynchronous classifier was introduced. This proof-of-concept was then validated in one participant with SCI and used to detect attempted hand open and palmar grasp movements.

This thesis recognizes the importance of localizing the sources conveying movement information, and it was shown that indeed signals originating from *movement-related brain areas* encode movement information. However, other non-brain sources, so-called artifacts like eye dipole movements or electrode cable movements, affect EEG signals and can easily be picked up by the movement decoder. These artifacts can therefore cause improper high decoding performances when they are correlated with limb movements. These artifacts must therefore be avoided by the paradigm design and the experimental setup.

3.2 Findings in Relation to the State of the Art

3.2.1 Decoding Executed Movement Trajectories

This thesis showed in Ofner and Müller-Putz [1] for the first time that hand positions – besides hand velocities – can be directly decoded from LFTD EEG signals. The employed paradigm allowed self-chosen continuous movements, and it was evaluated by calculating the correlation coefficient between the measured and the reconstructed hand trajectory. Notably, this paradigm did not suffer from an over-optimistic estimation of the correlation coefficient as it could be the case for classical center-out-reaching paradigms [231]. This is because the signals to be correlated cycle through multiple periods, yielding less noisy estimates of the correlation coefficient. However, a question that could not be answered satisfactorily in the thesis's first publication [1] is the location of the sources conveying movement information. In movement decoding experiments, care must be taken that non-brain signals do not influence the decoding results. Such

non-brain signals could be, for example, eye dipole shifts, electrode cable movements, electrode cap movements, or muscle artifacts. Therefore, another study [5] was carried out, which showed that LFTD EEG signals originating from the primary sensorimotor area, indeed convey trajectory information. However, the EEG can be contaminated with artifacts correlated to movements. These findings of the thesis were then later corroborated in Kobler et al. [232] where position and velocity were decoded from LFTD EEG signals, and primary sensorimotor and premotor areas were shown to encode end-effector velocities. Since the beginning of this PhD thesis, several more non-invasive studies confirmed that arm and finger trajectories are encoded in low-frequency EEG [232–236] and MEG [207, 237, 238] signals. These findings are supported by a growing body of invasive ECoG [239–244] and LFP [109, 245] studies, which also show that low-frequency brain signals encode movement information. Note that invasive recordings are less prone to movements artifacts than non-invasive recordings, and their findings are therefore less likely to be falsified.

Despite the initial success in decoding movements from EEG, a conclusive closed-loop online movement trajectory LFTD-based decoder has so far not been shown for EEG signals. The main reason is probably the low decoding performance. Invasive studies based on LFTD signals achieved some success here [245, 246], but it has to be seen whether these results can be translated to non-invasive recording techniques.

Decoding Methods The executed movement trajectory decoding studies in this thesis [1, 5] employed a multiple linear regression. This method yielded a limited decoding performance with a Pearson correlation coefficient of around 0.7. This raises the question of whether more sophisticated methods can improve the decoding performance. This paragraph gives an overview of the decoding methods that have been studied by now. Included are EEG, MEG, and ECoG studies based on LFTD signals, which often share a similar signal processing pipeline. Studies based on frequency-domain features are included when the respective decoding principles could be applied to time-domain signals as well.

Alongside multiple linear regression, also PLS regression [232], kernel ridge regression [233], particle filter [234], and Kalman filter [247] were by now explored for trajectory decoding from EEG low-frequency signals. In an MEG study, speed (a scalar) and direction were decoded separately with Kalman filters and a multilayer perceptron, succeeding the direct decoding of the velocity vector [237]. ECoG studies applied sparse linear regression [241, 242, 248], or regularized multi-way PLS regression [249]. Particularly, the latter regression type can deliver a good trade-off between prediction accuracies and trajectory smoothness. Furthermore, generalized additive models (GAMs) were combined with PLS regression [249]. GAMs are interesting as they allow non-linearity but are still tractable due to their otherwise linear structure. Another ECoG study applied an artificial neural network to decode trajectories [250]. The authors combined a convolutional neural network with a recurrent neural network for this purpose. A different and interesting concept is the usage of separate decoding models for different movement states. The consideration is that decoder models are not universally valid but only for certain

movement states, and that incorporating prior information of the movement state in the models can improve the decoding [243, 251].

Unfortunately, none of the enumerated methods provided a substantial improvement to the decoding performance, and a promising novel methodological research direction for non-invasive trajectory decoding would be required.

3.2.2 Decoding Imagined Movement Trajectories

MI experiments with non-disabled participants are usually carried out to assess the feasibility of a motor-task-based BCI algorithm for application in persons with SCI. Furthermore, MI experiments are in general less prone to movements artifacts, which makes it easier to obtain valid classification or decoding results. This thesis translated in [2] the decoding of executed movements to the decoding of imagined movements. It was shown that movement trajectories can be decoded in an MI task, and that the SMA contributes to the decoding. The contribution of the SMA is also indicated by the findings in the accompanying study in [6]. Imagined movement trajectories were also successfully decoded by Kim et al. [233], which was published simultaneously with [2]. In that study, participants executed and imagined arm movements. Arm movements were imagined according to the movements of a robotic arm, and additionally to another human's arm. In their analysis, they found that the decoding accuracy dropped substantially when eye movement-related activity was removed with a linear spatial filter from the EEG. This indicates that the EEG data were contaminated with eye movement-related activity. In general, it highlights once more the importance of artifact avoidance by the paradigm design and the usage of proper artifact cleaning methods. Interestingly, a non-linear movement decoder based on kernel ridge regression did not show that performance drop. However, that raises the question if non-linear eye movement-related activity remained in the EEG after applying a linear spatial filter.

The first report of an EEG-based trajectory decoder for imagined movements was already published in 2011. Bradberry et al. [252] pursued their initial movement decoding studies [205, 206], and showed the online decoding of imagined movement trajectories from LFTD EEG signals. However, this work was soon after criticized as it was shown that a random decoder could achieve the same decoding performance [253, 254]. In the time since also brain oscillations have been shown to encode imagined movement trajectories in mu, beta and, low-gamma bands [255].

3.2.3 Decoding Movement Targets and Directions

The efforts to decode the trajectories of arm movements in [1] did not yield a satisfactory decoding performance with a Pearson correlation coefficient of around 0.7. Even less promising were the results of the imagined movement trajectory decoding with a correlation coefficient of around 0.3 [2]. The decoding performance had to be improved beyond any conceivable level for a realistic chance to control a neuroprosthesis or a robotic arm. Therefore, this PhD thesis changed its focus from the decoding of continuous movement parameters to the simpler problem of decoding discrete movement

parameters. The objective was now to decode movement parameters from a small set of possible states which involves the decoding of less information per time interval from the EEG. Thus, a regression problem was turned into a classification problem. For that purpose, the decoding of movement targets was analyzed in this thesis in [7]. The decoding of movement targets/directions from EEG, MEG, ECoG and LFP from low-frequency signals is already reported in the literature, see section 1.4 and the more recent papers [246, 256–258]. The novelty of this thesis was the calculation of classifier patterns in [7] combined with source imaging, which allowed the analysis of the discriminative sources exploited by the classifier in the source space. Later, Úbeda et al. [259] corroborated the target decoding results by applying trajectory decoding to decode targets from LFTD EEG signals eventually. The authors first fitted a line through a decoded trajectory, and then identified the target by the direction in which this line pointed. Furthermore, the authors showed that targets could be decoded during executed movements but not during passive movements (i.e., when the hand was moved by the experimenter). This suggests that proprioceptive feedback alone does not modulate LFTD EEG signals so that movement trajectories and then movement targets can be decoded from it. Handiru et al. [260] developed a supervised factor analysis method and decoded movement directions also from time-domain EEG signals but in the source space.

An issue in some studies, including [7] from this thesis, is the potential confusion of movement targets and movement directions. In the employed paradigms, a movement target corresponded to exactly one movement direction and vice versa. Thus, it is not clear whether targets or directions have been decoded. Tanaka et al. [261] indicates that both movement directions and movements targets could modulate EEG signals.

The decoding of movement targets or movement directions was not further pursued in this thesis. Even if movement directions could be decoded with sufficient accuracy, it would be difficult to translate them into a control signal for existing motor neuroprostheses because they do not yet provide the necessary movement functionality [20]. Since a change from continuous trajectory decoding to simpler paradigms was envisaged, this PhD thesis focused instead on a control paradigm also suitable for existing motor neuroprostheses: the decoding of single limb movements.

3.2.4 Decoding of Single Limb Movements from Non-Disabled Persons

This PhD thesis focused eventually on the decoding of single limb movements because they can be exploited as control signals for both existing motor neuroprostheses and robotic arms. The following movements were identified as meaningful control classes and analyzed in this thesis in [3]: hand open, hand close, pronation, supination, elbow extension, and elbow flexion. This publication showed that ME and MI of these movements can be classified with a linear classifier from LFTD EEG signals. Furthermore, this publication shows – a novelty in that context – the corresponding patterns of the classifier [262, 263], which confirm that the classifier exploited brain signals but not movement artifacts or eye artifacts. Later, Zhao et al. [264] analyzed the published

data from [3] and improved the MI classification accuracy with a convolutional neural network.

Movements have already been classified from low-frequency EEG [265–267], MEG [267–269] and ECoG signals [270]. However, this thesis analyzed in [3] a different or more extensive movement set compared to the existing studies. Closely related to the decoding of single limb movements is – at least technically – the decoding of grasps as both movement types can be considered as discrete events. Several studies have by now demonstrated grasp decoding from EEG [271–273], ECoG [274], and LFP [275] with LFTD signals. This demonstrates once more that LFTD signals indeed carry various information about discrete movements.

This thesis analyzed executed movements and imagined movements [3]. While the classification accuracies for executed movements were reasonable, the classification accuracies for imagined movements were mediocre and barely above chance level. In a complementary study, it was therefore analyzed if the classification accuracies of imagined movements can be improved by presenting the user realistic cues instead of abstract cues, i.e., a video of a moving hand vs. an animation of a geometric object [8]. The rationale behind is that visual input has been shown to at least partly substitute missing proprioceptive input [276], and this substitution effect might help to yield higher classification accuracies in an MI paradigm where a modulation of the proprioceptive input is missing. How this approach can benefit an online classifier is admittedly still an open question as a typical chicken or egg dilemma exists: the classifier output would depend on the observation of the correct movement, and the movement would depend on the correct classifier output. Despite this question cannot be answered at this point, the study had its purpose as it was a first attempt to analyze the influence of the visual input on LFTD signals, and it could inform decisions about future research directions. This study found indeed that classification accuracies are improved by showing realistic cues. However, the discrimination was also improved when the realistic cues were only observed without a simultaneous movement imagination (as opposed to the abstract cues). Whether and how this is related to the human mirror system has to be studied [277]. The initial mirror system studies [277, 278] found that the mirror system in non-human subjects is only active when meaningful movements are observed but not during meaningless movements such as those in this thesis's study. However, later, it became clear that this is different for humans, and meaningless movements can also cause an activation of the human mirror system [277]. The outcome of this study raised the question if (1) the increase in classification accuracy was solely a consequence of the perception of the realistic visual input and independent of any movement intention related processes, (2) or if the realistic visual input modulated movement intention related processes. For an LFTD-based online classifier, only the latter option could potentially provide a performance benefit.

3.2.5 Decoding of Single Limb Movements from Persons with SCI

The final study in Ofner et al. [4] showed for the first time the successful classification of different single movements of the same limb (hand open, pronation, supination) and grasps (palmar, lateral) in tetraplegic persons using EEG signals. A significant paradigm change eventually overcame the mediocre MI classification performance observed in [3]. So far, in this thesis, MI was unquestionably considered as a suitable proxy for the expected classification performance in persons with SCI. Mostly, because MI [102, 279, 280], particularly kinesthetic MI [224], has been proven as an applicable mental control strategy for oscillation-based BCIs in persons with and without SCI [28, 35, 36, 77, 191, 196, 199, 281–283] since the late 90s [280]. However, it has been shown by now that attempted movements can yield more pronounced patterns in the frequency-domain than MI [229]. This indicates that MI in non-disabled persons may lead to an underestimation of the classification accuracy achievable in persons with SCI when they attempt movements. Furthermore, this underestimation might even be more severe for movement-related LFTD signals, in particular, for LFTD signals accompanying discrete movement events, which are, in fact, MRCPs [114, 115]. MRCPs have been shown to exist also in persons with SCI during *attempted* movements but are altered [284–286]. In line with these findings, Fukuma et al. [287] could decode attempted movements from paralyzed persons suffering from brachial plexus root avulsion, and additionally from one amputee by using LFTD MEG signals. These insights and findings raised doubts as to whether MI is the proper mental control strategy in an EEG-based movement control paradigm, and were the reason why attempted movements instead of MI were used in the paradigm in the final study [4]. This change presumably led then to the successful classification of movements in persons with SCI.

This thesis furthermore introduced a proof-of-concept of an online closed-loop movement decoder and tested this decoder on a person with SCI [4]. Four factors contributed to the successful demonstration of this concept. First, the movement decoder exploited LFTD EEG signals, which contain the discriminative movement information. Second, an sLDA classifier was modified to detect the MRCPs asynchronously. Third, the study participant was attempting movements instead of imagining movements. Fourth, a training paradigm was created, which elicited more MRCPs-like signals than other typical cue-based paradigms, like the Graz BCI paradigm [288]. So far, only MEG studies have shown a closed-loop control using LFTD signals in non-disabled participants [289] and paralyzed participants [287]. However, the evaluations were based on a cue-based paradigm. An asynchronous closed-loop control has also been implemented with MEG LFTD signals [290, 291], but the online performance results are either not provided or were not better than with a random decoder (the online decoding itself was not the main objective in both publications but the effects of BCI training).

3.2.6 Findings in Relation to Movement-Related Invasive BCIs in Humans

This thesis focused on the derivation of a natural and intuitive movement control signal from EEG. However, to put the results in a broader context, this section includes an update of the state of the art of movement-related invasive BCIs since the start of this thesis. The initial studies of continuous effector or cursor control in non-human primates [92, 93, 176, 182, 183] were subsequently translated to humans. Whereas initially only a rudimentary robotic arm or cursor control [187, 188] by tetraplegic persons was possible, the following studies quickly improved these results. Hochberg et al. [292] showed a 3D control of a robotic arm, including grasp functionality, by tetraplegic persons. Later, Collinger et al. [293] demonstrated a 7D control of a robotic arm by a tetraplegic person (3D translation, 3D orientation, 1D grasping). Wodlinger et al. [294] extended then the 7D control to a 10D control by enhancing the grasping functionality. The control of robotic arms was then eventually translated to the control of FES-based motor neuroprostheses in persons with SCI, and reach and grasp function were restored [295, 296].

All studies so far employed microarrays and decoded from neuronal firing rates and in case of [296] additionally from LFP high-frequency band power. Beside these microarray studies, also a few ECoG studies with movement-related online control exist. The control of a robotic arm by exploiting high-gamma ECoG signals was demonstrated in [111, 297, 298]. Milekovic et al. [246] by contrast, used LFTD ECoG signals to control a 1D cursor. Unlike the microarray studies mentioned above, the cited ECoG studies except [246] classified discrete movement classes instead of continuous movements, and all ECoG study participants executed the movements.

It is apparent that particularly microarray-based BCIs decode more movement information than non-invasive BCIs. While non-invasive BCIs were shown to control cursors or motor neuroprostheses [20, 33], a *natural and high-dimensional* online control of a motor neuroprosthesis or a robotic arm has not yet been convincingly demonstrated. This thesis advanced the current state of the art for non-invasive BCIs, especially for the decoding of discrete movements from EEG, but a movement control at the level of invasive BCIs is currently not foreseeable.

3.2.7 Other Movement Encoding Features

In addition to LFTD signals, EEG oscillations in classical BCI frequency bands, i.e., mu, beta, and gamma bands, have been shown by now to encode trajectories of arm movements [255, 299], movement directions [300, 301], movement phases during rhythmic movements [302], and hand synergies in grasping movements [303]. Korik et al. [255] found that the trajectory information in these frequency bands even surpasses the one in LFTD signals. Also, different grasps were shown to be encoded in EEG oscillations [273]. Those findings are not entirely consistent with the existing movement decoding literature [304]. However, it only points out the need for further studies to investigate the different feature types carrying movement information, and eventually integrate them

into a consistent theory. Another frequency band providing rich movement information is the high-gamma band (starting from ca. 50 Hz), which has been shown to encode various movement parameters in EEG [267, 305], ECoG [111, 210, 218, 241, 243, 244, 274, 306–308] and LFP [107, 109, 309, 310] studies. However, due to the low-pass effects of the brain structures [48], high-gamma band signals are hardly accessible with EEG in single-trial classification. Furthermore, brain connectivity analysis can support the extraction of movement trajectories from delta, theta, and gamma bands [311].

3.3 Training Paradigm Aspects

Paradigm design is a fundamental process in every BCI experiment, and many design decisions have a direct influence on the outcome of the study. During this PhD several important factors for movement decoding experiment have been identified and led to innovative paradigms, especially in [2, 4]. This section discusses important factors related to the choice of movement strategy, the acquisition of training data, and the visualization of the cue.

The problem of the choice of the appropriate movement strategy has already been introduced in the previous section. In short, MI in non-disabled persons leads to a strong underestimation of the expected performance in persons with SCI for discrete movement events (c.f. MI and attempted movement classification accuracies in [3] and [4], respectively). Whether ME, instead of MI, is a better choice is however open. It provides a more realistic estimation of the classification accuracy, but it may yield more dissimilar MRCPs than MI. At least two potentials of the MRCPs, the readiness potential and the motor potential, are affected in a complex way. Whereas the elicited *readiness potential* is more similar between ME and attempted movements in non-disabled and spinal cord injured persons, respectively, MI elicits a more similar *motor potential* [284]. Furthermore, MRCPs are modulated by the change in sensory feedback, which is present during ME but altered or not at all during MI or attempted movements [115]. It may be acceptable to ignore those differences when *testing the performance* of a particular decoder in non-disabled persons, but those differences become important if one wants to *tune the paradigm* to elicit more pronounced MRCPs.

Another problem is the acquisition of training data. A common approach is to measure behavior and find encodings of it in brain signals. However, this approach is not possible with persons with SCI due to the lack of respective movement function. As a workaround – which was also followed in this thesis – study participants are forced by the paradigm in a strict set of rules. For example, participants are only allowed to attempt certain movements at certain times and with certain characteristics (e.g., speed, duration, trajectory). However, there are two major problems to that workaround. The first problem is how those rules are enforced by the paradigm on the study participant. Often, the paradigm induces artifacts (e.g., eye movements when presenting a target, or a reference trajectory which should be followed) or evoked potentials (e.g., visual evoked potentials due to the cue). The second and even more serious problem is the unnatural setting. *Study participants are often reduced to agents who are remotely con-*

trolled by the paradigm. However, the brain signals generated under such unnatural and artificial conditions differ from brain signals generated during self-paced and self-chosen movements as in realistic scenarios [312–314]. Unsupervised decoder training methods – which do not enforce a certain movement – can enable more realistic self-controlled training paradigms. Such unsupervised decoder were proposed, e.g., by Gürel and Mehring [315] for trajectory decoding or Schwemmer et al. [316] for discrete movement decoding. Furthermore, study participants are in a state of increased attention: to follow the paradigm rules, and possibly also to observe the results of the BCI. As a consequence, the associated increased cognitive load might alter the brain signals as suggested by a study which investigated the influence of the attention level on MRCPs [317].

Moreover, the visual appearance of a cue is important. A cue visualized like a human body part can affect the EEG signals – probably due to the engagement of the putative human mirror system [318]. This thesis has shown that the mere observation of a moving hand in a video clip causes already a movement specific modulation of LFTD signals while abstract video clips do not cause a movement specific modulation [8]. Furthermore, a readiness potential occurs before an observation of a predicted human movement [319], and also brain oscillations are modulated by observation of human movements [320–323]. Thus, the visual type of the cue affects the EEG and can activate the motor system. However, whether this activation facilitates or impedes the training of a movement decoder model is not clear. If the modulation of LFTD signals by movement observation is sufficiently similar to the modulation of LFTD signals by movement intention (which has yet to be shown for LFTD signals), an initial movement decoder could be bootstrapped using a movement observation or a movement copy task. In a movement observation task, the prospective BCI user observes a realistically visualized, e.g., human arm, performing movements while the EEG is recorded. Subsequently, an initial decoder model is trained on these EEG data. This initial decoder can then be further improved in an adaptive online training, then using an attempted movement task instead of a movement observation task. However, when initially a movement copy task instead of a movement observation task is performed (i.e., attempting an observed movement), two processes can generate brain signals. One process due to the movement attempt and the other one due to the movement observation. These processes could generate interfering brain signals when the attempted movement is not in synchrony with the observed movement, and in turn, distort the training data for the movement decoder. Another potential application of a realistically visualized human arm is its possible incorporation in one's body schema with the so-called rubber hand illusion. After successful incorporation, an observed movement of the visualized arm can activate the somatosensory cortex and thus partly substitute the missing somatosensory feedback [276]. This could increase the movement information encoded in the EEG. However, it is an open question of how this can be exploited in an online classifier when visual feedback is only available after a movement has been decoded.

3.4 Sensory Feedback

In general, brain activity is generated by interacting neuronal networks and local processing within these networks. Thus, the input from other brain areas or the periphery drives neuronal circuits, which then can generate measurable output in the EEG. However, persons with SCI have typically no or altered sensory signals from the periphery of paralyzed body parts. When developing an EEG-based movement decoder, it is therefore essential to understand what effect the loss of sensory input has on the EEG signals generated by motor networks on cortical areas. This section discusses current findings and relates them to this thesis.

Galan et al. [324] found that the absence of sensory feedback affects EEG scalp potentials and the movement decoding performance. The authors induced an ischemic nerve block and compared executed and attempted movements in non-disabled subjects. In particular, they found that cortical activity was reduced for attempted movements during the movement preparation phase on the precentral area, and during the movement phase on the precentral and postcentral areas. Furthermore, the decoding performance of wrist movements lowered to chance level. This study supports the idea that the modulation of LFTD EEG signals is mainly caused by sensory feedback (i.e., thalamocortical connections relaying afferents) modulating the activity in cortical neuronal networks. However, their findings are limited by the fact that an ischemic nerve block only prevents sensory feedback from being sent from the peripheral nervous system to the central nervous system. The spinal cord networks can still generate impulses, which are then sent to the brain, and they could affect the cortical neural networks differently than in the case of an actual spinal cord injury. Bansal et al. [325] draws a more differentiated picture and found that low-frequency LFP signals on the primary motor cortex and the ventral pre-motor cortex are modulated by motor output and sensory input. They conclude that (1) sensory feedback (i.e., thalamocortical connections), (2) corticocortical connections, and (3) local network spiking activity modulate low-frequency LFP signals.

The findings from this PhD thesis support the idea that cortical areas relevant for EEG-based movement decoding are at least modulated by corticocortical connections, i.e., motor output from other brain areas. Whether sensory feedback adds additional information to the decoded movement signals was not investigated. However, the comparison of the decoding accuracies between this thesis's studies in [3] and [4] (sensory feedback vs. no sensory feedback) do not suggest a critical role of sensory feedback. Also, Ubeda et al. [259] showed that passive movements lead to a poor decoding performance compared to executed movements. Thus, sensory feedback is not the leading cause for the encoded movement information in LFTD EEG signals. In line with that, an ECoG study [307] achieved better movement classification using high-gamma band signals from motor areas than from sensory areas. However, other ECoG studies [308, 326] found movement information in the high-gamma band rather on sensory than motor areas. In summary, sensory feedback does not seem to be necessary to decode movements from EEG, but some contradicting findings need to be resolved in the future.

3.5 Unification of Discrete and Continuous Movement Parameters

LFTD signals associated with continuous and discrete movements have been strictly separated in this thesis so far, although they share the same frequency band and arise from overlapping cortical areas. It is therefore possible that they are the same phenomenon, and that the same cortical processes generate the respective LFTD EEG signals. This paragraph speculates whether the LFTD signals arising from both movement types can be united.

An important question one needs to ask is: are continuous movements encoded in continuously active brain sources? It may be that continuous movements are encoded instead as discrete impulses which are continuously evoked during continuous movements. The reader may imagine an outstretched arm which is continuously moved in front of the body, like in [5]. This arm movement would be composed of single movements (left, right, up, down) executed in a specific sequence and with a specific timing. Let us assume that every single movement of the arm causes movement specific MRCPs. One direct consequence of such a hypothetical evoked MRCPs series is that the movement frequency of body parts is represented in the EEG signals, due to recurrent MRCPs associated with every single movement. For example, when the arm is repetitively moved with a frequency of 1 Hz from left to right and back similar as in [2], a signal would be evoked in the EEG carrying that frequency. Interestingly, this is precisely what has been found [2], and it would explain why linear decoding models for continuous movements work to a certain degree (linear models can only decode frequencies supplied by the input). Now, MRCPs have a relatively long duration around 2 s. They will overlap in a continuous natural movement and could appear then as a continuous LFTD signal. Due to the overlap, they will not resemble the shape of typical MRCPs anymore, and will probably not contain all the subcomponents of individual MRCPs. It is thinkable that, e.g., the motor potential is evoked as in single movements but that potentials related to movement planning disappear as they are superseded by the motor potential, or happen at different time scales as explained in the next paragraph.

We do not execute jerky movements but rather round and well-connected movements. This is achieved by planning a movement sequence or a movement trajectory [327, 328]. Thus, continuous LFTD EEG signals could contain "low-level" potentials (e.g., motor potential) directly associated with the activation of muscle groups or muscle synergies [329, 330] (i.e., coactivation of muscles), and "high-level" potentials associated with movement plans. The hypothetical "high-level" potentials may appear on a longer timescale as they relate to planning and encode a movement sequence, and are in this case not exploitable by a linear movement decoder. The "high-level" potentials could encode so-called complex movements [331, 332] or motor primitives [333–335] which are then composed into movement sequences.

In summary, it may be that continuous LFTD EEG signals are timely-overlapping MRCPs subsets, which encode the single movements that constitute a continuous movement. The single movements correlate with kinematic parameters of the limb (e.g.,

velocity of the hand), which could explain why LFTD EEG signals encode kinematic parameters of the limb. Thus, the decoding of kinematic parameters of continuous movements would then be, in fact, a decoding of discrete movements.

3.6 Limitation of this Thesis

The attainable outcome of this PhD thesis is bounded by several limitations regarding the performance and reliability of the decoder, and the recording technique.

Performance The performance of the BCI in the final study [4] is not on a level as it would be necessary for an effective motor neuroprosthesis control. While the classification accuracy of different discrete movements is promising, the detection performance (i.e., true positive rate, false positive rate) is not. However, the validity of this statement is itself limited because the conducted single case study does not allow any inference about the performance at the group level. Another performance limitation is the user itself. With oscillation-based BCIs, BCI usage can be seen as a skill which can be trained by the user, like playing the piano. Whether the user can train the generation of MRCPs was not investigated in this PhD thesis, but Jochumsen et al. [336] showed that the detection of MRCPs is not trainable, even over months. This would constitute a disadvantage compared to oscillation-based BCIs, and that performance improvements can only be achieved with better signal recording, processing and decoding, and more natural training paradigms, but not with user training. A further performance limitation is the slow control rate achievable with LFTD signals. For an effective continuous control of an end effector, the user must be able to quickly compensate decoding errors or react to sudden changes in the environment. However, LFTD signals are per definition low-frequency signals and therefore cannot change quickly. Thus, it is not possible to promptly generate control commands, especially not at control rates around 10 Hz, which have proven to be advantageous [337].

Reliability The brain signals underlying LFTD signals are potentially MRCPs. While MRCPs provide substantial movement information for non-invasive BCIs, they are also susceptible to various behavioral influences. For example, level of intention, exerted force, movement speed, movement complexity, internal or external target selection are all factors that influence MRCPs [115], and this poses a serious challenge to a movement decoder. A movement decoder will need to reliably predict the movement even when the MRCPs vary in response to movement class-unrelated behavior. Furthermore, if the decoder should support many MRCPs variations, the MRCPs variations may eventually overlap between classes and prevent a successful movement discrimination. This is an inherent problem of MRCPs and not yet solved.

Recording Technique EEG provides excellent time-resolution. Furthermore, it allows the safe and easy recording of brain signals from many brain regions simultaneously. However, EEG is limited by two main factors: a low signal-to-noise ratio and the limited

information encoded in macroscale brain signals. The low signal-to-noise ratio impedes a reliable detection and discrimination of MRCPs. Whether this can be overcome with better signal processing and classification techniques has to be seen. The latter limitation is, however, more severe: if macroscale signals like EEG contain the necessary movement information required for an online trajectory decoder, with a performance comparable to invasive studies, is uncertain. The intuitiveness and naturalness of the control commands possible with EEG and the controllable degrees-of-freedom are limited in comparison to invasive recording techniques – at least from today's perspective.

3.7 Summary and Conclusion

This PhD thesis researched continuous and discrete movements and their non-invasive decoding from brain signals with EEG. Several outcomes have been generated. Most remarkably, this thesis showed that EEG signals encode movement information of continuous and discrete upper limb movements in low-frequency EEG signals. Furthermore, these EEG signals encode movement information even when no afferent signals are sent to the brain due to a lesion in the spinal cord. Attempted movements have proven in that case as a suitable mental control strategy. Moreover, this thesis localized the sources of movement encoding signals on motor-related brain areas, demonstrating the validity of the results. Eventually, a proof-of-concept how to decode attempted discrete movements online from the EEG of a person with complete SCI has been introduced and demonstrated. Thus, this thesis has shown that EEG signals of persons with SCI encode information of various movements of the upper limb. If the decoding performance can be improved, particularly attempted discrete movements could one day be used to intuitively control motor prostheses or robotic arms with a non-invasive BCI.

3.8 Outlook

Training Paradigm It is expected that future research focuses on the development of better training paradigms. A training paradigm should evoke MRCPs similar to real-life conditions so that the classifier can be trained with valid data. This is probably only possible when the BCI user is not forced into a strict set of rules on how and when to attempt movements (c.f. section 3.3). More realistic training paradigms could be implemented by using unsupervised decoding methods [315, 316] which do not require a strict paradigm. They could allow the BCI user to attempt movements in a more natural setting. Furthermore, the influence of goal-directed vs. non-goal-directed movements [338] needs to be further studied in the context of movement decoding, e.g., closing the hand to grasp a bottle vs. closing the hand without an object. Thus, more realistic MRCPs could be provided by suitable training paradigms which employ goal-directed movements as in the prospective usage scenarios for motor neuroprostheses or robotic arms.

Theoretical LFTD Framework A weak point in the current EEG-based movement decoding research is the lack of a comprehensive theoretical framework of how *movement-related* LFTD signals are generated. Although correlations with kinematic movement parameters (e.g., position or velocity) were found in the EEG, this does not imply that the EEG LFTD signals encode these kinematic parameters intrinsically. LFTD EEG signals could, for example, encode kinetic parameters like muscle activation correlating with the before mentioned movement parameters [339]. The kinematic parameter encoding would be in that view the result of biomechanics. However, the decoding of, e.g., the velocity, would then be suboptimal if it does not have a perfect correlation with the intrinsically encoded movement parameter. In case the brain indeed intrinsically encodes kinematic movement parameters, they have to be encoded in some brain coordinate system. For a successful movement decoding, this brain coordinate system needs to be transformed into the world coordinate system used to represent the decoded movements. A linear decoder can only perform affine transformations of the brain coordinate system, which could result in the loss of movement information. Also, the center of the brain coordinate system needs to be determined. Yoshimura et al. [340] and Tanaka et al. [261] indicate that the EEG encodes both intrinsic and extrinsic coordinate systems. A theoretical framework explaining the genesis of LFTD signals, the parameter encoding, or the brain's coordinate system, could help to develop better decoding models based on EEG signals.

Artificial Neural Networks Some of the issues mentioned earlier, like the transformation of the brain coordinate system, the decoding of appropriate movement parameters, or the sensitivity of MRCPs to behavioral and environmental influences, could be overcome with a classifier featuring a non-linear decoding model while retaining good generalization properties. A promising candidate for such a decoder would be an ANN. An ANN could provide the required non-linearity to transform brain coordinates to world coordinates. Furthermore, the ANN could learn a model of the spinal cord and the musculoskeletal system, which may allow the decoding of kinematic parameters even when the EEG encodes intrinsically kinetic parameters. The ANN could then decode the kinetic parameters and transform them via the learned model of the spinal cord and the musculoskeletal system into kinematic parameters.

One type of ANNs, recurrent neural networks, are particularly suitable for time sequences like MRCPs. Special network elements like long short-term memory (LSTM) blocks [341], help to avoid the typical training problem of recurrent neural networks (i.e., vanishing gradient). ANNs can also easily exploit other frequency bands and apply the proper feature extraction inherently in the network. Particularly, the high-gamma band is a rich source of movement information [107, 109, 218, 241, 243, 244, 274, 306] which, however, could not yet be successfully exploited on a single-trial basis with EEG signals. Thus, recurrent neural networks could turn out as an all-in-one solution to decode movement parameters from EEG. However, even LSTM-based recurrent neural networks require much more training samples as are usually recorded. Before exploring this approach, one needs to first come up with a solution on how to increase the number

of training samples by one or two orders. Also, clever training algorithms based on transfer learning may help. It is thinkable that the whole BCI community makes an effort to record and share data from thousands of study participants, and that general artificial neural network models are build which are then adapted to the individual user using relatively few training samples. This approach is common in, e.g., object recognition tasks where pre-trained models are publicly available. Only the last layers of this pre-trained models are then retrained for the specific application [342].

Other Approaches An inherent problem of MRCPs is the strong sensitivity to behavioral or environmental influences (e.g., movement speed, cue representation, internal or external target selection [115]). A classifier would have to learn all the different possible MRCPs associated with a movement, which could be difficult to realize. However, also the classification performance will suffer because the intra-class variances will necessarily increase, leading to a stronger class overlap and more false classifications. This can only be overcome if movement information can be decoded from the brain – probably in early potentials of the MRCPs – which is invariant to these influences, like movement goals [338] or movement targets [7]. A complementary approach is to learn the voluntary modulation of brain signals like slow-cortical potentials [59] or oscillations [198, 199], and use them as control signals. This approach does not suffer from a strong sensitivity to environmental influences. Future research could try to combine movement decoding and voluntarily modulation of brain signals to build intuitive and reliable BCIs.

Another possibility to increase the BCI performance is to stimulate the brain areas encoding movement information. Transcranial direct current stimulation (tDCS) can enhance the modulation of brain oscillations by the user [33]. If a similar effect can be found with movement-related LFTD EEG signals, it may boost the decoding performance.

As the decodable movement information from the EEG is rather low, clever designed shared-control mechanisms for robotic arms or motor neuroprostheses need to be developed as a remedy. Shared control systems are context-aware and include the state of the environment and the control device in the control signal generation [343]. Initial simple approaches have already been demonstrated, e.g., Rohm et al. [191]. A sophisticated shared-control system could continuously scan the environment of the BCI user for interact-able objects, and infer the desired movement from the object and from residual movements (e.g., looking at a water glass or bringing the hand close to the water glass). A robotic arm could then execute the movement. A BCI could provide for such a sophisticated shared-control system a high-level control signal. This control signal could be used, for example, as a start signal for the movement or for target selection.

Bibliography

1. Ofner, P. & Müller-Putz, G. R. *Decoding of Velocities and Positions of 3D Arm Movement from EEG* in *2012 34th Annual International Conference of the IEEE Engineering in Medicine and Biology Society* (IEEE, 2012), 6406–6409.
2. Ofner, P. & Müller-Putz, G. R. Using a Noninvasive Decoding Method to Classify Rhythmic Movement Imaginations of the Arm in Two Planes. *IEEE Transactions on Biomedical Engineering* **62,** 972–981 (2015).
3. Ofner, P., Schwarz, A., Pereira, J. & Müller-Putz, G. R. Upper Limb Movements Can Be Decoded from the Time-domain of Low-frequency EEG. *PLoS ONE* **12,** e0182578 (2017).
4. Ofner, P. *et al.* Attempted Arm and Hand Movements Can Be Decoded from Low-frequency EEG from Persons with Spinal Cord Injury. *Scientific Reports* **9,** 7134 (2019).
5. Ofner, P., Pereira, J. & Müller-Putz, G. R. *Decoding of Executed Movements and Source Imaging* in *Proceedings of the 6th International Brain-Computer Interface Conference 2014* (Graz University of Technology Publishing House, 2014), 026-1–026-4. ISBN: 978-3-85125-378-8.
6. Ofner, P. & Müller-Putz, G. R. *Time-domain Correlations of Imagined Arm Positions with Brain Sources* in *Proceedings of the BMT 2013* (Walter de Gruyter GmbH, 2013).
7. Ofner, P. & Müller-Putz, G. R. *Movement Target Decoding from EEG and the Corresponding Discriminative Sources: A Preliminary Study* in *2015 37th Annual International Conference of the IEEE Engineering in Medicine and Biology Society* (IEEE, 2015), 1468–1471.
8. Ofner, P., Kersch, P. & Müller-Putz, G. R. *Visual Input Affects the Decoding of Imagined Movements of the Same Limb* in *Proceedings of the 7th Graz Brain-Computer Interface Conference 2017* (Graz University of Technology Publishing House, 2017), 367–372.
9. Ferriman, A. BMJ Readers Choose The" Sanitary Revolution" As Greatest Medical Advance since 1840. *British Medical Journal* **334,** 111 (2007).
10. Singh, A., Tetreault, L., Kalsi-Ryan, S., Nouri, A. & Fehlings, M. G. Global Prevalence and Incidence of Traumatic Spinal Cord Injury. *Clinical Epidemiology* **6,** 309–331 (2014).

11. Van den Berg, M. E. L., Castellote, J. M., Mahillo-Fernandez, I. & de Pedro-Cuesta, J. Incidence of Spinal Cord Injury Worldwide: A Systematic Review. *Neuroepidemiology* **34,** 184–92 (3 2010).

12. Sekhon, L. H. & Fehlings, M. G. Epidemiology, Demographics, and Pathophysiology of Acute Spinal Cord Injury. *Spine* **26,** 2–12 (24 Suppl 2001).

13. Anderson, K. D. Targeting Recovery: Priorities of the Spinal Cord-injured Population. *Journal of Neurotrauma* **21,** 1371–1383 (10 2004).

14. Snoek, G. J., IJzerman, M. J., Hermens, H. J., Maxwell, D. & Biering-Sorensen, F. Survey of the Needs of Patients with Spinal Cord Injury: Impact and Priority for Improvement in Hand Function in Tetraplegics. *Spinal Cord* **42,** 526–532 (9 2004).

15. Collinger, J. L. *et al.* Functional Priorities, Assistive Technology, and Brain-Computer Interfaces After Spinal Cord Injury. *Journal of Rehabilitation Research and Development* **50,** 145–160 (2 2013).

16. Johnstone, B. R., Jordan, C. J. & Buntine, J. A. A Review of Surgical Rehabilitation of the Upper Limb in Quadriplegia. *Paraplegia* **26,** 317–339 (5 1988).

17. Keith, M. W. & Peljovich, A. Surgical Treatments to Restore Function Control in Spinal Cord Injury. *Handbook of Clinical Neurology* **109,** 167–179 (2012).

18. Kilgore, K. L., Peckham, P. H., Thrope, G. B., Keith, M. W. & Gallaher-Stone, K. A. Synthesis of Hand Grasp Using Functional Neuromuscular Stimulation. *IEEE Transactions on Biomedical Engineering* **36,** 761–770 (1989).

19. Rupp, R. & Gerner, H. J. Neuroprosthetics of the Upper Extremity–clinical Application in Spinal Cord Injury and Challenges for the Future. *Acta Neurochirurgica. Supplement* **97,** 419–426 (Pt 1 2007).

20. Rupp, R., Rohm, M., Schneiders, M., Kreilinger, A. & Müller-Putz, G. R. Functional Rehabilitation of the Paralyzed Upper Extremity After Spinal Cord Injury by Noninvasive Hybrid Neuroprostheses. *Proceedings of the IEEE* **103,** 954–968 (2015).

21. Mulcahey, M. J., Smith, B. T. & Betz, R. R. Evaluation of the Lower Motor Neuron Integrity of Upper Extremity Muscles in High Level Spinal Cord Injury. *Spinal Cord* **37,** 585–591 (8 1999).

22. Dietz, V. & Curt, A. Neurological Aspects of Spinal-cord Repair: Promises and Challenges. *The Lancet. Neurology* **5,** 688–694 (8 2006).

23. Tuga, M. R., Rupp, R., Liebetanz, D., Mikut, R. & Reischl, M. Concept of a Co-adaptive Training Environment for Human-machine Interfaces Based on EMG-control. *Biomedizinische Technik. Biomedical Engineering* **58 Suppl 1** (2013).

24. Merletti, R., Parker, P. A. & Parker, P. J. *Electromyography: Physiology, Engineering, and Non-invasive Applications* (John Wiley & Sons, 2004).

25. Huo, X. & Ghovanloo, M. Evaluation of a Wireless Wearable Tongue-computer Interface by Individuals with High-level Spinal Cord Injuries. *Journal of Neural Engineering* **7,** 26008 (2 2010).

26. Nathan, R. H. & Ohry, A. Upper Limb Functions Regained in Quadriplegia: A Hybrid Computerized Neuromuscular Stimulation System. *Archives of Physical Medicine and Rehabilitation* **71,** 415–421 (6 1990).

27. Kilgore, K. L. *et al.* An Implanted Upper-extremity Neuroprosthesis Using Myoelectric Control. *The Journal of Hand Surgery* **33,** 539–550 (4 2008).

28. Pfurtscheller, G., Müller, G. R., Pfurtscheller, J., Gerner, H. J. & Rupp, R. 'thought'–control of Functional Electrical Stimulation to Restore Hand Grasp in a Patient with Tetraplegia. *Neuroscience Letters* **351,** 33–36 (1 2003).

29. Warren, D. J. *et al.* Recording and Decoding for Neural Prostheses. *Proceedings of the IEEE* **104,** 374–391 (2016).

30. Vidal, J. J. Toward Direct Brain-Computer Communication. *Annual Review of Biophysics and Bioengineering* **2,** 157–180 (1973).

31. Wolpaw, J. R., Birbaumer, N., McFarlan, D., Pfurtscheller, G. & Vaughan, T. M. Brain–Computer Interfaces for Communication and Control. *Clinical Neurophysiology* **113,** 767–91 (2002).

32. Millán, J. D. R. *et al.* Combining Brain-Computer Interfaces and Assistive Technologies: State-of-the-art and Challenges. *Frontiers in Neuroscience* **4** (2010).

33. He, B., Baxter, B., Edelman, B. J., Cline, C. C. & Ye, W. W. Noninvasive Brain-Computer Interfaces Based on Sensorimotor Rhythms. *Proceedings of the IEEE* **103,** 907–925 (2015).

34. Chaudhary, U., Birbaumer, N. & Ramos-Murguialday, A. Brain-Computer Interfaces for Communication and Rehabilitation. *Nature Reviews Neurology* **12,** 513–525 (9 2016).

35. Pfurtscheller, G., Guger, C., Müller, G., Krausz, G. & Neuper, C. Brain Oscillations Control Hand Orthosis in a Tetraplegic. *Neuroscience Letters* **292,** 211–214 (3 2000).

36. Müller-Putz, G. R., Scherer, R., Pfurtscheller, G. & Rupp, R. EEG-based Neuroprosthesis Control: A Step Towards Clinical Practice. *Neuroscience Letters* **382,** 169–174 (1-2 2005).

37. Kandel, E. R., Schwartz, J. H., Jessell, T. M., Siegelbaum, S. A. & Hudspeth, A. J. *Principles of Neural Science* 1760 pp. ISBN: 0071390111 (McGraw-Hill Education Ltd, 2012).

38. Wolpaw, J. R. & Wolpaw, E. W. *Brain–Computer Interfaces: Principles and Practice* 3–12 (Oxford University Press New York, USA, 2012).

39. Stark, E. & Abeles, M. Predicting Movement from Multiunit Activity. *Journal of Neuroscience* **27,** 8387–8394 (31 2007).

40. Brown, E. N., Kass, R. E. & Mitra, P. P. Multiple Neural Spike Train Data Analysis: State-of-the-art and Future Challenges. *Nature Neuroscience* **7,** 456–461 (5 2004).

41. Nunez, P. L., Nunez, M. D. & Srinivasan, R. Multi-scale Neural Sources of EEG: Genuine, Equivalent, and Representative. a Tutorial Review. *Brain Topography* **32,** 193–214 (2019).

42. Edlinger, G., Wach, P. & Pfurtscheller, G. On the Realization of an Analytic High-resolution EEG. *IEEE Transactions on Biomedical Engineering* **45,** 736–745 (1998).

43. Ramoser, H., Muller-Gerking, J. & Pfurtscheller, G. Optimal Spatial Filtering of Single Trial Eeg during Imagined Hand Movement. *IEEE Transactions on Rehabilitation Engineering* **8,** 441–446 (2000).

44. Grosse-Wentrup, M., Liefhold, C., Gramann, K. & Buss, M. Beamforming in Noninvasive Brain–computer Interfaces. *IEEE Transactions on Biomedical Engineering* **56,** 1209–1219 (2009).

45. Michel, C. M. & Murray, M. M. Towards the Utilization of EEG As a Brain Imaging Tool. *NeuroImage* **61,** 371–385 (2012).

46. Edelman, B. J., Baxter, B. & He, B. EEG Source Imaging Enhances the Decoding of Complex Right-hand Motor Imagery Tasks. *IEEE Transactions on Biomedical Engineering* **63,** 4–14 (1 2016).

47. Schomer, D. L. & Da Silva, F. L. *Niedermeyer's Electroencephalography: Basic Principles, Clinical Applications, and Related Fields* (Lippincott Williams & Wilkins, 2012).

48. Buzsáki, G., Anastassiou, C. A. & Koch, C. The Origin of Extracellular Fields and Currents — EEG, ECoG, LFP and Spikes. *Nature Reviews Neuroscience* **13,** 407–420 (2012).

49. Einevoll, G. T., Kayser, C., Logothetis, N. K. & Panzeri, S. Modelling and Analysis of Local Field Potentials for Studying the Function of Cortical Circuits. *Nature Reviews Neuroscience* **14,** 770–785 (2013).

50. Williamson, S. J., Lü, Z.-L., Karron, D. & Kaufman, L. Advantages and Limitations of Magnetic Source Imaging. *Brain Topography* **4,** 169–180 (1991).

51. Nunez, P. L., Srinivasan, R., *et al. Electric Fields of the Brain: The Neurophysics of EEG* (Oxford University Press, USA, 2006).

52. Ogawa, S., Lee, T.-M., Kay, A. R. & Tank, D. W. Brain Magnetic Resonance Imaging with Contrast Dependent on Blood Oxygenation. *Proceedings of the National Academy of Sciences of the United States of America* **87,** 9868–9872 (1990).

53. Menon, R. S., Gati, J. S., Goodyear, B. G., Luknowsky, D. C. & Thomas, C. G. Spatial and Temporal Resolution of Functional Magnetic Resonance Imaging. *Biochemistry and Cell Biology* **76,** 560–571 (1998).

54. Kemper, V. G., Martino, F. D., Emmerling, T. C., Yacoub, E. & Goebel, R. High Resolution Data Analysis Strategies for Mesoscale Human Functional MRI at 7 and 9.4 T. *NeuroImage* **164,** 48–58 (2018).

55. Logothetis, N. K., Pauls, J., Augath, M., Trinath, T. & Oeltermann, A. Neurophysiological Investigation of the Basis of the fMRI Signal. *Nature* **412,** 150 (2001).

56. Ferrari, M. & Quaresima, V. A Brief Review on the History of Human Functional Near-infrared Spectroscopy (fNIRS) Development and Fields of Application. *NeuroImage* **63,** 921–935 (2012).

57. Pfurtscheller, G. *et al.* The Hybrid BCI. *Frontiers in Neuroscience* **4,** 30 (2010).

58. Zander, T. O. & Kothe, C. Towards Passive Brain-Computer Interfaces: Applying Brain-Computer Interface Technology to Human-machine Systems in General. *Journal of Neural Engineering* **8,** 025005 (2 2011).

59. Birbaumer, N. *et al.* A Spelling Device for the Paralysed. *Nature* **398,** 297–298 (6725 1999).

60. Nijboer, F. *et al.* A P300-based Brain–computer Interface for People with Amyotrophic Lateral Sclerosis. *Clinical Neurophysiology* **119,** 1909–1916 (2008).

61. Sellers, E. W., Vaughan, T. M. & Wolpaw, J. R. A Brain-Computer Interface for Long-term Independent Home Use. *Amyotrophic Lateral Sclerosis* **11,** 449–455 (2010).

62. Vansteensel, M. J. *et al.* Fully Implanted Brain–computer Interface in a Locked-in Patient with ALS. *New England Journal of Medicine* **375,** 2060–2066 (2016).

63. Pokorny, C. *et al.* The Auditory P300-based Single-switch Brain–computer Interface: Paradigm Transition from Healthy Subjects to Minimally Conscious Patients. *Artificial Intelligence in Medicine* **59,** 81–90 (2013).

64. Carlson, T. & del R. Millán, J. Brain-controlled Wheelchairs: A Robotic Architecture. *IEEE Robotics & Automation Magazine* **20,** 65–73 (2013).

65. Fernández-Rodríguez, Á., Velasco-Álvarez, F. & Ron-Angevin, R. Review of Real Brain-controlled Wheelchairs. *Journal of Neural Engineering* **13,** 061001 (6 2016).

66. Bensch, M. *et al.* Nessi: An EEG-controlled Web Browser for Severely Paralyzed Patients. *Computational Intelligence and Neuroscience,* 71863 (2007).

67. Halder, S. *et al.* Brain-controlled Applications Using Dynamic P300 Speller Matrices. *Artificial Intelligence in Medicine* **63,** 7–17 (2015).

68. Martinez-Cagigal, V., Gomez-Pilar, J., Alvarez, D. & Hornero, R. An Asynchronous P300-based Brain-Computer Interface Web Browser for Severely Disabled People. *IEEE Transactions on Neural Systems and Rehabilitation Engineering* **25,** 1332–1342 (8 2017).

69. Münßinger, J. I. *et al.* Brain Painting: First Evaluation of a New Brain-Computer Interface Application with ALS-patients and Healthy Volunteers. *Frontiers in Neuroscience* **4,** 182 (2010).

70. Botrel, L., Holz, E. M. & Kübler, A. Brain Painting V2: Evaluation of P300-based Brain-Computer Interface for Creative Expression by an End-user Following the User-centered Design. *Brain-Computer Interfaces* **2,** 135–149 (2015).

71. Pinegger, A., Hiebel, H., Wriessnegger, S. C. & Müller-Putz, G. R. Composing Only by Thought: Novel Application of the P300 Brain-Computer Interface. *PLoS ONE* **12,** e0181584 (2017).

72. Krepki, R., Blankertz, B., Curio, G. & Müller, K.-R. The Berlin Brain-Computer Interface (BBCI) – Towards a New Communication Channel for Online Control in Gaming Applications. *Multimedia Tools and Applications* **33,** 73–90 (2007).

73. Finke, A., Lenhardt, A. & Ritter, H. The Mindgame: A P300-based Brain-Computer Interface Game. *Neural Networks* **22,** 1329–1333 (9 2009).

74. Daly, J. J. & Wolpaw, J. R. Brain-Computer Interfaces in Neurological Rehabilitation. *The Lancet. Neurology* **7,** 1032–1043 (11 2008).

75. Wang, W. *et al.* Neural Interface Technology for Rehabilitation: Exploiting and Promoting Neuroplasticity. *Physical Medicine and Rehabilitation Clinics of North America* **21,** 157–178 (1 2010).

76. Pichiorri, F. *et al.* Brain-Computer Interface Boosts Motor Imagery Practice during Stroke Recovery. *Annals of Neurology* **77,** 851–865 (2015).

77. Biasiucci, A. *et al.* Brain-actuated Functional Electrical Stimulation Elicits Lasting Arm Motor Recovery After Stroke. *Nature Communications* **9** (2018).

78. Ramos-Murguialday, A. *et al.* Brain-machine Interface in Chronic Stroke Rehabilitation: A Controlled Study. *Annals of Neurology* **74,** 100–108 (2013).

79. Mrachacz-Kersting, N., Kristensen, S. R., Niazi, I. K. & Farina, D. Precise Temporal Association between Cortical Potentials Evoked by Motor Imagination and Afference Induces Cortical Plasticity. *The Journal of Physiology* **590,** 1669–1682 (2012).

80. Evarts, E. V. Pyramidal Tract Activity Associated with a Conditioned Hand Movement in the Monkey. *Journal of Neurophysiology* **29,** 1011–1027 (1966).

81. Mountcastle, V. B., Lynch, J. C., Georgopoulos, A., Sakata, H. & Acuna, C. Posterior Parietal Association Cortex of the Monkey: Command Functions for Operations within Extrapersonal Space. *Journal of Neurophysiology* **38,** 871–908 (1975).

82. Georgopoulos, A. P., Schwartz, A. B. & Kettner, R. E. Neuronal Population Coding of Movement Direction. *Science* **233,** 1416–1419 (4771 1986).

83. Branco, M. P., de Boer, L. M., Ramsey, N. F. & Vansteensel, M. J. Encoding of Kinetic and Kinematic Movement Parameters in the Sensorimotor Cortex: A Brain-Computer Interface Perspective. *European Journal of Neuroscience* (2019).

84. Georgopoulos, A. P., Kalaska, J. F., Caminiti, R. & Massey, J. T. On the Relations between the Direction of Two-dimensional Arm Movements and Cell Discharge in Primate Motor Cortex. *Journal of Neuroscience* **2,** 1527–1537 (11 1982).

85. Wise, S. P., Weinrich, M. & Mauritz, K. H. Motor Aspects of Cue-related Neuronal Activity in Premotor Cortex of the Rhesus Monkey. *Brain Research* **260,** 301–305 (2 1983).

86. Alexander, G. E. & Crutcher, M. D. Preparation for Movement: Neural Representations of Intended Direction in Three Motor Areas of the Monkey. *Journal of Neurophysiology* **64,** 133–150 (1 1990).

87. Aflalo, T. *et al.* Neurophysiology. Decoding Motor Imagery from the Posterior Parietal Cortex of a Tetraplegic Human. *Science* **348,** 906–910 (6237 2015).

88. Snyder, L. H., Batista, A. P. & Andersen, R. A. Intention-related Activity in the Posterior Parietal Cortex: A Review. *Vision Research* **40,** 1433–1441 (10-12 2000).

89. Kreiman, G., Koch, C. & Fried, I. Imagery Neurons in the Human Brain. *Nature* **408,** 357–361 (6810 2000).

90. Fetz, E. E. Operant Conditioning of Cortical Unit Activity. *Science* **163,** 955–958 (3870 1969).

91. Fetz, E. E. & Finocchio, D. V. Correlations between Activity of Motor Cortex Cells and Arm Muscles during Operantly Conditioned Response Patterns. *Experimental Brain Research* **23,** 217–240 (3 1975).

92. Taylor, D. M., Tillery, S. I. H. & Schwartz, A. B. Direct Cortical Control of 3D Neuroprosthetic Devices. *Science* **296,** 1829–1832 (5574 2002).

93. Carmena, J. M. *et al.* Learning to Control a Brain-machine Interface for Reaching and Grasping by Primates. *PLoS Biology* **1,** E42 (2 2003).

94. Lebedev, M. A. *et al.* Cortical Ensemble Adaptation to Represent Velocity of an Artificial Actuator Controlled by a Brain-machine Interface. *Journal of Neuroscience* **25,** 4681–4693 (19 2005).

95. Fetz, E. E. Volitional Control of Neural Activity: Implications for Brain-Computer Interfaces. *The Journal of Physiology* **579,** 571–579 (Pt 3 2007).

96. Buzsáki, G. *Rhythms of the Brain* 464 pp. ISBN: 0199828237 (OUP USA, 2011).

97. Berger, H. Über das Elektrenkephalogramm des Menschen. *Archiv Für Psychiatrie* **87,** 527–570 (1927).

98. Chatrian, G. E., Petersen, M. C. & Lazarte, J. A. The Blocking of the Rolandic Wicket Rhythm and Some Central Changes Related to Movement. *Electroencephalography and Clinical Neurophysiology* **11,** 497–510 (1959).

99. Pfurtscheller, G. & Neuper, C. Motor Imagery Activates Primary Sensorimotor Area in Humans. *Neuroscience Letters* **239,** 65–68 (2-3 1997).

100. Pfurtscheller, G. & Aranibar, A. Event-related Cortical Desynchronization Detected by Power Measurements of Scalp EEG. *Electroencephalography and Clinical Neurophysiology* **42,** 817–826 (6 1977).

101. Friedrich, E. V. C., Neuper, C. & Scherer, R. Whatever Works: A Systematic User-centered Training Protocol to Optimize Brain-Computer Interfacing Individually. *PLoS ONE* **8,** e76214 (9 2013).

102. Pfurtscheller, G. & Lopes da Silva, F. H. Event-related Eeg/meg Synchronization and Desynchronization: Basic Principles. *Clinical Neurophysiology* **110,** 1842–1857 (11 1999).

103. Myrden, A. & Chau, T. A Passive EEG-BCI for Single-Trial Detection of Changes in Mental State. *IEEE Transactions on Neural Systems and Rehabilitation Engineering* **25,** 345–356 (2017).

104. Walter, C., Rosenstiel, W., Bogdan, M., Gerjets, P. & Spüler, M. Online EEG-based Workload Adaptation of an Arithmetic Learning Environment. *Frontiers in Human Neuroscience* **11** (2017).

105. Rickert, J. *et al.* Encoding of Movement Direction in Different Frequency Ranges of Motor Cortical Local Field Potentials. *Journal of Neuroscience* **25,** 8815–8824 (39 2005).

106. Zhuang, J., Truccolo, W., Vargas-Irwin, C. & Donoghue, J. P. Decoding 3-D Reach and Grasp Kinematics from High-frequency Local Field Potentials in Primate Primary Motor Cortex. *IEEE Transactions on Biomedical Engineering* **57,** 1774–1784 (7 2010).

107. Flint, R. D., Ethier, C., Oby, E. R., Miller, L. E. & Slutzky, M. W. Local Field Potentials Allow Accurate Decoding of Muscle Activity. *Journal of Neurophysiology* **108,** 18–24 (2012).

108. Scherberger, H., Jarvis, M. R. & Andersen, R. A. Cortical Local Field Potential Encodes Movement Intentions in the Posterior Parietal Cortex. *Neuron* **46,** 347–354 (2 2005).

109. Milekovic, T., Truccolo, W., Grün, S., Riehle, A. & Brochier, T. Local Field Potentials in Primate Motor Cortex Encode Grasp Kinetic Parameters. *Neuroimage* **114,** 338–355 (2015).

110. Leuthardt, E. C., Schalk, G., Wolpaw, J. R., Ojemann, J. G. & Moran, D. W. A Brain–Computer Interface Using Electrocorticographic Signals in Humans. *Journal of Neural Engineering* **1,** 63–71 (2004).

111. Yanagisawa, T. *et al.* Electrocorticographic Control of a Prosthetic Arm in Paralyzed Patients. *Annals of Neurology* **71,** 353–361 (2011).

112. Birbaumer, N. Slow Cortical Potentials: Plasticity, Operant Control, and Behavioral Effects. *The Neuroscientist* **5,** 74–78 (1999).

113. Birbaumer, N., Hinterberger, T., Kubler, A. & Neumann, N. The Thought-translation Device (TTD): Neurobehavioral Mechanisms and Clinical Outcome. *IEEE Transactions on Neural Systems and Rehabilitation Engineering* **11,** 120–123 (2003).

114. Kornhuber, H. H. & Deecke, L. *Hirnpotentialänderungen Beim Menschen Vor Und Nach Willkürbewegungen Dargestellt Mit Magnetbandspeicherung Und Rückwartsanalyse* in *Pflugers Archiv-European Journal of Physiology* **281** (1964), 52.

115. Shibasaki, H. & Hallett, M. What Is the Bereitschaftspotential? *Clinical Neurophysiology* **117,** 2341–2356 (2006).

116. Niazi, I. K., Mrachacz-Kersting, N., Jiang, N., Dremstrup, K. & Farina, D. Peripheral Electrical Stimulation Triggered by Self-paced Detection of Motor Intention Enhances Motor Evoked Potentials. *IEEE Transactions on Neural Systems and Rehabilitation Engineering* **20,** 595–604 (2012).

117. Sburlea, A. I. *et al.* Detecting Intention to Walk in Stroke Patients from Premovement EEG Correlates. *Journal of NeuroEngineering and Rehabilitation* **12** (2015).

118. Liu, D. *et al.* EEG-based Lower-limb Movement Onset Decoding: Continuous Classification and Asynchronous Detection. *IEEE Transactions on Neural Systems and Rehabilitation Engineering* **26,** 1626–1635 (2018).

119. Müller-Putz, G. R., Scherer, R., Neuper, C. & Pfurtscheller, G. Steady-state Somatosensory Evoked Potentials: Suitable Brain Signals for Brain–computer Interfaces? *IEEE Transactions on Neural Systems and Rehabilitation Engineering* **14,** 30–37 (2006).

120. Breitwieser, C., Pokorny, C. & Müller-Putz, G. R. A Hybrid Three-class Brain–computer Interface System Utilizing SSSEPs and Transient ERPs. *Journal of Neural Engineering* **13,** 066015 (2016).

121. Pokorny, C., Breitwieser, C. & Müller-Putz, G. R. The Role of Transient Target Stimuli in a Steady-state Somatosensory Evoked Potential-based Brain–computer Interface Setup. *Frontiers in Neuroscience* **10** (2016).

122. Abiri, R., Borhani, S., Sellers, E. W., Jiang, Y. & Zhao, X. A Comprehensive Review of EEG-based Brain–Computer Interface Paradigms. *Journal of Neural Engineering* **16,** 011001 (2019).

123. Regan, D. Comparison of Transient and Steady-state Methods. *Annals of the New York Academy of Sciences* **388,** 45–71 (1982).

124. Herrmann, C. S. Human EEG Responses to 1-100 Hz Flicker: Resonance Phenomena in Visual Cortex and Their Potential Correlation to Cognitive Phenomena. *Experimental Brain Research* **137,** 346–353 (2001).

125. Middendorf, M., McMillan, G., Calhoun, G. & Jones, K. S. Brain-Computer Interfaces Based on the Steady-state Visual-evoked Response. *IEEE Transactions on Rehabilitation Engineering* **8,** 211–214 (2000).

126. Zhu, D., Bieger, J., Molina, G. G. & Aarts, R. M. A Survey of Stimulation Methods Used in SSVEP-based BCIs. *Computational Intelligence and Neuroscience* **2010,** 1–12 (2010).

127. Sutton, S., Tueting, P., Zubin, J. & John, E. R. Information Delivery and the Sensory Evoked Potential. *Science* **155,** 1436–1439 (3768 1967).

128. Polich, J. Updating P300: An Integrative Theory of P3a and P3b. *Clinical Neurophysiology* **118,** 2128–2148 (2007).

129. Donchin, E. & Coles, M. G. H. Is the P300 Component a Manifestation of Context Updating? *Behavioral and Brain Sciences* **11,** 357 (1988).

130. Farwell, L. A. & Donchin, E. Talking off the Top of Your Head: Toward a Mental Prosthesis Utilizing Event-related Brain Potentials. *Electroencephalography and Clinical Neurophysiology* **70,** 510–523 (6 1988).

131. Fazel-Rezai, R. *et al.* P300 Brain Computer Interface: Current Challenges and Emerging Trends. *Frontiers in Neuroengineering* **5,** 14 (2012).

132. Brouwer, A.-M. & van Erp, J. B. F. A Tactile P300 Brain-Computer Interface. *Frontiers in Neuroscience* **4,** 19 (2010).

133. Kübler, A. *et al.* A Brain-Computer Interface Controlled Auditory Event-related Potential (P300) Spelling System for Locked-in Patients. *Annals of the New York Academy of Sciences* **1157,** 90–100 (2009).

134. Schalk, G., Wolpaw, J. R., McFarland, D. J. & Pfurtscheller, G. EEG-based Communication: Presence of an Error Potential. *Clinical Neurophysiology* **111,** 2138–2144 (2000).

135. Kreilinger, A., Neuper, C. & Müller-Putz, G. R. Error Potential Detection during Continuous Movement of an Artificial Arm Controlled by Brain–computer Interface. *Medical & Biological Engineering & Computing* **50,** 223–230 (2012).

136. Chavarriaga, R., Sobolewski, A. & del R. Millán, J. Errare Machinale Est: The Use of Error-related Potentials in Brain-machine Interfaces. *Frontiers in Neuroscience* **8** (2014).

137. Dias, C. L., Sburlea, A. I. & Müller-Putz, G. R. Masked and Unmasked Error-related Potentials during Continuous Control and Feedback. *Journal of Neural Engineering* **15,** 036031 (2018).

138. Weiskopf, N. *et al.* Principles of a Brain-Computer Interface (BCI) Based on Real-time Functional Magnetic Resonance Imaging (fMRI). *IEEE Transactions on Biomedical Engineering* **51,** 966–970 (2004).

139. Birbaumer, N., Ruiz, S. & Sitaram, R. Learned Regulation of Brain Metabolism. *Trends in Cognitive Sciences* **17,** 295–302 (2013).

140. Yoo, S.-S. *et al.* Brain–computer Interface Using Fmri: Spatial Navigation by Thoughts. *Neuroreport* **15,** 1591–1595 (2004).

141. Bauernfeind, G., Leeb, R., Wriessnegger, S. C. & Pfurtscheller, G. Development, Set-up and First Results for a One-channel Near-infrared Spectroscopy System / Entwicklung, Aufbau Und Vorläufige Ergebnisse Eines Einkanal- Nahinfrarot-spektroskopie-systems. *Biomedizinische Technik/biomedical Engineering* **53,** 36–43 (2008).

142. Naseer, N. & Hong, K.-S. fNIRS-based Brain-Computer Interfaces: A Review. *Frontiers in Human Neuroscience* **9** (2015).

143. Mellinger, J. *et al.* An MEG-based Brain–Computer Interface (BCI). *NeuroImage* **36,** 581–593 (2007).

144. Lebedev, M. A. & Nicolelis, M. A. L. Brain-machine Interfaces: Past, Present and Future. *Trends in Neurosciences* **29,** 536–546 (9 2006).

145. Oostenveld, R. & Praamstra, P. The Five Percent Electrode System for High-resolution EEG and Erp Measurements. *Clinical Neurophysiology* **112,** 713–719 (4 2001).

146. Pinegger, A., Wriessnegger, S. C., Faller, J. & Müller-Putz, G. R. Evaluation of Different EEG Acquisition Systems Concerning Their Suitability for Building a Brain–computer Interface: Case Studies. *Frontiers in Neuroscience* **10,** 441 (2016).

147. Dannhauer, M., Lanfer, B., Wolters, C. H. & Knösche, T. R. Modeling of the Human Skull in EEG Source Analysis. *Human Brain Mapping* **32,** 1383–1399 (2010).

148. Hjorth, B. An On-line Transformation of EEG Scalp Potentials into Orthogonal Source Derivations. *Electroencephalography and Clinical Neurophysiology* **39,** 526–530 (1975).

149. McFarland, D. J., McCane, L. M., David, S. V. & Wolpaw, J. R. Spatial Filter Selection for EEG-based Communication. *Electroencephalography and Clinical Neurophysiology* **103,** 386–394 (3 1997).

150. Pearson, K. Liii. on Lines and Planes of Closest Fit to Systems of Points in Space. *The London, Edinburgh, and Dublin Philosophical Magazine and Journal of Science* **2,** 559–572 (11 1901).

151. Hotelling, H. Analysis of a Complex of Statistical Variables into Principal Components. *Journal of Educational Psychology* **24,** 417 (1933).

152. Makeig, S., Bell, A. J., Jung, T.-P. & Sejnowski, T. J. *Independent Component Analysis of Electroencephalographic Data* in *Advances in neural information processing systems* (1996), 145–151.

153. James, C. J. & Hesse, C. W. Independent Component Analysis for Biomedical Signals. *Physiological Measurement* **26,** R15–R39 (1 2005).

154. Blankertz, B., Tomioka, R., Lemm, S., Kawanabe, M. & Muller, K. Optimizing Spatial Filters for Robust EEG Single-Trial Analysis. *IEEE Signal Processing Magazine* **25,** 41–56 (2008).

155. Grosse-Wentrup, M. & Buss, M. Multiclass Common Spatial Patterns and Information Theoretic Feature Extraction. *IEEE Transactions on Biomedical Engineering* **55,** 1991–2000 (2008).

156. Michel, C. M. *et al.* EEG Source Imaging. *Clinical Neurophysiology* **115,** 2195–2222 (2004).

157. Oppenheim, A. V. & Schafer, R. W. *Discrete-time Signal Processing* 3rd Edition. ISBN: 978-0131988422 (Pearson, 2009).

158. Ang, K. K., Chin, Z. Y., Wang, C., Guan, C. & Zhang, H. Filter Bank Common Spatial Pattern Algorithm on BCI Competition IV Datasets 2a and 2b. *Frontiers in Neuroscience* **6,** 39 (2012).

159. Krusienski, D. J., McFarland, D. J. & Wolpaw, J. R. Value of Amplitude, Phase, and Coherence Features for a Sensorimotor Rhythm-based Brain-Computer Interface. *Brain Research Bulletin* **87,** 130–134 (1 2012).

160. Wei, Q., Wang, Y., Gao, X. & Gao, S. Amplitude and Phase Coupling Measures for Feature Extraction in an EEG-based Brain–Computer Interface. *Journal of Neural Engineering* **4,** 120–129 (2007).

161. Billinger, M., Brunner, C. & Müller-Putz, G. R. Single-Trial Connectivity Estimation for Classification of Motor Imagery Data. *Journal of Neural Engineering* **10,** 046006 (2013).

162. Bashashati, A., Fatourechi, M., Ward, R. K. & Birch, G. E. A Survey of Signal Processing Algorithms in Brain-Computer Interfaces Based on Electrical Brain Signals. *Journal of Neural Engineering* **4,** R32–R57 (2 2007).

163. Lotte, F., Congedo, M., Lécuyer, A., Lamarche, F. & Arnaldi, B. A Review of Classification Algorithms for EEG-based Brain-Computer Interfaces. *Journal of Neural Engineering* **4,** R1–R13 (2 2007).

164. Lotte, F. *et al.* A Review of Classification Algorithms for EEG-based Brain-Computer Interfaces: A 10 Year Update. *Journal of Neural Engineering* **15,** 031005 (3 2018).

165. Duda, R. O., Hart, P. E. & Stork, D. G. *Pattern Classification* ISBN: 0471056693 (Wiley John + Sons, 2000).

166. Blankertz, B., Lemm, S., Treder, M., Haufe, S. & Müller, K.-R. Single-Trial Analysis and Classification of Erp Components–a Tutorial. *Neuroimage* **56,** 814–825 (2 2011).

167. Schirrmeister, R. T. *et al.* Deep Learning with Convolutional Neural Networks for Eeg Decoding and Visualization. *Human Brain Mapping* **38,** 5391–5420 (11 2017).

168. LeCun, Y., Bengio, Y. & Hinton, G. Deep Learning. *Nature* **521,** 436–444 (2015).

169. Vidaurre, C., Schloogl, A., Cabeza, R., Scherer, R. & Pfurtscheller, G. A Fully On-line Adaptive BCI. *IEEE Transactions on Biomedical Engineering* **53,** 1214–1219 (2006).

170. Vidaurre, C., Sannelli, C., Müller, K.-R. & Blankertz, B. Co-adaptive Calibration to Improve BCI Efficiency. *Journal of Neural Engineering* **8,** 025009 (2011).

171. Faller, J. *et al.* A Co-adaptive Brain-Computer Interface for End Users with Severe Motor Impairment. *PLoS ONE* **9,** e101168 (2014).

172. Pan, S. J. & Yang, Q. A Survey on Transfer Learning. *IEEE Transactions on Knowledge and Data Engineering* **22,** 1345–1359 (2010).

173. Jayaram, V., Alamgir, M., Altun, Y., Scholkopf, B. & Grosse-Wentrup, M. Transfer Learning in Brain-computer Interfaces. *IEEE Computational Intelligence Magazine* **11,** 20–31 (2016).

174. Lu, S., Guan, C. & Zhang, H. Unsupervised Brain Computer Interface Based on Intersubject Information and Online Adaptation. *IEEE Transactions on Neural Systems and Rehabilitation Engineering* **17,** 135–145 (2009).

175. Robinson, N. & Vinod, A. P. Noninvasive Brain-Computer Interface: Decoding Arm Movement Kinematics and Motor Control. *IEEE Systems, Man, and Cybernetics Magazine* **2,** 4–16 (2016).

176. Wessberg, J. *et al.* Real-time Prediction of Hand Trajectory by Ensembles of Cortical Neurons in Primates. *Nature* **408,** 361–365 (6810 2000).

177. Serruya, M. D., Hatsopoulos, N. G., Paninski, L., Fellows, M. R. & Donoghue, J. P. Instant Neural Control of a Movement Signal. *Nature* **416,** 141–142 (6877 2002).

178. Mulliken, G. H., Musallam, S. & Andersen, R. A. Decoding Trajectories from Posterior Parietal Cortex Ensembles. *Journal of Neuroscience* **28,** 12913–12926 (2008).

179. Musallam, S., Corneil, B. D., Greger, B., Scherberger, H. & Andersen, R. A. Cognitive Control Signals for Neural Prosthetics. *Science* **305,** 258–262 (5681 2004).

180. Santhanam, G., Ryu, S. I., Yu, B. M., Afshar, A. & Shenoy, K. V. A High-performance Brain-Computer Interface. *Nature* **442,** 195–198 (7099 2006).

181. Kim, H. K. *et al.* Continuous Shared Control for Stabilizing Reaching and Grasping with Brain-Machine Interfaces. *IEEE Transactions on Biomedical Engineering* **53,** 1164–1173 (2006).

182. Velliste, M., Perel, S., Spalding, M. C., Whitford, A. S. & Schwartz, A. B. Cortical Control of a Prosthetic Arm for Self-feeding. *Nature* **453,** 1098–1101 (2008).

183. Moritz, C. T., Perlmutter, S. I. & Fetz, E. E. Direct Control of Paralysed Muscles by Cortical Neurons. *Nature* **456,** 639–642 (2008).

184. Pohlmeyer, E. A. *et al.* Toward the Restoration of Hand Use to a Paralyzed Monkey: Brain-controlled Functional Electrical Stimulation of Forearm Muscles. *PLoS ONE* **4,** e5924 (2009).

185. Townsend, B. R., Subasi, E. & Scherberger, H. Grasp Movement Decoding from Premotor and Parietal Cortex. *Journal of Neuroscience* **31,** 14386–14398 (2011).

186. Carmena, J. M. Stable Ensemble Performance with Single-neuron Variability during Reaching Movements in Primates. *Journal of Neuroscience* **25,** 10712–10716 (2005).

187. Hochberg, L. R. *et al.* Neuronal Ensemble Control of Prosthetic Devices by a Human with Tetraplegia. *Nature* **442,** 164–171 (7099 2006).

188. Kim, S.-P., Simeral, J. D., Hochberg, L. R., Donoghue, J. P. & Black, M. J. Neural Control of Computer Cursor Velocity by Decoding Motor Cortical Spiking Activity in Humans with Tetraplegia. *Journal of Neural Engineering* **5,** 455–476 (4 2008).

189. Schalk, G. *et al.* Two-dimensional Movement Control Using Electrocorticographic Signals in Humans. *Journal of Neural Engineering* **5,** 75–84 (2008).

190. Tavella, M., Leeb, R., Rupp, R. & d. R. Millán, J. *Towards Natural Non-invasive Hand Neuroprostheses for Daily Living* in *2010 Annual International Conference of the IEEE Engineering in Medicine and Biology* (2010), 126–129.

191. Rohm, M. *et al.* Hybrid Brain–computer Interfaces and Hybrid Neuroprostheses for Restoration of Upper Limb Functions in Individuals with High-level Spinal Cord Injury. *Artificial Intelligence in Medicine* **59,** 133–142 (2013).

192. Müller-Putz, G. R. & Pfurtscheller, G. Control of an Electrical Prosthesis with an SSVEP-based BCI. *IEEE Transactions on Biomedical Engineering* **55,** 361–364 (2008).

193. Ortner, R., Allison, B. Z., Korisek, G., Gaggl, H. & Pfurtscheller, G. An SSVEP Bci to Control a Hand Orthosis for Persons with Tetraplegia. *IEEE Transactions on Neural Systems and Rehabilitation Engineering* **19,** 1–5 (2011).

194. Horki, P., Neuper, C., Pfurtscheller, G. & Müller-Putz, G. Asynchronous Steady-state Visual Evoked Potential Based BCI Control of a 2-DoF Artificial Upper Limb. *Biomedizinische Technik/biomedical Engineering* **55,** 367–374 (2010).

195. Horki, P., Solis-Escalante, T., Neuper, C. & Müller-Putz, G. Combined Motor Imagery and SSVEP Based BCI Control of a 2 DoF Artificial Upper Limb. *Medical and Biological Engineering and Computing* **49,** 567–577 (2011).

196. Müller-Putz, G., Scherer, R., Pfurtscheller, G. & Neuper, C. Temporal Coding of Brain Patterns for Direct Limb Control in Humans. *Frontiers in Neuroscience* **4,** 34 (2010).

197. Gomez-Rodriguez, M. *et al.* Closing the Sensorimotor Loop: Haptic Feedback Facilitates Decoding of Motor Imagery. *Journal of Neural Engineering* **8,** 036005 (2011).

198. Wolpaw, J. R. & McFarland, D. J. Control of a Two-dimensional Movement Signal by a Noninvasive Brain-Computer Interface in Humans. *Proceedings of the National Academy of Sciences of the United States of America* **101,** 17849–17854 (51 2004).

199. McFarland, D. J., Sarnacki, W. A. & Wolpaw, J. R. Electroencephalographic (EEG) Control of Three-dimensional Movement. *Journal of Neural Engineering* **7,** 036007 (2010).

200. Polikov, V. S., Tresco, P. A. & Reichert, W. M. Response of Brain Tissue to Chronically Implanted Neural Electrodes. *Journal of Neuroscience Methods* **148,** 1–18 (2005).

201. Bjornsson, C. S. *et al.* Effects of Insertion Conditions on Tissue Strain and Vascular Damage during Neuroprosthetic Device Insertion. *Journal of Neural Engineering* **3,** 196–207 (2006).

202. Nicolelis, M. A. L. *et al.* Chronic, Multisite, Multielectrode Recordings in Macaque Monkeys. *Proceedings of the National Academy of Sciences of the United States of America* **100,** 11041–11046 (19 2003).

203. Jackson, A. & Fetz, E. E. Interfacing with the Computational Brain. *IEEE Transactions on Neural Systems and Rehabilitation Engineering* **19,** 534–541 (2011).

204. Lv, J., Li, Y. & Gu, Z. Decoding Hand Movement Velocity from Electroencephalogram Signals during a Drawing Task. *Biomedical Engineering Online* **9,** 64 (2010).

205. Bradberry, T. J., Gentili, R. J. & Contreras-Vidal, J. L. Reconstructing Three-dimensional Hand Movements from Noninvasive Electroencephalographic Signals. *Journal of Neuroscience* **30,** 3432–3437 (2010).

206. Bradberry, T. J., Rong, F. & Contreras-Vidal, J. L. Decoding Center-out Hand Velocity from MEG Signals during Visuomotor Adaptation. *NeuroImage* **47,** 1691–1700 (2009).

207. Toda, A., Imamizu, H., Kawato, M. & Sato, M.-a. Reconstruction of Two-dimensional Movement Trajectories from Selected Magnetoencephalography Cortical Currents by Combined Sparse Bayesian Methods. *NeuroImage* **54,** 892–905 (2011).

208. Georgopoulos, A. P., Langheim, F. J. P., Leuthold, A. C. & Merkle, A. N. Magnetoencephalographic Signals Predict Movement Trajectory in Space. *Experimental Brain Research* **167,** 132–135 (2005).

209. Acharya, S., Fifer, M. S., Benz, H. L., Crone, N. E. & Thakor, N. V. Electrocorticographic Amplitude Predicts Finger Positions during Slow Grasping Motions of the Hand. *Journal of Neural Engineering* **7,** 046002 (2010).

210. Kubánek, J., Miller, K. J., Ojemann, J. G., Wolpaw, J. R. & Schalk, G. Decoding Flexion of Individual Fingers Using Electrocorticographic Signals in Humans. *Journal of Neural Engineering* **6,** 066001 (2009).

211. Pistohl, T., Ball, T., Schulze-Bonhage, A., Aertsen, A. & Mehring, C. Prediction of Arm Movement Trajectories from ECoG-recordings in Humans. *Journal of Neuroscience Methods* **167,** 105–114 (2008).

212. Schalk, G. *et al.* Decoding Two-dimensional Movement Trajectories Using Electrocorticographic Signals in Humans. *Journal of Neural Engineering* **4,** 264–275 (2007).

213. Mehring, C. *et al.* Inference of Hand Movements from Local Field Potentials in Monkey Motor Cortex. *Nature Neuroscience* **6,** 1253–1254 (12 2003).

214. Hammon, P., Makeig, S., Poizner, H., Todorov, E. & Sa, V. D. Predicting Reaching Targets from Human EEG. *IEEE Signal Processing Magazine* **25,** 69–77 (2008).

215. Wang, Y. & Makeig, S. *Predicting Intended Movement Direction Using EEG from Human Posterior Parietal Cortex* in *International Conference on Foundations of Augmented Cognition* (2009), 437–446.

216. Waldert, S. *et al.* Hand Movement Direction Decoded from MEG and EEG. *Journal of Neuroscience* **28,** 1000–1008 (2008).

217. Wang, W. *et al.* Decoding and Cortical Source Localization for Intended Movement Direction with MEG. *Journal of Neurophysiology* **104,** 2451–2461 (2010).

218. Ball, T., Schulze-Bonhage, A., Aertsen, A. & Mehring, C. Differential Representation of Arm Movement Direction in Relation to Cortical Anatomy and Function. *Journal of Neural Engineering* **6,** 016006 (2009).

219. Mehring, C. *et al.* Comparing Information about Arm Movement Direction in Single Channels of Local and Epicortical Field Potentials from Monkey and Human Motor Cortex. *Journal of Physiology-Paris* **98,** 498–506 (2004).

220. Gu, Y. *et al.* Offline Identification of Imagined Speed of Wrist Movements in Paralyzed Als Patients from Single-Trial EEG. *Frontiers in Neuroscience* **3,** 62 (2009).

221. Gu, Y., Dremstrup, K. & Farina, D. Single-Trial Discrimination of Type and Speed of Wrist Movements from EEG Recordings. *Clinical Neurophysiology* **120,** 1596–1600 (2009).

222. Yom-Tov, E. & Inbar, G. F. Detection of Movement-related Potentials from the Electro-encephalogram for Possible Use in a Brain-Computer Interface. *Medical and Biological Engineering and Computing* **41,** 85–93 (2003).

223. Fatourechi, M., Ward, R. K. & Birch, G. E. A Self-paced Brain–Computer Interface System with a Low False Positive Rate. *Journal of Neural Engineering* **5,** 9–23 (2007).

224. Neuper, C., Scherer, R., Reiner, M. & Pfurtscheller, G. Imagery of Motor Actions: Differential Effects of Kinesthetic and Visual–motor Mode of Imagery in Single-Trial EEG. *Cognitive Brain Research* **25,** 668–677 (2005).

225. Croft, R. J. & Barry, R. J. Removal of Ocular Artifact from the EEG: A Review. *Neurophysiologie Clinique/Clinical Neurophysiology* **30,** 5–19 (1 2000).

226. Schlögl, A. *et al.* A Fully Automated Correction Method of EOG Artifacts in EEG Recordings. *Clinical Neurophysiology* **118,** 98–104 (2007).

227. Farrar, D. E. & Glauber, R. R. Multicollinearity in Regression Analysis: The Problem Revisited. *The Review of Economics and Statistics* **49,** 92 (1967).

228. Grahn, J. A. & Brett, M. Rhythm and Beat Perception in Motor Areas of the Brain. *Journal of Cognitive Neuroscience* **19,** 893–906 (2007).

229. Blokland, Y. *et al. Detection of Event-related Desynchronization during Attempted and Imagined Movements in Tetraplegics for Brain Switch Control* in *2012 34th Annual International Conference of the IEEE Engineering in Medicine and Biology Society* (2012), 3967–3969.

230. Cui, R. & MacKinnon, C. D. The Effect of Temporal Accuracy Constraints on Movement-related Potentials. *Experimental Brain Research* **194,** 477–488 (2009).

231. Antelis, J. M., Montesano, L., Ramos-Murguialday, A., Birbaumer, N. & Minguez, J. On the Usage of Linear Regression Models to Reconstruct Limb Kinematics from Low Frequency EEG Signals. *PLoS ONE* **8,** e61976 (2013).

232. Kobler, R. J., Sburlea, A. I. & Müller-Putz, G. R. Tuning Characteristics of Low-frequency EEG to Positions and Velocities in Visuomotor and Oculomotor Tracking Tasks. *Scientific Reports* **8** (2018).

233. Kim, J.-H., Biessmann, F. & Lee, S.-W. Decoding Three-dimensional Trajectory of Executed and Imagined Arm Movements from Electroencephalogram Signals. *IEEE Transactions on Neural Systems and Rehabilitation Engineering* **23,** 867–876 (2015).

234. Zhang, J., Wei, J., Wang, B., Hong, J. & Wang, J. Nonlinear EEG Decoding Based on a Particle Filter Model. *BioMed Research International* **2014,** 1–13 (2014).

235. Paek, A. Y., Agashe, H. A. & Contreras-Vidal, J. L. Decoding Repetitive Finger Movements with Brain Activity Acquired Via Non-invasive Electroencephalography. *Frontiers in Neuroengineering* **7** (2014).

236. Agashe, H. A., Paek, A. Y., Zhang, Y. & Contreras-Vidal, J. L. Global Cortical Activity Predicts Shape of Hand during Grasping. *Frontiers in Neuroscience* **9** (2015).

237. Yeom, H. G. *et al.* A Study on Decoding Models for the Reconstruction of Hand Trajectories from the Human Magnetoencephalography. *BioMed Research International* **2014,** 1–8 (2014).

238. Yeom, H. G., Kim, J. S. & Chung, C. K. Estimation of the Velocity and Trajectory of Three-dimensional Reaching Movements from Non-invasive Magnetoencephalography Signals. *Journal of Neural Engineering* **10,** 026006 (2013).

239. Talakoub, O. *et al.* Reconstruction of Reaching Movement Trajectories Using Electrocorticographic Signals in Humans. *PLoS ONE* **12,** e0182542 (2017).

240. Hotson, G. *et al.* Coarse Electrocorticographic Decoding of Ipsilateral Reach in Patients with Brain Lesions. *PLoS ONE* **9,** e115236 (2014).

241. Nakanishi, Y. *et al.* Prediction of Three-dimensional Arm Trajectories Based on ECoG Signals Recorded from Human Sensorimotor Cortex. *PLoS ONE* **8,** e72085 (8 2013).

242. Nakanishi, Y. *et al.* Mapping ECoG Channel Contributions to Trajectory and Muscle Activity Prediction in Human Sensorimotor Cortex. *Scientific Reports* **7,** 45486 (2017).

243. Bundy, D. T., Pahwa, M., Szrama, N. & Leuthardt, E. C. Decoding Three-dimensional Reaching Movements Using Electrocorticographic Signals in Humans. *Journal of Neural Engineering* **13,** 026021 (2016).

244. Nakanishi, Y. *et al.* Decoding Fingertip Trajectory from Electrocorticographic Signals in Humans. *Neuroscience Research* **85,** 20–27 (2014).

245. Stavisky, S. D., Kao, J. C., Nuyujukian, P., Ryu, S. I. & Shenoy, K. V. A High Performing Brain-machine Interface Driven by Low-frequency Local Field Potentials Alone and Together with Spikes. *Journal of Neural Engineering* **12,** 036009 (3 2015).

246. Milekovic, T. *et al.* An Online Brain–machine Interface Using Decoding of Movement Direction from the Human Electrocorticogram. *Journal of Neural Engineering* **9,** 046003 (2012).

247. Robinson, N., Guan, C. & Vinod, A. P. Adaptive Estimation of Hand Movement Trajectory in an EEG Based Brain–computer Interface System. *Journal of Neural Engineering* **12,** 066019 (2015).

248. Shin, D., Kambara, H., Yoshimura, N. & Koike, Y. Control of a Robot Arm Using Decoded Joint Angles from Electrocorticograms in Primate. *Computational Intelligence and Neuroscience* **2018,** 2580165 (2018).

249. Eliseyev, A. & Aksenova, T. Stable and Artifact-resistant Decoding of 3d Hand Trajectories from ECoG Signals Using the Generalized Additive Model. *Journal of Neural Engineering* **11,** 066005 (2014).

250. Xie, Z., Schwartz, O. & Prasad, A. Decoding of Finger Trajectory from ECoG Using Deep Learning. *Journal of Neural Engineering* **15,** 036009 (2018).

251. Flamary, R. & Rakotomamonjy, A. Decoding Finger Movements from ECoG Signals Using Switching Linear Models. *Frontiers in Neuroscience* **6** (2012).

252. Bradberry, T. J., Gentili, R. J. & Contreras-Vidal, J. L. Fast Attainment of Computer Cursor Control with Noninvasively Acquired Brain Signals. *Journal of Neural Engineering* **8,** 036010 (2011).

253. Poli, R. & Salvaris, M. Comment on 'fast Attainment of Computer Cursor Control with Noninvasively Acquired Brain Signals'. *Journal of Neural Engineering* **8,** 058001 (2011).

254. Bradberry, T. J., Gentili, R. J. & Contreras-Vidal, J. L. Reply to Comment on 'fast Attainment of Computer Cursor Control with Noninvasively Acquired Brain Signals'. *Journal of Neural Engineering* **8,** 058002 (2011).

255. Korik, A., Sosnik, R., Siddique, N. & Coyle, D. Decoding Imagined 3D Hand Movement Trajectories from EEG: Evidence to Support the Use of Mu, Beta, and Low Gamma Oscillations. *Frontiers in Neuroscience* **12** (2018).

256. Wang, Z. *et al.* Decoding Onset and Direction of Movements Using Electrocorticographic (ECoG) Signals in Humans. *Frontiers in Neuroengineering* **5** (2012).

257. Robinson, N., Guan, C., Vinod, A. P., Ang, K. K. & Tee, K. P. Multi-class EEG Classification of Voluntary Hand Movement Directions. *Journal of Neural Engineering* **10,** 056018 (2013).

258. Lew, E. Y. L., Chavarriaga, R., Silvoni, S. & del R. Millán, J. Single Trial Prediction of Self-paced Reaching Directions from EEG Signals. *Frontiers in Neuroscience* **8** (2014).

259. Úbeda, A., Azorı´ n, J. M., Chavarriaga, R. & del R. Millán, J. Classification of Upper Limb Center-out Reaching Tasks by Means of EEG-based Continuous Decoding Techniques. *Journal of Neuroengineering and Rehabilitation* **14** (2017).

260. Handiru, V. S., Vinod, A. P. & Guan, C. EEG Source Space Analysis of the Supervised Factor Analytic Approach for the Classification of Multi-directional Arm Movement. *Journal of Neural Engineering* **14,** 046008 (2017).

261. Tanaka, H., Miyakoshi, M. & Makeig, S. Dynamics of Directional Tuning and Reference Frames in Humans: A High-density EEG Study. *Scientific Reports* **8** (2018).

262. Liao, X., Yao, D., Wu, D. & Li, C. Combining Spatial Filters for the Classification of Single-Trial EEG in a Finger Movement Task. *IEEE Transactions on Biomedical Engineering* **54,** 821–831 (2007).

263. Haufe, S. *et al.* On the Interpretation of Weight Vectors of Linear Models in Multivariate Neuroimaging. *NeuroImage* **87,** 96–110 (2014).

264. Zhao, D., Tang, F., Si, B. & Feng, X. Learning Joint Space–time–frequency Features for EEG Decoding on Small Labeled Data. *Neural Networks* **114,** 67–77 (2019).

265. Vučković, A. & Sepulveda, F. Delta Band Contribution in Cue Based Single Trial Classification of Real and Imaginary Wrist Movements. *Medical and Biological Engineering and Computing* **46,** 529–539 (2008).

266. Vučković, A. & Sepulveda, F. A Two-stage Four-class BCI Based on Imaginary Movements of the Left and the Right Wrist. *Medical Engineering & Physics* **34,** 964–971 (2012).

267. Quandt, F. *et al.* Single Trial Discrimination of Individual Finger Movements on One Hand: A Combined MEG and EEG Study. *NeuroImage* **59,** 3316–3324 (2012).

268. Sugata, H. *et al.* Neural Decoding of Unilateral Upper Limb Movements Using Single Trial MEG Signals. *Brain Research* **1468,** 29–37 (2012).

269. Sugata, H. *et al.* Common Neural Correlates of Real and Imagined Movements Contributing to the Performance of Brain–machine Interfaces. *Scientific Reports* **6** (2016).

270. Wissel, T. *et al.* Hidden Markov Model and Support Vector Machine Based Decoding of Finger Movements Using Electrocorticography. *Journal of Neural Engineering* **10,** 056020 (2013).

271. Schwarz, A., Ofner, P., Pereira, J., Sburlea, A. I. & Müller-Putz, G. R. Decoding Natural Reach-and-grasp Actions from Human EEG. *Journal of Neural Engineering* **15,** 016005 (2017).

272. Jochumsen, M. *et al.* Classification of Hand Grasp Kinetics and Types Using Movement-related Cortical Potentials and EEG Rhythms. *Computational Intelligence and Neuroscience* **2017,** 1–8 (2017).

273. Iturrate, I. *et al.* Human EEG Reveals Distinct Neural Correlates of Power and Precision Grasping Types. *NeuroImage* **181,** 635–644 (2018).

274. Pistohl, T., Schulze-Bonhage, A., Aertsen, A., Mehring, C. & Ball, T. Decoding Natural Grasp Types from Human ECoG. *NeuroImage* **59,** 248–260 (2012).

275. Mollazadeh, M. *et al.* Spatiotemporal Variation of Multiple Neurophysiological Signals in the Primary Motor Cortex during Dexterous Reach-to-grasp Movements. *Journal of Neuroscience* **31,** 15531–15543 (2011).

276. Shokur, S. *et al.* Expanding the Primate Body Schema in Sensorimotor Cortex by Virtual Touches of an Avatar. *Proceedings of the National Academy of Sciences of the United States of America* **110,** 15121–15126 (2013).

277. Rizzolatti, G. & Craighero, L. The Mirror-Neuron System. *Annual Review of Neuroscience* **27,** 169–192 (2004).

278. Di Pellegrino, G., Fadiga, L., Fogassi, L., Gallese, V. & Rizzolatti, G. Understanding Motor Events: A Neurophysiological Study. *Experimental Brain Research* **91,** 176–180 (1992).

279. Lang, W., Cheyne, D., Höllinger, P., Gerschlager, W. & Lindinger, G. Electric and Magnetic Fields of the Brain Accompanying Internal Simulation of Movement. *Brain Research. Cognitive Brain Research* **3,** 125–129 (2 1996).

280. Pfurtscheller, G., Neuper, C., Flotzinger, D. & Pregenzer, M. EEG-based Discrimination between Imagination of Right and Left Hand Movement. *Electroencephalography and Clinical Neurophysiology* **103,** 642–651 (6 1997).

281. Meng, J. *et al.* Noninvasive Electroencephalogram Based Control of a Robotic Arm for Reach and Grasp Tasks. *Scientific Reports* **6** (2016).

282. Soekadar, S. R. *et al.* Hybrid EEG/EOG-based Brain/neural Hand Exoskeleton Restores Fully Independent Daily Living Activities After Quadriplegia. *Science Robotics* **1,** eaag3296 (2016).

283. Vidaurre, C., Klauer, C., Schauer, T., Ramos-Murguialday, A. & Müller, K.-R. EEG-based BCI for the Linear Control of an Upper-limb Neuroprosthesis. *Medical Engineering & Physics* **38,** 1195–1204 (2016).

284. Castro, A., Diaz, F. & Sumich, A. Long-term Neuroplasticity in Spinal Cord Injury Patients: A Study on Movement-related Brain Potentials. *International Journal of Psychophysiology* **87,** 205–214 (2013).

285. Xu, R. *et al.* Movement-related Cortical Potentials in Paraplegic Patients: Abnormal Patterns and Considerations for BCI-rehabilitation. *Frontiers in Neuroengineering* **7** (2014).

286. Lacourse, M. G., Cohen, M. J., Lawrence, K. E. & Romero, D. H. Cortical Potentials during Imagined Movements in Individuals with Chronic Spinal Cord Injuries. *Behavioural Brain Research* **104,** 73–88 (1-2 1999).

287. Fukuma, R. *et al.* Real-time Control of a Neuroprosthetic Hand by Magnetoencephalographic Signals from Paralysed Patients. *Scientific Reports* **6** (2016).

288. Pfurtscheller, G. & Neuper, C. Motor Imagery and Direct Brain-Computer Communication. *Proceedings of the IEEE* **89,** 1123–1134 (2001).

289. Fukuma, R. *et al.* Closed-loop Control of a Neuroprosthetic Hand by Magnetoencephalographic Signals. *PLoS ONE* **10,** e0131547 (2015).

290. Yanagisawa, T. *et al.* Induced Sensorimotor Brain Plasticity Controls Pain in Phantom Limb Patients. *Nature Communications* **7** (2016).

291. Fukuma, R. *et al.* Training in Use of Brain–machine Interface-controlled Robotic Hand Improves Accuracy Decoding Two Types of Hand Movements. *Frontiers in Neuroscience* **12** (2018).

292. Hochberg, L. R. *et al.* Reach and Grasp by People with Tetraplegia Using a Neurally Controlled Robotic Arm. *Nature* **485,** 372–375 (2012).

293. Collinger, J. L. *et al.* High-performance Neuroprosthetic Control by an Individual with Tetraplegia. *The Lancet* **381,** 557–564 (9866 2013).

294. Wodlinger, B. *et al.* Ten-dimensional Anthropomorphic Arm Control in a Human Brain-Machine Interface: Difficulties, Solutions, and Limitations. *Journal of Neural Engineering* **12,** 016011 (2014).

295. Bouton, C. E. *et al.* Restoring Cortical Control of Functional Movement in a Human with Quadriplegia. *Nature* **533,** 247–250 (2016).

296. Ajiboye, A. B. *et al.* Restoration of Reaching and Grasping Movements through Brain-controlled Muscle Stimulation in a Person with Tetraplegia: A Proof-of-concept Demonstration. *The Lancet* **389,** 1821–1830 (2017).

297. Fifer, M. S. *et al.* Simultaneous Neural Control of Simple Reaching and Grasping with the Modular Prosthetic Limb Using Intracranial EEG. *IEEE Transactions on Neural Systems and Rehabilitation Engineering* **22,** 695–705 (2014).

298. Hotson, G. *et al.* Individual Finger Control of a Modular Prosthetic Limb Using High-density Electrocorticography in a Human Subject. *Journal of Neural Engineering* **13,** 026017 (2016).

299. Heger, D., Jäkel, R., Putze, F., Lösch, M. & Schultz, T. *Filling a Glass of Water: Continuously Decoding the Speed of 3D Hand Movements from EEG Signals* in *2012 34th Annual International Conference of the IEEE Engineering in Medicine and Biology Society* (2012), 4095–4098.

300. Loza, C. A., Philips, G. R., Hazrati, M. K., Daly, J. J. & Principe, J. C. *Classification of Hand Movement Direction Based on EEG High-gamma Activity* in *2014 36th Annual International Conference of the IEEE Engineering in Medicine and Biology Society* (IEEE, 2014).

301. Shiman, F. *et al.* Classification of Different Reaching Movements from the Same Limb Using EEG. *Journal of Neural Engineering* **14,** 046018 (2017).

302. Seeber, M., Scherer, R. & Müller-Putz, G. R. EEG Oscillations Are Modulated in Different Behavior-related Networks during Rhythmic Finger Movements. *The Journal of Neuroscience* **36,** 11671–11681 (2016).

303. Pei, D., Patel, V., Burns, M., Chandramouli, R. & Vinjamuri, R. Neural Decoding of Synergy-based Hand Movements Using Electroencephalography. *IEEE Access* **7,** 18155–18163 (2019).

304. Zeng, H. *et al.* The Advantage of Low-delta Electroencephalogram Phase Feature for Reconstructing the Center-out Reaching Hand Movements. *Frontiers in Neuroscience* **13,** 480 (2019).

305. Ball, T. *et al.* Movement Related Activity in the High Gamma Range of the Human EEG. *NeuroImage* **41,** 302–310 (2008).

306. Flint, R. D. *et al.* Extracting Kinetic Information from Human Motor Cortical Signals. *NeuroImage* **101,** 695–703 (2014).

307. Jiang, T. *et al.* Characterization and Decoding the Spatial Patterns of Hand Extension/flexion Using High-density ECoG. *IEEE Transactions on Neural Systems and Rehabilitation Engineering* **25,** 370–379 (2017).

308. Thomas, T. M. *et al.* Decoding Native Cortical Representations for Flexion and Extension at Upper Limb Joints Using Electrocorticography. *IEEE Transactions on Neural Systems and Rehabilitation Engineering* **27,** 293–303 (2019).

309. Ince, N. F. *et al.* High Accuracy Decoding of Movement Target Direction in Non-human Primates Based on Common Spatial Patterns of Local Field Potentials. *PLoS ONE* **5,** e14384 (2010).

310. Flint, R. D., Lindberg, E. W., Jordan, L. R., Miller, L. E. & Slutzky, M. W. Accurate Decoding of Reaching Movements from Field Potentials in the Absence of Spikes. *Journal of Neural Engineering* **9,** 046006 (2012).

311. Li, T., Xue, T., Wang, B. & Zhang, J. Decoding Voluntary Movement of Single Hand Based on Analysis of Brain Connectivity by Using EEG Signals. *Frontiers in Human Neuroscience* **12** (2018).

312. Touge, T., Werhahn, K. J., Rothwell, J. C. & Marsden, C. D. Movement-related Cortical Potentials Preceding Repetitive and Random-choice Hand Movements in Parkinson's Disease. *Annals of Neurology* **37,** 791–799 (1995).

313. Jankelowitz, S. & Colebatch, J. Movement-related Potentials Associated with Self-paced, Cued and Imagined Arm Movements. *Experimental Brain Research* **147,** 98–107 (2002).

314. Pereira, J., Sburlea, A. I. & Müller-Putz, G. R. EEG Patterns of Self-paced Movement Imaginations Towards Externally-cued and Internally-selected Targets. *Scientific Reports* **8** (2018).

315. Gürel. Unsupervised Adaptation of Brain-machine Interface Decoders. *Frontiers in Neuroscience* **6,** 164 (2012).

316. Schwemmer, M. A. *et al.* Meeting Brain–computer Interface User Performance Expectations Using a Deep Neural Network Decoding Framework. *Nature Medicine* **24,** 1669–1676 (2018).

317. Aliakbaryhosseinabadi, S., Kamavuako, E. N., Jiang, N., Farina, D. & Mrachacz-Kersting, N. Influence of Dual-tasking with Different Levels of Attention Diversion on Characteristics of the Movement-related Cortical Potential. *Brain Research* **1674,** 10–19 (2017).

318. Rizzolatti, G., Cattaneo, L., Fabbri-Destro, M. & Rozzi, S. Cortical Mechanisms Underlying the Organization of Goal-directed Actions and Mirror Neuron-based Action Understanding. *Physiological Reviews* **94,** 655–706 (2014).

319. Kilner, J. M., Vargas, C., Duval, S., Blakemore, S.-J. & Sirigu, A. Motor Activation Prior to Observation of a Predicted Movement. *Nature Neuroscience* **7,** 1299–1301 (2004).

320. Cochin, S., Barthelemy, C., Lejeune, B., Roux, S. & Martineau, J. Perception of Motion and qEEG Activity in Human Adults. *Electroencephalography and Clinical Neurophysiology* **107,** 287–295 (1998).

321. Muthukumaraswamy, S. D., Johnson, B. W. & McNair, N. A. Mu Rhythm Modulation during Observation of an Object-directed Grasp. *Cognitive Brain Research* **19,** 195–201 (2004).

322. Neuper, C., Scherer, R., Wriessnegger, S. & Pfurtscheller, G. Motor Imagery and Action Observation: Modulation of Sensorimotor Brain Rhythms during Mental Control of a Brain–computer Interface. *Clinical Neurophysiology* **120,** 239–247 (2009).

323. Bourguignon, M. *et al.* Primary Motor Cortex and Cerebellum Are Coupled with the Kinematics of Observed Hand Movements. *NeuroImage* **66,** 500–507 (2013).

324. Galán, F., Baker, M. R., Alter, K. & Baker, S. N. Degraded EEG Decoding of Wrist Movements in Absence of Kinaesthetic Feedback. *Human Brain Mapping* **36,** 643–654 (2014).

325. Bansal, A. K., Vargas-Irwin, C. E., Truccolo, W. & Donoghue, J. P. Relationships among Low-frequency Local Field Potentials, Spiking Activity, and Three-dimensional Reach and Grasp Kinematics in Primary Motor and Ventral Premotor Cortices. *Journal of Neurophysiology* **105,** 1603–1619 (2011).

326. Ryun, S., Kim, J. S., Jeon, E. & Chung, C. K. Movement-related Sensorimotor High-gamma Activity Mainly Represents Somatosensory Feedback. *Frontiers in Neuroscience* **11** (2017).

327. Saleh, M., Takahashi, K. & Hatsopoulos, N. G. Encoding of Coordinated Reach and Grasp Trajectories in Primary Motor Cortex. *Journal of Neuroscience* **32,** 1220–1232 (2012).

328. Wong, A. L., Haith, A. M. & Krakauer, J. W. Motor Planning. *The Neuroscientist* **21,** 385–398 (2014).

329. Yokoyama, H. *et al.* Cortical Correlates of Locomotor Muscle Synergy Activation in Humans: An Electroencephalographic Decoding Study. *iScience* (2019).

330. Bizzi, E. & Cheung, V. C. K. The Neural Origin of Muscle Synergies. *Frontiers in Computational Neuroscience* **7** (2013).

331. Graziano, M. S. A., Taylor, C. S. R. & Moore, T. Complex Movements Evoked by Microstimulation of Precentral Cortex. *Neuron* **34,** 841–851 (2002).

332. Graziano, M. S. A., Aflalo, T. N. S. & Cooke, D. F. Arm Movements Evoked by Electrical Stimulation in the Motor Cortex of Monkeys. *Journal of Neurophysiology* **94,** 4209–4223 (2005).

333. Hall, T. M., de Carvalho, F. & Jackson, A. A Common Structure Underlies Low-frequency Cortical Dynamics in Movement, Sleep, and Sedation. *Neuron* **83,** 1185–1199 (2014).

334. Liao, J. Y. & Kirsch, R. F. Characterizing and Predicting Submovements during Human Three-dimensional Arm Reaches. *PLoS ONE* **9,** e103387 (2014).

335. Miranda, J. G. V. *et al.* Complex Upper-limb Movements Are Generated by Combining Motor Primitives That Scale with the Movement Size. *Scientific Reports* **8** (2018).

336. Jochumsen, M., Niazi, I. K., Nedergaard, R. W., Navid, M. S. & Dremstrup, K. Effect of Subject Training on a Movement-related Cortical Potential-based Brain-Computer Interface. *Biomedical Signal Processing and Control* **41,** 63–68 (2018).

337. Shanechi, M. M. *et al.* Rapid Control and Feedback Rates Enhance Neuroprosthetic Control. *Nature Communications* **8** (2017).

338. Pereira, J., Ofner, P., Schwarz, A., Sburlea, A. I. & Müller-Putz, G. R. EEG Neural Correlates of Goal-directed Movement Intention. *NeuroImage* **149,** 129–140 (2017).

339. Todorov, E. Reply to 'one Motor Cortex, Two Different Views'. *Nature Neuroscience* **3,** 963–964 (2000).

340. Yoshimura, N., Tsuda, H., Kawase, T., Kambara, H. & Koike, Y. Decoding Finger Movement in Humans Using Synergy of EEG Cortical Current Signals. *Scientific Reports* **7** (2017).

341. Hochreiter, S. & Schmidhuber, J. Long Short-term Memory. *Neural Computation* **9,** 1735–1780 (1997).

342. Yosinski, J., Clune, J., Bengio, Y. & Lipson, H. *How Transferable Are Features in Deep Neural Networks?* in *Advances in neural information processing systems* (2014), 3320–3328.

343. Müller-Putz, G. *et al.* Towards Noninvasive Hybrid Brain–Computer Interfaces: Framework, Practice, Clinical Application, and Beyond. *Proceedings of the IEEE* **103,** 926–943 (2015).

Appendix

All primary and secondary publications of this PhD thesis are collected in this appendix. Table A.1 and Table A.2 give an estimation of the contribution of every author.

Table A.1: Author contributions of primary publications.

#	*Author*	*Work*	*Contribution*
1	**P. Ofner**	85 %	study design, scripts, recording, analysis, interpretation, writing
	G.R. Müller-Putz	15 %	idea, study design, interpretation, writing
2	**P. Ofner**	90 %	idea, study design, scripts, recording, analysis, interpretation, writing
	G.R. Müller-Putz	10 %	study design, interpretation, writing
3	**P. Ofner**	80 %	idea, study design, scripts, recording, analysis, interpretation, writing
	A. Schwarz	10 %	study design, recording, writing
	J. Pereira	5 %	writing
	G.R. Müller-Putz	5 %	study design, interpretation, paper review
4	**P. Ofner**	70 %	idea, study design, scripts, recording, analysis, interpretation, writing
	A. Schwarz	10 %	study design, recording, writing
	J. Pereira	10 %	study design, recording, writing
	D. Wyss	4 %	recruitment of study participants
	R. Wildburger	1 %	clinical supervision
	G.R. Müller-Putz	5 %	study design, interpretation, paper review

Table A.2: Author contributions of secondary publications.

#	*Author*	*Work*	*Contribution*
1	**P. Ofner**	45 %	study design, scripts, analysis, interpretation, writing
	J. Pereira	40 %	study design, scripts, recording
	G.R. Müller-Putz	15 %	idea, study design, interpretation, paper review
2	**P. Ofner**	90 %	idea, study design, scripts, recording, analysis, interpretation, writing
	G.R. Müller-Putz	10 %	study design, interpretation, paper review
3	**P. Ofner**	90 %	idea, study design, scripts, recording, analysis, interpretation, writing
	G.R. Müller-Putz	10 %	study design, interpretation, paper review
4	**P. Ofner**	50 %	idea, study design, scripts, analysis, interpretation, writing
	P. Kersch	40 %	study design, scripts, recording, paper review
	G.R. Müller-Putz	10 %	study design, interpretation, paper review

Primary Publication I

34th Annual International Conference of the IEEE EMBS
San Diego, California USA, 28 August - 1 September, 2012

Decoding of velocities and positions of 3D arm movement from EEG*

Patrick Ofner[1] and Gernot R. Müller-Putz[1]

***Abstract*— A brain-computer interface (BCI) can be used to control a limb neuroprosthesis with motor imaginations (MI) to restore limb functionality of paralyzed persons. However, existing BCIs lack a natural control and need a considerable amount of training time or use invasively recorded biosignals. We show that it is possible to decode velocities and positions of executed arm movements from electroencephalography signals using a new paradigm without external targets. This is a step towards a non-invasive BCI which uses natural MI. Furthermore, training time will be reduced, because it is not necessary to learn new mental strategies.**

I. INTRODUCTION

A brain-computer interface (BCI) [1] measures biosignals originating in the brain and uses them to control devices. One important application of a BCI is the restoration of upper limb functionality of paralyzed persons [2]. The ideal solution is to detect natural movement imaginations in a non-invasive way and continuously control an arm neuroprosthesis. Here, natural means that the actually imagined arm movement (in a certain direction with a certain speed) is also executed by the arm neuroprosthesis. Thus, there exists a direct-link between motor imagination (MI) and arm neuroprosthesis movement. In this work, we assume that an arm neuroprosthesis capable of executing natural movements exists and face the problem of detecting natural movements.

Sensorimotor rhythms (SMR) [3] based BCIs detect power modulations in certain frequency bands in electroencephalography (EEG) signals [4] induced by MI. In [5] imaginations of foot movements were used for closing and opening the right hand of a patient with tetraplegia. The switching between different phases of the lateral grasp with left hand MI was shown in [2]. SMR based BCIs have the advantage of operating non-invasively, but MIs are artificially assigned to neuroprosthesis movements. Thus, MIs are not natural.

Gratifyingly, there are evidences that low frequency signals measured from cortex carry valuable information regarding arm movement trajectories. It was shown in [6] that it is possible to decode two-dimensional movement trajectories when controlling a joystick. Signals were recorded with electrocorticography (ECoG). A low frequency time-domain signal was found which correlates with movement trajectories. This signal component was referenced as local motor potential (LMP). In [7] it was shown that the arm movement direction of subjects performing a center-out task can be decoded from ECoG. Decoding information was carried by movement-related potentials as well as spectral amplitude modulations in low frequencies (< 2 Hz) and in the high gamma band. [8] successfully decoded arm movement trajectories from subjects using low frequency components from ECoG signals. There, subjects performed two-dimensional movements to random targets.

[9] proofed that three-dimensional executed arm movements can also be decoded from EEG, probably paving the way to a new generation of BCIs which decode non-invasively natural arm movement imaginations. In [9] low-pass filtered (< 1 Hz) signals were used to decode arm velocities during a center-out reaching task. It is probable that these low frequency components measured from EEG are the same as those measured from the ECoG, although yet a proof remains.

In this work we were basing on the approach from [9] and investigated if it is possible to decode arm movements from EEG (velocities and positions) using a new paradigm without external targets.

II. METHODOLOGY

A. Subjects

Five healthy right-handed subjects (3 females) participated in the experiment. Subjects s1, s2 and s3 had prior experience with BCI measurements. Subjects were seated in an armchair with their left forearm fully supported by the armrest.

B. Paradigm

Subjects moved their right arm continuously and self-chosen in front of the body in all three dimensions. We call this a continuous and self-chosen movement task. The hand was closed and the thumb was on the upside. Subjects were instructed to perform natural, round (not jaggy) and in speed varying arm movements when a trial started. To suppress eye movements, subjects were asked to fixate their gaze on a cross presented on a screen in front of them. Further restrictions were not imposed. We recorded ten trials, each lasted 65 s. For further analysis, we only used the last 60 s of a trial to exclude movement onset effects. Thus, in total we obtained 10 min movement data from each subject. The start of a trial was indicated by a short beep tone. Breaks were inserted between trials with a subject specific duration (usually around 1 min) to avoid fatigue of arm and shoulder muscles. No feedback was provided.

*This work is supported by the European ICT Programme Project FP7-224631. This paper only reflects the authors' views and funding agencies are not liable for any use that may be made of the information contained herein.

[1]Both authors are with the Institute of Knowledge Discovery, Graz University of Technology, Krenngasse 37, 8010 Graz, Austria.

Correspondence to Patrick Ofner (patrick.ofner@tugraz.at)

978-1-4577-1787-1/12/$26.00 ©2012 IEEE

C. Signal recording

Forty-nine Ag/AgCl electrodes spread over sensorimotor and frontal areas were used to record EEG signals from the scalp. Three electrooculography (EOG) electrodes were positioned above the nasion, and below the outer canthi of the eye. Reference was placed on the left ear, ground on the right ear. All electrode impedances were below 5 kΩ. After band-pass filtering between 0.01 Hz and 200 Hz with an eighth-order Chebyshev filter and applying a notch filter at 50 Hz, signals were sampled with 512 Hz using four g.USBamp amplifiers (g.tec, Graz, Austria). x/y/z coordinates of the right hand of the subjects were tracked with the Kinect sensor device (Microsoft, Redmond, USA) using the OpenNI framework (http://www.openni.org) and the NiTE middleware (PrimeSense, Tel-Aviv, Israel). We rotated the coordinate system so that the x-axis was going from right to left, the y-axis from down to up and the z-axis from front to back relative to the subject. EEG, EOG and hand positions were recorded with a customized TOBI Signal Server [10] and Matlab (MathWorks, Massachusetts, USA). After recording, we removed linear trends from raw EEG signals per trial. We filtered signals with a 100 Hz zero-phase, fourth order, low-pass Butterworth filter and down sampled to 256 Hz to reduce computational effort.

D. Decoder

1) Velocity: The velocity decoder was originally described in [9] and is only summarized here. It transforms EEG signals into instantaneous velocity signals of the (right) hand. In a preprocessing step, we low-pass filtered with a fifth-order Butterworth filter with a cutoff frequency of 1 Hz. Then, we calculated time differences of the filtered signals and normalized to a mean value of 0 and a standard deviation of 1. The resulting signals are referenced as $S_n[t]$, where n is the EEG channel number and t is the time step. The actual decoder comprises three linear models:

$$v_x = a_x + \sum_{n=1}^{N}\sum_{k=0}^{L} b_{nkx} S_n[t - kT] \quad (1)$$

$$v_y = a_y + \sum_{n=1}^{N}\sum_{k=0}^{L} b_{nky} S_n[t - kT] \quad (2)$$

$$v_z = a_z + \sum_{n=1}^{N}\sum_{k=0}^{L} b_{nkz} S_n[t - kT] \quad (3)$$

v_i is the velocity of the hand in the i-th dimension, N is the number of EEG channels, L is the number of time lags used for decoding. T is the interval between two time lags and was set to 11.7 ms, which is 3 times the smallest time step when using a sampling rate of 256 Hz. a_i and b_{nki} are the weights of the linear models. The weights were found with multiple linear regressions. As dependent variables we used 1 Hz low-pass filtered and differentiated measured x/y/z coordinates of the hand.

2) Position: Here we present an adaption of the velocity decoder which decodes *directly* hand positions of executed movements from EEG. The differentiation of the position yields the velocity. Thus, one can suppose removing the differentiation step in the velocity decoder described above would give us the actual position of the hand. We found that frequencies below 0.5 Hz negatively influence correlations. Therefore, instead of just removing the differentiation, we replaced the low-pass filter and the differentiation with a band-pass filter with cutoff frequencies at 0.5 Hz and 2 Hz. The output of the three linear models is now the position of the hand. To compute the model weights with multiple linear regressions, the band-pass filtered (0.5 Hz - 2 Hz) measured coordinates of the hand were used as dependent variables.

E. Analysis

To assess the quality of the velocity decoder we calculated for each subject Pearson correlation coefficients (r) between decoded x/y/z velocities and 1 Hz low-pass filtered measured x/y/z velocities from the Kinect. We used a 30-fold cross-validation, that means we tested against 20 s of data. For the position decoder, measured hand positions were band-pass filtered from 0.5 to 2 Hz and correlated with the decoded positions. To exclude a possible decoding of eye movements instead of brain activity, we also decoded velocities and positions from EOG.

Each channel at each time lag has three weights (b_{nkx}, b_{nky}, b_{nkz}, corresponding to the x/y/z coordinates). These weights form a vector contributing (weighted with the EEG signal) to the final velocity or position, respectively. To assess the contribution from each channel at each time lag, we computed the euclidean norm over these weight-vectors and averaged over cross-validation folds.

III. RESULTS

A. Velocity Decoder

For each subject, the mean value and standard deviation of r over all 30 cross-validation folds, when decoding velocity from EEG, are shown in Table I. The mean value and standard deviation of r over all subjects in x, y and z axis are 0.70/0.77/0.62 ± 0.13/0.11/0.15. Decoding from normally distributed random data yield maximal absolute r values of 0.03/0.12/0.07. Table II shows r when decoding from EOG. Here, the mean value and standard deviation of r over all subjects are 0.35/0.33/0.23 ± 0.22/0.20/0.16.

TABLE I
SUBJECTS MEAN VALUES AND STANDARD DEVIATIONS OF r OVER CROSS-VALIDATION FOLDS WHEN DECODING VELOCITY FROM EEG

	s1	s2	s3	s4	s5
v_x	0.53±0.09	0.71±0.08	0.79±0.07	0.74±0.11	0.73±0.10
v_y	0.84±0.06	0.78±0.09	0.71±0.09	0.78±0.09	0.71±0.13
v_z	0.71±0.08	0.54±0.16	0.67±0.06	0.50±0.16	0.67±0.12

A common weight pattern between equivalent time lags was not found across subjects. Subjects show basically at least a contribution from premotor/supplementary motor area or primary motor/sensory area. All subjects show contribution peaks at time lags 35 ms and 82 ms and a high contribution plateau between. The same contribution distribution over

TABLE II

SUBJECTS MEAN VALUES AND STANDARD DEVIATIONS OF r OVER CROSS-VALIDATION FOLDS WHEN DECODING VELOCITY FROM EOG

	s1	s2	s3	s4	s5
v_x	0.27±0.17	0.46±0.17	0.15±0.18	0.44±0.20	0.42±0.19
v_y	0.42±0.12	0.28±0.18	0.13±0.14	0.48±0.18	0.33±0.18
v_z	0.25±0.17	0.17±0.16	0.20±0.14	0.18±0.16	0.33±0.15

time lags can be observed when decoding from random data drawn from the standard normal distribution. Exemplarily, Fig. 1 shows the contribution of each EEG channel at each time lag averaged over cross-validation folds for subject s3.

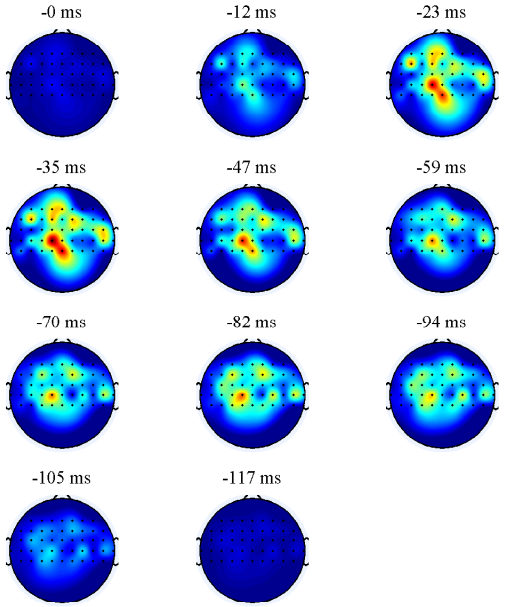

Fig. 1. Velocity decoder: Qualitative contribution of each channel at each time lag for s3. The largest contribution is colored red, the smallest blue.

An example of decoded and low-pass filtered measured velocities for subject s3 are shown in Fig. 2. The decoder was tested on run 1 and trained on runs 2 to 10.

B. Position Decoder

For each subject, the mean value and standard deviation of r over all 30 cross-validation folds, when decoding position from EEG, are shown in Table III. The mean value and standard deviation of r over all subjects in x, y and z axes are 0.70/0.78/0.62 ± 0.12/0.09/0.14. Decoding from normally distributed random data yield maximal absolute r values of 0.01/0.07/0.04. Table IV shows r when decoding from EOG. Here, the mean value and standard deviation of r over all subjects are 0.33/0.32/0.22 ± 0.22/0.19/0.14.

A common weight pattern between equivalent time lags was not found across subjects. Contributions from the 105 ms

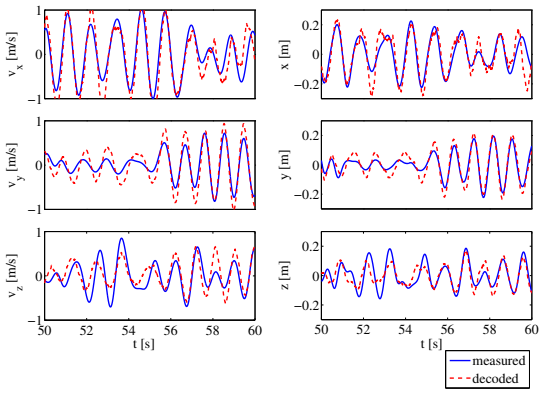

Fig. 2. Decoder example: Measured and decoded velocities (left) and positions (right) from subject 3 in the time domain.

TABLE III

SUBJECTS MEAN VALUES AND STANDARD DEVIATIONS OF r OVER CROSS-VALIDATION FOLDS WHEN DECODING POSITION FROM EEG

	s1	s2	s3	s4	s5
x	0.52±0.08	0.71±0.06	0.79±0.08	0.75±0.09	0.73±0.10
y	0.84±0.04	0.81±0.05	0.73±0.08	0.80±0.09	0.74±0.11
z	0.71±0.08	0.54±0.16	0.66±0.07	0.54±0.17	0.64±0.11

time lag were similar to contributions from the 35 ms time lag of the velocity decoder. All subjects show contributions peaks at time lags 12 ms and 105 ms and low contributions otherwise. The same contribution distribution can be observed when decoding from normally distributed random data. Exemplarily, Fig. 3 shows the contributions for subject s3.

An example of decoded and band-pass filtered measured positions for subject 3 are shown in Fig. 2.

IV. DISCUSSION

In this paper we proofed that velocity and position decoding from executed arm movements in three dimensions without external targets is possible from EEG. r values were reasonable high. In [9] r values for x/y/z-axes were 0.19/0.38/0.32, which are two to almost four times smaller than correlations measured in this work. The coordinate systems were comparable, only the x and z axes were inverted. Reasons for this discrepancy could be that we did not presented targets – movements were self-chosen – and we omitted the first 5 s of runs to exclude possible existing

TABLE IV

SUBJECTS MEAN VALUES AND STANDARD DEVIATIONS OF r OVER CROSS-VALIDATION FOLDS WHEN DECODING POSITION FROM EOG

	s1	s2	s3	s4	s5
x	0.23±0.13	0.45±0.17	0.10±0.21	0.43±0.15	0.42±0.18
y	0.40±0.12	0.27±0.15	0.11±0.13	0.49±0.17	0.32±0.16
z	0.22±0.14	0.20±0.16	0.17±0.12	0.23±0.13	0.31±0.14

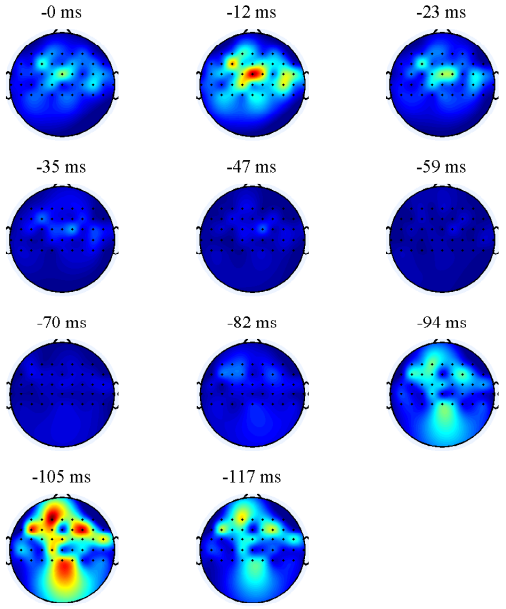

Fig. 3. Position decoder: Qualitative contribution of each channel at each time lag for s3. The largest contribution is colored red, the smallest blue.

movement onset effects. However, in the center-out reaching task used in [9] it is likely that movements were completed within 5 s. In [11] similar low r values (0.37/0.24 for x/y-axes) were obtained when decoding hand velocities from EEG during a drawing task restricted to left/right/up/down movements. Movement trajectories were self-chosen as in our work. However, because of the restriction to only four movement directions, it is obvious that executed movements were jerky and not continuous. Thus, it is possible that our relative high correlations are due to continuous movements (instead of "stop-and-go" movements).

The risk that our promising results are due to eye activity can be neglected, because the gaze of subjects was controlled, and decoding from EOG yield lower correlations than decoding from EEG. However, it is interesting that EOG based correlations were not close to 0. One reason could be that subjects moved their eyes correlated with movements over a short period of time. Another explanation is that we measured brain activity even perhaps at EOG electrodes. Low frequency biosignals are conducted better over the head than high frequency biosignals. Thus, low frequency EEG components are widespread over the scalp, and therefore even EOG electrodes could contain decodable movement information.

A common weight pattern between equivalent time lags was not observable across subjects. Weights probably include a spatial filter – in addition to the actual decoder part – to reduce the signal-to-noise ratio of the measured velocity/position coding sources. If this spatial filter is highly tuned to the head properties of a person (e.g. geometry, conductivity), each person would have an individual weight pattern. If there is more than one area on the cortex coding velocity/position information, the weight pattern differences between subjects would be even more distinct. Subjects show basically at least a contribution from premotor/supplementary motor area or primary motor/sensory area. This is similar to [9] where high contributions from precentral gyrus, postcentral gyrus, and inferior parietal lobule were found, and to [11] where premotor, posterior parietal and occipital areas showed the largest contributions (using low frequency signals for decoding). Interestingly, the contribution course over time lags can also be obtained when decoding from random data. Thus, the contribution course over time lags has to be attributed to general properties of the multiple linear regression.

A non-invasive position decoding could be the basis to control an arm neuroprosthesis in a natural manner. The position of the hand is controlled by the user with natural MI, and inverse kinematics is used to move the joints of the arm neuroprosthesis in their proper position. Furthermore, the training time will be formidable reduced, because it is not necessary to learn new mental strategies.

REFERENCES

[1] J. R. Wolpaw, N. Birbaumer, D. J. McFarland, G. Pfurtscheller, and T. M. Vaughan, "Brain-computer interfaces for communication and control," *Clinical Neurophysiology*, vol. 113, no. 6, pp. 767–791, 2002.

[2] G. R. Müller-Putz, R. Scherer, G. Pfurtscheller, and R. Rupp, "EEG-based neuroprosthesis control: a step towards clinical practice," *Neuroscience Letters*, vol. 382, pp. 169–174, 2005.

[3] G. Pfurtscheller, C. Neuper, G. R. Müller, B. Obermaier, G. Krausz, A. Schlögl, R. Scherer, B. Graimann, C. Keinrath, D. Skliris, M. Wörtz, G. Supp, and C. Schran, "Graz-BCI: state of the art and clinical applications," *IEEE Transactions on Neural Systems and Rehabilitation Engineering*, vol. 11, pp. 177–180, 2003.

[4] G. Pfurtscheller and F. H. L. D. Silva, "Event-related eeg/meg synchronization and desynchronization: basic principles," *Clinical Neurophysiology*, vol. 110, no. 11, pp. 1842–1857, 1999.

[5] G. Pfurtscheller, G. R. Müller, J. Pfurtscheller, H. J. Gerner, and R. Rupp, ""Thought"-control of functional electrical stimulation to restore handgrasp in a patient with tetraplegia," *Neuroscience Letters*, vol. 351, pp. 33–36, 2003.

[6] G. Schalk, J. Kubánek, K. J. Miller, N. R. Anderson, E. C. Leuthardt, J. G. Ojemann, D. Limbrick, D. Moran, L. A. Gerhardt, and J. R. Wolpaw, "Decoding two-dimensional movement trajectories using electrocorticographic signals in humans," *Journal of Neural Engineering*, vol. 4, no. 3, pp. 264–275, 2007.

[7] T. Ball, A. Schulze-Bonhage, A. Aertsen, and C. Mehring, "Differential representation of arm movement direction in relation to cortical anatomy and function," *Journal of Neural Engineering*, vol. 6, no. 1, 2009.

[8] T. Pistohl, T. Ball, A. Schulze-Bonhage, A. Aertsen, and C. Mehring, "Prediction of arm movement trajectories from ecog-recordings in humans," *Journal of Neuroscience Methods*, vol. 167, no. 1, pp. 105–114, 2008.

[9] T. J. Bradberry, R. J. Gentili, and J. L. Contreras-Vidal, "Reconstructing three-dimensional hand movements from noninvasive electroencephalographic signals," *Journal of Neuroscience*, vol. 30, pp. 3432–3437, 2010.

[10] C. Breitwieser, A. Kreilinger, C. Neuper, and G. R. Müller-Putz, "The TOBI hybrid BCI – the data acquisition module," in *Proceedings of the First TOBI Workshop 2010*, 2010, p. 58.

[11] J. Lv, Y. Li, and Z. Gu, "Decoding hand movement velocity from electroencephalogram signals during a drawing task," *BioMedical Engineering OnLine*, vol. 9, no. 64, 2010.

Primary Publication II

Appendix

Using a Noninvasive Decoding Method to Classify Rhythmic Movement Imaginations of the Arm in Two Planes

Patrick Ofner, *Student Member, IEEE*, and Gernot R. Müller-Putz*, *Member, IEEE*

***Abstract*—A brain–computer interface (BCI) can help to overcome movement deficits in persons with spinal-cord injury. Ideally, such a BCI detects detailed movement imaginations, i.e., trajectories, and transforms them into a control signal for a neuroprosthesis or a robotic arm restoring movement. Robotic arms have already been controlled successfully by means of invasive recording techniques, and executed movements have been reconstructed using noninvasive decoding techniques. However, it is unclear if detailed imagined movements can be decoded noninvasively using electroencephalography (EEG). We made progress toward imagined movement decoding and successfully classified horizontal and vertical imagined rhythmic movements of the right arm in healthy subjects using EEG. Notably, we used an experimental design which avoided muscle and eye movements to prevent classification results being affected. To classify imagined movements of the same limb, we decoded the movement trajectories and correlated them with assumed movement trajectories (horizontal and vertical). We then assigned the decoded movements to the assumed movements with the higher correlation. To train the decoder, we applied partial least squares, which allowed us to interpret the classifier weights although channels were highly correlated. To conclude, we showed the classification of imagined movements of one limb in two different movement planes in seven out of nine subjects. Furthermore, we found a strong involvement of the supplementary motor area. Finally, as our classifier was based on the decoding approach, we indirectly showed the decoding of imagined movements.**

***Index Terms*—Brain–computer interface, electroencephalography (EEG), movement decoding, movement imagery.**

I. Introduction

A BRAIN–COMPUTER interface (BCI) [1] records brain signals and transforms them into control signals for devices. One group of potential BCI users are persons with spinal-cord injury (SCI) [2]. Such users will have lost control of body parts and a BCI in combination with a neuroprosthesis, e.g., functional electrical stimulation, can be used to restore motor functions. Ideally, a person with SCI imagines a certain movement, which is executed instantly by means of the system. The BCI is used to decode the movement imagination (MI), and a neuroprosthesis is used to generate the movement. An optimal BCI would decode the actual detailed MI, i.e., the user imagines with, e.g., the hand a movement on a certain trajectory, and the exact trajectory should be decoded by the BCI. Thus, a direct link between the MI and a paralyzed body part would be reestablished, giving the user the possibility to control movements in an entirely natural way. Of course, in addition to a decoder, this also necessitates a highly sophisticated neuroprosthesis and compensation for the lacking sensory (especially proprioceptive) feedback to execute precise movements. Today, neuroprostheses can restore some movement functionality [3], but are still not capable of performing natural human arm movements with similar degrees of freedom and precision. Also, sensory feedback compensation or restoration is still under research [4], [5]. However, the work presented here is solely about the MI decoding part of a neuroprosthesis.

Promising results have been reported for invasive BCIs with intracortically implanted arrays, also called brain–machine interfaces (BMIs). In [6], a person with SCI controlled a cursor and a robotic arm; in [7], two persons with tetraplegia caused by brainstem stroke controlled a robotic arm; a person with a motor complete injury due to spinocerebellar degeneration, but with generally intact sensation, controlled a seven-degree-of-freedom robotic arm in [8]. BMIs provide good brain signal qualities; however, the implantation requires the opening of the skull and the penetration of the pia mater, which can cause serious infections. Probably, one would feel more comfortable with an alternative and that is where noninvasive BCIs come in. Furthermore, experiments can be conducted with less effort and costs.

Today's noninvasive BCIs can detect the process of MI [9], but not the detailed MI itself (i.e., imagined trajectories). They are based on power changes in sensorimotor rhythms (SMR) accompanying MI [10]. In the work of Pfurtscheller *et al.* [11], foot MI was used to restore the lateral grasp in a tetraplegic patient's right hand. Müller-Putz *et al.* [2] showed the switching between different lateral grasp phases with left hand MI, and just recently, [12], [13] showed the restoration of hand and elbow functions. The control of a 2-D and 3-D cursor, respectively, has been demonstrated in [14] and [15] by biofeedback training. Potentially, instead of the cursor, a robotic arm or neuroprosthesis could also have been controlled. Although these BCIs restored substantial movement functionality, or could be extended to that, they were not controlled in a familiar and natural way by the user. SMR-based BCIs often require an

Manuscript received June 24, 2014; revised November 12, 2014; accepted November 25, 2014. Date of publication December 4, 2014; date of current version February 16, 2015. This work was supported by the European ICT Programme Project FP7-224631. *Asterisk indicates corresponding author.*

P. Ofner is with the Institute for Knowledge Discovery, Graz University of Technology, and also with BioTechMed-Graz.

*G. R. Müller-Putz is with the Institute for Knowledge Discovery, Graz University of Technology, 8010 Graz, Austria, and also with BioTechMed-Graz, 8010 Graz, Austria (e-mail: gernot.mueller@tugraz.at).

Color versions of one or more of the figures in this paper are available online at http://ieeexplore.ieee.org.

Digital Object Identifier 10.1109/TBME.2014.2377023

Appendix

artificial association between MI and movement functionality. Classification performance is crucial, and scientists are, therefore, forced to use the best classifiable MIs and not the most similar MIs. Furthermore, as the user has to learn a new mental strategy, SMR-based BCIs often require a long training period of weeks or months. However, the learning period for a *decoder* based BCI should be substantially reduced because MIs are natural and have already been learned. Therefore, the learning of a new mental strategy is no longer necessary.

Although Yuan *et al.* [16] found a correlation between mu and beta band activity with the speed of imagery hand clenching, the traditional mu and beta bands used in SMR-based BCIs are rather associated with general movement activity but contain only little information about movement trajectories [17]–[19]. Interestingly, low-frequency (<4 Hz) time-domain brain signals measured with electroencephalography (EEG), electrocorticography (ECoG), or magnetoencephalography (MEG) seem to provide proper decodable information about movement trajectories. Two-dimensional hand positions during arm movements have been predicted in the work of Pistohl *et al.* [20] from human ECoG low-frequency time-domain signals. Schalk *et al.* [21] decoded 2-D movement trajectories during joystick control, and Milekovic *et al.* [22] demonstrated an online classification of 1-D joystick movement directions. The decoding of movement directions during a center-out task has been shown by Ball *et al.* [18]. Acharya *et al.* [23] reported about finger position decoding during slow hand grasps. Movement decoding has also been investigated in human MEG signals. The prediction of movement trajectories in a pentagon copying task with a 2-D joystick has been reported by Georgopoulos *et al.* in [24], and Bradberry *et al.* [25] decoded hand velocities in a center-out drawing task. Toda *et al.* [26] reconstructed 2-D index fingertip trajectories during pointing movements. Also, 3-D velocity decoding of movements in a center-out task has already been reported by Yeom *et al.* [27]. Waldert *et al.* [17] decoded hand movement directions on a single-trial basis. Wang *et al.* [28] decoded four different wrist MIs in a 2-D center-out task. Jerbi *et al.* [29] found phase locking between slow oscillatory brain rhythms and time-varying hand speed. Finally, movements have been decoded from EEG too. Bradberry *et al.* [30] decoded hand movement velocities in a center-out out reaching task, and Lv *et al.* [31] decoded hand movement velocities during a drawing task in four directions. Our group showed the 3-D decoding of hand velocities and positions in a continuous self-chosen movement task [32]. Notably, we used longer lasting movements, about 1 min during each trial, instead of short lasting center-out reaching movements, which last usually around 1 s. The often used correlation measure of short lasting movements can be misinterpreted (see [33]). This is because a short-time window does not contain multiple periods of the movement position signal at low frequencies. However, as we used longer lasting movements, this was not an issue in our work.

The aforementioned EEG studies had in common that they all used low-frequency and mostly time-domain signals to decode or classify executed movements. However, our targeted subjects are persons with SCI who are mainly restricted to MI; thus, the next step is to try to decode MI from healthy subjects. Vučković and Sepulveda already showed the classification of imagined wrist movements using delta band features [34], [35]. Gu *et al.* found in healthy subjects [36] and in amyotrophic lateral sclerosis patients [37] that the speed of imagined wrist movements (fast and slow) is encoded in the movement-related cortical potential. Thus, discrete imagined movement types of the same limb (wrist) and velocities have been already decoded from low EEG frequencies. However, finally, we would like to decode imagined continuous movement trajectories of the arm and use it as a control signal for neuroprostheses. Bradberry *et al.* [38] made a first attempt to control a computer cursor in 2-D with decoded imagined finger/arm movements. However, only one target was presented on a screen in each trial, and Poli and Salvaris [39] showed that a random cursor also hits this target after some time, and they reached similar decoding results. Thus, we designed a new experiment where subjects imagined arm movements and decoded them (preliminary results have been shown in [40] and [41]). However, there is one substantial issue. We have to know the imagined movement trajectories—either the hand velocity or position—to train and test the decoder. But the imagined trajectories must be determined without inducing eye movements, which excludes following a known cursor trajectory on a computer screen. That would cause eye dipole movements which would heavily influence the recorded EEG and the decoder might be trained on eye movements instead of MI. Of course, methods exist which can rid the EEG of eye movements. They are also used in this study, but usually they just attenuate the influence of eye movements. There is no guarantee that they remove the influence completely. In addition to this influence caused by the electrical fields of the eye dipoles, eye movements could potentially modulate brain sources. In this case, eye movements instead of MI would be decoded again. Indeed, Pesaran *et al.* [42] showed that eye movements modulate the neural activity in the dorsal premotor area in monkeys. Therefore, we avoided eye movements in our experimental design.

In our work, subjects imagined rhythmic arm movements either in the horizontal or vertical plane. These movements were synchronized to the beats of a metronome. Thus, we knew the imagined movement trajectories. Afterward, we decoded the MI trajectories for a few seconds from low-frequency time-domain signals and, then, classified the movement plane. In the following, we analyze the performance of the decoder-based classifier and show the involved brain regions in the sensor and source space.

II. Methods

A. Subjects

We recruited nine healthy and right-handed subjects (four females and five males). Most of them had already participated in BCI experiments. They were aged between 23 and 37 with a mean value of 26.1 and a standard deviation of 4.3.

B. Paradigm

Subjects were comfortably seated in an arm chair with a computer screen in front of them displaying cues. They imagined

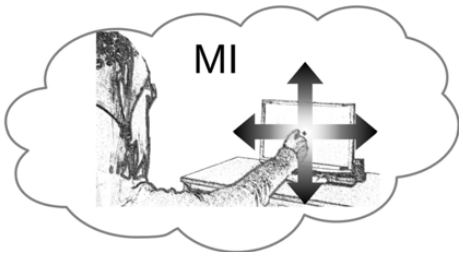

Fig. 1. Subjects imagined rhythmic movements in the horizontal or vertical plane. The gaze was fixated on a cross on the screen.

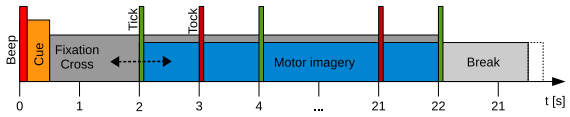

Fig. 2. Sequence of a trial. At second 0, a cue appeared (an arrow pointing right or up) together with a beep to gain the subject's attention, followed by a gaze-fixation cross. Between 1.5 and 2.5 s started a metronome to tick for 20 s.

horizontal or vertical repetitive rhythmic arm movements from left to right and back, or from bottom to top and back, respectively, for 20 s within each trial (see Fig. 1). The cue was an arrow pointing to the right, indicating horizontal movements starting from the left, or pointing upwards, indicating vertical movements starting from the bottom. Subjects were asked to imagine natural, round, not jagged movements with the extended right arm. During the trial, a cross was shown on the screen to fixate the gaze of the subject and to suppress eye movements. We instructed subjects to synchronize the MIs to beep tones with a rhythm of 1 Hz presented by a computer. As a beep tone corresponded to an end position of the imagined trajectories, MIs were actually done with 0.5 Hz. See Fig. 2 for the exact sequence of a trial. We recorded ten trials per run and eight runs, in total 80 trials with equally distributed classes. To remove the influence of eye movements from the EEG using a linear regression method, we also recorded one run with 30-s-long deliberate eye movements. Furthermore, we recorded four runs (each of 30 s) of baseline EEG without any beep tones and MI. These runs were used to calculate the noise covariance matrices needed for source imaging.

C. Recording

We recorded the EEG with 68 electrodes covering frontal, central, and parietal areas. Reference was placed on the left mastoid, ground on the right mastoid. Additionally, we recorded the electrooculogram with three electrodes placed above the nasion and below the outer canthi of the eyes. All signals were recorded with five g.USBamp amplifiers (g.tec medical engineering GmbH, Schiedlberg, Austria). We applied an eighth-order Butterworth bandpass filter with cutoff frequencies at 0.01 and 100 Hz, a Notch filter at 50 Hz, and then sampled the signals with 256 Hz. For subsequent source imaging, we also measured the positions of the electrodes with a CMS 20 EP system (Zebris Medical GmbH, Isny, Germany).

D. Preprocessing

Using EEGLAB [43], we computed the independent components (ICs) with the extended infomax independent component analysis [44] in the frequency range 0.2–70 Hz (fourth-order zero-phase Butterworth filter) and searched for ICs suspected to be muscle, eye, technical artifacts, or ICs obviously common to all electrodes. Then, we removed artifact contaminated ICs from the original unfiltered data. Subsequently, we applied a zero-phase antialiasing filter and downsampled data to 16 Hz for computational convenience. To get the signal of interest—which was expected to be at the movement frequency of 0.5 Hz—we bandpass filtered the data with a second-order zero-phase Butterworth filter with cutoff frequencies at 0.4 and 0.6 Hz. We found empirically the filter order and the bandwidth which worked for us. Finally, we removed possible remaining eye artifacts [45] and removed samples when their absolute value exceeds a threshold of 4.4 times the median absolute deviation (MAD) [46] of a channel. MAD is a robust deviation measure and corresponds to three times the standard deviation with normally distributed data. This caused a removal of 6.2–19.8% of data.

E. Partial Least Squares

As multicollinearity [47] is a serious issue in our data and prevents the interpretation of, e.g., multiple linear regression weights, we used partial least squares (PLS) [48], [49]. PLS is a method used to model the relation between observed variables. It considers the internal structure of the data by using latent (hidden, unobservable) variables. Furthermore, it can deal with many noisy and multicollinear variables. PLS has its usefulness in modeling, regression, classification, and dimension reduction applications. PLS is a key component in our classification method and source contribution analysis, and hence, we give a brief general overview of PLS modeling and PLS regression. PLS regression is used for decoding in Section II-F; PLS modeling is used to find the sources involved in movement decoding in Sections II-G and II-H.

1) Modelling: Let $\mathbf{X}$ be an $n \times N$ matrix of predictor variables (i.e., EEG data), and $\mathbf{Y}$ be an $n \times M$ matrix of response variables (i.e., movement positions). The rows of these matrices correspond to observations and the columns to predictor and response variables, respectively. In PLS, $\mathbf{X}$ and $\mathbf{Y}$ are decomposed into:

$$\mathbf{X} = \mathbf{T}\mathbf{P}^{\mathrm{T}} + \mathbf{E} \tag{1}$$

$$\mathbf{Y} = \mathbf{U}\mathbf{Q}^{\mathrm{T}} + \mathbf{F}. \tag{2}$$

$\mathbf{T}$ and $\mathbf{U}$ are the latent variables and are called scores. $\mathbf{T}$ and $\mathbf{U}$ are $n \times P$ matrices with n observations and P components. In general, $\mathbf{T}$ is an orthogonal matrix, and in our case, $\mathbf{T}$ was also orthonormal, which makes a normalization step unnecessary. $\mathbf{P}$ and $\mathbf{Q}$ are the so-called loadings and can be seen as regression weights to approximate the original data ($\mathbf{X}$ and $\mathbf{Y}$ matrices) with $\mathbf{E}$ and $\mathbf{F}$ as the residuals. $\mathbf{P}$ is of dimension $N \times P$, and $\mathbf{Q}$ is $M \times P$. The basic idea in PLS is now to find scores $\mathbf{T}$ and $\mathbf{U}$ with maximum covariance between them. In that way, $\mathbf{T}$ multiplied by the loadings $\mathbf{Q}^{\mathrm{T}}$ is also a good predictor of $\mathbf{Y}$

with a residual matrix $\mathbf{G}$:

$$\mathbf{Y} = \mathbf{T}\mathbf{Q}^{\mathrm{T}} + \mathbf{G}. \tag{3}$$

Thus, $\mathbf{T}$ models the structure behind $\mathbf{X}$ and $\mathbf{Y}$ in the latent variable space. $\mathbf{T}$ is calculated from $\mathbf{X}$ using the weight matrix $\mathbf{W}$ with dimension $N \times P$:

$$\mathbf{T} = \mathbf{X}\mathbf{W}. \tag{4}$$

How $\mathbf{W}$ is calculated depends on the actual PLS algorithm; here, we used the SIMPLS algorithm [50]. Now, the loadings are useful for interpreting the relations between predictor and response variables, even when there are serious multicollinearities as the scores $\mathbf{T}$ are orthogonal.

2) Regression: PLS can also be used as a regression method. Inserting (4) in (3) gives

$$\mathbf{Y} = \mathbf{X}\mathbf{W}\mathbf{Q}^{\mathrm{T}} + \mathbf{G}. \tag{5}$$

With the $N \times M$ dimensional matrix

$$\mathbf{B} = \mathbf{W}\mathbf{Q}^{\mathrm{T}}. \tag{6}$$

$\mathbf{Y}$ can be approximated as $\hat{\mathbf{Y}}$:

$$\hat{\mathbf{Y}} = \mathbf{X}\mathbf{B} \tag{7}$$

where the columns of $\mathbf{B}$ contain the linear regression coefficients for each dimension of the response variable. Please note that we have shown the general case of a multidimensional response variable, but in the remaining part of this study, we only deal with 1-D response variables, i.e., $\hat{\mathbf{Y}}$ has the dimension $n \times 1$.

F. Calculation of the Classification Accuracy

Our classification approach is based on the decoding principle [30], [32]. We decoded the horizontal and vertical component of the MI and correlated each one with an assumed sinusoidal movement trajectory, and then assigned the MI to the component with the higher correlation, this being a two-class classification. The imagined movement positions in the horizontal/vertical plane were assumed to follow a 0.5-Hz sinus curve over time. The left/bottom end position corresponded to -90° and the right/top end position to $+90^{\circ}$. This is justified as movements started from a position with maximum deflection, accelerated, and reached their maximum speed in the middle, then decelerated and stopped at the other end point, and so forth.

We extracted the EEG and the assumed movement positions in a certain decoding window w within train trials and independently trained two linear models (the horizontal and the vertical model) with PLS regression. The decoding window w ranged from 2 to 18 s after the metronome began to tick; thus, we omitted the first and last 2 s of every MI phase to avoid any transient response of the zero-phase filter. We trained each model using the full-channel EEG from the current time step and from three time lags at 62.5, 125, and 187.5 ms as the predictor variables, and the assumed movement trajectory as the response variable. Thus, the input dimension of each model was 273 (68 channels, four time points, one bias), and the output dimension was 1. Equations (8) (horizontal or H-model) and (9) (vertical or V-model) show the two linear models used for position decoding. N is the number of channels, L the number of time lags, T the interval between time lags, $S_n[t]$ is the preprocessed EEG signal at electrode n at time point t, h and v are the decoded positions in the horizontal and vertical plane, respectively, and a and b are the coefficients found with the two PLS regressions:

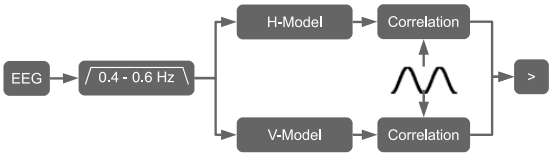

Fig. 3. Classification method is based on the decoding approach. The EEG signal is bandpass filtered and the horizontal and vertical positions are decoded. Afterward, the decoded positions are correlated with the assumed sinusoidal positions, and the trial is classified as horizontal or vertical MI depending on which decoding model yielded the higher correlation.

$$h[t] = a_{\mathrm{h}} + \sum_{n=1}^{N}\sum_{k=0}^{L} b_{n\,k\,\mathrm{h}} S_n[t - kT] \tag{8}$$

$$v[t] = a_{\mathrm{v}} + \sum_{n=1}^{N}\sum_{k=0}^{L} b_{n\,k\,\mathrm{v}} S_n[t - kT]. \tag{9}$$

To classify a trial, we used the same decoding window w as in the training step to extract the EEG from the trial and applied the H- and V-models to the extracted EEG and decoded the positions. Subsequently, we correlated the output of each model with a 0.5-Hz sinusoidal oscillation (Pearson correlation coefficient, r) and assigned the trial to the class (horizontal or vertical) corresponding to the model yielding the higher correlation. See Fig. 3 for a visualization of the classification method. To assess the classification method, we used a 10×10 fold cross-validation, trained the regression models with the trials in each train set, and classified the trials in the corresponding test sets. Finally, we calculated the classification accuracy for each cross-validation fold.

To test the validity of our approach, we assumed a 0.7-Hz sinusoidal trajectory (instead of the correct one with 0.5 Hz) and shifted the 0.4–0.6-Hz bandpass applied in the preprocessing step to 0.6–0.8 Hz. As the subjects did not imagined movements with this frequency, there should be no correlation with this trajectory and no significant classification accuracies should be reached. Furthermore, we calculated the classification accuracies when using electrodes only from the sensorimotor area and the supplementary motor area (SMA). Here, we used 24 electrodes of our custom made electrode caps; the electrodes covered positions close to FC1, FCz, FC2, C3, C1, Cz, C2, C4, CP3, CP1, CPz, CP2, CP4 (10–20 system).

G. Sensor Space Contributions

It is of great interest to determine the electrodes contributing the most to the classification, either to validate the method or to gain more knowledge about the underlying processes. However, the channels were highly correlated and multiple linear regression weights would not be interpretable (see Sections III and IV

for further information); therefore, we used PLS to analyze the relations between EEG and MI.

In the contribution analysis, we used the whole EEG dataset as training data for the PLS. Keeping the PLS model in Section II-E in mind, the predictor variables in $\mathbf{X}$ correspond to the EEG data including time lags, and the response variable in $\mathbf{Y}$ corresponds to the assumed movement position. The $n \times P$ latent variables $\mathbf{T}$ are the sources containing decodable movement information and expand over the channels and time lags. The $1 \times P$ loadings $\mathbf{Q}$ can be seen as regression weights, which show the MI information contained in every single latent variable. The projection of the $P = 272$ latent variables (68 channels $\cdot$ 4 time lags) back to the channel and time lag space is given through the loadings $\mathbf{P}$. We independently decoded the horizontal and vertical MI component and, therefore, used two models with their own set of loadings and scores, i.e., the H- and V-models. For these models, two interpretable $(N \cdot (L+1) \times 1)$-dimensional vectors can be obtained:

$$\mathbf{c}_\mathrm{h} = \mathbf{P}_\mathrm{h}\mathbf{Q}_\mathrm{h}^\mathrm{T} \tag{10}$$

$$\mathbf{c}_\mathrm{v} = \mathbf{P}_\mathrm{v}\mathbf{Q}_\mathrm{v}^\mathrm{T}. \tag{11}$$

$\mathbf{c}_\mathrm{h}$ and $\mathbf{c}_\mathrm{v}$ consist of the back projections of the latent variables into the channel/time lag space, summed and weighted by their importance to the decoding procedure. In this study, we are solely interested in the origin of the decoding sources, and not, e.g., in the decoder internals. Thus, we averaged the elements of $\mathbf{c}_\mathrm{h}$ and $\mathbf{c}_\mathrm{v}$ over the time lags, which changed the dimensions of $\mathbf{c}_\mathrm{h}$ and $\mathbf{c}_\mathrm{v}$ from $N \cdot (L+1) \times 1$ (channel/time lag space) to $N \times 1$ (channel space). Then, we calculated the 2-norm of corresponding entries in $\mathbf{c}_\mathrm{h}$ and $\mathbf{c}_\mathrm{v}$ and call that the contribution of a channel. The contributions are proportional to the amplitudes of the latent variables projected to the channels and the importance of the latent variables for the decoding.

H. Source Space Contributions

To analyze the contributions in the source space, we used the same procedure as described in Section II-G, but with brain sources instead of electrode channels. We used the software Brainstorm [51], computed boundary element head models with the Colin27 brain model included in Brainstorm and subject individual electrode positions, rereferenced the data to a common average reference (a prerequisite of Brainstorm's source imaging algorithms), and estimated the (full) noise covariance matrices based on the baseline runs with a shrinkage regularization [52]. Subsequently, we computed 15 028 brain sources using standardized low-resolution brain electromagnetic tomography [53]. The source orientations were constrained normal to the cortex. Unusual high loadings in the loading matrix $\mathbf{Q}$ indicated overfitting. As a remedy and because of limited computing resources, we limited the number of latent variables to 150.

III. Results

A. Classification Accuracies

We used the method described in Section II-F to calculate the classification accuracies. Here, the decoding window w was fixed to 2–18 s after the start of the metronome. Table I shows the mean values and standard deviations over all cross-validation folds for all subjects. The significance level is 59% with $\alpha = 0.05$ [54]. The grand average over all nine subjects is $64 \pm 10\%$. Seven subjects reached a significant classification accuracy.

TABLE I
OBTAINED CLASSIFICATION ACCURACIES WITH THE MEAN VALUES AND STANDARD DEVIATIONS OVER THE CROSS-VALIDATION FOLDS

subject	**s1**	**s2**	s3	**s4**	**s5**	s6	**s7**	**s8**	**s9**	avg.
mean value [%]	65	61	51	75	65	48	68	75	74	64
std. dev. [%]	17	17	16	14	16	18	15	16	14	10

Subjects with significant classification results are written in bold. The average values were calculated using subjects' mean classification. values.

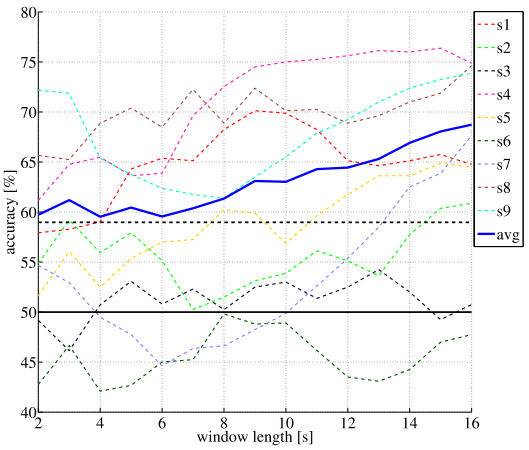

Fig. 4. Dependency of the classification accuracy on the decoding window w length. Averaged values over all subjects except s3 and s6 are shown as a blue solid line. The solid black horizontal line marks the chance level; the dashed black horizontal line represents the significance level ($\alpha = 0.05$).

To analyze the influence of the decoding window length, we changed the window length in 1-s steps from 2 to 16 s. The window always started 2 s after the cue presentation. The classification accuracies in dependence on the decoding window length are shown in Fig. 4. An increase of the classification accuracy over the window length is observable for subjects s2, s4, s5, s7, s8, and s9. Subjects s2 and s9 show initial peaks; s1 shows a peak in the middle. Furthermore, Fig. 4 shows the averaged accuracies over all subjects except those subjects which never reached a significant classification accuracy (s3 and s6). A simple linear regression analysis shows a significant dependence of the averaged classification accuracy on the window length ($p < 0.05$). The fitted regression line (not shown) has a slope of 0.66, indicating a positive dependence of the classification accuracy on the window length, and the window length explains $R^2 = 89\%$ of the variance of the classification accuracy.

Table II shows the classification accuracies when assuming a wrong movement trajectory, i.e., a sinusoidal trajectory with

Appendix

TABLE II
OBTAINED CLASSIFICATION ACCURACIES WITH THE MEAN VALUES AND STANDARD DEVIATIONS OVER THE CROSS-VALIDATION FOLDS WHEN ASSUMING A 0.7-HZ MOVEMENT TRAJECTORY

subject	s1	s2	s3	s4	s5	s6	s7	s8	s9	avg.
mean value [%]	43	50	46	42	43	53	44	53	54	48
std. dev. [%]	18	16	17	18	16	17	16	17	16	5

The average values were calculated using subjects' mean classification values.

TABLE III
OBTAINED CLASSIFICATION ACCURACIES WITH THE MEAN VALUES AND STANDARD DEVIATIONS OVER THE CROSS-VALIDATION FOLDS WHEN USING ELECTRODES ONLY FROM THE SENSORIMOTOR AREA AND THE SMA

subject	**s1**	**s2**	s3	**s4**	s5	s6	s7	**s8**	**s9**	avg.
mean value [%]	63	65	48	77	56	57	57	71	84	64
std. dev. [%]	15	17	18	13	15	20	17	15	13	11

Subjects with significant classification results are written in bold. The average values were calculated using subjects' mean classification. values.

TABLE IV
PEARSON CORRELATION COEFFICIENT AVERAGED OVER ALL TEST TRIALS WHEN DECODING POSITIONS USING THE H/V MODEL AND IMAGINING HORIZONTAL/VERTICAL MOVEMENTS

subject	s1		s2		s3		s4		s5	
model	H	V	H	V	H	V	H	V	H	V
hor MI	**0.55**	0.46	**0.23**	0.18	**0.02**	0.05	**0.52**	0.09	**0.11**	−0.06
vert MI	0.47	**0.71**	0.20	**0.43**	0.07	**0.10**	0.06	**0.49**	−0.03	**0.18**
subject	s6		s7		s8		s9		avg	
model	H	V	H	V	H	V	H	V	H	V
hor MI	**0.21**	0.22	**0.19**	−0.04	**0.41**	0.05	**0.49**	0.23	**0.30**	0.13
vert MI	0.22	**0.07**	−0.03	**0.11**	0.01	**0.35**	0.25	**0.63**	0.14	**0.34**

TABLE V
SIGNIFICANT DIFFERENCES BETWEEN CORRELATIONS REACHED WITH THE H- AND V-MODEL WHEN IMAGING HORIZONTAL OR VERTICAL MOVEMENTS, TESTED WITH A BONFERRONI CORRECTED SIGN TEST

subject	s1	s2	s3	s4	s5	s6	s7	s8	s9
horizontal MI	∗			∗	∗		∗	∗	∗
vertical MI	∗	∗		∗	∗		∗	∗	∗

Significant differences ($\alpha = 0.05$) are marked with an asterisk.

TABLE VI
BONFERRONI CORRECTED SIGN TEST IF THE CORRELATIONS REACHED WITH AN H- OR V-MODEL AND HORIZONTAL OR VERTICAL MI HAD A NONZERO MEDIAN

subject	s1		s2		s3		s4		s5	
model	H	V	H	V	H	V	H	V	H	V
hor MI	∗	∗	∗	∗		∗	∗		∗	∗
vert MI	∗	∗	∗	∗	∗	∗		∗		∗
subject	s6		s7		s8		s9			
model	H	V	H	V	H	V	H	V		
hor MI	∗	∗	∗		∗		∗	∗		
vert MI	∗			∗		∗	∗	∗		

Significant differences ($\alpha = 0.05$) are marked with an asterisk.

0.7 Hz. Here, none of the subjects reached a significant classification accuracy above 59% with $\alpha = 0.05$. The classification accuracies are statistically significantly lower than the classification accuracies yielded by the correct movement trajectory, i.e., 0.5 Hz, with respect to the median value (sign test, $p < 0.05$).

Table III shows the classification accuracies when using electrodes only from the sensorimotor area and the SMA. Subjects s1, s2, s4, s8, and s9 reached again a significant classification accuracy, but not s5 and s7 as when using all electrodes. However, the classification accuracies of both electrode configurations (all versus sensorimotor/SMA electrodes) do not differ statistically significantly with respect to the median value (sign test, $p = 1$).

The classification of a trial depended on whether the V- or H-model yield the higher correlation. Table IV shows the mean value over all test trials of the Pearson correlation coefficient, and the grand average over all subjects. The subjects' averaged standard deviations over the test trials are 0.35 (horizontal MI/H-model), 0.40 (horizontal MI/V-model), 0.38 (vertical MI/H-model), and 0.33 (vertical MI/V-model). For subjects with a significant classification accuracy, correlations are always higher when decoding a MI with the correct (= associated) model as opposed to with the wrong model. We used a Bonferroni corrected sign test to test for statistical significant differences between correlations obtained with the H- and V-models while fixating the type of MI, i.e., we tested if the differences between paired correlations had a nonzero median distribution. Table V shows the significant differences ($\alpha = 0.05$) when imaging horizontal or vertical movements, respectively. Subjects s3 and s6 showed no significant difference between correlations yielded by the H- and V-models and, therefore, did not reach a significant classification accuracy. Subject s2 only showed a significant difference when decoding vertical MI, not when decoding horizontal MI. This is consistent with the observation that s2 reached the lowest significant classification accuracy. Furthermore, we used a Bonferroni corrected sign test and $\alpha = 0.05$ to test whether the correlations had a nonzero median (see Table VI). All subjects which reached a significant classification accuracy had a median correlation significantly different from 0 when decoding MI with the associated decoding model. Subjects s4, s7, and s8 showed no significant difference from a zero median when decoding an MI with a notassociated decoding model, which was expected. However, the other subjects have significant nonzero medians when decoding an MI with a not-associated decoding model. We selected the sign test because correlation coefficients are not normally distributed (due to the range limitation).

B. Sensor Space Contributions

Due to high correlations between channels, we used PLS regression. To assess the amount of correlation, we calculated the Pearson correlation coefficient between all channel

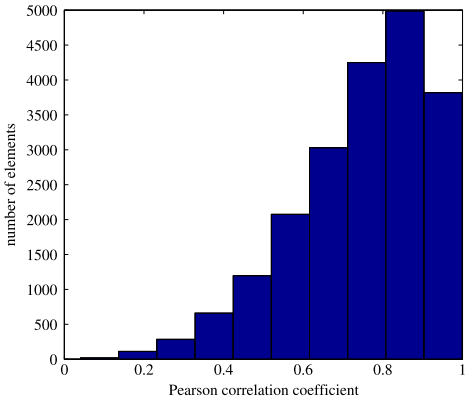

Fig. 5. Histogram showing a large number of high Pearson correlation coefficients between EEG channels. Included are all channel combinations and subjects.

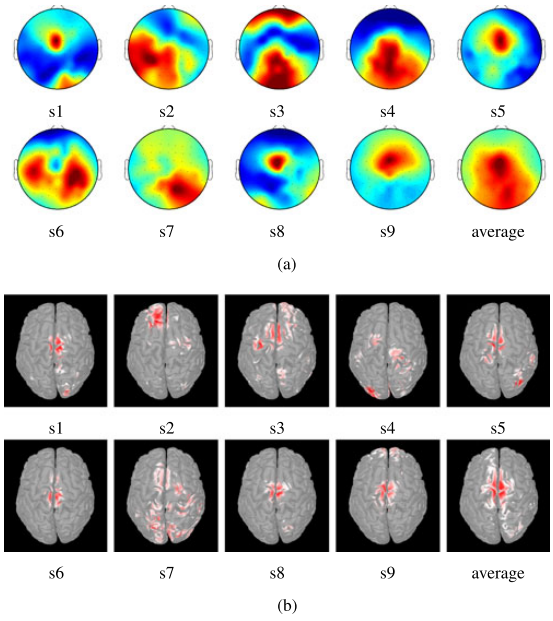

Fig. 6. Contribution of the channels and brain sources, respectively, to the decoded positions for each subject and the average. (a) Contributions of the channels. Red is mapped to the maximum value, blue corresponds to zero. (b) Contribution of the brain sources. Contributions below 50% of each subjects maximum contribution are not shown. Red is mapped to the maximum value, white to 50% of the maximum value.

combinations for each subject. Here, we used preprocessed data between 2 and 18 s after the start of the metronome. Fig. 5 shows a histogram of the Pearson correlation coefficient including coefficients from all channel combinations and subjects. The histogram shows a substantial number of high channel correlations, which make traditional regression weights uninterpretable.

We analyzed the contribution of each channel to the decoding as described in Section II-G. Fig. 6(a) shows the contribution of the channels to the decoded positions for all subjects. Additionally, the average over all subjects is shown. Before averaging, we normalized all maps to the corresponding maximum contribution. Subjects s1, s5, s8, and s9 show strong contributions from channels over the SMA. A contribution of the SMA and the parietal area can be observed in the averaged plot.

C. Source Space Contributions

Analogous to the sensor level analysis, we calculated the decoding contribution of each voxel or brain source, respectively. Fig. 6(b) shows the contributions of the voxels for all subjects and the average based on normalized maps. All subjects except s2 show an involvement of central motor regions. Subjects s1, s5, s8, and s9 show focal contributions from the SMA. The averaged plot indicates contributions from the SMA.

IV. Discussion

We showed the successful classification of rhythmic MI in two orthogonal planes (horizontal versus vertical). Seven out of nine subjects reached a significant classification accuracy. Moreover, as our classification method is based on the decoder presented in [30] and [32], we indirectly showed the decoding of MI from EEG.

The correlations were lower than the correlations reached in a decoding experiment performed by our group with executed movements [32]. There, average correlation coefficients of 0.70 (X) and 0.78 (Y) were measured, but here we obtained 0.30 (X) and 0.34 (Y). Reasons could be that executed movements are better decodable than imagined movements, or that movement execution is an easier task than MI. That is to say subjects probably make more errors when imagining a given trajectory because of the lack of direct feedback, which would be necessary for movement corrections. Unfortunately, these correlations are too low to control an arm neuroprosthesis in an efficient manner, and the correlations' standard deviations are relatively large which would cause an unstable decoding performance.

All subjects with a significant classification accuracy reached higher correlations with an MI associated decoding model than with the not-associated decoding model. However, the correlations obtained with a not-associated model were often not close to zero. A reason could be some 0.5-Hz oscillations common to both MI classes, maybe due to the MI itself or induced by the metronome beats.

A key point in our classification approach is the narrow-band filter. The decoder algorithms in [30] and [32] used solely linear operations. These linear operations could only amplify or damp *existing* frequency components, but not add or delete frequency components (that would only be possible with nonlinear operations). Therefore, the EEG has to contain decodable movement information in frequencies corresponding to movement frequencies (we do *not* exclude that other EEG frequencies may contain decodable movement information as well, but those frequencies must be exploited with nonlinear methods). As our movement frequency was fixed to 0.5 Hz, we were only interested in the EEG frequencies around 0.5 Hz and set a bandpass filter appropriately to increase the signal-to-noise ratio. EEG signals with frequencies below or above 0.5 Hz would have had

Appendix

zero correlation with the assumed 0.5-Hz movement trajectories (with respect to infinite long signals). We designed a stable narrow-band filter, but with a low order. That way, the output of the filter was still able to follow the input appropriately. In order to validate our classifier, we tested our classifier also with an assumed 0.7-Hz movement trajectory and obtained no statistically significant classification results. Therefore, our classifier is expected to be indeed based on correlations between the EEG and 0.5-Hz oscillations. However, we lack a neurophysiological explanation why low EEG frequencies correspond to movement frequencies, but observations and reasoning with respect to linear operations. An understanding of the basic principles behind movement decoding is desirable and should be a priority task of all involved researchers to take forward decoding.

We assumed sinusoidal movement trajectories, which proved to be sufficient to demonstrate the decoding. However, there may be better assumptions which are closer to the imagined trajectories, e.g., triangular trajectories, which could yield better correlations. A sinusoidal trajectory is the most canonical form comprising of one frequency, other trajectories would comprise more frequency components and, therefore, would typically necessitate a broader bandpass filter.

The decoded positions were correlated with a sinus. However, the positions were not perfectly decoded but with a certain error. Therefore, the estimated correlations were expected to be more accurate the longer the decoding window. Because of that, classification accuracies were also expected to increase with a longer decoding window. Indeed, an increase of the classification accuracy over the window length was apparent for six out of seven subjects with a significant classification accuracy, and the averaged classification accuracies depend statistically significant on the window length. Notably, three out of seven subjects with a significant classification accuracy show an apparent classification peak in the beginning or middle, respectively. This indicates a second opposing effect, and we suspect that some subjects experienced a decrease in their concentration level over the trial length.

We would like to point out that the decoding window was necessary because of our experimental design. Our design goal was to avoid eye movements by design and to decode imagined instead of executed movements. That way, we were able to analyze MI decoding without provoking eye/muscle artifacts. However, in a final end-user application, such a decoding window would be undesirable and imagined movement trajectories should be decoded instantly.

The sources underlying the classification are of interest for assessing the validity of the classification results. Our experimental design avoided eye, muscle, and electrode cable movements, and the metronome beats were exactly the same in both classes. Furthermore, a classification based on electrodes only from the sensorimotor area and SMA did not yield statistically significant classification accuracies as when using all electrodes. Therefore, the discriminative information must have originated in brain sources and not in artifacts or external sources. However, due to large channel correlations, it would not have been possible to interpret the weights of, e.g., a multiple linear regression, a problem known in statistics as multicollinearity [47]. Intuitively, if two variables are correlated, weights have to be shared in some ratio across them. Thus, a variable which correlates with many other variables would tend to get a lower weight than when not correlated with others. A multiple linear regression still predicts the response variable, but the weights would not be interpretable. Therefore, we used the PLS regression which revealed common contribution patterns between subjects in the sensor as well as in the source space. Strong contributions from subareas of the SMA are observable, which become even more clear in the averaged sensor and source space plots. Interestingly, subjects s3 and s6 did not achieve a significant classification accuracy, but show a clear involvement of central motor areas. An explanation could be the fact that s3 and s6 indeed partly reached significant correlations, but with no exploitable difference between the classes allowing a classification. The SMA is responsible for higher level motor tasks. Therefore, the brain sources contributing to the decoding are neurophysiologically plausible and indicate that we indeed decoded from brain signals. This is consistent with the MEG studies [17], [27] showing central regions carrying movement trajectory/direction information. Notably, SMR power modulations triggered by MI occur mainly on the sensorimotor cortex [10], [55], although Yuan *et al.* [56] showed modulations also on the SMA. As the regions are different, SMR modulations and low-frequency time-domain signals are probably two different movement-related processes. However, the literature about macroscale brain sources containing movement trajectory/direction information is not always consistent and shows also involvements of other brain regions. Toda *et al.* [26] showed the involvement of primary sensorimotor, higher motor, and parietal regions when decoding 2-D finger trajectories from MEG. Lv *et al.* [31] reported larger weights in motor, posterior parietal, and occipital areas when decoding hand movement velocities during a drawing task. Jerbi *et al.* [29] found phase locking between slow oscillatory MEG activity and time-varying hand speed in the contralateral primary motor cortex. Wang *et al.* [28] revealed that the contralateral motor area and the left inferior frontal gyrus encode intended movement directions. Bradberry *et al.* [30] found involvements of the contralateral primary sensorimotor region and the inferior parietal lobule when decoding 3-D movements trajectories from EEG. As there is some inconsistence, the involved brain regions and the exact movement conditions (e.g., self-chosen/target, repetitive, execution/imagery, trajectory/direction decoding) should be investigated in future studies. A limitation of our source space analysis is that we used a template head model instead of subject individual models acquired from magnetic resonance imaging scans. Individual models would increase the spatial accuracy of the estimated sources.

We restricted the number of latent variables (scores) to 150 in the source space analysis because of two reasons. First, it was not computationally feasible to use all latent variables. Second, we have observed exceptionally large loadings when using a high number of latent variables. This is an indication of overfitting, and probably because the PLS cannot find more orthonormal latent variables than in the sensor space.

We do not know if metronome beats were a prerequisite for the MI decoding presented in this study. They possibly caused

class-unspecific brain oscillations, which were subsequently class-specifically modulated by the MI, and then decoded. In functional magnetic resonance imaging studies, Grahn and Brett [57] found that rhythm perception elicits higher activation in the SMA and basal ganglia. Bengtsson *et al.* [58] reported a higher activation of the dorsal premotor cortex, SMA, pre-SMA, and lateral cerebellum when listening to rhythmic sequences. This indicates a clear involvement of the SMA during beat perception, and according to our findings, the SMA is also involved when decoding MI. However, the relation between the decoding of rhythmic MI and the perception of rhythmic beats is yet unknown and has to be analyzed in further studies. Nevertheless, the metronome beats could not have influenced (but probably facilitated) the classification results as the beats were exactly the same in both classes. In other words, the metronome beats could at most be a necessary condition but not a sufficient condition for decoding MI.

Our work shows the EEG-based classification of two different imagined movement trajectories with the same limb, and we excluded an unintentional artifact-based classification. Furthermore, we showed that the main contributions originate in the SMA. This is also an important finding for persons with SCI as the SMA is involved in higher level motor control and, therefore, does not rely on an intact sensorimotor feedback loop. Thus, decoding should be applicable to persons with SCI. For a practical neuroprosthesis control, the decoder needs to be substantially improved, and the generalization to nonrhythmic and nonrestricted MI remains unknown. However, we have shown that MI decoding from EEG basically works.

Acknowledgment

This paper only reflects the authors' views and funding agencies are not liable for any use that may be made of the information contained herein.

References

[1] J. R. Wolpaw *et al.*, "Brain-computer interfaces for communication and control," *Clin. Neurophysiol.*, vol. 113, no. 6, pp. 767–791, 2002.
[2] G. R. Müller-Putz *et al.*, "EEG-based neuroprosthesis control: A step towards clinical practice," *Neurosci. Lett.*, vol. 382, pp. 169–174, 2005.
[3] J. Hobby *et al.*, "Restoration of tetraplegic hand function by use of the neurocontrol freehand system," *J. Hand Surg. Br.*, vol. 26, no. 5, pp. 459–464, 2001.
[4] R. R. Riso *et al.*, "Cognitive feedback for use with FES upper extremity neuroprostheses," *IEEE Trans. Biomed. Eng.*, vol. 38, no. 1, pp. 29–38, Jan. 1991.
[5] L. A. Johnson *et al.*, "Direct electrical stimulation of the somatosensory cortex in humans using electrocorticography electrodes: A qualitative and quantitative report," *J. Neural Eng.*, vol. 10, no. 3, pp. 1–7, 2013.
[6] L. R. Hochberg *et al.*, "Neuronal ensemble control of prosthetic devices by a human with tetraplegia," *Nature*, vol. 442, pp. 164–171, 2006.
[7] L. R. Hochberg *et al.*, "Reach and grasp by people with tetraplegia using a neurally controlled robotic arm," *Nature*, vol. 485, pp. 372–375, 2012.
[8] J. L. Collinger *et al.*, "High-performance neuroprosthetic control by an individual with tetraplegia," *Lancet*, vol. 381, no. 9866, pp. 557–564, 2013.
[9] G. Pfurtscheller *et al.*, "Graz-BCI: State of the art and clinical applications," *IEEE Trans. Neural Syst. Rehabil. Eng.*, vol. 11, no. 2, pp. 177–180, Jun. 2003.
[10] G. Pfurtscheller and F. H. L. D. Silva, "Event-related EEG/MEG synchronization and desynchronization: Basic principles," *Clin. Neurophysiol.*, vol. 110, no. 11, pp. 1842–1857, 1999.
[11] G. Pfurtscheller *et al.*, ""Thought"-control of functional electrical stimulation to restore handgrasp in a patient with tetraplegia," *Neurosci. Lett.*, vol. 351, pp. 33–36, 2003.
[12] M. Rohm *et al.*, "Hybrid brain-computer interfaces and hybrid neuroprostheses for restoration of upper limb functions in individuals with high-level spinal cord injury," *Artif. Intell. Med.*, vol. 59, no. 2, pp. 133–142, 2013.
[13] A. Kreilinger *et al.*, "Neuroprosthesis control via noninvasive hybrid brain-computer interface," *IEEE Intell. Syst.*, vol. 28, no. 5, pp. 40–43, 2013, to be published.
[14] J. R. Wolpaw and D. J. McFarland, "Control of a two-dimensional movement signal by a noninvasive brain–computer interface in humans," *Proc. Nat. Acad. Sci.*, vol. 101, no. 51, pp. 17849–17854, 2004.
[15] D. J. McFarland *et al.*, "Electroencephalographic (EEG) control of three-dimensional movement," *J. Neural Eng.*, vol. 7, no. 3, pp. 1–9, 2010.
[16] H. Yuan *et al.*, "Relationship between speed and EEG activity during imagined and executed hand movements," *J. Neural Eng.*, vol. 7, no. 2, pp. 1–10, 2010.
[17] S. Waldert *et al.*, "Hand movement direction decoded from MEG and EEG," *J. Neurosci.*, vol. 28, no. 4, pp. 1000–1008, 2008.
[18] T. Ball *et al.*, "Differential representation of arm movement direction in relation to cortical anatomy and function," *J. Neural Eng.*, vol. 6, no. 1, pp. 1–16, 2009.
[19] Y. Nakanishi *et al.*, "Prediction of three-dimensional arm trajectories based on ECoG signals recorded from human sensorimotor cortex," *PLoS One*, vol. 8, no. 8, pp. 1–9, 2013.
[20] T. Pistohl *et al.*, "Prediction of arm movement trajectories from ECoG-recordings in humans," *J. Neurosci. Methods*, vol. 167, no. 1, pp. 105–114, 2008.
[21] G. Schalk *et al.*, "Decoding two-dimensional movement trajectories using electrocorticographic signals in humans," *J. Neural Eng.*, vol. 4, no. 3, pp. 264–275, 2007.
[22] T. Milekovic *et al.*, "An online brain–machine interface using decoding of movement direction from the human electrocorticogram," *J. Neural Eng.*, vol. 9, no. 4, pp. 1–14, 2012.
[23] S. Acharya *et al.*, "Electrocorticographic amplitude predicts finger positions during slow grasping motions of the hand," *J. Neural Eng.*, vol. 7, no. 4, pp. 1–13, 2010.
[24] A. P. Georgopoulos *et al.*, "Magnetoencephalographic signals predict movement trajectory in space," *Exp. Brain Res.*, vol. 167, no. 1, pp. 132–135, 2005.
[25] T. J. Bradberry *et al.*, "Decoding center-out hand velocity from meg signals during visuomotor adaptation," *NeuroImage*, vol. 47, no. 4, pp. 1691–1700, 2009.
[26] A. Toda *et al.*, "Reconstruction of two-dimensional movement trajectories from selected magnetoencephalography cortical currents by combined sparse Bayesian methods," *NeuroImage*, vol. 54, no. 2, pp. 892–905, 2011.
[27] H. G. Yeom *et al.*, "Estimation of the velocity and trajectory of three-dimensional reaching movements from non-invasive magnetoencephalography signals," *J. Neural Eng.*, vol. 10, no. 2, pp. 1–9, 2013.
[28] W. Wang *et al.*, "Decoding and cortical source localization for intended movement direction with meg," *J. Neurophysiol.*, vol. 104, no. 5, pp. 2451–2461, 2010.
[29] K. Jerbi *et al.*, "Coherent neural representation of hand speed in humans revealed by MEG imaging," *Proc. Nat. Acad. Sci.*, vol. 104, no. 18, pp. 7676–7681, 2007.
[30] T. J. Bradberry *et al.*, "Reconstructing three-dimensional hand movements from noninvasive electroencephalographic signals," *J. Neurosci.*, vol. 30, pp. 3432–3437, 2010.
[31] J. Lv *et al.*, "Decoding hand movement velocity from electroencephalogram signals during a drawing task," *Biomed. Eng. Online*, vol. 9, no. 64, pp. 1–21, 2010.
[32] P. Ofner and G. R. ller-MüPutz, "Decoding of velocities and positions of 3D arm movement from EEG," in *Proc. Annu. Int. Conf. IEEE Eng. Med. Biol. Soc.*, 2012, pp. 6406–6409.
[33] J. M. Antelis *et al.*, "On the usage of linear regression models to reconstruct limb kinematics from low frequency EEG signals," *PLoS One*, vol. 8, no. 4, pp. 1–14, 2013.
[34] A. Vučković and F. Sepulveda, "Delta band contribution in cue based single trial classification of real and imaginary wrist movements," *Med. Biol. Eng. Comput.*, vol. 46, no. 6, pp. 529–539, 2008.
[35] A. Vučković and F. Sepulveda, "A two-stage four-class BCI based on imaginary movements of the left and the right wrist," *Med. Eng. Phys.*, vol. 34, no. 7, pp. 964–971, 2012.

[36] Y. Gu *et al.*, "Single-trial discrimination of type and speed of wrist movements from EEG recordings," *Clin. Neurophysiol.*, vol. 120, no. 8, pp. 1596–1600, 2009.
[37] Y. Gu *et al.*, "Offline identification of imagined speed of wrist movements in paralyzed ALS patients from single-trial EEG," *Front Neurosci.*, vol. 3, no. 62, pp. 1–7, 2009.
[38] T. J. Bradberry *et al.*, "Fast attainment of computer cursor control with noninvasively acquired brain signals," *J. Neural Eng.*, vol. 8, no. 3, pp. 1–9, 2011.
[39] R. Poli, and M. Salvaris, "Comment on 'fast attainment of computer cursor control with noninvasively acquired brain signals'," *J. Neural Eng.*, vol. 8, no. 5, pp. 1–3, 2011.
[40] P. Ofner and G. R. Müller-Putz, "Towards a novel control paradigm based on decoding imagined movements from EEG," in *Proc. 5th Int. Brain-Comput. Interface Meeting: Defining Future*, 2013, pp. 62–63.
[41] P. Ofner and G. R. Müller-Putz, "EEG-based classification of imagined arm trajectories," in *Proc. 2nd Int. Conf. NeuroRehabilitation*, 2014, pp. 611–620.
[42] B. Pesaran *et al.*, "Dorsal premotor neurons encode the relative position of the hand, eye, and goal during reach planning," *Neuron*, vol. 51, no. 1, pp. 125–134, 2006.
[43] A. Delorme and S. Makeig, "EEGLAB: An open source toolbox for analysis of single-trial EEG dynamics including independent component analysis," *J. Neurosci Methods*, vol. 134, pp. 9–21, 2004.
[44] T. W. Lee *et al.*, "Independent component analysis using an extended infomax algorithm for mixed sub-Gaussian and super-Gaussian sources," *Neural Comput.*, vol. 11, no. 2, pp. 417–441, 1999.
[45] A. Schlögl *et al.*, "A fully automated correction method of EOG artifacts in EEG recordings," *Clin. Neurophysiol.*, vol. 118, no. 1, pp. 98–104, 2007.
[46] F. Mosteller and J. W. Tukey, *Data Analysis and Regression*. Reading, MA, USA: Addison-Wesley, 1977.
[47] D. E. Farrar and R. R. Glauber, "Multicollinearity in regression analysis: The problem revisited," *Rev. Econ. Statist.*, vol. 49, no. 1, pp. 92–107, 1967.
[48] S. Wold *et al.*, "PLS-regression: A basic tool of chemometrics," *Chemometr. Intell. Lab. Syst.*, vol. 58, no. 2, pp. 109–130, 2001.
[49] R. Rosipal and N. Krämer, "Overview and recent advances in partial least squares," in *Subspace, Latent Structure and Feature Selection* (ser. Lecture Notes in Computer Science, vol. 3940). Berlin, Germany, Springer, 2006, pp. 34–51.
[50] S. de Jong, "Simpls: An alternative approach to partial least squares regression," *Chemometr. Intell. Lab. Syst.*, vol. 18, no. 3, pp. 251–263, 1993.
[51] F. Tadel *et al.*, "Brainstorm: A user-friendly application for MEG/EEG analysis," *Comput. Intell. Neurosci*, vol. 2011, p. 879716, 2011.
[52] J. Schäfer and K. Strimmer, "A shrinkage approach to large-scale covariance matrix estimation and implications for functional genomics," *Statist. Appl. Genet. Mol. Biol.*, vol. 4, no. 1, pp. 1–30, 2005.
[53] R. D. Pascual-Marqui, "Standardized low-resolution brain electromagnetic tomography (sLORETA): Technical details," *Methods Find Exp. Clin. Pharmacol.*, vol. 24, pp. 5–12, 2002.
[54] M. Billinger *et al.*, "Is it significant? Guidelines for reporting BCI performance," in *Towards Practical Brain-Computer Interfaces*. Berlin, Germany: Springer, 2012, pp. 333–354.
[55] H. Yuan *et al.*, "Cortical imaging of event-related (de)synchronization during online control of brain-computer interface using minimum-norm estimates in frequency domain," *IEEE Trans. Neural Syst. Rehabil. Eng.*, vol. 16, no. 5, pp. 425–431, Oct. 2008.
[56] H. Yuan *et al.*, "Negative covariation between task-related responses in alpha/beta-band activity and bold in human sensorimotor cortex: An EEG and fMRI study of motor imagery and movement," *NeuroImage*, vol. 49, no. 3, pp. 2596–2606, 2010.
[57] J. A. Grahn and M. Brett, "Rhythm and beat perception in motor areas of the brain," *J. Cogn. Neurosci.*, vol. 19, no. 5, pp. 893–906, 2007.
[58] S. L. Bengtsson *et al.*, "Listening to rhythms activates motor and premotor cortices," *Cortex*, vol. 45, no. 1, pp. 62–71, 2009.

Patrick Ofner (S'14) received the B.Sc. and M.Sc. degrees in information and communications technology from the Graz University of Technology, Graz, Austria, in 2008 and 2011, respectively, where he is working toward the Ph.D. degree under the mentorship of Dr. G. R. Müller-Putz.

He is currently a Scientific Project Assistant at the BCI Lab of the Institute for Knowledge Discovery, Graz University of Technology. His research interests includes movement decoding, EEG source imaging, biosignal processing, and machine learning.

Gernot R. Müller-Putz received the M.Sc. and Ph.D. degrees from the Graz University of Technology, Graz, Austria, in 2000 and 2004, respectively. He also received the "venia docendi" for medical informatics from the Faculty of Computer Science, Graz University of Technology.

He is currently the Head of the Institute for Knowledge Discovery, Graz University of Technology, and its associated BCI Lab. Since October 2014, he has been a full Professor for semantic data analysis at the Graz University of Technology. He has gained extensive experience in the field of biosignal analysis, brain–computer interface research, EEG-based neuroprosthesis control, hybrid BCI systems, the human somatosensory system, and assistive technology over the past 15 years. He has also managed several national and international projects and is currently partner in 2 EU FP7 projects (BackHome, ABC) and coordinator of BNCI Horizon 2020. Recently, he has received a Horizon 2020 project, MoreGrasp, which will be coordinated by him. Furthermore, he organized and hosted six international Brain–Computer Interface Conferences over the last 13 years in Graz, the last one in September 2014 in Graz. He is also steering board member for the International BCI Meeting, which takes place in the U.S. usually every three years (last time in 2013).

Dr. Müller-Putz is the Review Editor of *Frontiers in Neuroprosthetics*. Since 2014, he has been an Associate Editor of the *Brain-Computer Interface Journal* and of the IEEE TRANSACTIONS OF BIOMEDICAL ENGINEERING.

Primary Publication III

PLOS ONE

RESEARCH ARTICLE

Upper limb movements can be decoded from the time-domain of low-frequency EEG

Patrick Ofner, Andreas Schwarz, Joana Pereira, Gernot R. Müller-Putz*

Institute of Neural Engineering, BCI-Lab, Graz University of Technology, Graz, Austria

* gernot.mueller@tugraz.at

OPEN ACCESS

Citation: Ofner P, Schwarz A, Pereira J, Müller-Putz GR (2017) Upper limb movements can be decoded from the time-domain of low-frequency EEG. PLoS ONE 12(8): e0182578. https://doi.org/10.1371/journal.pone.0182578

Editor: Dingguo Zhang, Shanghai Jiao Tong University, CHINA

Received: February 6, 2017

Accepted: July 20, 2017

Published: August 10, 2017

Data Availability Statement: Data are available from the BNCI Horizon 2020 database at http://bnci-horizon-2020.eu/database/data-sets (accession number 001-2017) and from Zenodo at DOI 10.5281/zenodo.834976.

Funding: This work is supported by the European ICT Programme Project H2020-643955 "MoreGrasp" and the ERC Consolidator Grant ERC-681231 "Feel Your Reach". The funders had no role in study design, data collection and analysis, decision to publish, or preparation of the manuscript.

Abstract

How neural correlates of movements are represented in the human brain is of ongoing interest and has been researched with invasive and non-invasive methods. In this study, we analyzed the encoding of single upper limb movements in the time-domain of low-frequency electroencephalography (EEG) signals. Fifteen healthy subjects executed and imagined six different sustained upper limb movements. We classified these six movements and a rest class and obtained significant average classification accuracies of 55% (movement vs movement) and 87% (movement vs rest) for executed movements, and 27% and 73%, respectively, for imagined movements. Furthermore, we analyzed the classifier patterns in the source space and located the brain areas conveying discriminative movement information. The classifier patterns indicate that mainly premotor areas, primary motor cortex, somatosensory cortex and posterior parietal cortex convey discriminative movement information. The decoding of single upper limb movements is specially interesting in the context of a more natural non-invasive control of e.g., a motor neuroprosthesis or a robotic arm in highly motor disabled persons.

Introduction

Understanding how the human brain encodes movements is essential for the development of an intuitive and natural control of a motor neuroprosthesis or a robotic arm. Neuroprostheses based on functional electrical stimulation (FES) [1] can be already used to restore movement function of spinal cord injured (SCI) persons [2]. These neuroprostheses often rely on a shoulder joystick as a control signal, and end users with SCI need to learn to control movements, such as grasping, with contralateral shoulder movements. However, this control would have a more natural feel for the end user if the movement intention is decoded with a brain-computer interface (BCI), and subsequently translated into a control signal for a neuroprosthesis or robotic arm. It has been shown with tetraplegic human subjects that invasive BCIs allow the control of a robotic arm with up to 10 degrees of freedom (DoF) [3–6]. Invasive BCIs have a better signal-to-noise ratio than non-invasive BCIs, but require extensive surgery, and the suitability for long-term use is still unclear due to neural tissue response. Non-invasive BCIs based on electroencephalography (EEG) signals on the other hand do not require surgery and are easier to setup. They often rely on power modulations of sensorimotor rhythms (SMR)

Competing interests: The authors have declared that no competing interests exist.

accompanying movement imagination (MI) (see also event-related (de)synchronization [7]) but other brain rhythms can also be exploited [8,9]. These power modulations can act as the control signals for a neuroprosthesis [2,10–12]. Using an SMR-based BCI, our group has already shown the restoration of the lateral grasp of a tetraplegic (C4/5 ASIA A) user with MI of both feet [12]. In a later study, we demonstrated the switching between different lateral grasp phases in a person with SCI (C5 ASIA A) with an SMR-based BCI and the Freehand system [10]. Recently, Rohm et al. and Kreilinger et al. [11,13] restored not only hand but also elbow functions of a tetraplegic end user (a review can be found in Rupp et al. [2]). However, SMR-based BCIs can usually only detect spatially well separated patterns in the EEG as elicited by, for example, right hand MI vs left hand MI, although recent research suggests more spatially specific detections [14,15]. Furthermore, SMR-based BCIs usually require repetitive MI of movements. This often requires BCI users to learn unnatural MI commands, such as using repetitive left hand MI to control right hand functions [16]. However, for a more natural control the imagined movement should be as close as possible to the actual neuroprosthesis movement. In this context, continuous decoding of movement trajectories from the time-domain of the EEG has been investigated. Bradberry et al. showed in an offline study the decoding of 3D hand velocities [17], later our group showed the decoding of 3D positions in a continuous movement task [18] and the decoding of imagined movement trajectories [19]. Furthermore, Agashe et al. decoded hand joint angular velocities [20], and also hand movement directions were decoded non-invasively [21]. The current state of the art allows decoding of movement trajectories and directions from EEG, however the low correlation with the real or intended movement prevents a reliable and accurate control.

Another possibility to make neuroprosthesis or robotic arm control more natural is to decode additional information about the type or quality of an imagined movement, which has been done in the time-domain as well as in the frequency-domain of EEG. Gu et al. found that the speed of imagined wrist movements is encoded in the time-domain in motor-related cortical potentials (MRCPs) [22–24], and Yuan et al. found such a relationship in the mu and beta rhythm with executed/imagined hand movements [25]. Jochumsen et al. [26] decoded from MRCPs movement force and speed during executed and imagined grasping movements in healthy persons, and attempted movements in stroke patients. Also MIs related to the same limb were classified based on EEG power modulations in the frequency domain: Edelman et al. [15] classified repetitive imagined hand flexion/extension and forearm supination/pronation, Yong and Menon showed the classification of repetitive imagined grasp and elbow movements [14]. Based on these findings, the natural control experience can be enhanced if, e.g. an imagined repetitive supination of the arm is used to control the supination of, e.g. a robotic arm. Furthermore, detecting different MIs related to the same limb increases the number of control possibilities compared to classical SMR-based BCIs, which often only detect left/right hand and foot MI. However, repetitive MIs are also not optimal since one usually does not execute repetitive hand/arm movements when manipulating objects. Of special interest are therefore sustained MIs, such as single supination. Vučković and Sepulveda showed the classification of sustained wrist extension/flexion and forearm pronation/supination MIs from the frequency-domain of the EEG in the delta and gamma band [27,28]. Gu et al. classified imagined wrist extension and wrist rotation based on power-modulations in the mu and beta band and the rebound rate of MRCPs but did not find any statistical difference in the rebound rate of MRCPs [23].

In this work we hypothesize that executed and imagined sustained movements from the same limb can be decoded from low-frequency time-domain signals (< 3 Hz). We applied a multiclass classification comprising of 6 movement classes: elbow flexion/extension, forearm supination/pronation, and hand open/close. Additionally, these movements were classified

against a rest class. We measured 15 healthy subjects in two separate ME and MI sessions. To the best of our knowledge, this high number of different sustained movements of the same limb has not been studied before using low-frequency time-domain EEG signals. Furthermore, we show for the first time for EEG-based movement decoding the classifier patterns [29] in the source space, which allows the estimation of the brain regions exploited by the classifier. Generally, the purpose of this work is to get a better understanding if and how single sustained upper limb movements are encoded in the time-domain of low-frequency EEG signals.

Methods

Subjects

We recruited 15 healthy subjects aged between 22 and 40 years with a mean age of 27 years (standard deviation 5 years). Nine subjects were female, and all the subjects except s1 were right-handed. The subjects received payment for their participation. Written informed consent was obtained from all subjects, and the study was conducted in accordance with the protocol approved by the ethics committee of the Medical University of Graz (approval number 28–108 ex 15/16).

Paradigm

Subjects sat on a chair and their right arm was fully supported by an exoskeleton with anti-gravity support (Hocoma, Switzerland) to avoid muscle fatigue, see Fig 1A (the individual in this figure has given written informed consent, as outlined in PLOS consent form, to publish these case details).

We measured each subject in two sessions on two different days, which were not separated by more than one week. In the first session the subjects performed ME, and MI in the second session. The subjects performed six movement types which were the same in both sessions and comprised of elbow flexion/extension, forearm supination/pronation and hand open/close; all with the right upper limb (see Fig 1B). All movements started at a neutral position: the hand half open, the lower arm extended to 120 degree and in a neutral rotation, i.e. thumb on the inner side. Additionally to the movement classes, a rest class was recorded in which subjects were instructed to avoid any movement and to stay in the starting position. In the ME session, we instructed subjects to execute sustained movements. In the MI session, we asked subjects to perform kinesthetic MI [30] of the movements done in the ME session (subjects performed one ME run immediately before the MI session to support kinesthetic MI).

The paradigm was trial-based and cues were displayed on a computer screen in front of the subjects, Fig 2 shows the sequence of the paradigm. At second 0, a beep sounded and a cross popped up on the computer screen (subjects were instructed to fixate their gaze on the cross). Afterwards, at second 2, a cue was presented on the computer screen, indicating the required task (one out of six movements or rest) to the subjects. At the end of the trial, subjects moved back to the starting position. In every session, we recorded 10 runs with 42 trials per run. We presented 6 movement classes and a rest class and recorded 60 trials per class in a session.

Recording

The EEG was measured from 61 channels covering frontal, central, parietal and temporal areas using active electrodes and four 16-channel amplifiers (g.tec medical engineering GmbH, Austria). Reference was placed on the right mastoid, ground on AFz. We used an 8^{th} order Chebyshev bandpass filter from 0.01 Hz to 200 Hz and sampled with 512 Hz. Power line interference was suppressed with a notch filter at 50 Hz. In addition we measured the arm joint angles for

a

b

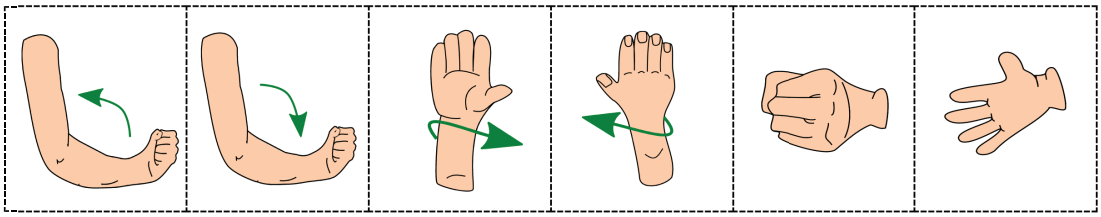

Fig 1. Experimental setup and movements. a: Subjects sat in a chair and executed/imagined movements according to cues presented on a computer screen in front of them. **b:** Subjects executed/imagined: elbow flexion, elbow extension, forearm supination, forearm pronation, hand close, and hand open.

https://doi.org/10.1371/journal.pone.0182578.g001

the exoskeleton using customized software and finger positions with a 5DT Data Glove (5DT, USA) for determining movement onsets. Prior to each session, we measured the electrode positions with a CMS 20 EP system (Zebris Medical GmbH, Germany). The individual electrode positions were used for source imaging.

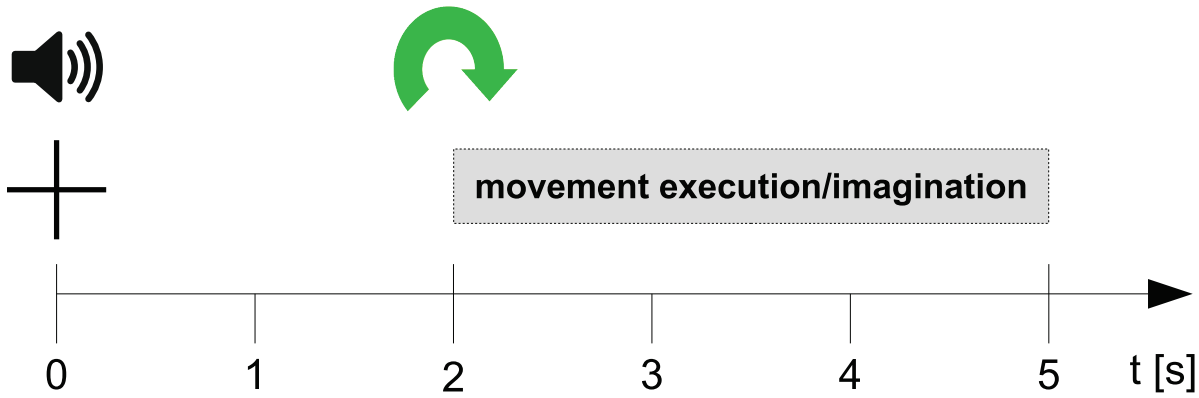

Fig 2. Trial sequence. At second 0, a cross appeared together with a beep sound; at second 2, the cue was presented and subjects executed/imagined a sustained movement or avoided any movement, respectively. After the trial, a break with a random duration of 2 s to 3 s followed.

https://doi.org/10.1371/journal.pone.0182578.g002

Movement onset detection

To detect movement onsets in ME sessions we used sensor data from the exoskeleton and the data glove. The elbow and wrist sensors (exoskeleton) were used to detect elbow flexion/extension and forearm pronation/supination onsets, respectively. For opening/closing onsets we performed a principal component analysis on the data glove sensor data and used only the first principal component for further processing. A movement was detected when the absolute difference between the sensor data and the preceding time average (from -1 s to -0.5 s) crossed a threshold. Thresholds were chosen dependent on each sensor to ensure timely detection of movement onsets and to minimize false positive detections (typically, movements were detected not more than 80 ms later than a human expert would detect them when visually inspecting the sensor data). In order to account for systematic detection time differences between the classes (e.g. different sensor thresholds and different inertiae of limb parts), we time-shifted the mean value of the detection times of each class toward the mean value of all classes. Thus, on average the movement onsets (wrt. to the cue) of the movement classes were all the same. For the classes without overt movements (i.e., the rest class and the MI classes), we assumed a virtual movement onset. This virtual movement onset was individually calculated for each subject as the average movement onset of the movement classes. In this manner, all classes were still comparable.

Preprocessing

We used EEGLAB to detect and remove noisy channels (1.4 channels per subject on average) based on the joint probability of each channel. We downsampled the data to 256 Hz to save computation time. Thereafter we marked artefacts by band-pass filtering (0.3 Hz—70 Hz, 4^{th} order zero-phase Butterworth filter) the data and using EEGLAB[31] to find (1) values above/below thresholds of -200 μV and 200 μV, respectively, (2) trials with abnormal joint probabilities, and (3) trials with abnormal kurtosis. The methods (2) and (3) used as threshold 5 times the standard deviation of their statistic to detect artefact contaminated trials. The artefact contaminated trials were only marked for removal but not yet removed. Afterwards, we filtered the original (unfiltered) 256 Hz EEG data with a zero-phase 4^{th} order Butterworth filter between 0.3 Hz and 3 Hz and re-referenced the data to a common average reference. Subsequently, we discarded the trials previously marked as artefact contaminated.

Classification

The preprocessed signals were classified with a shrinkage regularized linear discriminant analysis (sLDA) classifier [32,33] which was embedded in the discriminative spatial pattern (DSP) [29] framework described in the next section.

We conducted two types of classifications: first, we classified all 6 movement classes against each other. Second, we aggregated all movement classes into one class and classified it against the rest class. We refer to these classification types as mov-vs-mov and mov-vs-rest classifications, respectively. In the mov-vs-rest classification we randomly removed trials from the aggregated movement class to ensure equal trial numbers in both classes. As mov-vs-mov was a multiclass classification comprising of 6 classes, we applied an 1-vs-1 classification strategy yielding 15 binary classifiers. To validate the classification we employed a 10x10-fold cross-validation.

We employed two classification approaches using EEG data from: (1) single time points and (2) time windows with different lengths (0.2–1 s). Single time point classification gives a higher time resolution of the accuracy course and is more suitable to analyze the information distribution over time. Furthermore, the corresponding classifier patterns can be readily obtained with the DSP method described in the next section. The time window based classification, on the other hand, is expected to increase the classification accuracy. Because every method has its benefits, we analyzed both approaches in this work and refer to them as "single time point" and "time window" based classifications.

Classifier patterns

We calculated the classifier pattern based on the discriminative spatial pattern (DSP) method [29]. This method allows the calculation of an (s)LDA classifier and the corresponding patterns simultaneously. An LDA can be formulated as an optimization problem of Fisher's' criterion and consecutively as a generalized eigenvalue problem. When this generalized eigenvalue problem is solved for the eigenvector corresponding to the largest eigenvalue one obtains the LDA weight vector. DSP also solves this generalized eigenvalue problem for the remaining eigenvectors and one obtains a weight matrix. This weight matrix can then be inverted to obtain the pattern.

Let x(t) be a vector of the EEG channels at time t with dimension [channels x 1], w_t the computed LDA weight vector at time t with dimension [channels x 1], and the scalar y(t) the projection of the original EEG channels to the LDA space. Then the LDA can be formulated as

$$x(t)^T \cdot w_t = y(t) \tag{1}$$

and w_t corresponds to the eigenvector with the largest eigenvalue. With DSP we get a weight matrix instead where the first column (when sorted by the eigenvalue) corresponds to the LDA solution:

$$x(t)^T \cdot W_t(:,1) = y(t) \tag{2}$$

This weight matrix can be inverted to obtain the pattern a_t corresponding to the LDA weights:

$$A_t = W_t^{-1} \tag{3}$$

$$a_t = A_t(1,:) \tag{4}$$

In fact, we obtained an sLDA weight vector because we calculated the within-class scatter matrix (a factor in the Fisher's criterion) using shrinkage regularization. We calculated the patterns for every time step in the time window from -0.4 s to 0.4 s relative to the movement onset (indicated by the subscript t).

In general terms, a pattern explains how a source, e.g. a specific brain area or independent component, is projected on the channels. Noteworthy, "source" can refer to two different concepts: first, the sources constituting a classifier (manifesting as a pattern) in channel space (i.e. scalp potential distribution), second, the brain sources found with source imaging methods, i.e. voxels. This section refers solely to patterns and the next section shows how source imaging was applied to transform this pattern to the source (voxel) space. Each element in a pattern vector shows with what impact a source is projected on the associated channel. It is important to bear in mind that a pattern itself does not have any physical representation, i.e. it has no physical unit. However, a common physical unit would be a necessity when averaging and interpreting patterns. If we multiply (scale) a source with its pattern, we get the projection to the channel space in the same physical unit as the source, e.g. if the source corresponds to Volt, the resulting scaled pattern corresponds to Volt too. In the case of LDA, however, we do not have a single source but two classes in the channel space projected into an one dimensional LDA space. Thus, we are interested in the distance between the two classes in the LDA space. In our scaling approach we use the distance between the two class means in the LDA space as a scaling factor for a_t. Let $\mu_{0,t}$ and $\mu_{1,t}$ be vectors with dimension [channels x 1] representing the class means of the two classes in the channel space, then the scaled pattern can be calculated as:

$$a_{scaled,t} = (\mu_{0,t}^T \cdot w_t - \mu_{1,t}^T \cdot w_t) \cdot a_t \quad (5)$$

With this scaling we get a pattern which has the same physical unit as the original channel space. The pattern shows the differences of the class means in the original space as exploited by the LDA classifier. We then transformed this pattern from the channel space into the source space using standardized low-resolution brain electromagnetic tomography (sLORETA) [34], see the next section for more details.

As we applied an 1-vs-1 classification strategy, we obtained several binary classifiers and therefore also several patterns (e.g. a supination vs pronation pattern). To obtain the final classifier patterns we grouped the patterns according to the two classification types: movement vs movement patterns (mov-vs-mov) and movement vs rest patterns (mov-vs-rest). Patterns belonging to a group were averaged using their absolute values. We took the absolute values because a pattern expresses the difference between two classes and its signs depend on the order of the classes and should therefore not be considered. Finally, we averaged the patterns over non-overlapping 100 ms time segments located between -0.4 s and 0.4 s relative to the movement onset, i.e. yielding 9 patterns per classification type for each session and subject. Additionally, we time averaged over the whole -0.4 s to 0.4 s period. Fig 3 summarizes the procedure.

Source space

EEG source imaging methods allow to infer from the EEG (i.e. scalp potential distribution) the underlying sources in the brain. The EEG signals are attributed to the "channel space", whereas the inferred brain sources are attributed to the "source space" and are often estimated (normalized) current densities [35].

We transformed the LDA patterns (obtained from single EEG time-points) from the channel space into the source space to increase the spatial resolution of the patterns obtained. For this purpose, we used the software Brainstorm [36]. A desirable property of scaled LDA

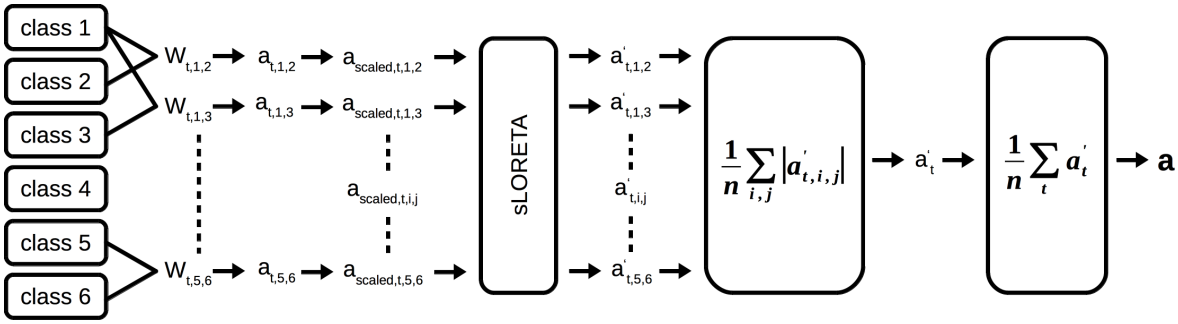

Fig 3. Calculation of a mov-vs-mov pattern. Patterns are calculated from each 1-vs-1 classifier; subsequently scaled and transformed into the source space; we then calculated the absolute value and averaged over patterns. Finally, we averaged over non-overlapping time segments. The same processing pipeline applies to the mov-vs-rest pattern.

https://doi.org/10.1371/journal.pone.0182578.g003

patterns compared to LDA weights is that they correspond to measured scalp potentials and can be subjected to source imaging methods similar as EEG channels. Boundary element head models were calculated based on subject individual electrode positions and the ICBM152 template head model (ICBM152 is a head model based on a non-linear average of 152 subjects). We estimated the full noise covariance matrices based on the EEG data from the period 0.5 to 2 s after trial start and applied shrinkage regularization [37]. Finally, we computed 15002 brain sources, i.e. voxels, with sLORETA [34] (the dipole orientations were unconstrained).

Classifier pattern statistics

Group level statistics was done by nonparametric permutation testing [38,39] of the classifier patterns in the source space. The statistical testing was done separately for each ME/MI and mov-vs-mov/mov-vs-rest pattern. Beside the actual classifier patterns, we calculated random classifier patterns by shuffling class labels once for each subject. As a test statistic, we used the difference between the actual classifier patterns and the random classifier patterns averaged over all subjects. We obtained the permutation distribution of the test statistic by enumerating all $2^{15} = 32768$ actual/random classifier pattern combinations. For that, we used the maximum of the voxels in each enumeration step to account for multiple comparisons (in case of 100 ms time segments, we used the maximum of the whole -0.4 s to 0.4 s period). We then established a threshold corresponding to $\alpha = 0.05$. All voxels with a test statistic exceeding the threshold were considered significant.

Results

Classification accuracies

Single time point classification. The ME classification accuracies are shown in Fig 4A (mov-vs-mov) and Fig 4B (mov-vs-rest). The mov-vs-mov average classification accuracy over all subjects reached a maximum of 42% (9% standard deviation) at 0.13 s after movement onset and the mov-vs-rest average classification accuracy reached a maximum of 81% (7% standard deviation) at movement onset (0.0 s). Accuracies were calculated from -2 s to 2 s relative to the movement onset with a time resolution of 1/16 s. Classification accuracies are statistically significant above 24% (mov-vs-mov) and 65% (mov-vs-rest) for a single subject, and above 18% (mov-vs-mov) and 54% (mov-vs-rest) for the average ($\alpha = 0.05$, adjusted wald interval [40,41], Bonferroni corrected for the length of the analyzed time window). We calculated the

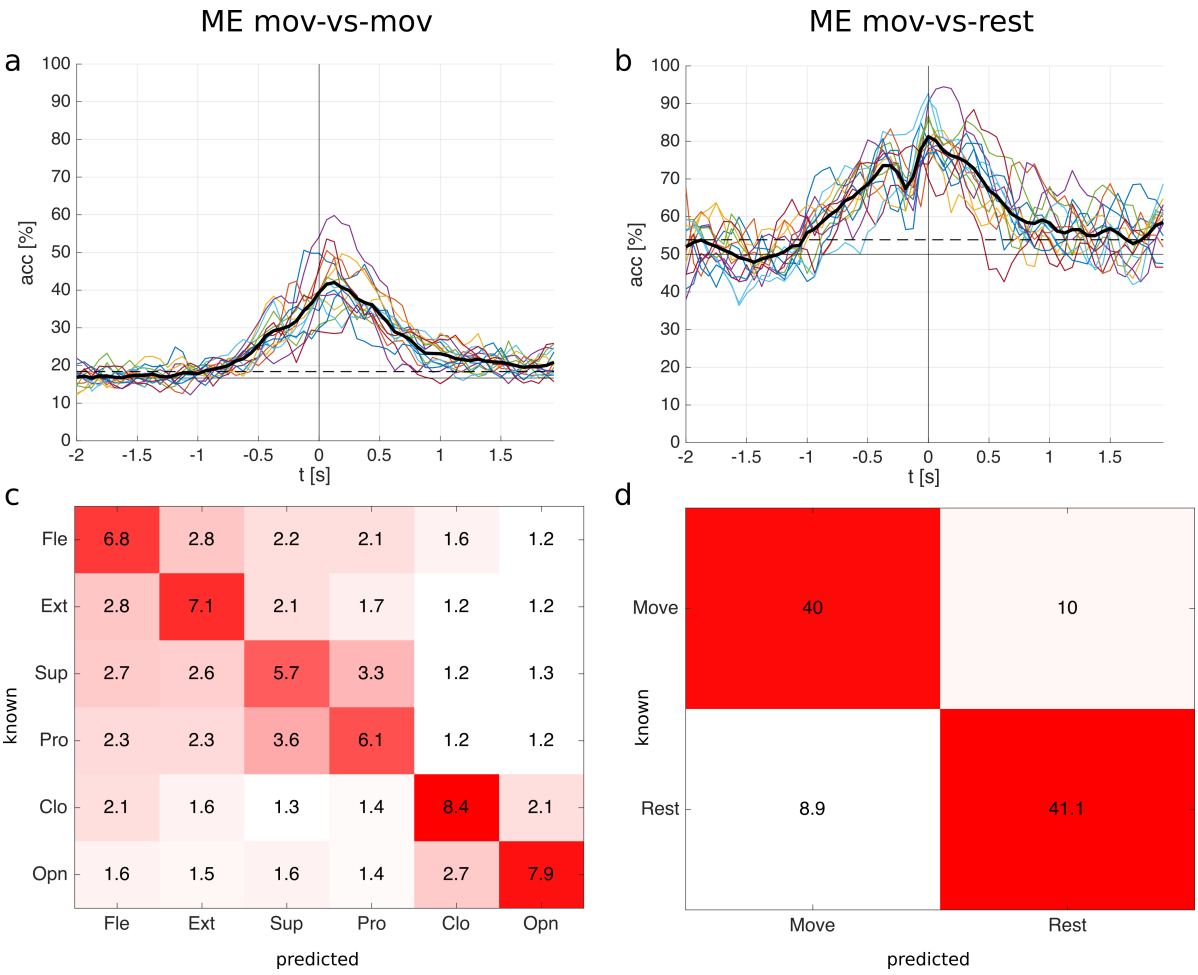

Fig 4. ME classification results for the single time point classification. a: mov-vs-mov classification accuracies of all 15 subjects and the average (thick black line). Time point 0 s corresponds to the movement onset. **b:** mov-vs-rest classification accuracies. The horizontal solid line in a and b is the chance level; the horizontal dashed line is the significance level for the average. **c:** mov-vs-mov confusion matrix (occurrences sum to 100%) with classes elbow flexion (Fle), elbow extension (Ext), forearm supination (sup), forearm pronation (pro), hand close (Clo), and hand open (Opn). **d:** mov-vs-rest confusion matrix. Confusion matrices were calculated at the time point with the highest average classification accuracy (mov-vs-mov: 0.13 s; mov-vs-rest: 0.0 s).

https://doi.org/10.1371/journal.pone.0182578.g004

significance levels based on the average number of trials available after artefact removal. In mov-vs-mov and mov-vs-rest all subjects reached a significant classification accuracy, see Table 1 which shows the individual maximum classification accuracies. The mov-vs-mov averaged classification accuracy becomes significant at -0.94 s and stays significant until the end of the analyzed time window (2 s); the mov-vs-rest averaged classification accuracy is significant between -1.0 s and 1.69 s, see Fig 4A and 4B.

Confusion matrices are shown in Fig 4C (mov-vs-mov) and Fig 4D (mov-vs-rest). They correspond to the timepoints when the average classification accuracies reached a maximum. The confusion matrices show relative numbers, i.e. the occurrences sum up to 100%. If a

Table 1. Maximum ME classification accuracies for the single time point classification.

ME	s1	s2	s3	s4	s5	s6	s7	s8	s9	s10	s11	s12	s13	s14	s15	avg
mov-vs-mov [%]	**51**	**51**	**39**	**60**	**36**	**38**	**36**	**40**	**49**	**50**	**39**	**43**	**42**	**54**	**40**	44 ± 7
mov-vs-rest [%]	**85**	**81**	**83**	**94**	**87**	**93**	**78**	**81**	**83**	**80**	**79**	**86**	**91**	**88**	**81**	85 ± 5

Included is the average and standard deviation over subjects. Significant classification accuracies are bold.

https://doi.org/10.1371/journal.pone.0182578.t001

movement was wrongly predicted, it was often predicted as a movement involving the same joints, see Fig 4C. In other words, movements involving different joints (e.g. open vs pronation) are better distinguishable than movements involving the same joints (e.g. open vs close).

Fig 5 shows the MI classification accuracies. The mov-vs-mov average classification accuracy over all subjects reached a maximum of 23% (3% standard deviation) at -0.13 s; the mov-vs-rest average classification accuracy reached a maximum of 68% (8% standard deviation) at 0.06 s. Accuracies are significant above 24% (mov-vs-mov) and 65% (mov-vs-rest) for a single subject, and above 18% (mov-vs-mov) and 54% (mov-vs-rest) for the average ($\alpha = 0.05$, adjusted wald interval, Bonferroni corrected for the length of the analyzed time window). Ten subjects reached a significant classification accuracy in mov-vs-mov and 15 subjects in mov-vs-rest, see Table 2. The mov-vs-mov average classification becomes significant between -0.56 s and 0.81 s; the mov-vs-rest average classification is significant between -0.69 s and 0.81 s, see Fig 5A and 5B.

The averaged maximum mov-vs-mov accuracies are 1.8 times higher for ME than for MI, the averaged maximum mov-vs-rest accuracies are 1.2 times higher for ME than for MI (cf. Table 1 and Table 2). The ME and MI accuracies are significantly different for mov-vs-mov and mov-vs-rest ($p < 5{\cdot}10^{-4}$, two-sided Wilcoxon signed rank test).

MI confusion matrices are shown in Fig 5C (mov-vs-mov) and Fig 5D (mov-vs-rest). They qualitatively show similar patterns as in ME, i.e. MI involving different joint are better discriminable than MI involving same joints.

Time window classification. Beside classifying on single time points, we also classified time windows of the EEG. The analyzed time windows ranged from 200 ms to 1 s, and features were taken in 100 ms time intervals within these time windows (see Table 3). Fig 6 shows the subjects' averaged ME/MI classification accuracies for the different window lengths as well as single time-point classification (relative to the movement onset) for comparison. The maximum averaged classification accuracies, the respective time points and standard deviations can be read from Table 4 (ME) and Table 5 (MI), respectively. Accuracies are significant above 18% (ME/MI mov-vs-mov) and 54% (ME/MI mov-vs-rest) ($\alpha = 0.05$, adjusted wald interval, Bonferroni corrected for the length of the analyzed time window).

A one-way repeated measures ANOVA was conducted to compare the effect of the window length on the classification accuracy (at the time point of maximum average classification accuracy). There was a statistically significant effect for the window length for ME mov-vs-mov [$F(5,70) = 59.2$, $p_{GG} = 7.0e\text{-}11$], ME mov-vs-rest [$F(5,70) = 7.1$, $p_{GG} = 0.002$], MI mov-vs-mov [$F(5,70) = 21.6$, $p = 5.0e\text{-}13$], and MI mov-vs-rest [$F(5,70) = 3.5$, $p_{GG} = 0.02$]. Mauchly's test indicated that the sphericity assumption had been violated for ME mov-vs-mov, ME mov-vs-rest and MI mov-vs-rest ($p < 0.05$), and a Greenhouse-Geisser correction was applied in these cases. Post hoc tests with Dunn & Šidák's method were performed between groups and results are shown in Fig 7.

Motor-related cortical potentials

The grand-average MRCPs for all movements and the rest condition are shown in Fig 8 (ME) and Fig 9 (MI). MRCPs are aligned to the movement onset for ME and the virtual movement

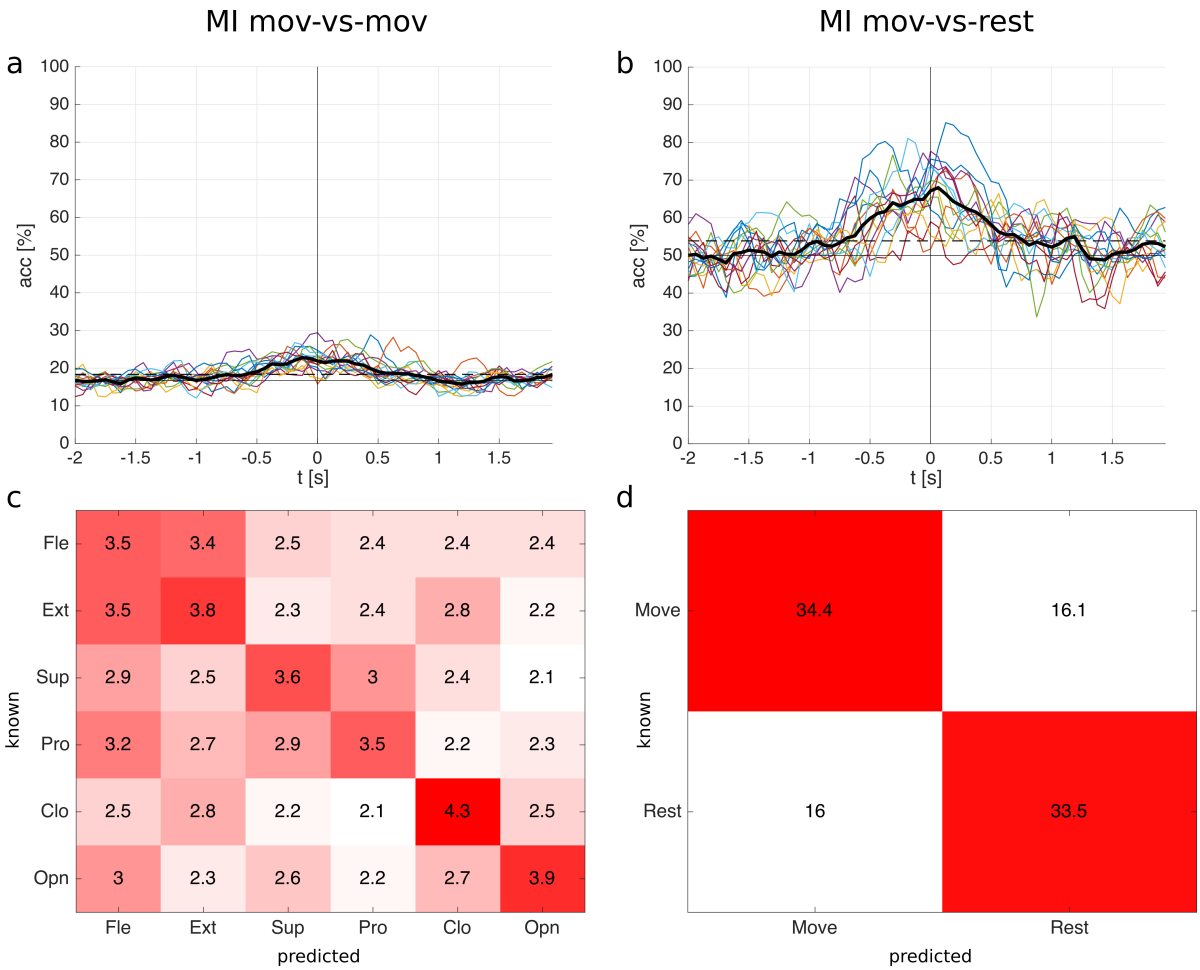

Fig 5. MI classification results for the single time point classification. a: mov-vs-mov classification accuracies of all 15 subjects and the average (thick black line). Time point 0 s corresponds to the movement onset. **b:** mov-vs-rest classification accuracies. The horizontal solid line in a and b is the chance level; the horizontal dashed line is the significance level for the average. **c:** mov-vs-mov confusion matrix (occurrences sum to 100%). **d:** mov-vs-rest confusion matrix. Confusion matrices were calculated at the time point with the highest average classification accuracy (mov-vs-mov: -0.13 s; mov-vs-rest: 0.06 s).

https://doi.org/10.1371/journal.pone.0182578.g005

onset for MI, respectively. We show the grand-average MRCPs for channels FCz, C3, Cz, and C4, here Laplace filtered to increase the spatial resolution, the preprocessing was otherwise the

Table 2. Maximum MI classification accuracies for the single time point classification.

MI	s1	s2	s3	s4	s5	s6	s7	s8	s9	s10	s11	s12	s13	s14	s15	avg
mov-vs-mov [%]	**29**	23	23	**29**	**24**	**24**	**24**	**26**	**28**	23	22	**28**	**27**	**25**	23	25 ± 2
mov-vs-rest [%]	**71**	**72**	**68**	**78**	**77**	**81**	**66**	**85**	**68**	**66**	**77**	**66**	**74**	**73**	**76**	73 ± 6

Included is the average and standard deviation over subjects. Significant classification accuracies are bold.

https://doi.org/10.1371/journal.pone.0182578.t002

Table 3. Time windows used for classification.

window length [s]	number of time points fed into the classifier
0 (single time point)	1
0.2	3
0.4	5
0.6	7
0.8	9
1	11

https://doi.org/10.1371/journal.pone.0182578.t003

same as for the classification. Laplace filtering was done by subtracting the mean voltage of the four surrounding orthogonal electrodes from the center electrode [42]. Generally, ME MRCPs are more pronounced than MI MRCPs (especially on Cz), and the rest condition shows smaller but otherwise similar shaped responses as the movements. The MRCPs show the largest response on Cz (ME) and on FCz (MI), respectively.

Fig 10 shows the ME MRCPs averaged over all subjects with respect to their joint movements. MRCPs on Cz for forearm supination/pronation and elbow flexion/extension are more pronounced than for hand close/open. Elbow and forearm pronation/supination movements have similar MRCPs prior to movement onset and show differences in the latency of their negative peak (around 50 ms and 300 ms, respectively). Also differences in the MRCPs of movements belonging to the same joint are observable (see S1 Fig). The negative peak at Cz in hand opening is 0.3 μV larger than in hand closing. Almost no differences in latency or amplitude can be found between forearm pronation and supination. Elbow flexion leads to earlier MRCPs at Cz (around 60 ms) and weaker MRCPs (about 0.3 μV) than elbow extension. Such a detailed and fair comparison of the MI MRCPs between conditions is not reasonable, since the real imagined movement onset cannot be given.

Classifier patterns

We calculated 9 classifier patterns per subject, per classification type (mov-vs-mov and mov-vs-rest), and per movement condition (ME, MI), ranging from -0.4 s to 0.4 s relative to movement onset. Additionally, we calculated classifier patterns averaged over this time period. We subjected these patterns to statistical analysis, as described in the Methods section, and show them in Fig 11. The figure shows the group averages of the differences between classifier patterns and random classifier patterns (i.e. reference patterns) and only significant voxels are colored.

Immediately before movement onset (around -100 ms), the ME mov-vs-mov patterns (see Fig 11A) are prominent on premotor areas (PM). Subsequently (0–100 ms), patterns intensify on the contralateral primary motor (M1), contralateral somatosensory cortex (S1) and the posterior parietal cortex (PPC). After 300 ms, patterns remain on M1 and S1. Patterns are shortly observable on an ipsilateral temporal area (100 ms). In the ME mov-vs-rest condition (see Fig 11B) patterns appear at movement onset (0 ms) contralaterally on PM, M1, S1 and PPC. The pattern on PM vanishes 100 ms after movement onset and the remaining patterns vanish almost entirely 200 ms after movement onset. S1 Video and S2 Video show the progression of the mov-vs-mov and mov-vs-rest patterns. The mov-vs-mov MI patterns are below the significance threshold (see Fig 11C). The mov-vs-rest MI patterns arise on central motor cortex areas at movement onset (see Fig 11D).

The time averaged ME patterns of mov-vs-mov and mov-vs-rest are similar and are located on PM, M1, S1 and PPC (see Fig 11E). The time averaged MI mov-vs-mov patterns are faintly

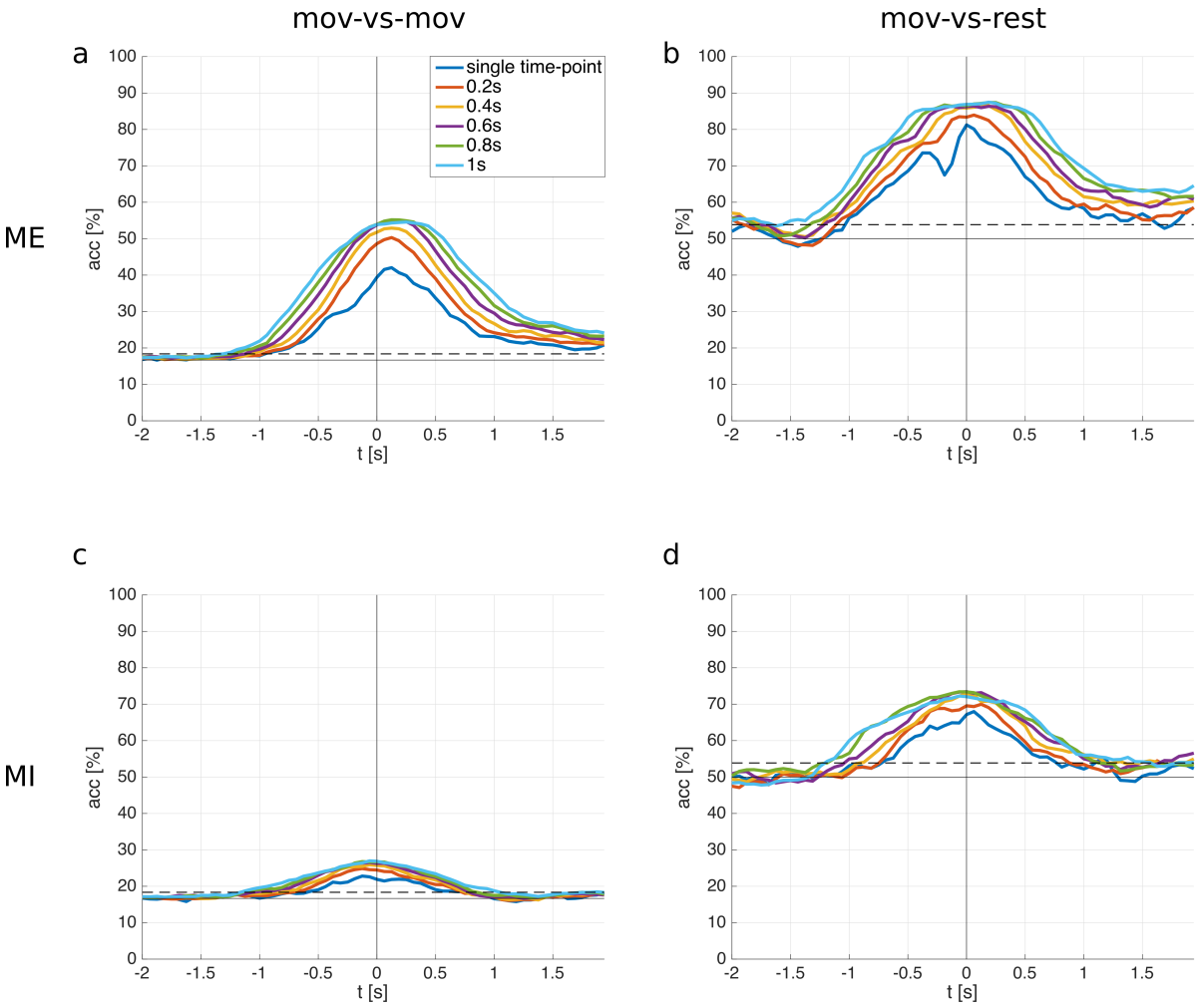

Fig 6. Classification accuracies for different window lengths. Time point 0 s corresponds to the movement onset. The horizontal solid lines are the chance level; the horizontal dashed lines are the significance levels. **a:** subject averaged ME mov-vs-mov classification accuracies. **b:** subject averaged ME mov-vs-rest classification accuracies. **c:** subject averaged MI mov-vs-mov classification accuracies. **d:** subject averaged MI mov-vs-rest classification accuracies.

https://doi.org/10.1371/journal.pone.0182578.g006

located on central areas (see Fig 11G), whereas the mov-vs-rest patterns have a more distinct representation on M1 and S1.

Discussion

We show in this work for the first time the successful classification of six different movements of the right arm from low-frequency time-domain EEG. Significant classification accuracies were reached during movement execution as well as during movement imagination. This proves that single and non-repetitive movements of the same limb can be decoded from time-

Table 4. ME classification accuracies for different window lengths.

ME	window length					
	0 s	0.2 s	0.4 s	0.6 s	0.8 s	1 s
mov-vs-mov						
max acc [%]	42	50	53	55	55	55
std dev [%]	9	9	10	10	9	9
time [s]	0.13	0.13	0.13	0.13	0.13	0.25
mov-vs-rest						
max acc [%]	81	84	87	86	87	87
std dev [%]	7	6	6	4	6	4
time [s]	0.0	0.06	0.19	-0.13	0.19	0.19

Included is the maximum of the average classification accuracy and the respective standard deviation and time point.

https://doi.org/10.1371/journal.pone.0182578.t004

domain EEG signals and differentiated against each other. However, despite the ME classification accuracies being promising, the MI classification accuracies are rather low. This may be because ME EEG signals were time-locked to the actual movement onset but MI EEG signals were time-locked to a virtual movement onset (which corresponded to the average ME onset of each subject). Thus, the ME onset was more accurate, and exact time-locking is important for classifying in the time-domain as the underlying signals change over time. One could overcome this issue by defining the virtual movement onset relative to occurring MRCPs [43] instead as a fixed time delay. Another explanation may be that ME produces more pronounced brain patterns than MI in the time-domain. This is indicated by studies analyzing MRCPs [43,44]. Interestingly, Sugata et al. did not find such a dissimilarity in classification accuracy between ME and MI in a magnetoencephalography (MEG) study using comparable features in grasping, pinching and elbow flexion [45]. Also Wang et al. obtained more comparable classification accuracies between ME and MI in a MEG based study employing a target decoding paradigm [46]. Beside that, attempted movements may produce more pronounced brain patterns than MI and therefore yield higher classification accuracies. They may cause a stronger activation of the motor system as indicated in Blokland et al. where classification accuracies in tetraplegic individuals were higher with attempted movements than MI using spectral features [47]. Furthermore, extensive user training could improve the expression of distinct brain patterns. User training can be highly beneficial in SMR-based BCIs [12,48], however it is still unclear if this is also true for time-domain signals in the context of movement decoding.

Table 5. MI classification accuracies for different window lengths.

MI	window length					
	0 s	0.2 s	0.4 s	0.6 s	0.8 s	1 s
mov-vs-mov						
max acc [%]	23	25	26	27	27	27
std dev [%]	2	3	4	3	4	3
time [s]	-0.13	-0.13	-0.06	-0.06	-0.13	-0.06
mov-vs-rest						
max acc [%]	68	70	73	73	73	72
std dev [%]	8	8	5	7	7	8
time [s]	0.06	0.13	0.0	0.0	-0.06	-0.06

Included is the maximum of the average classification accuracy and the respective standard deviation and time point.

https://doi.org/10.1371/journal.pone.0182578.t005

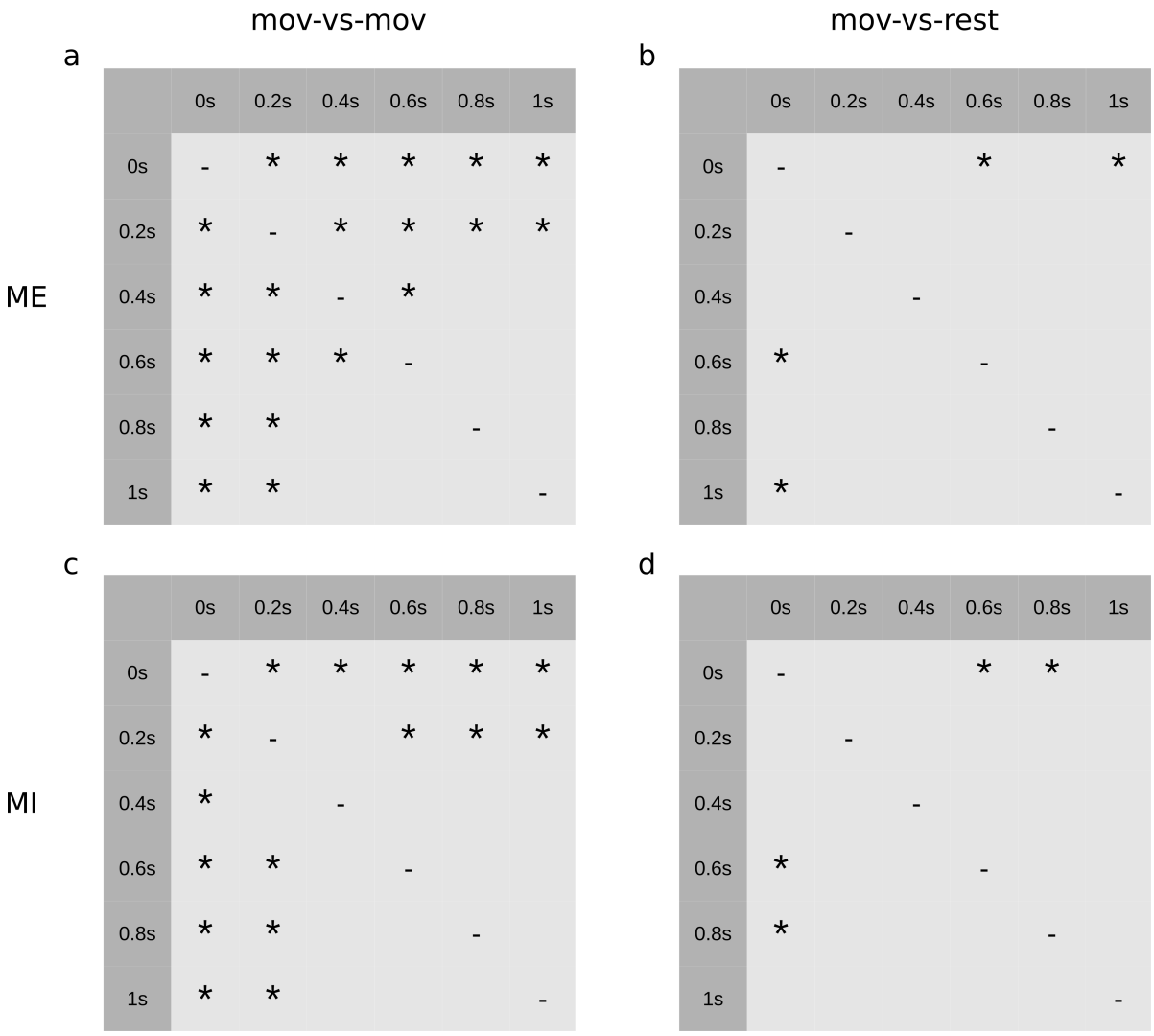

Fig 7. Post hoc tests with Dunn & Šidák's method between window lengths. A star indicates a statistically significant difference ($p < 0.05$) **a:** ME mov-vs-mov **b:** ME mov-vs-rest **c:** MI mov-vs-mov **d:** MI mov-vs-rest.

https://doi.org/10.1371/journal.pone.0182578.g007

Moreover, the obtained confusion matrices indicate that movements involving different joints (i.e. different muscle groups) are more discriminable than movements involving the same joints Consequently, for future applications it would be necessary to select the subset of classes which work best for BCI users but still allow a natural control. Furthermore, a hierarchical classifier concept may be beneficial: one meta classifier classifies movements of different joints (e.g. hand movement vs elbow movement), and subjacent classifiers classify movements of the same joint (e.g. hand open vs hand close).

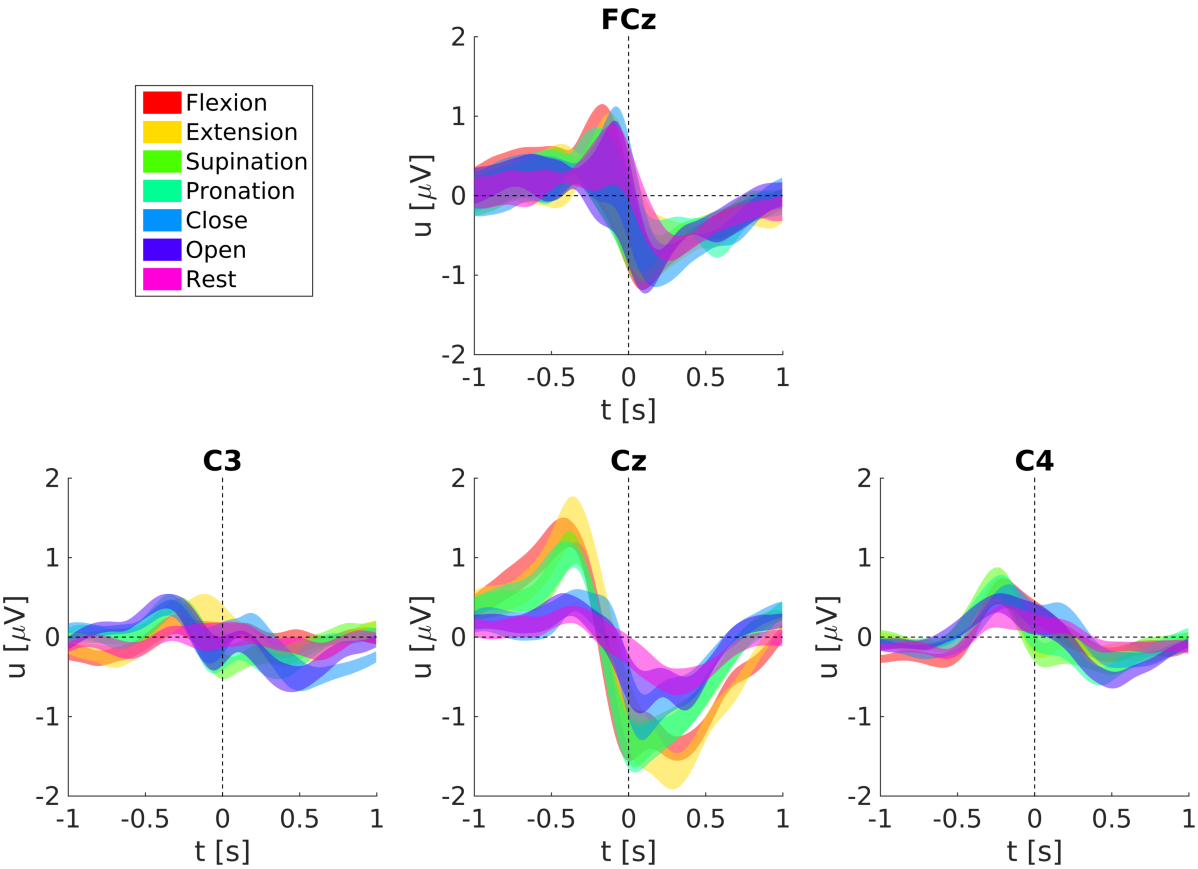

Fig 8. Grand-average MRCPs and respective standard errors during ME.

https://doi.org/10.1371/journal.pone.0182578.g008

A simple approach to improve the classification accuracy is to use more temporal information when classifying the EEG. Therefore, we also classified time windows instead of single time points of the EEG, and analysed the effect of the time window length. The results indicate that a time window of length 0.6 s is sufficient to reach the maximum possible classification accuracy (w.r.t. the methods used in this paper), longer time windows don't improve the classification performance and increase the computational load. Furthermore, ME classification profits more from a time window based approach than MI in case of mov-vs-mov. The improvement in classification performance can be due to the temporal spread of the discriminative information of the underlying signals (i.e. MRCPs) which is better captured with a time window based classification. Another reason may be that a time window based classification allows to fine-tune the employed 0.3–3 Hz bandpass filter. An LDA classifier which uses data from more than one time point is basically a finite impulse response filter with trainable filter coefficients, and can shrink or enlarge the 0.3–3 Hz passband to maximize the extracted discriminative information.

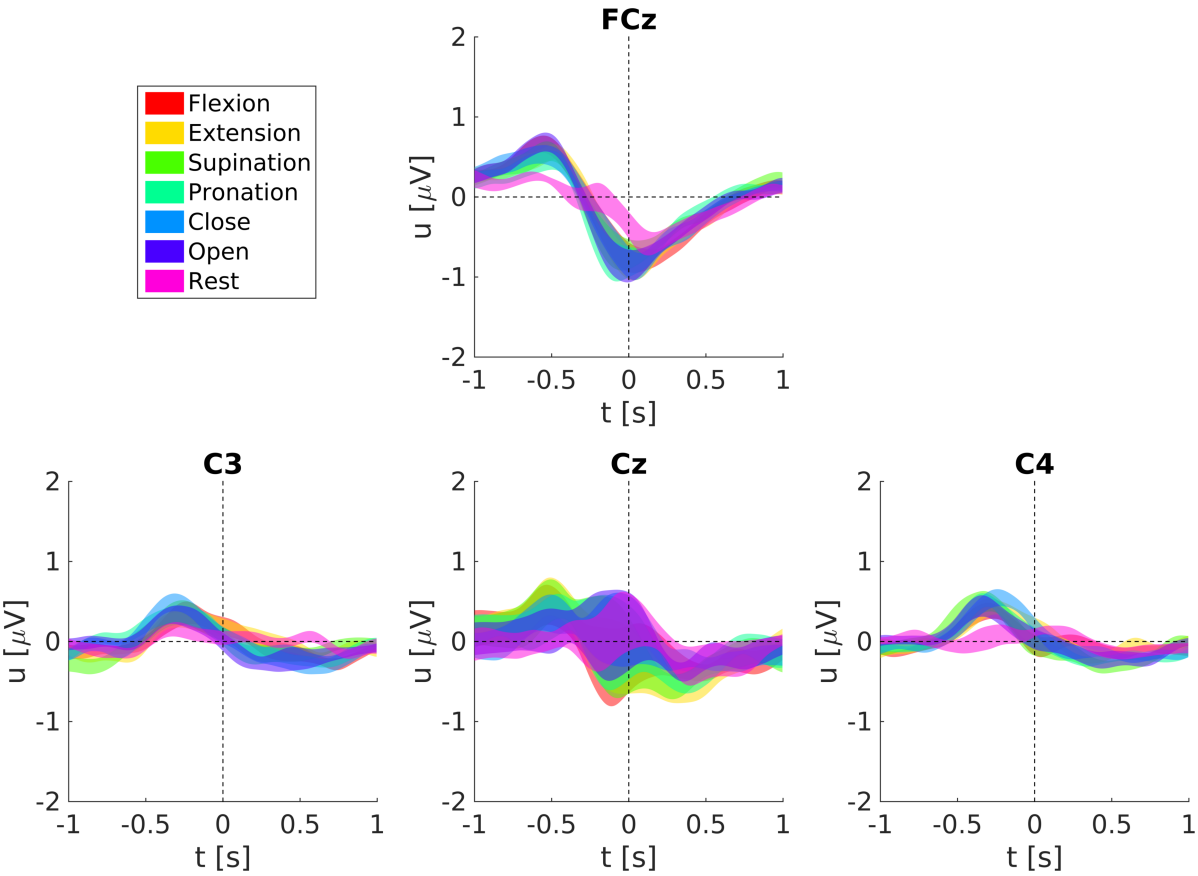

Fig 9. Grand-average MRCPs and respective standard errors during MI.

https://doi.org/10.1371/journal.pone.0182578.g009

Earlier, we pointed out some possibilities to boost the MI accuracy. However, a study conducted by Lacourse et al. [49] forments doubts if MI accuracy in healthy subjects is a good predictor for the performance in SCI subjects. They found that MRCPs during attempted and imagined hand movements in tetraplegic subjects are more similar than in a abled-bodied control group (there with executed and imagined movements). Furthermore, they found that MRCPs between tetraplegic subjects and abled-bodied subjects are different. This challenges the usefulness of using MI in abled-bodied subjects to predict the classification performance for SCI subjects. Nevertheless, our results show the general applicability in able-bodied subjects and point out the need for further research in SCI subjects with attempted movements.

Our work adds to the work of Vučković and Sepulveda who have shown that wrist extension/flexion and forearm pronation/supination can be decoded from the frequency-domain of EEG [27,28] (especially from the delta band). Here, we show that also the time-domain contains movement information related to individual joint movements. This is in line with previous research which shows that low-frequency time-domain EEG signals contain information about movement trajectories, speed and force [17–19,22,23,26]. Electrocorticography (ECoG)

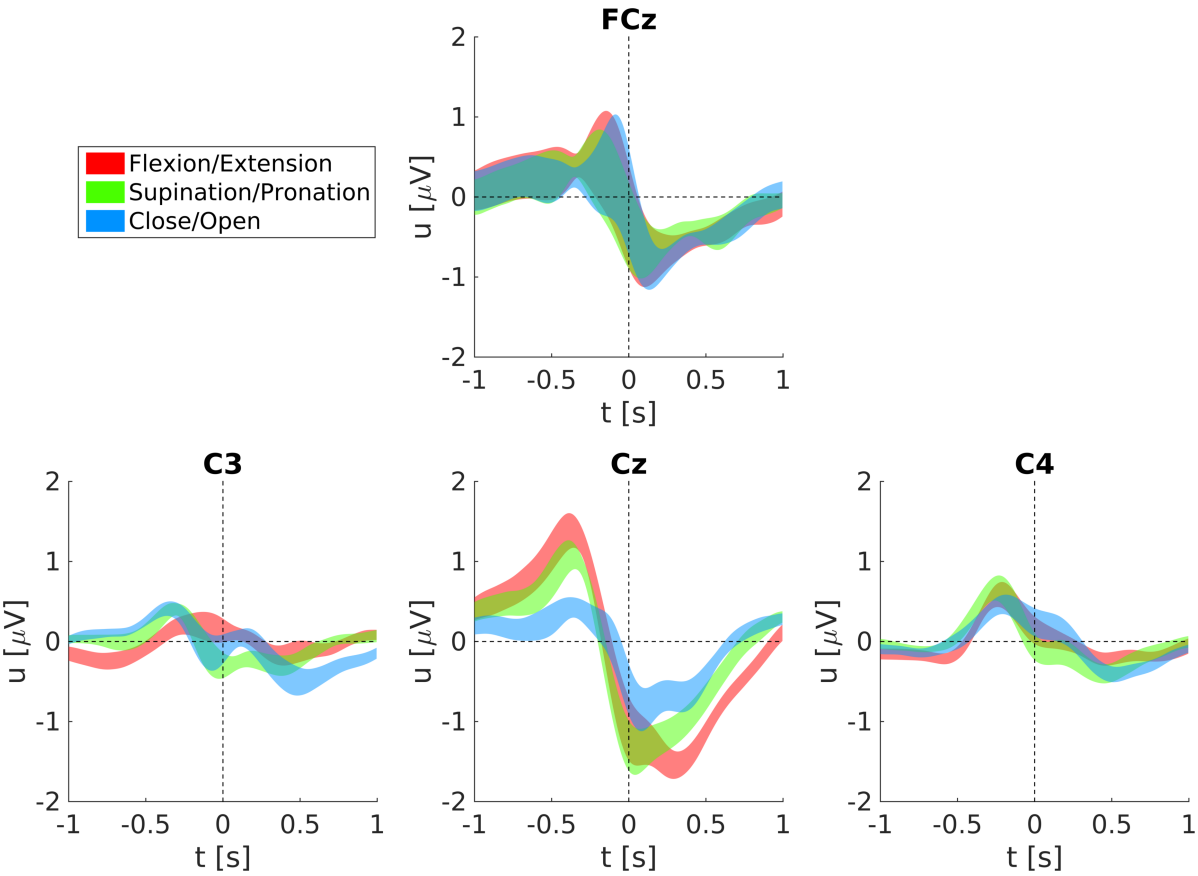

Fig 10. Grand-average ME MRCPs grouped with respect to their joint movements and respective standard errors. Shown are the averages of elbow extension/flexion, forearm supination/pronation and hand opening/closing.

https://doi.org/10.1371/journal.pone.0182578.g010

studies support this and indicate that low-frequency time-domain signals contain movement related information [50–54]. Interestingly, the frequency bands used in classical SMR-based BCIs, i.e. mu and beta band, contain less information about movement kinematics and muscle activity than low-frequency bands and the high-gamma band [55–57]. Mu and beta bands are more suitable to detect a movement intention than the details of the movement. However, our group recently found that these frequency bands can be separated in two types of large-scale networks where one network type is modulated by the movement phase of rhythmic finger movements [9].

To reliably detect the movement intention is of utmost importance for a neuroprosthesis control to avoid unexpected and potentially dangerous movements. In accordance with [26,58], we successfully classified between movements and a rest class based on low-frequency time-domain EEG. The classification of movement vs rest may be further improved by combining time-domain signals and power modulations in mu and beta bands [59].

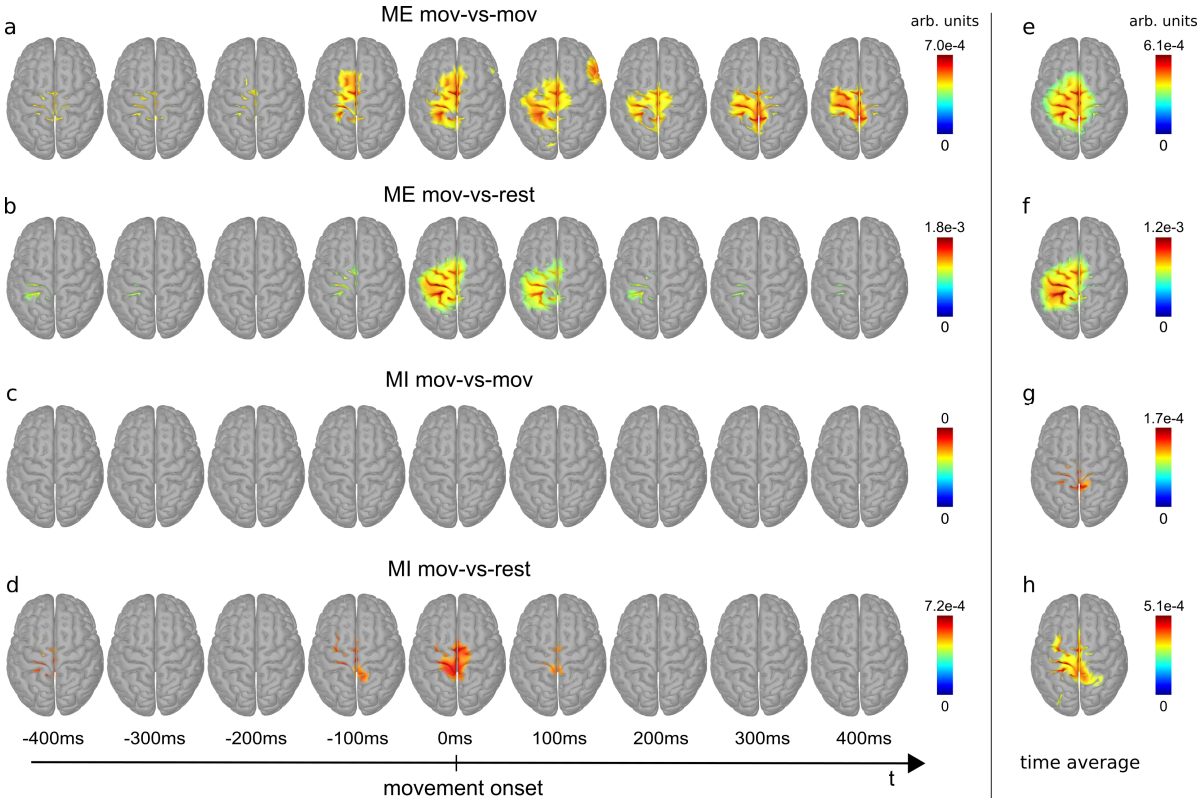

Fig 11. Classifier patterns. Shown are patterns between -0.4 s and 0.4 s relative to movement onset (**a**-**d**) and averaged over this time period (**e**-**h**). **a** and **e:** mov-vs-mov patterns during ME. **b** and **f:** mov-vs-rest patterns during ME. **c** and **g:** mov-vs-mov patterns during MI. **d** and **h:** mov-vs-rest patterns during MI. Only significant voxels are colored. Blue corresponds to zero, red to the maximum value.

https://doi.org/10.1371/journal.pone.0182578.g011

MRCPs can be retrieved with similar signal processing methods as low-frequency time-domain signals. They show a typical negative peak around movement onset like in our results [24]. Hence, our classification approach is based on MRCPs. Such MRCPs-like signals are also observable in both ME and MI rest classes, i.e. without any movement intention. It is reported that voluntary muscle relaxation causes similar potential changes to that of muscle contraction [24]. This may be an explanation at least for ME if the subjects were already preparing for some movement before the cue appeared on the screen, and then relaxed after the rest class cue was presented. This can be an issue for an asynchronous BCI trained with a cue based paradigm. An asynchronous BCI must be trained on a rest class which truly corresponds to a relaxation phase, and this requires a careful design of the training paradigm.

A novelty in the context of EEG-based movement decoding from a single limb is the analysis of the classifier patterns. These patterns show for ME that mainly M1, S1, PM, and PPC contain movement related information which can be decoded from low-frequency time-domain EEG signals. This is consistent with the general understanding that PM and PPC are involved in movement planning while M1 is active during the execution of the movement, and S1 receives proprioceptive feedback which is eventually integrated with other sensory input at

the PPC [60–62]. The ME mov-vs-mov patterns show also a slight and temporary involvement of a non-motor related ipsilateral temporal area. However, this lateral pattern cannot be attributed to movement artefacts as the mov-vs-rest classifier would be more susceptible to movement artefacts but does not have similar pronounced lateral pattern. This lateral pattern can be a consequence of the usage of a template head model and an incomplete electrode coverage on temporal sites. Another observation is that mov-vs-mov and mov-vs-rest patterns cover similar areas. Thus, general (mov-vs-rest) and detailed (mov-vs-mov) movement information can be decoded from the same brain areas. One can also observe that MI produces less pronounced patterns than ME, which is consistent with a lower classification accuracy for MI than ME. The MI patterns are also more centrally located.

We calculated classifier patterns instead of analyzing the weights of the LDA classifier because the EEG channels are highly correlated in lower frequencies [19] which causes a problem known as multicollinearity [63] and complicates their interpretation [64]. Classifier patterns were already used as a tool to spatially analyze brain processes [65]. They can be used to find EEG amplitude differences exploited by the classifier between experimental conditions.

The following limitations of our study can be identified. First, preprocessing filter and classification time windows were non-causal to avoid time shifts in the obtained results due to signal processing. However, for an online application causal filter and time windows must implemented. Second, the movement onsets obtained via external sensors are not as timely as movement onsets obtained via electromyography. Due to inertia of the body parts, muscle activity is usually detected before overt movements. Third, we used template head models instead of individual head models generated from magnetic resonance imaging scans for source imaging, which can increase the location error of sources and in turn decreases the sensitivity of the obtained patterns.

Future studies need to confirm if details of imagined or attempted movements can also be decoded from individuals with SCI and if the classifier performance is sufficient to control a neuroprosthesis or a robotic arm. Specifically, it has to be determined if the classification accuracies yielded by attempted movements in individuals with SCI correspond closer to the ME or MI accuracies reported in this work. The classifier patterns show that PM, M1 and S1 encode information about the details of the movement on the macroscale, and especially these areas have direct connections to the spinal cord [62,66]. These direct connections are impaired in SCI users, however, and this could have an influence on the information encoded in the MRCPs [49]. Further studies also need to analyze the influence of object interactions on the movement information encoded in low-frequency time-domain EEG signals.

Conclusion

We have demonstrated the successful decoding of single executed and imagined upper limb movements based on low-frequency time-domain EEG signals. These movements can be the basis for new mental control strategies aimed at a more natural neuroprosthesis or robotic arm control. Furthermore, we show that the patterns underlying the classification emerge from motor related brain areas.

Supporting information

S1 Fig. MRCPs for movements belonging to the same joints. Shown is the average over subjects.
(TIF)

S1 Video. Progression of the ME mov-vs-mov patterns. Patterns were calculated for single time points (i.e. not averaged over time) from -1 s to 1 s relative to movement onset. Statistical analysis was not performed.
(AVI)

S2 Video. Progression of the ME mov-vs-rest patterns. Patterns were calculated for single time points (i.e. not averaged over time) from -1 s to 1 s relative to movement onset. Statistical analysis was not performed.
(AVI)

Author Contributions

Conceptualization: PO AS GRMP.

Data curation: GRMP.

Formal analysis: PO.

Funding acquisition: GRMP.

Investigation: PO AS.

Methodology: PO AS JP GRMP.

Project administration: GRMP.

Resources: GRMP.

Software: PO.

Supervision: GRMP.

Visualization: PO.

Writing – original draft: PO.

Writing – review & editing: PO AS JP GRMP.

References

1. Rupp R, Gerner HJ. Neuroprosthetics of the upper extremity—clinical application in spinal cord injury and challenges for the future. Acta Neurochir Suppl. 2007; 97: 419–426.
2. Rupp R, Rudiger R, Martin R, Matthias S, Alex K, Muller-Putz GR. Functional Rehabilitation of the Paralyzed Upper Extremity After Spinal Cord Injury by Noninvasive Hybrid Neuroprostheses. Proc IEEE. 2015; 103: 954–968.
3. Hochberg LR, Serruya MD, Friehs GM, Mukand JA, Saleh M, Caplan AH, et al. Neuronal ensemble control of prosthetic devices by a human with tetraplegia. Nature. 2006; 442: 164–171. https://doi.org/10.1038/nature04970 PMID: 16838014
4. Hochberg LR, Bacher D, Jarosiewicz B, Masse NY, Simeral JD, Vogel J, et al. Reach and grasp by people with tetraplegia using a neurally controlled robotic arm. Nature. 2012; 485: 372–375. https://doi.org/10.1038/nature11076 PMID: 22596161
5. Collinger JL, Wodlinger B, Downey JE, Wang W, Tyler-Kabara EC, Weber DJ, et al. High-performance neuroprosthetic control by an individual with tetraplegia. Lancet. 2013; 381: 557–564. https://doi.org/10.1016/S0140-6736(12)61816-9 PMID: 23253623
6. Wodlinger B, Downey JE, Tyler-Kabara EC, Schwartz AB, Boninger ML, Collinger JL. Ten-dimensional anthropomorphic arm control in a human brain−machine interface: difficulties, solutions, and limitations. J Neural Eng. 2014; 12: 016011. https://doi.org/10.1088/1741-2560/12/1/016011 PMID: 25514320
7. Pfurtscheller G, da Silva FHL. Event-related EEG/MEG synchronization and desynchronization: basic principles. Clin Neurophysiol. 1999; 110: 1842–1857. PMID: 10576479

8. Wagner J, Makeig S, Gola M, Neuper C, Müller-Putz G. Distinct β Band Oscillatory Networks Subserving Motor and Cognitive Control during Gait Adaptation. J Neurosci. 2016; 36: 2212–2226. https://doi.org/10.1523/JNEUROSCI.3543-15.2016 PMID: 26888931
9. Seeber M, Scherer R, Müller-Putz GR. EEG oscillations are modulated in different behavior-related networks during rhythmic finger movements. J Neurosci. in press;
10. Müller-Putz GR, Scherer R, Pfurtscheller G, Rupp R. EEG-based neuroprosthesis control: a step towards clinical practice. Neurosci Lett. 2005; 382: 169–174.
11. Kreilinger A, Rohm M, Kaiser V, Leeb R, Rupp R, Mueller-Putz GR. Neuroprosthesis Control via a Non-invasive Hybrid Brain-Computer Interface. IEEE Intell Syst. 2013; 28: 40–43.
12. Pfurtscheller G, Gert P, Müller GR, Jörg P, Gerner HJ, Rüdiger R. "Thought"–control of functional electrical stimulation to restore hand grasp in a patient with tetraplegia. Neurosci Lett. 2003; 351: 33–36. PMID: 14550907
13. Rohm M, Schneiders M, Müller C, Kreilinger A, Kaiser V, Müller-Putz GR, et al. Hybrid brain-computer interfaces and hybrid neuroprostheses for restoration of upper limb functions in individuals with high-level spinal cord injury. Artif Intell Med. 2013; 59: 133–142. https://doi.org/10.1016/j.artmed.2013.07.004 PMID: 24064256
14. Yong X, Menon C. EEG classification of different imaginary movements within the same limb. PLoS One. 2015; 10: e0121896. https://doi.org/10.1371/journal.pone.0121896 PMID: 25830611
15. Edelman BJ, Baxter B, He B. EEG Source Imaging Enhances the Decoding of Complex Right-Hand Motor Imagery Tasks. IEEE Trans Biomed Eng. 2016; 63: 4–14. https://doi.org/10.1109/TBME.2015.2467312 PMID: 26276986
16. Pfurtscheller G, Guger C, Müller G, Krausz G, Neuper C. Brain oscillations control hand orthosis in a tetraplegic. Neurosci Lett. 2000; 292: 211–214. PMID: 11018314
17. Bradberry TJ, Gentili RJ, Contreras-Vidal JL. Reconstructing three-dimensional hand movements from noninvasive electroencephalographic signals. J Neurosci. 2010; 30: 3432–3437. https://doi.org/10.1523/JNEUROSCI.6107-09.2010 PMID: 20203202
18. Ofner P, Müller-Putz GR. Decoding of velocities and positions of 3D arm movement from EEG. Conf Proc IEEE Eng Med Biol Soc. 2012; 2012: 6406–6409. https://doi.org/10.1109/EMBC.2012.6347460 PMID: 23367395
19. Ofner P, Müller-Putz GR. Using a noninvasive decoding method to classify rhythmic movement imaginations of the arm in two planes. IEEE Trans Biomed Eng. 2015; 62: 972–981. https://doi.org/10.1109/TBME.2014.2377023 PMID: 25494495
20. Agashe HA, Paek AY, Zhang Y, Contreras-Vidal JL. Global cortical activity predicts shape of hand during grasping. Front Neurosci. 2015; 9: 121. https://doi.org/10.3389/fnins.2015.00121 PMID: 25914616
21. Waldert S, Preissl H, Demandt E, Braun C, Birbaumer N, Aertsen A, et al. Hand movement direction decoded from MEG and EEG. J Neurosci. 2008; 28: 1000–1008. https://doi.org/10.1523/JNEUROSCI.5171-07.2008 PMID: 18216207
22. Gu Y, Farina D, Murguialday AR, Dremstrup K, Montoya P, Birbaumer N. Offline Identification of Imagined Speed of Wrist Movements in Paralyzed ALS Patients from Single-Trial EEG. Front Neurosci. 2009; 3: 62. https://doi.org/10.3389/neuro.20.003.2009 PMID: 20582286
23. Gu Y, Dremstrup K, Farina D. Single-trial discrimination of type and speed of wrist movements from EEG recordings. Clin Neurophysiol. 2009; 120: 1596–1600. https://doi.org/10.1016/j.clinph.2009.05.006 PMID: 19535289
24. Shibasaki H, Hiroshi S, Mark H. What is the Bereitschaftspotential? Clin Neurophysiol. 2006; 117: 2341–2356. https://doi.org/10.1016/j.clinph.2006.04.025 PMID: 16876476
25. Yuan H, Perdoni C, He B. Relationship between speed and EEG activity during imagined and executed hand movements. J Neural Eng. 2010; 7: 026001.
26. Jochumsen M, Niazi IK, Taylor D, Farina D, Dremstrup K. Detecting and classifying movement-related cortical potentials associated with hand movements in healthy subjects and stroke patients from single-electrode, single-trial EEG. J Neural Eng. 2015; 12: 056013. https://doi.org/10.1088/1741-2560/12/5/056013 PMID: 26305233
27. Vučković A, Sepulveda F. Delta band contribution in cue based single trial classification of real and imaginary wrist movements. Med Biol Eng Comput. 2008; 46: 529–539. https://doi.org/10.1007/s11517-008-0345-8 PMID: 18418635
28. Vučković A, Sepulveda F. A two-stage four-class BCI based on imaginary movements of the left and the right wrist. Med Eng Phys. 2012; 34: 964–971. https://doi.org/10.1016/j.medengphy.2011.11.001 PMID: 22119365

29. Liao X, Yao D, Wu D, Li C. Combining Spatial Filters for the Classification of Single-Trial EEG in a Finger Movement Task. IEEE Trans Biomed Eng. 2007; 54: 821–831. https://doi.org/10.1109/TBME.2006.889206 PMID: 17518278

30. Neuper C, Scherer R, Reiner M, Pfurtscheller G. Imagery of motor actions: differential effects of kinesthetic and visual-motor mode of imagery in single-trial EEG. Brain Res Cogn Brain Res. 2005; 25: 668–677. https://doi.org/10.1016/j.cogbrainres.2005.08.014 PMID: 16236487

31. Delorme A, Makeig S. EEGLAB: an open source toolbox for analysis of single-trial EEG dynamics including independent component analysis. J Neurosci Methods. 2004; 134: 9–21. https://doi.org/10.1016/j.jneumeth.2003.10.009 PMID: 15102499

32. Peck R, Van Ness J. The use of shrinkage estimators in linear discriminant analysis. IEEE Trans Pattern Anal Mach Intell. 1982; 4: 530–537. PMID: 21869073

33. Blankertz B, Lemm S, Treder M, Haufe S, Müller K-R. Single-trial analysis and classification of ERP components—A tutorial. Neuroimage. 2011; 56: 814–825. https://doi.org/10.1016/j.neuroimage.2010.06.048 PMID: 20600976

34. Pascual-Marqui RD. Standardized low-resolution brain electromagnetic tomography (sLORETA): technical details. Methods Find Exp Clin Pharmacol. 2002; 24 Suppl D: 5–12.

35. Michel CM, Murray MM, Lantz G, Gonzalez S, Spinelli L, de Peralta RG. EEG source imaging. Clin Neurophysiol. 2004; 115: 2195–2222. https://doi.org/10.1016/j.clinph.2004.06.001 PMID: 15351361

36. Tadel F, Baillet S, Mosher JC, Pantazis D, Leahy RM. Brainstorm: a user-friendly application for MEG/EEG analysis. Comput Intell Neurosci. 2011; 2011: 879716. https://doi.org/10.1155/2011/879716 PMID: 21584256

37. Schäfer J, Juliane S, Korbinian S. A Shrinkage Approach to Large-Scale Covariance Matrix Estimation and Implications for Functional Genomics. Stat Appl Genet Mol Biol. 2005; 4. https://doi.org/10.2202/1544-6115.1175 PMID: 16646851

38. Nichols TE, Holmes AP. Nonparametric permutation tests for functional neuroimaging: a primer with examples. Hum Brain Mapp. 2002; 15: 1–25. PMID: 11747097

39. Maris E, Oostenveld R. Nonparametric statistical testing of EEG- and MEG-data. J Neurosci Methods. 2007; 164: 177–190. https://doi.org/10.1016/j.jneumeth.2007.03.024 PMID: 17517438

40. Billinger M, Martin B, Ian D, Vera K, Jing J, Allison BZ, et al. Is It Significant? Guidelines for Reporting BCI Performance. Biological and Medical Physics, Biomedical Engineering. 2012. pp. 333–354.

41. Müller-Putz GR, Scherer R, Brunner C, Leeb R, Pfurtscheller G. Better than random? A closer look on BCI results. Int J Bioelectromagn. 2008; 10: 52–55.

42. Hjorth B. An on-line transformation of EEG scalp potentials into orthogonal source derivations. Electroencephalogr Clin Neurophysiol. 1975; 39: 526–530. PMID: 52448

43. Niazi IK, Jiang N, Tiberghien O, Nielsen JF, Dremstrup K, Farina D. Detection of movement intention from single-trial movement-related cortical potentials. J Neural Eng. 2011; 8: 066009. https://doi.org/10.1088/1741-2560/8/6/066009 PMID: 22027549

44. do Nascimento OF, Nielsen KD, Voigt M. Movement-related parameters modulate cortical activity during imaginary isometric plantar-flexions. Exp Brain Res. 2006; 171: 78–90. https://doi.org/10.1007/s00221-005-0247-z PMID: 16320044

45. Sugata H, Hisato S, Masayuki H, Takufumi Y, Kojiro M, Shiro Y, et al. Common neural correlates of real and imagined movements contributing to the performance of brain–machine interfaces. Sci Rep. 2016; 6: 24663. https://doi.org/10.1038/srep24663 PMID: 27090735

46. Wang W, Sudre GP, Xu Y, Kass RE, Collinger JL, Degenhart AD, et al. Decoding and cortical source localization for intended movement direction with MEG. J Neurophysiol. 2010; 104: 2451–2461. https://doi.org/10.1152/jn.00239.2010 PMID: 20739599

47. Blokland Y, Vlek R, Karaman B, Özin F, Thijssen D, Eijsvogels T, et al. Detection of event-related desynchronization during attempted and imagined movements in tetraplegics for brain switch control. Conf Proc IEEE Eng Med Biol Soc. 2012; 2012: 3967–3969. https://doi.org/10.1109/EMBC.2012.6346835 PMID: 23366796

48. Wolpaw JR, McFarland DJ. Control of a two-dimensional movement signal by a noninvasive brain-computer interface in humans. PNAS. 2004; 101: 17849–17854. https://doi.org/10.1073/pnas.0403504101 PMID: 15585584

49. Lacourse MG, Cohen MJ, Lawrence KE, Romero DH. Cortical potentials during imagined movements in individuals with chronic spinal cord injuries. Behav Brain Res. 1999; 104: 73–88. PMID: 11125744

50. Hotson G, Fifer MS, Acharya S, Benz HL, Anderson WS, Thakor NV, et al. Coarse electrocorticographic decoding of ipsilateral reach in patients with brain lesions. PLoS One. 2014; 9: e115236. https://doi.org/10.1371/journal.pone.0115236 PMID: 25545500

51. Schalk G, Kubánek J, Miller KJ, Anderson NR, Leuthardt EC, Ojemann JG, et al. Decoding two-dimensional movement trajectories using electrocorticographic signals in humans. J Neural Eng. 2007; 4: 264–275. https://doi.org/10.1088/1741-2560/4/3/012 PMID: 17873429

52. Pistohl T, Ball T, Schulze-Bonhage A, Aertsen A, Mehring C. Prediction of arm movement trajectories from ECoG-recordings in humans. J Neurosci Methods. 2008; 167: 105–114. https://doi.org/10.1016/j.jneumeth.2007.10.001 PMID: 18022247

53. Hammer J, Fischer J, Ruescher J, Schulze-Bonhage A, Aertsen A, Ball T. The role of ECoG magnitude and phase in decoding position, velocity, and acceleration during continuous motor behavior. Front Neurosci. 2013; 7: 200. https://doi.org/10.3389/fnins.2013.00200 PMID: 24198757

54. Acharya S, Fifer MS, Benz HL, Crone NE, Thakor NV. Electrocorticographic amplitude predicts finger positions during slow grasping motions of the hand. J Neural Eng. 2010; 7: 046002. https://doi.org/10.1088/1741-2560/7/4/046002 PMID: 20489239

55. Bundy DT, Pahwa M, Szrama N, Leuthardt EC. Decoding three-dimensional reaching movements using electrocorticographic signals in humans. J Neural Eng. 2016; 13: 026021. https://doi.org/10.1088/1741-2560/13/2/026021 PMID: 26902372

56. Ball T, Schulze-Bonhage A, Aertsen A, Mehring C. Differential representation of arm movement direction in relation to cortical anatomy and function. J Neural Eng. 2009; 6: 016006. https://doi.org/10.1088/1741-2560/6/1/016006 PMID: 19155551

57. Shin D, Watanabe H, Kambara H, Nambu A, Isa T, Nishimura Y, et al. Prediction of muscle activities from electrocorticograms in primary motor cortex of primates. PLoS One. 2012; 7: e47992. https://doi.org/10.1371/journal.pone.0047992 PMID: 23110153

58. López-Larraz E, Montesano L, Gil-Agudo Á, Minguez J. Continuous decoding of movement intention of upper limb self-initiated analytic movements from pre-movement EEG correlates. J Neuroeng Rehabil. 2014; 11: 153. https://doi.org/10.1186/1743-0003-11-153 PMID: 25398273

59. Ibáñez J, Serrano JI, del Castillo MD, Monge-Pereira E, Molina-Rueda F, Alguacil-Diego I, et al. Detection of the onset of upper-limb movements based on the combined analysis of changes in the sensorimotor rhythms and slow cortical potentials. J Neural Eng. 2014; 11: 056009. https://doi.org/10.1088/1741-2560/11/5/056009 PMID: 25082789

60. Andersen RA, Snyder LH, Bradley DC, Xing J. Multimodal representation of space in the posterior parietal cortex and its use in planning movements. Annu Rev Neurosci. 1997; 20: 303–330. https://doi.org/10.1146/annurev.neuro.20.1.303 PMID: 9056716

61. Aflalo T, Kellis S, Klaes C, Lee B, Shi Y, Pejsa K, et al. Neurophysiology. Decoding motor imagery from the posterior parietal cortex of a tetraplegic human. Science. 2015; 348: 906–910. https://doi.org/10.1126/science.aaa5417 PMID: 25999506

62. Kandel E. Principles of Neural Science, Fifth Edition. McGraw Hill Professional; 2013.

63. Farrar DE, Glauber RR. Multicollinearity in Regression Analysis: The Problem Revisited. Rev Econ Stat. 1967; 49: 92.

64. Haufe S, Stefan H, Frank M, Kai G, Sven D, John-Dylan H, et al. On the interpretation of weight vectors of linear models in multivariate neuroimaging. Neuroimage. 2014; 87: 96–110. https://doi.org/10.1016/j.neuroimage.2013.10.067 PMID: 24239590

65. Ofner P, Muller-Putz GR. Movement target decoding from EEG and the corresponding discriminative sources: A preliminary study. Conf Proc IEEE Eng Med Biol Soc. 2015; 2015: 1468–1471. https://doi.org/10.1109/EMBC.2015.7318647 PMID: 26736547

66. Dum RP, Strick PL. The origin of corticospinal projections from the premotor areas in the frontal lobe. J Neurosci. 1991; 11: 667–689. PMID: 1705965

Primary Publication IV

www.nature.com/scientificreports

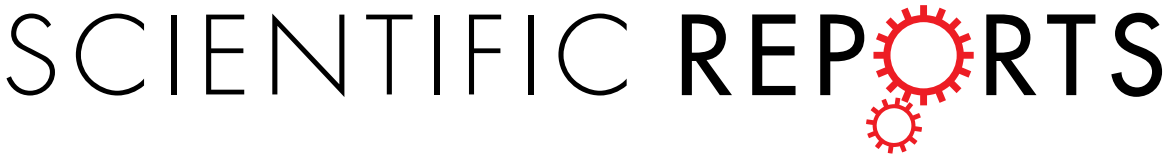

OPEN

Attempted Arm and Hand Movements can be Decoded from Low-Frequency EEG from Persons with Spinal Cord Injury

Received: 11 January 2019
Accepted: 26 April 2019
Published online: 09 May 2019

Patrick Ofner[1], Andreas Schwarz[1], Joana Pereira[1], Daniela Wyss[2], Renate Wildburger[2] & Gernot R. Müller-Putz[1]

We show that persons with spinal cord injury (SCI) retain decodable neural correlates of attempted arm and hand movements. We investigated hand open, palmar grasp, lateral grasp, pronation, and supination in 10 persons with cervical SCI. Discriminative movement information was provided by the time-domain of low-frequency electroencephalography (EEG) signals. Based on these signals, we obtained a maximum average classification accuracy of 45% (chance level was 20%) with respect to the five investigated classes. Pattern analysis indicates central motor areas as the origin of the discriminative signals. Furthermore, we introduce a proof-of-concept to classify movement attempts online in a closed loop, and tested it on a person with cervical SCI. We achieved here a modest classification performance of 68.4% with respect to palmar grasp vs hand open (chance level 50%).

Persons with cervical spinal cord injury (SCI) have lost the majority of voluntary motor control functions. In addition to paralysis of the lower limbs, upper limb functionality is usually severely limited. Brain-computer interfaces (BCIs)[1] in combination with upper-limb motor neuroprostheses[2,3] have been proposed as a remedy[4–6]. A BCI can detect user induced changes in brain-signals and transform them into control signals for neuroprostheses or robotic arms[5–16]. Brain signals can be recorded invasively or non-invasively for this purpose. In the present work, we focus on and apply the non-invasive electroencephalography (EEG) recording technique. EEG-based BCIs for neuroprostheses control rely typically on changes of oscillations originating from sensorimotor areas[17,18] to detect and differentiate executed, imagined or attempted movements involving different body parts[15]. However, oscillation-based BCIs could impose non-intuitive control paradigms (e.g. repetitive foot motor imagery to control a hand function). In recent years, low-frequency time-domain signals have also gained attention in the BCI field as these have been shown to encode even more information about movements such as trajectories[19–23], see[24] for a review. Movement-related cortical potentials (MRCPs)[25,26] in particular were shown to encode, e.g., reaching directions/targets[27–29], or force[30].

MRCPs are particularly interesting when designing an intuitive control paradigm for a BCI. For example, MRCPs encode even various single movements of the same limb, such as hand open, hand close, or different grasp types[31–33], which could be detected by an EEG-based BCI and transformed into movements via a neuroprosthesis. As a result of this a person with SCI would only need to attempt to open the right hand in order to actually open it, and analogously, to close it. This eventually allows a natural control paradigm. In this work, we thus analyzed MRCPs in participants with SCI during attempted movements.

This work comprises two parts. In the first part, we analyzed whether attempted arm and hand movements of participants with SCI can be classified from MRCPs. We have shown in our previous work[31,32] that low-frequency time-domain EEG signals (which capture MRCPs) encode information about hand and arm movements of the same limb in able-bodied participants. The translation of these results to participants with SCI, however, is still lacking. MRCPs in participants with SCI are present during movement imagination and movement attempts but there is evidence that they are altered[34–36]. As a result of this they may not be encoding the same information as in able-bodied participants. We therefore analyzed whether single movement attempts (i.e. hand open, palmar

[1]Graz University of Technology, Institute of Neural Engineering, BCI-Lab, Graz, Austria. [2]AUVA rehabilitation clinic, Tobelbad, Austria. Correspondence and requests for materials should be addressed to G.R.M.P. (email: gernot.mueller@tugraz.at)

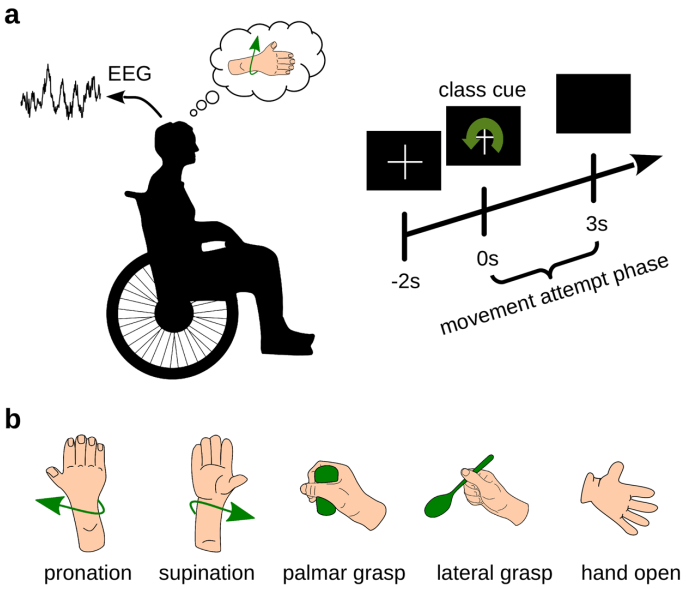

Figure 1. Offline Paradigm. (**a**) Participants with SCI sat in their wheelchairs and attempted the movement requested on a computer screen. (**b**) Illustration of the attempted movements.

participant	sex	age [years]	dominant hand	tested hand	time since lesion [years | months]		AIS	NLI
P01	male	35	right	right	0	11	B	sub C6
P02	male	42	right	right	0	10	D	sub C1
P03	male	62	right	right	0	7	B	sub C5
P04	female	20	right	right	16	9	B	C5
P05	male	57	right	right	0	9	A	sub C4
P06	male	78	right	right	0	7	D	sub C5
P07	male	27	right	left	0	4	C	sub C4
P08	male	69	right	right	2	0	B	C7
P09	male	53	right	right	6	2	A	sub C4
P10	male	55	right	right	1	11	A	sub C6

Table 1. Status of participants. Includes American Spinal Injury Association Impairment Scale (AIS) and Neurological Level of Injury (NLI). Explanation of AIS scores: A = complete, B = sensory incomplete, C = motor incomplete, D = motor incomplete.

grasp, lateral grasp, supination, and pronation) can be classified based on low-frequency time-domain EEG signals in participants with SCI. Furthermore, we analyzed movement-related differences of the neural correlate.

In the second part, we propose a proof-of-concept of an MRCPs-based online classifier for self-paced attempted hand movements (hand open vs palmar grasp). In this proof-of-concept study, we describe the necessary adaptations of the training paradigm and the classifier, and present the online results of two sessions in a participant with SCI.

Results

Movement classification. *Classification accuracies.* We measured 10 participants with cervical SCI, each of whom was seated in a wheelchair in front of a computer screen. Instructions were given on the computer screen to the participants, and according to the instructions, they attempted or executed one of the following movements: pronation, supination, palmar grasp, lateral grasp or hand open. The offline paradigm is shown in Fig. 1. Participants executed or attempted a movement depending on their individual SCI status (see Table 1 and Supplementary Table 1)[37]. We performed an offline analysis and classified the 5 movements from the band-pass filtered EEG signals (0.3 to 3 Hz) with a shrinkage linear discriminant analysis (sLDA) classifier. This yielded a grand average accuracy, which peaked with 45.3% at 1.1 s after class cue presentation. The confidence interval at this peak was [40.3%, 50.3%] (calculated based on a t-distribution[38]). A plot of the participants' classification

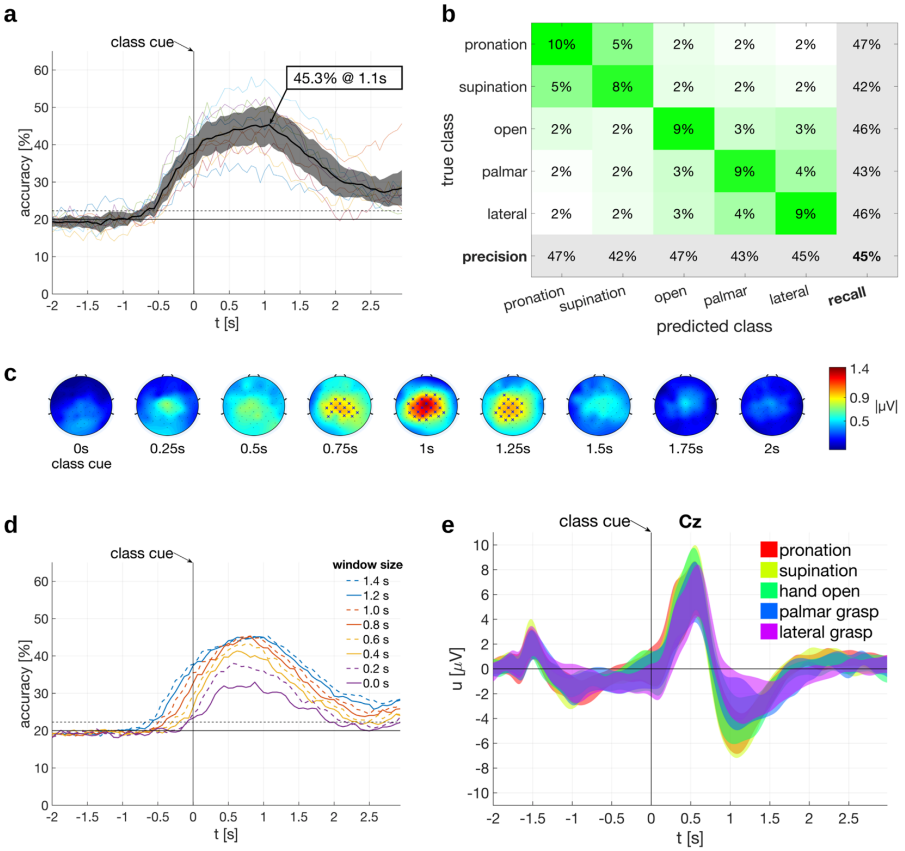

Figure 2. Offline Results for the full set of participants (n = 10). All times are relative to the trial start (**a**) Classification accuracy as a function of time. Grand-average classification accuracy and its respective 95% confidence interval is shown in black, individual classification accuracies are shown in thin, colored traces (feature extraction window size = 1.4 s). The grand average classification accuracy peak is marked. (**b**) Confusion matrix at peak grand average classification accuracy. (**c**) Difference Topoplots. Statistically significant differences on electrodes are marked with an "x". (**d**) Grand average classification accuracies for different feature extraction window sizes (0 s corresponds to one sample). (**e**) Grand average time courses of the electrical potentials on electrode Cz with 95% confidence intervals.

participant	p01	p02	p03	p04	p05	p06	p07	p08	p09	p10
peak acc [%]	35.1	47.7	50.2	52.8	52.7	58.2	40.4	47.7	44.2	42.1
peak latency [s]	2.4	3.3	3.1	3.1	3	2.8	3.1	2.2	3.1	2.9

Table 2. Peak classification accuracies per participant, and respective latencies with a feature extraction window size of 1.4 s.

accuracies and the grand average can be found in Fig. 2a. The plot includes the 95% confidence interval of the grand average (based on a t-distribution[38]). The chance level for 5 classes is 20% and the significance level for the grand average was determined as 22.3% ($\alpha = 0.05$, adjusted wald interval[39,40], Bonferroni corrected for the length of the analyzed time interval). Additionally, the peak accuracies for individual participants with their corresponding latencies are shown in Table 2. The confusion matrix in Fig. 2b, calculated at the peak of the grand average accuracy, shows that all classes are discriminable but classes involving common joints are more prone to be misclassified than classes involving separate joints. We classified EEG samples using a time window of 1.4 s length which was shifted along the trial, and aligned the classification accuracies to the center of this time window (we refer to this time window as feature extraction window). Similar to[31], we then also compared different lengths of feature extraction windows. One can see in Fig. 2d and Supplementary Table 2 that the classification accuracies start saturating with feature extraction windows above 1 s. We therefore did not test feature extraction windows

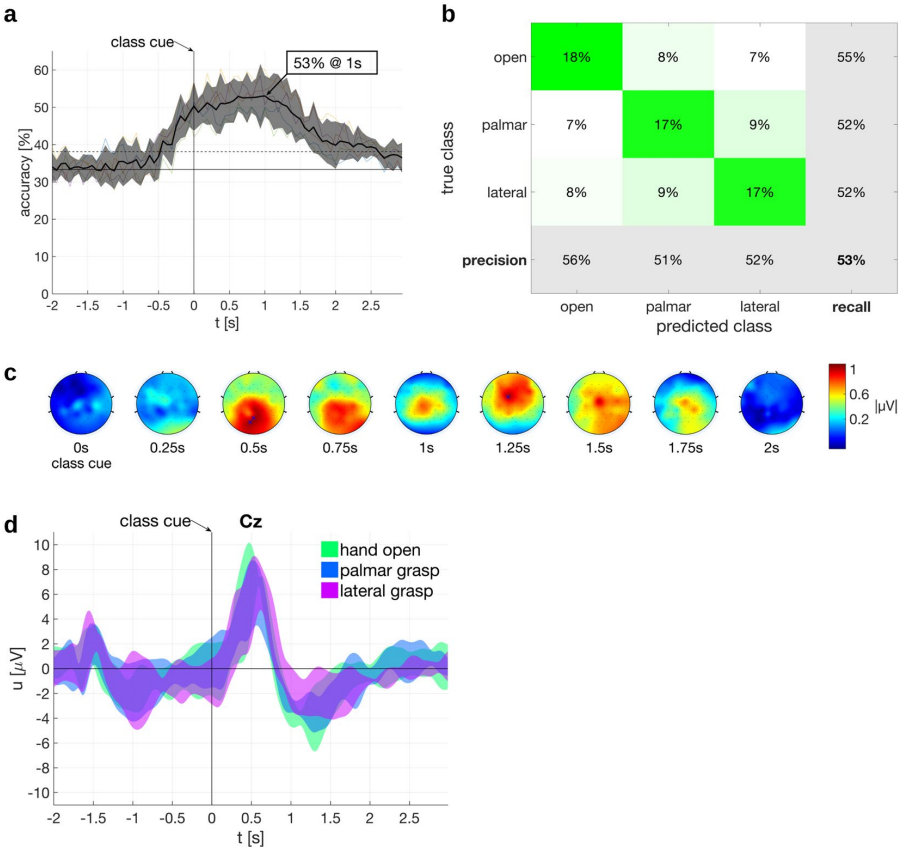

Figure 3. Offline Results for the subset of participants (n = 5) with no active hand movement comprising only of palmar grasp, lateral grasp and hand open classes. All times are relative to trial start (**a**) Classification accuracies of individual participants (thin traces) and the grand average (black thick line) with its respective 95% confidence interval. The classification accuracy peak is marked. (**b**) Confusion matrix at peak grand average classification accuracy. (**c**) Difference Topoplots. Statistically significant differences on electrodes are marked with an "x". (**d**) Grand average time courses of the electrical potentials on electrode Cz with 95% confidence intervals.

longer than 1.4 s and selected this window length for the classification analyses. The reader must keep in mind here that the filter and feature extraction windows were non-causal.

The motor skills of our participants were not homogeneous and some of them had a remaining but impaired hand function or could rotate the forearm. We therefore selected a subset comprising 5 participants who have a motor score of 0 or 1 for finger flexors and finger abductors on the International Standards for Neurological Classification of Spinal Cord Injury (ISNCSCI) impairment scale[37], i.e. no active hand movement. This subset was then subjected to a 3-class classification (palmar grasp, lateral grasp, hand open). By this means we analyzed exclusively those movement classes which could not be executed by the participants. Figure 3a shows the time course of the classification accuracies. The grand average peak was 53.0% at 1 s after class cue presentation with a 95% confidence interval of [47.5%, 58.6%] (the chance level is 33.3% and significance level is 38.1%). The confusion matrix in Fig. 3b indicates that all classes can be discriminated.

MRCPs. The trial averaged electrical potential on the central electrode Cz shows the typical pattern emerging in a synchronous paradigm (c.f. Fig. 2e). 500 ms after the presentation of the class cue, a positive peak developed corresponding to the cognitive processing of the cue. This positive peak is then followed by a negative peak around 1 s after cue presentation which we attribute to the movement attempt and related to MRCPs. Also the averaged potentials of the 5 participant subset (i.e. without active hand movement) have qualitatively similar features (c.f. Fig. 3d). Signals were non-causal filtered between 0.3 to 3 Hz with a monopolar reference. The 95% confidence intervals are based on a t-distribution[38] over participants.

	positive peak				negative peak			
	amplitude [μV]		latency [s]		amplitude [μV]		latency [s]	
class	mean	std dev	mean	std dev	mean	std dev	mean	std dev
pronation	8.01	2.97	0.44	0.14	−5.48	2.38	1.10	0.09
supination	8.44	3.79	0.49	0.13	−6.05	2.15	1.05	0.11
hand open	8.17	3.36	0.51	0.11	−5.33	2.41	1.35	0.59
palmar grasp	6.56	3.34	0.53	0.08	−4.45	2.02	1.41	0.41
lateral grasp	6.68	2.86	0.56	0.08	−3.68	2.19	1.27	0.21

Table 3. Descriptive statistics of the positive and negative peaks of the electrical potentials on Cz. Latency is relative to the class cue.

The early positive and the later negative peaks were defined as points-of-interest, and we analyzed whether their amplitude or latency contains discriminative information for the 5 movement classes. Descriptive statistics can be found in Table 3 which indicates differences of the peaks in the amplitudes and time latencies with respect to the movement classes. Moreover, a nonparametric Friedmann test ($\alpha = 0.05$) found a statistically significant effect of the class on the amplitude of the positive and negative peak ($[\chi^2(4) = 16.3, p = 0.0026]$, $[\chi^2(4) = 20.3, p = 0.0004]$), as well as on the latency of the positive and negative peak ($[\chi^2(4) = 22.1, p = 0.0002]$, $[\chi^2(4) = 12.2, p = 0.0158]$). Thus, the early positive and the later negative peak contain discriminative information about the movement class.

Difference topoplots. We calculated the differences between the topoplots of each class (see Section *Difference topoplots* for further explanations). This allowed us to check the origin of the brain signals containing discriminative information. The resulting plots are termed difference topoplots in this work, and can be seen in Figs 2c and 3c where we averaged over the full set of participants and the subset, respectively. For both sets, the difference topoplot sequences indicate differences on the central motor cortex, which peak around second 1. This means that at the time point of maximum classification accuracy, signals do indeed originate from plausible, i.e. movement-related, brain regions and not from other sources. The subset difference topoplots furthermore show an involvement of the occipital cortex around 1.5 s. Statistically significant differences at time points and electrodes are marked ($\alpha = 0.05$, one-tailed nonparametric permutation test).

Proof-of-Concept of an online classifier. We presented the offline classification of attempted movements in the previous section, here we introduce a proof-of-concept to demonstrate the classification of hand open vs palmar grasp in a closed-loop for a participant with SCI. We recruited participant P09 who has an ISNCSCI motor score of 0 for elbow extensors, finger flexors and finger abductors, i.e. total paralysis of the hand, and measured two sessions on different days.

We introduced a new training paradigm for the classifier. One must keep in mind that the offline paradigm is synchronous and has a cue which requires a cognitive processing, which is then reflected in the EEG potential. Figure 2e is a convenient example of this. However, in a self-paced paradigm the cue-related potential would not be generated at all but only the MRCPs (associated to the negative peak). Therefore, it is imperative that the classifier is trained on MRCPs which are affected to the least extent possible by the cue. Figure 4a shows the training paradigm used for the proof-of-concept study. We used a training paradigm where the class cue was presented immediately at the trial start. This class cue was then replaced by the ready cue, a green filled circle, which started shrinking at a random speed. When the shrinking ball hit the circumference of a small white circle, representing the go cue, the participant was required to attempt the movement.

The trial-averaged electrode potential of Cz, time locked to the go cue (second 0), is shown in Fig. 4c. One can see in Fig. 4c that the positive peak before the negative peak is reduced. The depicted potentials include 95% confidence intervals based on a t-distribution[38] over trials. The potentials corresponding to the two sessions differ right after the movement attempt at around 0.5 s to 1 s, which corresponds to the characteristic negative deflection of MRCPs. Interestingly, it was noted that there is a second negativity around 1.5 s to 2 s exclusively for the second session. This difference between sessions might be due to slightly different instructions to the participant. We asked for a sustained single movement attempt in the first session and for a short single movement attempt in the second session. The additional positive peak between 2 s and 2.5 s is well separated from the negative peak and could have been induced by the sudden disappearance of the cues on the computer screen at trial end. Overall, we can see that the potential time course is closer to that of typical MRCPs[25,26]. This training paradigm is therefore apparently more applicable to train a self-paced movement classifier than the offline paradigm. Using this new training paradigm and additional rest trials, we trained a 3-class online classifier to detect hand open, palmar grasp and rest state.

Subsequently, we evaluated the classifier using the test paradigm shown in Fig. 4b. The class cue (hand open, palmar grasp, rest) was shown together with a white cross in the beginning of a trial. After 5 s, the class cue disappeared and the white cross was shown for the next 60 s. The participant was instructed to perform in this 60 s period multiple self-paced movement attempts if it was a hand open or palmar grasp trial, or to remain inactive in rest trials. During recording, the online classifier was constantly active and provided feedback. When a movement was detected, a hand open or palmar grasp symbol was shown for 2 s on the computer screen. The participant was furthermore instructed to report a movement attempt by a soft speech sound 2 s after the movement attempt to mark movement events.

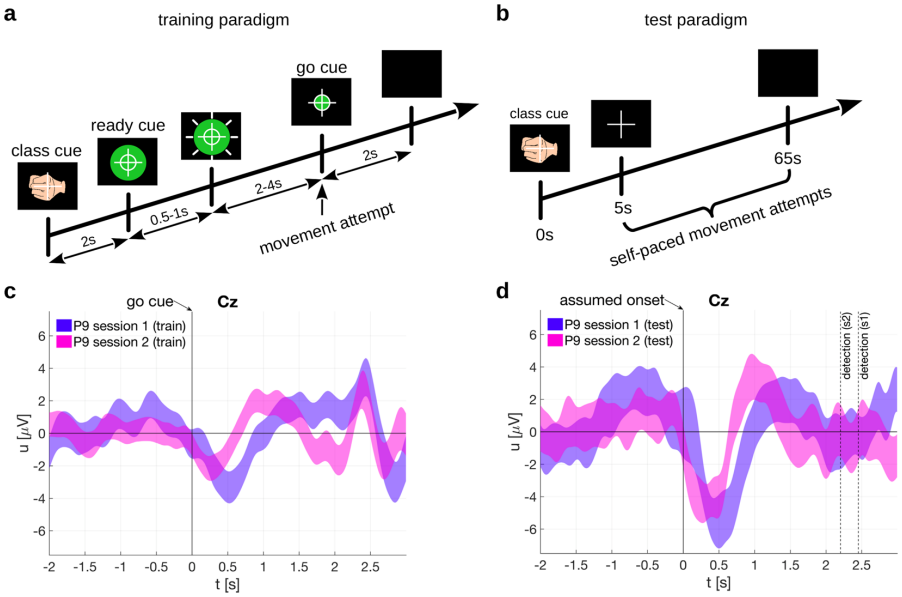

Figure 4. Training and test paradigms for online classification and respective electrode potentials. (**a**) Training paradigm. A green filled circle shrunk with a random speed. The participant attempted a movement (hand open or palmar grasp) when it hit the inner white circle, i.e. the go cue. (**b**) Test paradigm. The participant repeatedly attempted self-paced movements. (**c**) 95% confidence intervals of the electrode potentials on Cz, time locked to the go cue. (**d**) 95% confidence interval of the electrode potentials on Cz, time locked to the assumed movement onset (i.e. the movement detection time point corrected by the detection delay). Additionally, movement detection time points are shown for each session.

session	movement attempts	TP count	TPR [%]	FP/min	accuracy [%]	significance level [%]
1	188	50	26.6	3.2	66.0	62.4
2	130	48	36.9	3.6	70.8	65.3

Table 4. Online detection and classification results of both sessions.

We defined then a true positive window relative to these reported events. We considered a movement detection only as a true positive when it occurred within the true positive window (regardless of the movement class). The true positive rate (TPR) is then the number of true positives (TP) divided by the number of reported movement attempts multiplied by 100. Formally, the TPR is defined as $TPR = TP/P \cdot 100$, where P is the number of condition positives (i.e. the sum of true positives and false negatives). The classification accuracy regarding hand open vs palmar grasp was calculated based on true positives only, i.e. detections outside the true positive window were ignored. We also calculate the number of false positives per minute (FP/min). To do this, every detection within a rest trial was counted as a false positive and then normalized to a per minute rate. Eventually, we obtained an average classification accuracy of 68.4% over both sessions, and the individual session results can be found in Table 4.

Finally, we analyzed whether the classifier was indeed decoding from brain signals. First, we selected all true positives, i.e. all movement detections within the true positive window irrespective of the movement class. Next, we aligned to the assumed movement onset which is the time point of the movement detection minus the detection delay (c.f. Section *Detection delay*). The detection delay was 2.5 s in session 1 and 2.2 s in session 2. We then averaged over trials for each session, and show the electrode potential of Cz in Fig. 4d. The potentials show the typical negativity present in MRCPs and in the potentials elicited in the training paradigm, which is shown in Fig. 4c. The electrode potentials are shown separate for each movement class in Fig. 5. Second, we show in Fig. 6 the topoplots at the time lags used as features by the classifier (0 s to 1.4 s in 200 ms intervals). The topoplots (not to be confused with the difference topoplots) indicate that the classifier uses brain signals originating from lateral and central motor areas which is typical for MRCPs. Importantly, the EEG signals in Fig. 6 were causally filtered to show the reader what the classifier identified when it detected a true positive. The signals in Fig. 4c,d, however, were non-causally filtered to avoid phase distortion and ease the interpretation.

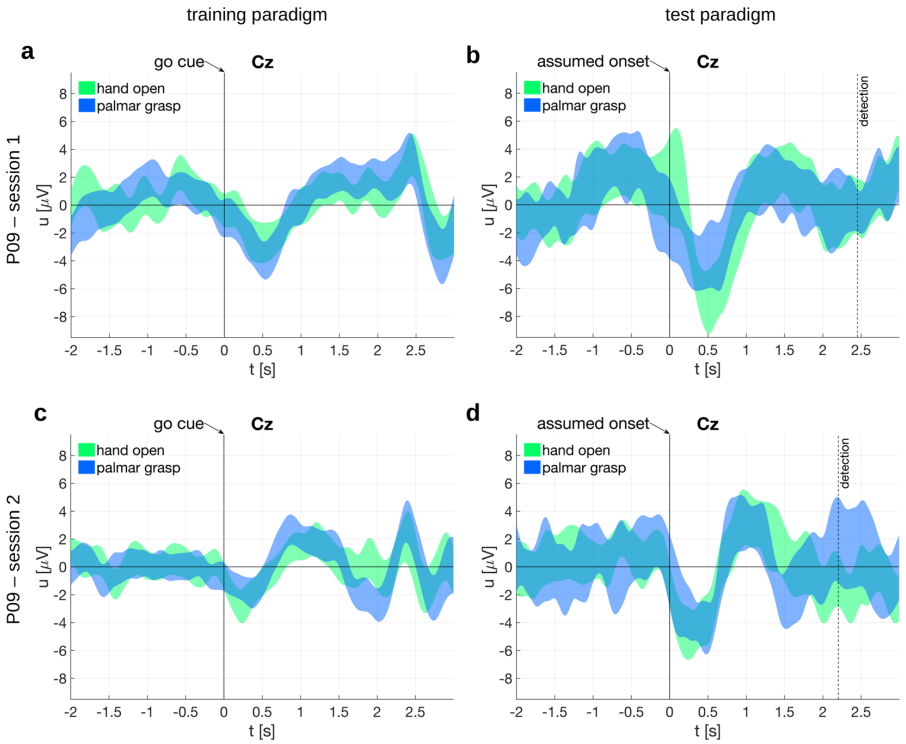

Figure 5. Electrode potentials at the proof-of-concept classification. Shown are the 95% confidence intervals at electrode Cz time locked to the go cue or assumed movement onset, respectively. (**a**) Session 1, training paradigm. (**b**) Session 1, test paradigm. (**c**) Session 2, training paradigm. (**d**) Session 2, test paradigm.

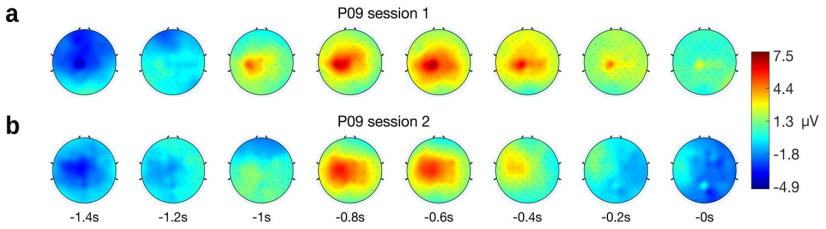

Figure 6. Topoplots from test paradigm. The topoplots are time-locked to true positive movement detections and second 0 corresponds to t_{train} (i.e. the detection time point minus 575 ms, see Section *Detection delay*). Thus, the time lags shown comprise the input features of the classifier. (**a**) Topoplot from session 1. (**b**) Topoplots from session 2.

Discussion

Movement classification. We showed that participants with cervical SCI having impaired upper limb movements encode information about attempted arm and hand movements in low-frequency time-domain EEG signals. This information can be used to discriminate hand open, palmar grasp, lateral grasp, pronation, and supination.

We showed in our previous work the decoding of arm and hand movements from MRCPs[31,32], i.e. low-frequency time domain signals. However, MRCPs are altered in participants with SCI[34–36]. It was therefore unclear if these participants encode similar information in the EEG as participants with an intact spinal cord. With respect to non-invasive recording techniques, it was so far only shown that low-frequency time-domain magnetoencephalography (MEG) signals can be used to discriminate a limited attempted movement set (hand open vs hand close) in participants with SCI[41]. To the best of our knowledge, this study is therefore the first to show that an extended arm/hand movement set can be classified from low-frequency time-domain EEG signals in participants with SCI.

We focused on low-frequency signals as they encode movement trajectories, movement directions, grasp types, speed or force in EEG[19–21,23,32,33,42–45] and ECoG signals[46–51]. Other frequency bands used in classical oscillation-based BCIs[5,6,17], i.e. mu and beta band, were found to encode a general movement state rather than movement parameters (how a movement is performed)[27,42,49,51–53]. However, recent studies extend these findings. For example, Iturrate *et al.*[33] found spectral power differences in the upper alpha and lower beta bands for power and precision grasps. Korik *et al.*[54] demonstrated the decoding of executed and imagined 3D hand movement trajectories from mu, beta, and low gamma bands. Future studies will have to further investigate the decoding of movement parameters from time-domain and frequency-domain features and consistently integrate the findings from both domains.

We found the EEG neural correlates of hand and arm movements differ in central brain areas. No apparent lateralization effect was observable. This is plausible as central brain areas like the Supplementary motor area (SMA), primary motor cortex (M1), and somatosensory cortex (S1) are involved in motor control[55,56]. However, a precise localization is not possible in the channel space. Furthermore, the accuracy plots and difference topoplots indicate that the movement information is spread over time. Moreover the electrical potential on Cz develops two distinctive peaks over time, a positive peak immediately after the cue followed by a negative peak. The positive peak is most likely a complex of P3 and positive slow wave potentials related to stimulus evaluation[57,58] and response selection[59,60]; earlier perception related potentials are filtered out due to their higher frequency components. The negative peak can be explained as an MRCP[25,26]. Both peaks differ in their amplitude and latency depending on the movement, however only the negative peak around 3 s after cue leads to significant differences in the difference topoplots. Furthermore, we obtained significant classification accuracies at both peak latencies (especially with a short feature extraction window). We therefore make the assumption that processes related to inferring the desired behavior (evaluation of rules) as well as movement related processes can be decoded from low-frequency EEG signals.

We found as in[31,32] that the classification accuracy improves with the length of the feature extraction window. This is expected as the discriminable information is spread over time. Moreover, the additional time inputs are weighted by the classifier which can be seen as a temporal filter. This filter could fine-tune the 0.3–3 Hz band-pass filter to extract the proper signals. The classification accuracies, however, show a saturation effect and time windows above 1 s add little or no improvement. Furthermore, we found that the discriminability is dependent on the joints involved in the movement. The confusion matrix indicates that movement classes with separate joints are better discriminable than movement classes with common joints, e.g. pronation is better discriminable from hand open than from supination. This was observed before in healthy participants[31], and it implies that related body parts are encoded closer in low-frequency time-domain EEG signals than less related body parts. Thus, their signal sources are spatially closer and/or the time courses of the generated signals are more similar.

One can observe in the classification accuracy plots that the accuracy raises above significance level before the cue onset, i.e. at a time period when no class information was yet available to the participants. We ascribe that effect to the employed zero-phase band-pass filter and the symmetric feature extraction window which were non-causal. Due to these non-causal features and the low-frequency band, future information in the signal is perceptibly spread back in time. This leads to discriminable signals even before the class cue onset.

Participants with SCI available for studies are often heterogeneous with respect to their residual movement functions, and despite all participants having restrictions in their upper limb movements, the degree of movement function nevertheless varied from person to person. We therefore run an additional analysis comprised only of participants with no active hand movements and a restricted movement set (hand open, palmar grasp, lateral grasp). We obtained a statistically significant classification accuracy which peaked again around 1 s. Furthermore, the emerging neural correlates were similar. As before, differences in central brain areas are observable, but additionally also on occipital areas, which could be related to the visual processing of the cue. However, this effect vanished in a larger group and could be a spurious finding due to the small group size. Also the electrical potential on Cz has a qualitatively similar shape, comprising of a positive peak followed by a negative peak.

Proof-of-concept of an online classifier. An online classifier ideally detects self-paced movements (i.e. movement vs. rest state), and simultaneously classifies them, for example as hand open or palmar grasp as in this work. The critical issue for an effective online classifier is the availability of applicable training data: the training paradigm should elicit MRCPs which are as close as possible to MRCPs elicited in a self-paced paradigm. However, cue-based paradigms similar to the Graz BCI paradigm[61] are not suitable to elicit clean MRCPs because they are usually contaminated with cue-related potentials (as we have observed in the first part of this study). An alternative would be a self-paced training paradigm where the classifier is trained by time-locking on the movement onset[62–67]. However, participants with SCI may have lost all movement functionality of the respective limb, and may not provide any measurable EMG signals to detect the movement onset. We therefore designed a suitable training paradigm and added ready and go cues in addition to the class cue. The class cue requires the retrieval and selection of memorized task rules, and separates these processes from the actual movement attempt. There were variable time intervals before the go cue in order to make class and ready cue associated potentials indiscernible when time-locking to the go cue and averaging. Another important point in our paradigm is that the ready and go cues have a class-independent appearance to avoid any class-related perception differences. Plus, by adding a fixation cross in the middle and a symmetrically shrinking green ball, eye movements can be minimized. Finally, both cross and green ball are still displayed for 2 seconds after the go cue to avoid further evoked potentials close to the go cue due to their disappearance. Furthermore, the predictability of the go cue as given by our training paradigm is critical. The literature shows that MRCPs preceding self-paced and regular-cued movements are similar in shape and topography[68–70]. On the downside, our training paradigm may be contaminated with a contingent negative variation (CNV) potential, which is elicited by a warning stimulus followed by an imperative stimulus[71,72]. The CNV comprises of two components, one occurs after the warning stimulus and one

before the imperative stimulus (i.e. the go cue in our paradigm). The last component in particular could form a potential complex with the Bereitschaftspotential (BP)[26]. However, for longer intervals between the warning and imperative stimulus (in the second range), the second component of the CNV and the late BP become similar in time course and scalp distribution[73–75]. Aside from these theoretical considerations, the potentials measured on participant P09 resemble the shape of band-pass filtered MRCPs. Interestingly, around 1.5 s to 2 s after the go cue we can observe a sustained positive potential deflection in training session 1 which is absent in training session 2. This difference in the potentials is probably due to differences in the movement strategy. Participant P09 was instructed to sustain the attempted movement until the end of the trial in training session 1 but not in training session 2. However, the majority of the EEG samples used for classifier training are from an interval before the deflection differences occur. The effect of the movement strategy on the evaluation outcome should be therefore negligible, which is also indicated by comparable classification accuracies in the two test sessions.

Interestingly, the hand open vs palmar grasp vs rest classifier had its maximum offline classification accuracy at $t_{train} = 1.875$ s (session 1) and $t_{train} = 1.625$ s (session 2), respectively. This means that the classifier found - using a 1.4 s long feature extraction window - the EEG samples from 0.475 s to 1.875 s (session 1), and from 0.225 s to 1.625 (session 2) most discriminative. Thus, the classifier was trained on an interval which started just before the negative potential peak on Cz and also covered the following positive deflection. This differs from the classifier in the offline paradigm, which on average used samples symmetrically around the negative peak. However, this shift could have been caused by the fact that we used a non-causal filter with the offline paradigm and/or that no rest class was present.

In addition to the training paradigm, we also designed an online test paradigm. This test paradigm elicited MRCPs which are similar in morphology to the MRCPs found in the training paradigm: they show a notable negative deflection followed by a positive deflection on Cz. This is to be expected since a classifier detects the trained pattern. However, the test MRCPs have larger amplitudes than the training MRCPs. One reason for this could be that self-paced movements cause similar yet more pronounced potential peaks than predictably cued movements[70]. Another reason could be the detection logic based on pre and post classes. It could be that the strict detection thresholds – which had to be exceeded by the pre, post and movement class – only allowed the detection of very pronounced MRCPs. Furthermore, the associated topoplots are interesting as they show a broad but central negativity followed by a lateralized positivity. This indicates that the classifier has indeed decoded brain signals, i.e. MRCPs, and not movement induced artefacts. However, the test paradigm was designed for a first proof-of-concept and this took place in a controlled environment, to avoid external influences. Future studies will need to evaluate and improve the classifier's generalization capabilities as MRCPs depend on various factors, like force and speed[30,76], goal-directedness[77], attention diversion[78], or externally or internally selected movement types[79]. This generalization is essential in the process of translating the research to the practical needs of end-users.

We obtained a TPR of around 30%, with more than 3 FP/min for participant P09. TPR and FP were calculated regardless of the movement class (hand open or palmar grasp). Furthermore, we obtained a classification accuracy of 68.4%. The classification accuracy was calculated using true positives only. False positives do not coincide with an intention to move and would impede the interpretation of the classification accuracy. The separation of TPR and FP/min from the classification accuracy allows evaluation of the movement detection performance separately from the movement classification. The detection of movements from MRCPs, particularly lower limb movements, is well reported in the literature[30,44,62–65,67,80]. Lower-limb MRCPs-based movement detection performances up to a TPR of 82.5% with FP/min of 1.38 are reported[62], which are nearly 3 times better than the performance reached in this work. However, those results were obtained in healthy participants, and lower limb movements produce more pronounced MRCPs than upper limb movements[81]. What is novel in our work is the simultaneous online classification of various self-paced hand movement attempts in a participant with SCI using EEG. It is noteworthy that we tested our classification approach on a participant with a chronic and complete cervical SCI, and without any remaining hand function (AIS A, NLI C4). Thus, an intact spinal cord is not a prerequisite to classify movements from MRCPs. To the best of our knowledge, only a study based on MEG applied a related protocol for movement online classification in participants with SCI[41], although this was cue-based. In this MEG study, two out of five paralyzed participants reached a significant and comparable classification accuracy of 83.3% and 66.7%, respectively, on classifying hand open vs hand close movement attempts.

The participant group size in the offline analysis ($n = 10$) is in the range of typical BCI studies but rather small compared to typical medical or general neuroscience standards. While we backed up all findings with state-of-the-art analysis and statistics, spurious findings cannot be fully excluded. Nevertheless, the classification and imaging findings are consistent with the literature, which strengthens our confidence in the interpretation of the results. Because of the limited group size and the resulting localization error, we refrained to do an analysis of the difference topoplots in the source space or to discuss the origin of the signal sources in detail. Moreover, we would like to point out that the band-pass filter was not systematically optimized with respect to the classification performance but based on previous studies[31,32]. Furthermore, the online classifier is a proof-of-concept. Other classification approaches based on, e.g. recurrent neural networks or hidden markov models for time series may provide a better detection and classification performance. In addition, we would like to highlight that the online training paradigm was in fact a cue-based paradigm. The influence of the class cue has been diminished, but a true self-paced training paradigm could yield more authentic MRCPs and therefore a better classification and detection performance. Moreover, we demonstrated our online classifier with a single person with SCI, and therefore cannot make any predictions of the expected performance or its variance in the population of persons with SCI.

We showed that various movement attempts of the upper limb can be classified offline from low-frequency time-domain EEG signals in participants with SCI. Furthermore, we have introduced a proof-of-concept on how to detect and classify movements in quasi real-time in a closed-loop setup. While the performance of the classifier is probably not yet sufficient to be used for neuroprosthesis control, we were able to show for the first time the general feasibility of classifying different single upper limb movements in an end-user with SCI.

Methods

Movement classification. *Participants.* We recruited and measured 10 participants with subacute and chronic cervical SCI in a rehabilitation center (AUVA rehabilitation clinic, Tobelbad, Austria). They were aged between 20 and 69 years and suffered their lesion 3 months to 16 years before the study. Inclusion criteria were legal age of 18 years and restricted hand function, whereas artificial ventilation was an exclusion criterion. Their neurological level of injury (NLI) ranged from C1 to C7 and their American Spinal Injury Association Impairment Scale (AIS) score ranged from A to D. See Table 1 and Supplementary Table 1 for details. Written informed consent was obtained from all participants or a witness. The study was conducted in accordance with the protocol approved by the ethics committee for the hospitals of the Austrian general accident insurance institution AUVA (approval number 3/2017).

Paradigm. Each of the participants sat in front of a computer screen with an arm resting on a pillow on their lap or on a table and they carried out the instructions given on the computer screen. At the trial start, a fixation cross and a beep sound were presented. We asked the participants to focus their gaze firmly on the cross which was displayed during the whole trial period of 5 s to avoid eye movements, see Fig. 1a. Furthermore, we instructed participants to avoid swallowing and eye blinking during the trial period. The class cue was displayed 2 s after the trial start for 3 s (i.e. until the end of the trial) and corresponded to one of 5 classes: pronation, supination, palmar grasp, lateral grasp or hand open (c.f. Fig. 1b). Based on the participants' residual motor abilities (c.f. Supplementary Table 1), they were asked to execute or attempt the corresponding movement immediately when the class cue appeared. Furthermore they were asked to avoid any other movement during the current cue phase. If the participants were able to execute a movement, they went back to their initial rest position after the trial period. Between trials, a break with a random period of 1 s to 3 s followed. We recorded 9 runs with 40 trials per run, i.e. 72 trials per class in total.

Recording. We measured the EEG with 61 electrodes covering frontal, central, parietal and temporal areas. Additionally, we measured the electrooculogram (EOG) with 3 electrodes placed above the nasion and below the outer canthi of the eyes. Reference was placed on the left earlobe and ground on AFF2h. Signals were recorded using four 16-channel g.USBamps biosignal amplifiers and a g.GAMMAsys/g.LADYbird active electrode system (g.tec medical engineering GmbH, Austria) with 256 Hz and a band-pass filter from 0.01 Hz to 100 Hz (8^{th} order Chebyshev filter). Power line interference was suppressed with a notch filter at 50 Hz.

Preprocessing. Signals were processed using Matlab R2017a (MathWorks, Massachusetts, USA) and the external toolboxes BioSig 3.3.0[82] and EEGLAB 14.1.1b[83,84]. In short, first (1) we removed noisy channels, next (2) we removed stationary artefacts with ICA, we then (3) detected trials with transient artefacts, and finally (4) we removed stationary and transient artefacts from a narrow band EEG signal (0.3–3 Hz). It is noteworthy that we performed steps 2 and 3 on the EEG signal using a broader frequency range of 0.3–70 Hz to ease the detection of artefacts. The ICA weights were then cached and subsequently applied in step 4.

First (1), we visually inspected signals and removed channels contaminated with perceptible noise. Additionally, we removed by default channel AFz as it is sensitive to eye blinks and eye movements.

Next (2), we removed stationary artefacts by filtering the signals from 0.3 Hz to 70 Hz (4^{th} order Butterworth zero-phase band-pass filter) and computed independent components (ICs) with the extended infomax independent component analysis (ICA) implemented in EEGLAB. We reduced the data dimensionality before computing the ICA with a principal component analysis (PCA) and retained principal components explaining 99% of the variance of the data. Furthermore, we computed the ICA only on samples with an absolute value of less than 10.4 times the median absolute deviation (MAD)[85] of a channel. MAD is robust deviation measure and the chosen threshold corresponds to 7 times the standard deviation for normally distributed data. We then identified the ICs contaminated with muscle and eye related artefacts, removed those ICs and projected the remaining ICs back to the original space.

Next (3), we detected transient artefacts using EEGLAB and marked trials for rejection with (1) values above/below $-100\,\mu V$ and $100\,\mu V$, respectively, (2) trials with abnormal joint probabilities, and (3) trials with abnormal kurtosis. The methods (2) and (3) used as threshold 5 times the standard deviation of their statistic to detect artefact contaminated trials.

Finally (4), we removed the previously computed and artefact contaminated ICs from the original data (i.e. 0.01–100 Hz filtered). For this purpose we applied the cached ICA weights, removed previously identified artefactual components, and back-projected to the channel space. Lastly, we applied a zero-phase 4^{th} order Butterworth band-pass filter from 0.3 Hz to 3 Hz as in[31], and excluded trials marked for rejection from further processing.

Classification. We re-referenced the preprocessed EEG signals to a common average reference (CAR) and classified the EEG with a multiclass shrinkage linear discriminant analysis (sLDA) classifier[86,87]. The input to the sLDA classifier were the EEG samples from all low noise channels. Furthermore, we used multiple causal and non-causal time points of the EEG as an input to the classifier. For this purpose, EEG samples spaced in 200 ms intervals were taken from a time window, i.e. the feature extraction window, and fed into the classifier (here we tested 8 different window lengths from 0 s to 1.4 s, see Supplementary Table 3 for the feature number). The output of the classifier was normalized with a softmax function to obtain probabilities.

We shifted the feature extraction window along the trial in steps of $1/16^{th}$ of a second, and calculated classification accuracies aligned to the center of the feature extraction window. Classification accuracies were validated with a trial-based 10×10 cross-fold validation.

Difference topoplots. The EEG channel layout corresponds to the 10-5 system[88]. Noisy channels which were excluded in the preprocessing step were interpolated with a biharmonic spline interpolation (griddata command in Matlab). We calculated the differences of the trial averaged electrode potentials for all class combinations (i.e. palmar grasp vs lateral grasp, hand open vs lateral grasp, etc.). Next, we computed the absolute values of all differences as we were only interested in the intensity of the differences and not in any polarity, and averaged over all class combinations. Finally, we averaged over non-overlapping 250 s time segments from 0 s to 3 s relative to the class cue. We refer to these average absolute potential differences as difference topoplots.

We found significant differences on channels and time points with a one-tailed nonparametric permutation test[89,90] with $\alpha = 0.05$. For this purpose, we shuffled class labels once for each participant and computed shuffled difference topoplots. The test statistic was the difference between the shuffled and unshuffled difference topoplots. We accounted for multiple comparisons by calculating the permutation distribution using the maximum test statistic over channels and time points.

Proof-of-concept of an online classifier. *Paradigm.* We employed two separate paradigms in the online classification, one to train the classifier (training paradigm), and one to evaluate the performance (test paradigm). The training paradigm comprises two different trial types: movement trials and rest trials. In a movement trial (c.f. Fig. 4a), a class cue together with a cross and a beep were displayed in the beginning of a trial. The class cue represented either hand open or palmar grasp. After 2 s, the class cue was replaced by the ready cue, a filled green circle with a smaller inner white circle. After a random time interval of 0.5 s to 1 s, the filled green circle started to shrink with a random speed to the size of the inner white circle in 2 s to 4 s. The participant was instructed to attempt the movement corresponding to the class cue when the filled green circle hit the inner white circle, i.e. the go cue. In session 1, we instructed the participant to attempt to open or grasp, and deliberately hold the position until the end of the trial, i.e. attempt a sustained movement. In session 2, we gave the instruction not to hold the position, but to make a short single movement attempt. In both sessions, the experimenter demonstrated the participant a hand open and a palmar grasp movement executed at a regular speed, and asked the participant to attempt to imitate these movements. The screen was then cleared 2 s later at the end of the trial. A break of 2 s to 3 s was between trials. The other trial type was a rest trial, where a cross was shown for 70 s and the participant was instructed to avoid any movement during this period. We recorded 5 movement runs, each comprises 30 movement trials, and 4 rest runs each comprises 1 rest trial. Thus, in total we recorded 150 movement trials (75 trials per movement class) and 4 rest trials.

In the test paradigm, the class cue (hand open, palmar grasp, rest), a fixation cross, and a beep were presented at the beginning of a trial. The class cue was then removed at 5 seconds and a 60 s long period of movement or rest, followed. In the case of a rest class cue, we instructed the participant to avoid any movement during this period. In the case of a movement related class cue, we instructed the participant to attempt multiple self-paced movements of the requested movement class during the 60 s period, see Fig. 4b. Furthermore, we instructed the participant to report any movement attempt 2 s afterwards by a soft speech sound. The experimenter then promptly pressed a button on the computer to mark the time point of a movement event. However, due to a misunderstanding, the participant reported movement attempts immediately afterwards in session 1, which is also reflected in different true positive window offsets (see Section *Definition of the true-positive window*). Moreover the participant was instructed to wait at least 3 s after reporting before attempting the next movement. The online classifier was constantly active and showed the corresponding movement icon (hand open or palmar grasp) for 2 s whenever a movement attempt was detected. We then recorded 6 runs in session 1 and 5 runs in session 2. Each run comprised of 4 movement trials and 1 rest trial.

Online classifier and detection thresholds. Recording, preprocessing, and classification were performed in a manner similar to the descriptions in Section *Movement classification* except that the feature extraction window and band-pass filter were causal and no ICA artifact removal was applied. Using the training paradigm (see Fig. 4a) and the previously described classifier with a 1.4 s long feature extraction window, we classified 3 classes: hand open, palmar grasp and rest. Rest trials were obtained by epoching the 70 s long original rest trials into 150 trials. Thus, the number of rest trials was equal to the total number of movement trials. We then calculated the offline classification accuracies on the time interval 1 s to 2 s after the go cue with a 10-fold cross-validation, and found the time point t_{train} with the highest offline classification accuracy ($t_{train} = 1.875$ s in training session 1, $t_{train} = 1.625$ s in training session 2, respectively). In addition to the 3 original movement/rest classes, we introduced a pre class and a post class to increase the robustness of the classifier. The pre and post classes respectively detect the early and late phases of MRCPs. These phases could otherwise increase the chance of detecting a wrong class if the MRCPs, which are spread over time, are not yet (or are no longer) fully covered by the feature extraction window. The pre class and post class features were gathered for this purpose from $t_{train} - 500$ ms and $t_{train} + 500$ ms, respectively. That is, the feature extraction window was shifted by -500 ms and 500 ms relative to t_{train}. Pre class and post class comprised features from both hand open and palmar grasp trials but no rest trials. The final online classifier was then trained with the classes hand open, palmar grasp, rest, pre and post. If the participant attempted a movement, an ideal output of the online classifier would show a peak of the pre class probability, followed 500 ms later by a peak of the hand open or palmar grasp class probability, and another 500 ms later by a peak of the post class probability. See Supplementary Fig. 1c,d for examples of the trial averaged classifier output.

Finally, we defined 3 time windows to detect the pre, movement, and post class probability peaks. Each time window was specified by time length and time position relative to a reference position t_0. The pre window ranged from -650 ms to -350 ms relative to t_0; the movement window ranged from -50 ms to 50 ms; the post window ranged from 350 ms to 650 ms. A movement was detected when all the following conditions were met: (1) pre

class probability is above 0.7 for at least 150 ms within the pre window, (2) hand open or palmar grasp class probability is above 0.9 during the movement window, and (3) post class probability is above 0.7 for at least 150 ms within the post window. The movement class (hand open or palmar grasp) with the higher probability within the movement window was then eventually detected. After a detection, a refractory period of 2 s was imposed. Supplementary Fig. 2 illustrates the thresholds and time windows. The thresholds were set before the evaluation and were not subsequently changed.

Detection delay. Different causes led to a delay between the movement attempt and the detection of the movement attempt. We assume that the participant started the movement attempt exactly at the go cue in the training paradigm. First, due to the time extension of the MRCPs, the filter delay, and the 1.4 s long feature extraction window, the point with the highest classification accuracy is delayed from the go cue and is given by t_{train}. Second, we introduced a delay by our pre, movement and post window based detection logic. We provide in the following a conservative estimation of the expected detection delay, i.e. the average maximum delay, under the assumption that the average post class classifier output is maximal 500 ms after t_{train} and symmetric (c.f. Supplementary Fig. 1c,d). This is a reasonable assumption, since the post class is trained on data 500 ms after t_{train}. For a conservative estimation, we assume that the average post class classifier output crosses the probability-threshold (0.7) for exactly the length of the time-threshold (150 ms, see the description of the detection logic in the previous section). Shorter probability-threshold crossings do not cause a detection, and longer crossings cause an earlier detection. The total average maximum detection delay then comprises (1) t_{train}, (2) the time delay from t_{train} to the center of the post window (500 ms), and (3) half of the time-threshold (150/2 ms; the other half is already covered by the previous point). Thus, the maximum detection delay between the movement attempt and the detection time point is on average $t_{train} + 500\,\text{ms} + 75\,\text{ms}$.

It is a conservative estimation because crossings of the post window probability-threshold for longer than 150 ms – but still centered on $t_{train} + 500$ ms – cause earlier crossings of the 150 ms time-threshold, and therefore shorter movement detection delays, see Supplementary Fig. 2. An exact assessment of the average detection delay would require the knowledge of the exact pre, movement, and post class probability distributions in the test paradigm which we cannot measure. Furthermore, we estimated the average of the detection delay and not the single trial detection delays which are not possible to determine.

Definition of the true-positive window. In order to evaluate the performance of the online classifier, we defined a true positive window and counted every detection within it as a true positive, and every detection outside it as a false positive. We set the length of the true-positive window to 2 s which allowed for a maximum of one detection due to the refractory period. The center of the true-positive window was set by an offset relative to the time points of the reported movement attempts, whereby the true-positive window should capture the assumed movement onset (i.e. the movement detection corrected by the detection delay). Thus, the offset should correspond to the average time difference between the assumed movement onset and the movement event marked by the experimenter. As the offset is not known a priori (i.e. there is no ground truth regarding the start of the movement attempt), we employed a systematic approach to determine it. We iterated the offset from 0 s to 5 s and calculated for each offset value the TP/FP ratio, to which we refer as detection ratio. The offset which maximized the detection ratio was then used as the offset for a session (leading to an offset of 2.2 s in session 1 and 4.2 s in session 2). See Supplementary Fig. 1a,b for the dependency of the detection ratio and classification accuracy on the offset.

As a remark, the FPs in the movement trials were solely used to determine the offset of the true-positive window but not to determine the FP/min rate shown in the results section. The FP/min rate was determined exclusively from rest trials.

Data Availability

Data are available from the BNCI Horizon 2020 database at http://bnci-horizon-2020.eu/database/data-sets (accession number 001–2019) and from Zenodo at https://doi.org/10.5281/zenodo.2222268.

References

1. Wolpaw, J. R., Birbaumer, N., McFarland, D. J., Pfurtscheller, G. & Vaughan, T. M. Brain-computer interfaces for communication and control. *Clin. Neurophysiol.* **113**, 767–791 (2002).
2. Rupp, R., Rohm, M., Schneiders, M., Kreilinger, A. & Muller-Putz, G. R. Functional Rehabilitation of the Paralyzed Upper Extremity After Spinal Cord Injury by Noninvasive Hybrid Neuroprostheses. *Proc. IEEE* **103**, 954–968 (2015).
3. Rupp, R. & Gerner, H. J. Neuroprosthetics of the upper extremity–clinical application in spinal cord injury and challenges for the future. *Acta Neurochir. Suppl.* **97**, 419–426 (2007).
4. Jackson, A. & Zimmermann, J. B. Neural interfaces for the brain and spinal cord—restoring motor function. *Nat. Rev. Neurol.* **8**, 690–699 (2012).
5. Müller-Putz, G. R., Scherer, R., Pfurtscheller, G. & Rupp, R. EEG-based neuroprosthesis control: a step towards clinical practice. *Neurosci. Lett.* **382**, 169–174 (2005).
6. Pfurtscheller, G., Müller, G. R., Pfurtscheller, J., Gerner, H. J. & Rupp, R. 'Thought' – control of functional electrical stimulation to restore hand grasp in a patient with tetraplegia. *Neurosci. Lett.* **351**, 33–36 (2003).
7. Wu, Z. *et al*. The Convergence of Machine and Biological Intelligence. *IEEE Intell. Syst.* **28**, 28–43 (2013).
8. Hochberg, L. R. *et al*. Neuronal ensemble control of prosthetic devices by a human with tetraplegia. *Nature* **442**, 164–171 (2006).
9. Hochberg, L. R. *et al*. Reach and grasp by people with tetraplegia using a neurally controlled robotic arm. *Nature* **485**, 372–375 (2012).
10. Collinger, J. L. *et al*. High-performance neuroprosthetic control by an individual with tetraplegia. *Lancet* **381**, 557–564 (2013).
11. Ajiboye, A. B. *et al*. Restoration of reaching and grasping movements through brain-controlled muscle stimulation in a person with tetraplegia: a proof-of-concept demonstration. *Lancet* **389**, 1821–1830 (2017).
12. Fifer, M. S. *et al*. Simultaneous neural control of simple reaching and grasping with the modular prosthetic limb using intracranial EEG. *IEEE Trans. Neural Syst. Rehabil. Eng.* **22**, 695–705 (2014).

13. Taylor, D. M., Tillery, S. I. H. & Schwartz, A. B. Direct cortical control of 3D neuroprosthetic devices. *Science* **296**, 1829–1832 (2002).
14. Meng, J. *et al*. Noninvasive Electroencephalogram Based Control of a Robotic Arm for Reach and Grasp Tasks. *Sci. Rep.* **6**, 38565 (2016).
15. Pfurtscheller, G., Guger, C., Müller, G., Krausz, G. & Neuper, C. Brain oscillations control hand orthosis in a tetraplegic. *Neurosci. Lett.* **292**, 211–214 (2000).
16. Rohm, M. *et al*. Hybrid brain-computer interfaces and hybrid neuroprostheses for restoration of upper limb functions in individuals with high-level spinal cord injury. *Artif. Intell. Med.* **59**, 133–142 (2013).
17. Pfurtscheller, G. & Lopes da Silva, F. H. Event-related EEG/MEG synchronization and desynchronization: basic principles. *Clin. Neurophysiol.* **110**, 1842–1857 (1999).
18. Pfurtscheller, G., Neuper, C., Flotzinger, D. & Pregenzer, M. EEG-based discrimination between imagination of right and left hand movement. *Electroencephalogr. Clin. Neurophysiol.* **103**, 642–651 (1997).
19. Bradberry, T. J., Gentili, R. J. & Contreras-Vidal, J. L. Reconstructing three-dimensional hand movements from noninvasive electroencephalographic signals. *J. Neurosci.* **30**, 3432–3437 (2010).
20. Ofner, P. & Muller-Putz, G. R. Decoding of velocities and positions of 3D arm movement from EEG. In *2012 Annual International Conference of the IEEE Engineering In Medicine and Biology Society*, https://doi.org/10.1109/embc.2012.6347460 (2012).
21. Ofner, P. & Muller-Putz, G. R. Using a Noninvasive Decoding Method to Classify Rhythmic Movement Imaginations of the Arm in Two Planes. *IEEE Transactions on Biomedical Engineering* **62**, 972–981 (2015).
22. Kim, J.-H., Bießmann, F. & Lee, S.-W. Decoding Three-Dimensional Trajectory of Executed and Imagined Arm Movements From Electroencephalogram Signals. *IEEE Trans. Neural Syst. Rehabil. Eng.* **23**, 867–876 (2015).
23. Paek, A. Y., Agashe, H. A. & Contreras-Vidal, J. L. Decoding repetitive finger movements with brain activity acquired via non-invasive electroencephalography. *Front. Neuroeng.* **7**, 3 (2014).
24. Robinson, N. & Vinod, A. P. Noninvasive Brain-Computer Interface: Decoding Arm Movement Kinematics and Motor Control. *IEEE Systems, Man, and Cybernetics Magazine* **2**, 4–16 (2016).
25. Shibasaki, H. & Hallett, M. What is the Bereitschaftspotential? *Clin. Neurophysiol.* **117**, 2341–2356 (2006).
26. Kornhuber, H. H. & Deecke, L. Hirnpotentialänderungen bei Willkürbewegungen und passiven Bewegungen des Menschen: Bereitschaftspotential und reafferente Potentiale. *Pflugers Arch. Gesamte Physiol. Menschen Tiere* **284**, 1–17 (1965).
27. Lew, E. Y. L., Chavarriaga, R., Silvoni, S. & Millán, J. D. R. Single trial prediction of self-paced reaching directions from EEG signals. *Front. Neurosci.* **8**, 222 (2014).
28. Úbeda, A., Azorín, J. M., Chavarriaga, R. & R Millán, J. D. Classification of upper limb center-out reaching tasks by means of EEG-based continuous decoding techniques. *J. Neuroeng. Rehabil.* **14**, 9 (2017).
29. Hammon, P., Makeig, S., Poizner, H., Todorov, E. & De Sa, V. Predicting Reaching Targets from Human EEG. *IEEE Signal Process. Mag.* **25**, 69–77 (2008).
30. Jochumsen, M., Niazi, I. K., Mrachacz-Kersting, N., Farina, D. & Dremstrup, K. Detection and classification of movement-related cortical potentials associated with task force and speed. *J. Neural Eng.* **10**, 056015 (2013).
31. Ofner, P., Schwarz, A., Pereira, J. & Müller-Putz, G. R. Upper limb movements can be decoded from the time-domain of low-frequency EEG. *PLoS One* **12**, e0182578 (2017).
32. Schwarz, A., Ofner, P., Pereira, J., Sburlea, A. I. & Müller-Putz, G. R. Decoding natural reach-and-grasp actions from human EEG. *J. Neural Eng.* **15**, 016005 (2018).
33. Iturrate, I. *et al*. Human EEG reveals distinct neural correlates of power and precision grasping types. *Neuroimage* **181**, 635–644 (2018).
34. Lacourse, M. G., Cohen, M. J., Lawrence, K. E. & Romero, D. H. Cortical potentials during imagined movements in individuals with chronic spinal cord injuries. *Behav. Brain Res.* **104**, 73–88 (1999).
35. Castro, A., Díaz, F. & Sumich, A. Long-term neuroplasticity in spinal cord injury patients: a study on movement-related brain potentials. *Int. J. Psychophysiol.* **87**, 205–214 (2013).
36. Xu, R. *et al*. Movement-related cortical potentials in paraplegic patients: abnormal patterns and considerations for BCI-rehabilitation. *Front. Neuroeng.* **7**, 35 (2014).
37. Marino, R. J. *et al*. International standards for neurological classification of spinal cord injury. *J. Spinal Cord Med.* **26**(Suppl 1), S50–6 (2003).
38. Gardner, M. J. & Altman, D. G. Confidence intervals rather than P values: estimation rather than hypothesis testing. *BMJ* **292**, 746–750 (1986).
39. Müller-Putz, G. R., Scherer, R., Brunner, C., Leeb, R. & Pfurtscheller, G. Better than random? A closer look on BCI results. *Int. J. Bioelectromagn.* **10**, 52–55 (2008).
40. Billinger, M. *et al*. Is It Significant? Guidelines for Reporting BCI Performance. In *Biological and Medical Physics, Biomedical Engineering* 333–354 (2012).
41. Fukuma, R. *et al*. Real-Time Control of a Neuroprosthetic Hand by Magnetoencephalographic Signals from Paralysed Patients. *Sci. Rep.* **6**, 21781 (2016).
42. Waldert, S. *et al*. Hand movement direction decoded from MEG and EEG. *J. Neurosci.* **28**, 1000–1008 (2008).
43. Gu, Y., Dremstrup, K. & Farina, D. Single-trial discrimination of type and speed of wrist movements from EEG recordings. *Clin. Neurophysiol.* **120**, 1596–1600 (2009).
44. Jochumsen, M., Niazi, I. K., Taylor, D., Farina, D. & Dremstrup, K. Detecting and classifying movement-related cortical potentials associated with hand movements in healthy subjects and stroke patients from single-electrode, single-trial EEG. *J. Neural Eng.* **12**, 056013 (2015).
45. Úbeda, A., Hortal, E., Iáñez, E., Perez-Vidal, C. & Azorín, J. M. Assessing movement factors in upper limb kinematics decoding from EEG signals. *PLoS One* **10**, e0128456 (2015).
46. Schalk, G. *et al*. Decoding two-dimensional movement trajectories using electrocorticographic signals in humans. *J. Neural Eng.* **4**, 264–275 (2007).
47. Pistohl, T., Ball, T., Schulze-Bonhage, A., Aertsen, A. & Mehring, C. Prediction of arm movement trajectories from ECoG-recordings in humans. *J. Neurosci. Methods* **167**, 105–114 (2008).
48. Acharya, S., Fifer, M. S., Benz, H. L., Crone, N. E. & Thakor, N. V. Electrocorticographic amplitude predicts finger positions during slow grasping motions of the hand. *J. Neural Eng.* **7**, 046002 (2010).
49. Flint, R. D. *et al*. Extracting kinetic information from human motor cortical signals. *Neuroimage* **101**, 695–703 (2014).
50. Pistohl, T., Schulze-Bonhage, A., Aertsen, A., Mehring, C. & Ball, T. Decoding natural grasp types from human ECoG. *Neuroimage* **59**, 248–260 (2012).
51. Bundy, D. T., Pahwa, M., Szrama, N. & Leuthardt, E. C. Decoding three-dimensional reaching movements using electrocorticographic signals in humans. *J. Neural Eng.* **13**, 026021 (2016).
52. Ball, T., Schulze-Bonhage, A., Aertsen, A. & Mehring, C. Differential representation of arm movement direction in relation to cortical anatomy and function. *J. Neural Eng.* **6**, 016006 (2009).
53. Hammer, J. *et al*. Predominance of Movement Speed Over Direction in Neuronal Population Signals of Motor Cortex: Intracranial EEG Data and A Simple Explanatory Model. *Cereb. Cortex* **26**, 2863–2881 (2016).
54. Korik, A., Sosnik, R., Siddique, N. & Coyle, D. Decoding Imagined 3D Hand Movement Trajectories From EEG: Evidence to Support the Use of Mu, Beta, and Low Gamma Oscillations. *Front. Neurosci.* **12**, 130 (2018).

55. Georgopoulos, A. Higher Order Motor Control. *Annu. Rev. Neurosci.* **14**, 361–377 (1991).
56. Kandel, E. *Principles of Neural Science, Fifth Edition*. (McGraw Hill Professional, 2013).
57. Polich, J. Updating P300: an integrative theory of P3a and P3b. *Clin. Neurophysiol.* **118**, 2128–2148 (2007).
58. Polich, J., Eischen, S. E. & Collins, G. E. P300 from a single auditory stimulus. *Electroencephalography and Clinical Neurophysiology/ Evoked Potentials Section* **92**, 253–261 (1994).
59. García-Larrea, L. & Cézanne-Bert, G. P3, positive slow wave and working memory load: a study on the functional correlates of slow wave activity. *Electroencephalogr. Clin. Neurophysiol.* **108**, 260–273 (1998).
60. Falkenstein, M., Hohnsbein, J. & Hoormann, J. Effects of choice complexity on different subcomponents of the late positive complex of the event-related potential. *Electroencephalogr. Clin. Neurophysiol.* **92**, 148–160 (1994).
61. Kalcher, J., Flotzinger, D., Neuper, C., Gölly, S. & Pfurtscheller, G. Graz brain-computer interface II: towards communication between humans and computers based on online classification of three different EEG patterns. *Med. Biol. Eng. Comput.* **34**, 382–388 (1996).
62. Niazi, I. K. *et al*. Detection of movement intention from single-trial movement-related cortical potentials. *J. Neural Eng.* **8**, 066009 (2011).
63. López-Larraz, E., Montesano, L., Gil-Agudo, Á. & Minguez, J. Continuous decoding of movement intention of upper limb self-initiated analytic movements from pre-movement EEG correlates. *J. Neuroeng. Rehabil.* **11**, 153 (2014).
64. Bhagat, N. A. *et al*. Design and Optimization of an EEG-Based Brain Machine Interface (BMI) to an Upper-Limb Exoskeleton for Stroke Survivors. *Front. Neurosci*. **10** (2016).
65. Liu, D. *et al*. EEG-Based Lower-Limb Movement Onset Decoding: Continuous Classification and Asynchronous Detection. *IEEE Trans. Neural Syst. Rehabil. Eng.* **26**, 1626–1635 (2018).
66. Niazi, I. K. *et al*. Detection of movement-related cortical potentials based on subject-independent training. *Med. Biol. Eng. Comput.* **51**, 507–512 (2013).
67. Sburlea, A. I., Montesano, L. & Minguez, J. Continuous detection of the self-initiated walking pre-movement state from EEG correlates without session-to-session recalibration. *J. Neural Eng.* **12**, 036007 (2015).
68. Cui, R. & MacKinnon, C. D. The effect of temporal accuracy constraints on movement-related potentials. *Exp. Brain Res.* **194**, 477–488 (2009).
69. Thickbroom, G. W. & Mastaglia, F. L. Cerebral events preceding self-paced and visually triggered saccades. A study of presaccadic potentials. *Electroencephalogr. Clin. Neurophysiol.* **62**, 277–289 (1985).
70. Jankelowitz, S. K. & Colebatch, J. G. Movement-related potentials associated with self-paced, cued and imagined arm movements. *Exp. Brain Res.* **147**, 98–107 (2002).
71. Walter, W. G. *et al*. Contingent Negative Variation: An Electric Sign of Sensori-Motor Association and Expectancy in the Human Brain. *Nature* **203**, 380–384 (1964).
72. Tecce, J. J. Contingent negative variation (CNV) and psychological processes in man. *Psychol. Bull.* **77**, 73–108 (1972).
73. Rohrbaugh, J., Syndulko, K. & Lindsley, D. Brain wave components of the contingent negative variation in humans. *Science* **191**, 1055–1057 (1976).
74. Prescott, J. The effects of response parameters on CNV amplitude. *Biol. Psychol.* **22**, 107–135 (1986).
75. Cui, R. Q. *et al*. High resolution spatiotemporal analysis of the contingent negative variation in simple or complex motor tasks and a non-motor task. *Clin. Neurophysiol.* **111**, 1847–1859 (2000).
76. Romero, D. H., Lacourse, M. G., Lawrence, K. E., Schandler, S. & Cohen, M. J. Event-related potentials as a function of movement parameter variations during motor imagery and isometric action. *Behav. Brain Res.* **117**, 83–96 (2000).
77. Pereira, J., Ofner, P., Schwarz, A., Sburlea, A. I. & Müller-Putz, G. R. EEG neural correlates of goal-directed movement intention. *Neuroimage* **149**, 129–140 (2017).
78. Aliakbaryhosseinabadi, S., Kamavuako, E. N., Jiang, N., Farina, D. & Mrachacz-Kersting, N. Influence of dual-tasking with different levels of attention diversion on characteristics of the movement-related cortical potential. *Brain Res.* **1674**, 10–19 (2017).
79. Touge, T., Werhahn, K. J., Rothwell, J. C. & Marsden, C. D. Movement-related cortical potentials preceding repetitive and random-choice hand movements in parkinson's disease. *Ann. Neurol.* **37**, 791–799 (1995).
80. Jiang, N., Gizzi, L., Mrachacz-Kersting, N., Dremstrup, K. & Farina, D. A brain–computer interface for single-trial detection of gait initiation from movement related cortical potentials. *Clin. Neurophysiol.* **126**, 154–159 (2015).
81. Martínez-Expósito, A., Ibáñez, J., Resquín, F. & Pons, J. L. Task Influence on Motor-Related Cortical Signals: Comparison Between Upper and Lower Limb Coordinated and Analytic Movements. In *Biosystems & Biorobotics* 1139–1143 (2016).
82. Schlogl, A. & Brunner, C. BioSig: A Free and Open Source Software Library for BCI Research. *Computer* **41**, 44–50 (2008).
83. Lee, T. W., Girolami, M. & Sejnowski, T. J. Independent component analysis using an extended infomax algorithm for mixed subgaussian and supergaussian sources. *Neural Comput.* **11**, 417–441 (1999).
84. Delorme, A. & Makeig, S. EEGLAB: an open source toolbox for analysis of single-trial EEG dynamics including independent component analysis. *J. Neurosci. Methods* **134**, 9–21 (2004).
85. Mosteller, F. *Data Analysis and Regression: A Second Course in Statistics*. (Pearson College Division, 1977).
86. Peck, R. & Van Ness, J. The use of shrinkage estimators in linear discriminant analysis. *IEEE Trans. Pattern Anal. Mach. Intell.* **4**, 530–537 (1982).
87. Blankertz, B., Lemm, S., Treder, M., Haufe, S. & Müller, K.-R. Single-trial analysis and classification of ERP components — A tutorial. *Neuroimage* **56**, 814–825 (2011).
88. Oostenveld, R. & Praamstra, P. The five percent electrode system for high-resolution EEG and ERP measurements. *Clin. Neurophysiol.* **112**, 713–719 (2001).
89. Nichols, T. E. & Holmes, A. P. Nonparametric permutation tests for functional neuroimaging: a primer with examples. *Hum. Brain Mapp.* **15**, 1–25 (2002).
90. Maris, E. & Oostenveld, R. Nonparametric statistical testing of EEG- and MEG-data. *J. Neurosci. Methods* **164**, 177–190 (2007).

Acknowledgements
This work is supported by the European ICT Programme Project H2020-643955 "MoreGrasp".

Author Contributions
P.O., A.S. and G.R.M.P. designed the study. P.O., A.S. and J.P. recorded the data. P.O. analysed the data. D.W. and R.W. recruited and provided the participants. P.O. wrote the original draft. All authors reviewed and edited the manuscript.

Additional Information
Supplementary information accompanies this paper at https://doi.org/10.1038/s41598-019-43594-9.

Competing Interests: The authors declare no competing interests.

Publisher's note: Springer Nature remains neutral with regard to jurisdictional claims in published maps and institutional affiliations.

Secondary Publication I

Proceedings of the 6th International Brain-Computer Interface Conference 2014 DOI:10.3217/978-3-85125-378-8-26

Decoding of Executed Movements and Source Imaging

Patrick Ofner[12], Joana Pereira[3] and Gernot R. Müller-Putz[12]

[1] Graz University of Technology, Graz, Austria
[2] BioTechMed-Graz, Graz, Austria
[3] University of Lisbon, Lisbon, Portugal
patrick.ofner@tugraz.at, gernot.mueller@tugraz.at

Abstract

A brain-computer interface (BCI) in combination with a neuroprosthesis can be used to restore movement in paralyzed persons. Usually, the control of such BCIs by the deliberate modulation of brain oscillations is unnatural and unintuitive. Recently, low-frequency brain signals have been found to encode movement information and can be used to decode movement trajectories. These signals are potential candidates for new types of BCIs which can be used to naturally control neuroprosthesis by imagining movement trajectories. We analyzed the contributing brain areas in the source space and found motor areas but also parietal and lateral areas encoding movement information.

1 Introduction

A brain-computer interface (BCI) allows the control of devices trough brain-signals. In combination with a neuroprosthesis, e.g., functional electrical stimulation (FES), a BCI can be used to restore motor functions in paralyzed persons [5]. One type of non-invasive BCIs – so called sensorimotor rhythm (SMR) BCIs – are usually based on the deliberate modulation of brain oscillations [7] by movement imagery (MI). However, the control of SMR-based BCIs is not natural and intuitive, because MIs are assigned artificially to control functions (e.g., a foot MI controls the elbow function). Furthermore, SMR-based BCIs do not decode the imagined movement trajectories, but the general activity at sensorimotor areas during MI. As opposed to non-invasive BCIs, invasive BCIs were already used to decode trajectories of imagined movements and to control robotic arms [2, 3]. On the downside, invasive BCIs have the drawback that they require a major surgical intervention with the risk of infection. Gratifyingly, Bradberry et al. [1] discovered that low-frequency electroencephalography (EEG) signals can be used to decode executed movement trajectories, and also our group decoded 3D hand positions from EEG signals [6]. In this work we decoded frontal and lateral hand movements from brain sources reconstructed from the EEG. Notably, we did not trained a decoder using all sources simultaneously and interpreted the decoder weights. This can lead to wrong interpretations as these weights must be seen as a filter and not as a pattern. Instead, we decoded the movements from each brain source separately and calculated the correlation coefficients with the measured movements, and obtained maps showing the involved brain regions when decoding movements.

2 Methods

2.1 Subjects

We recruited 8 right-handed and 1 left-handed subjects who got compensated for their participation (5 males, 4 females). Most of them had already participated in BCI experiments. Subjects sat comfortably in a chair with their arms supported by arm rests.

Proceedings of the 6th International Brain-Computer Interface Conference 2014 DOI:10.3217/978-3-85125-378-8-26

2.2 Paradigm

We recorded 3 runs. In the first run (frontal run) subjects moved their right arm in front of them while the gaze was fixated on a cross on a screen. The second run (lateral run) was similar to the first run, except that subjects moved their right arm laterally. In the third run (ball run), subjects moved their right arm in front of them again, but now observed and followed with the eyes a moving ball on the computer screen. Subjects were instructed to execute the arm movements independently from the ball movements. In all runs, we asked subjects to execute round, natural movements (not jaggy) with the extended right arm, and to keep the hand closed with the thumb being on the upper side. Each run comprised of 8 65 s long trials, with subject specific breaks between the trials to avoid muscle fatigue (usually around 1 minute). A trial started with the presentation of a cross (run 1 and 2) or a ball (run 3), respectively, on the computer screen. Two seconds later a beep chimed indicating to the user to start with the movement. In run 3, also a ball on the screen started to move. Additionally to the arm movement trials, we recorded two trials where we instructed the subjects to follow a moving ball on the screen with the eyes, but avoid any arm movement. These two trials were used to remove the influences of eye movements from the EEG with a linear regression method [8], and to calculate the noise covariance matrix used for source imaging (after removal of eye movements).

2.3 Recording

We recorded the EEG with 68 passive Ag/AgCl electrodes covering frontal, central and parietal areas, and the electrooculogram (EOG) with 3 electrodes placed above the nasion and the two outer canthi of the eyes. Reference was placed on the left mastoid, ground on the right mastoid. We assured that all impedances were below 5 kOhm. All biosignals were recorded with g.USBamp amplifiers (g.tec medical engineering GmbH, Schiedlberg, Austria). We applied an 8-th order Butterworth bandpass filter with cut off frequencies at 0.01 Hz and 100 Hz, a notch filter at 50 Hz, and then sampled the signals with 512 Hz. The position of the right hand was tracked with a Kinect sensor device (Microsoft, Redmond, US). Here, the x-axis was orientated leftward, y upward, and z backward with respect to the subject. We also recorded the electrode positions with a CMS 20 EP system (Zebris Medical GmbH, Isny, Germany).

2.4 Preprocessing

We computed the independent component analysis for each run in the frequency range 0.3 Hz – 70 Hz, using the extended infomax algorithm [4], and removed independent components suspected to be muscle or technical artefacts. Subsequently, we applied a zero-phase anti-aliasing filter and downsampled data to 16 Hz for computational convenience. Then we applied a zero-phase 4-th order Butterworth band-pass filter with cutoff frequencies interesting for decoding at 0.2 Hz and 2 Hz. Afterwards, we removed influences of eye movements on the EEG with a linear regression method [8], and removed samples exceeding a threshold of 5.9 times the median absolute deviation (MAD) of a channel to get rid of remaining artefacts. MAD is a robust deviation measure, and the threshold corresponds to 4 times the standard deviation when the data are normally distributed. Furthermore, we filtered the measured positions with the same band-pass filter as used for the EEG (i.e. 0.2 Hz – 2 Hz), and centered and scaled them to a standard deviation of one. Finally, we omitted the first 5 seconds of each trial to exclude possible existing movement onset effects.

Proceedings of the 6th International Brain-Computer Interface Conference 2014 DOI:10.3217/978-3-85125-378-8-26

2.5 Source Imaging

To transform the data from the sensor space into the source space we used the software Brainstorm [9]. We calculated the head model using the Colin27 model included in Brainstorm, and coregistered the electrode positions. Using the head model and a noise covariance matrix, we calculated 15028 brain sources with the weighted minimum norm estimation (wMNE) method. The noise covariance matrix was calculated from the two trials without arm movements after we removed eye movements from them.

2.6 Decoding

We analyzed all runs separately using a 10-fold cross-validation. For this purpose we divided each run in segments of 10 s length and assigned these segments to train and test sets. The decoder [6] itself comprised of 2 multiple linear regressions between a brain source (voxel) and the 2D position in the movement plane (frontal or lateral, respectively). We used the current time step and time lags at ca. 60, 130, 190 ms of the EEG as the input for the decoder. X and y positions were decoded in the frontal and ball runs, and y and z positions in the lateral run. We decoded the positions from the test sets, and calculated the Pearson correlation coefficients between the decoded and the measured 2D positions. Subsequently, we calculated the average of the correlation coefficients across the 10 test sets. Finally, we averaged the correlation coefficients over the movement plane dimensions, i.e. x/y or y/z, respectively. This procedure was performed for every single voxel, and we got one correlation coefficient for each voxel, run and subject.

To asses the chance level, we randomly permuted the coordinate segments and performed a 10-fold cross-validation as described above and repeated this procedure 50 times. Thus, we got 50 correlation coefficients for each voxel, run and subject, and then, fitted a normal distribution to these 50 chance correlation coefficients (this is reasonable as the correlation values are usually around 0 and not at the limits 1/-1). Subsequently, we calculated the p-values of the correlation coefficients based on the chance level distributions.

2.7 Results

The maximum correlation coefficient reached by a subject averaged over all subjects were (mean value/standard deviation) 0.47 ± 0.09 (frontal), 0.52 ± 0.13 (lateral), and 0.47 ± 0.10 (ball). The corresponding chance level correlations were 0.12 ± 0.03 (frontal), 0.12 ± 0.02 (lateral), and 0.11 ± 0.02 (ball). Figure 1 shows the subject averaged correlations of each voxel in each run and their average over the runs. Before averaging, all non-significant correlations were set to 0. Observable are higher correlations on the central and left motor cortex, parietal areas, and right lateral correlations.

3 Discussion

We have successfully decoded executed movements from frontal and lateral arm movements on a per brain source (voxel) basis. The subject averaged correlations indicate a contribution of the primary motor cortex. This was expected, as subjects executed movements. However, also contributions from parietal and lateral areas are observable. These contributions can be external sources projected onto the margins of the head model. Such an external source could be muscle activity, although muscle activity is thought to be most prominent in higher

Proceedings of the 6th International Brain-Computer Interface Conference 2014 DOI:10.3217/978-3-85125-378-8-26

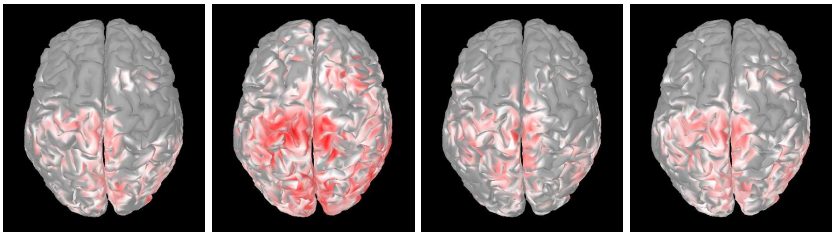

frontal run lateral run ball run average

Figure 1: Subject averaged correlations on a per voxel basis for all 3 runs and the average of them. Red corresponds to the maximum value of 0.33 in the lateral run, white to 50 % of the maximum value, and correlations below 50 % of the maximum are not shown.

frequency ranges. To summarize, the findings indicate that indeed brain sources carry decodable movement information, but the measurements are potentially contaminated by external sources.

References

[1] Trent J Bradberry, Rodolphe J Gentili, and José L Contreras-Vidal. Reconstructing three-dimensional hand movements from noninvasive electroencephalographic signals. *Journal of Neuroscience*, 30:3432–3437, 2010.

[2] Jennifer L Collinger, Brian Wodlinger, John E Downey, Wei Wang, Elizabeth C Tyler-Kabara, Douglas J Weber, Angus J C McMorland, Meel Velliste, Michael L Boninger, and Andrew B Schwartz. High-performance neuroprosthetic control by an individual with tetraplegia. *Lancet*, 381(9866):557–564, 2013.

[3] Leigh R Hochberg, Daniel Bacher, Beata Jarosiewicz, Nicolas Y Masse, John D Simeral, Joern Vogel, Sami Haddadin, Jie Liu, Sydney S Cash, Patrick van der Smagt, and John P Donoghue. Reach and grasp by people with tetraplegia using a neurally controlled robotic arm. *Nature*, 485:372–375, 2012.

[4] T W Lee, M Girolami, and T J Sejnowski. Independent component analysis using an extended infomax algorithm for mixed sub-gaussian and super-gaussian sources. *Neural Computation*, 11(2):417–441, 1999.

[5] G R Müller-Putz, R Scherer, G Pfurtscheller, and R Rupp. EEG-based neuroprosthesis control: a step towards clinical practice. *Neuroscience Letters*, 382:169–174, 2005.

[6] Patrick Ofner and Gernot R Müller-Putz. Decoding of velocities and positions of 3d arm movement from eeg. In *Engineering in Medicine and Biology Society (EMBC), 2012 Annual International Conference of the IEEE*, pages 6406–6409, 2012.

[7] Gert Pfurtscheller and Fernando H Lopes Da Silva. Event-related eeg/meg synchronization and desynchronization: basic principles. *Clinical Neurophysiology*, 110(11):1842–1857, 1999.

[8] A Schlögl, C Keinrath, D Zimmermann, R Scherer, R Leeb, and G Pfurtscheller. A fully automated correction method of eog artifacts in eeg recordings. *Clinical Neurophysiology*, 118(1):98–104, 2007.

[9] François Tadel, Sylvain Baillet, John C Mosher, Dimitrios Pantazis, and Richard M Leahy. Brainstorm: A user-friendly application for meg/eeg analysis. *Computational Intelligence and Neuroscience*, 2011.

Secondary Publication II

Biomed Tech 2013; 58 (Suppl. 1) © 2013 by Walter de Gruyter · Berlin · Boston. DOI 10.1515/bmt-2013-4432

TIME-DOMAIN CORRELATIONS OF IMAGINED ARM POSITIONS WITH BRAIN SOURCES

Ofner P[1] and Müller-Putz G R[1]

[1]Institute for Knowledge Discovery, Graz University of Technology, Austria

patrick.ofner@tugraz.at

Abstract: *We investigated how the assumed hand position of the right arm during movement imagination correlates with brain sources. Sources were calculated from the electroencephalogram (EEG) applying a brain imaging technique. We used frequencies below 1 Hz. In 4 out of 9 subjects, substantial correlations on the supplementary motor cortex were observed. This supports that decoding movement imaginations could be possible and it is neurophysiologically plausible.*

Keywords: *EEG, movement decoding, movement imagination*

Introduction

An important issue of tetraplegic persons is the restoration of the upper limb functionality. The nerves in the spinal cord are damaged and have to be bridged. For that purpose a functional electrical stimulation (FES) neuroprosthesis can be combined with a brain-computer interface (BCI) [1]. In general, a BCI measures brain signals and transforms them into control commands for devices. Here, the movement imagination (MI) is detected with a BCI and transformed into a real arm movement using the FES neuroprosthesis. Sensorimotor rhythms (SMR) based BCIs can detect power modulations in the mu-band accompanying MIs. However, SMR-based BCIs detect only the process of MI of a body part, but not the actual MI itself. As a consequence, different body parts usually have to be assigned to different neuroprosthesis movements. That means that e.g. a foot movement is assigned to an extension of the arm. A more natural control schema would be to decode the actual MI (e.g. the imagined position of the arm). Recent findings have shown that also low frequency time-domain signals (< 5 Hz) carry movement information when executing movements (e.g. [2]). In [3] low frequency electroencephalogram (EEG) components were used decode the velocity of executed arm movements. However, it is still an open question if this movement decoding can also be applied to imagined movements, and if so, which brain regions are involved. In this work we investigated if decoding of rhythmic movement imaginations is possible and which are the underlying brain regions.

Methods

Paradigm: We recruited 9 healthy right-handed subjects and measured the EEG during imagined arm movements. Subjects were seated comfortably in a chair, and in front of them was a computer screen displaying the cues. We asked subjects to imagine natural, round (not jaggy), repeated, rhythmic movements from left to right and back (transverse plane), and from bottom to top and back (sagittal plane). MIs were synchronised with a metronome with a frequency of 1 Hz. As a beat of the metronome corresponded to an endposition of the arm, the frequency of the imagined movements was 0.5 Hz. A trial started with a short beep tone together with a cue. The cue was either an arrow pointing right or up and was shown for 0.5 s. Subsequently, a cross was shown for the rest of the trial and subjects were asked to fixate their gaze on this cross to suppress eye movements. The metronome started beating 1.5–2.5 s after the trial start and stopped 20s later, this was also the end of the trial. We recorded 8 MI runs, each comprising 5 trials per movement plane. In this work we did not differentiate between the two different movement planes, leading to a combined set of 80 MI trials. To remove eye movements from the EEG with a linear regression method, we also recorded 2 runs with deliberate eye movements.
Recording: We recorded the EEG with 68 electrodes covering frontal, central and parietal areas. Reference was placed on the left ear, ground on the right ear. Furthermore, we recorded the electrooculogram (EOG) using 3 electrodes. Signals were acquired with g.USB amplifiers (g.tec, Graz, Austria) with a sampling frequency of 256 Hz and an 8th order Chebyshev bandpass filter with cut off frequencies at 0.01 Hz and 100 Hz and a notch filter at 50 Hz. The positions of the EEG electrodes were measured with a CMS 20EP system (Zebris Medical GmbH, Isny, Germany).
Preprocessing: To remove artefacts, we applied an independent component analysis and removed components suspected to be eye-, muscle- or technical artefacts. We also removed remaining influences of eye movements from the EEG with a linear regression method. For computational convenience, we applied an anti-aliasing filter and downsampled data to 16 Hz. Afterwards, we bandpass filtered the data with a zero-phase 4th order Butterworh filter with cut off frequencies at 0.3 Hz and 0.8 Hz, thus including the arm movement frequency of 0.5 Hz. To remove any remaining artefacts, we removed samples exceeding a threshold of 4.4 times the median absolute deviation. This corresponds approximately to 3 times the standard deviation when the data is normally distributed. We also removed samples 1 s before and after a detected artefact.
Analyis: We calculated the brain sources with the software Brainstorm. Here, we used the default anatomy data based on the Colin27 brain delivered with Brainstorm and cal-

Table 1: This table contains the maximum absolute canonical correlations over all brain sources for all subjects.

subject	s1	s2	s3	s4	s5	s6	s7	s8	s9
max abs corr	0.54	0.21	0.14	0.37	0.16	0.19	0.12	0.25	0.36

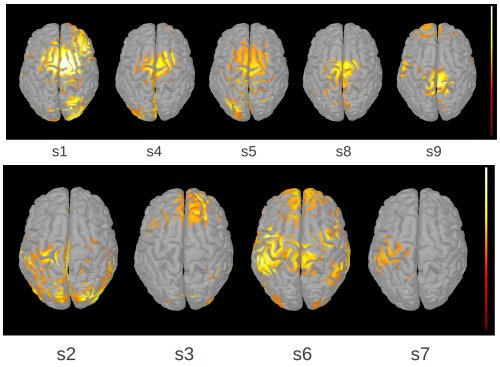

Figure 1: This figure shows the absolute canonical correlations for each subject. White (highest representable value) corresponds to a canonical correlation of 0.5 for s1, 0.4 for s4 and s9, 0.3 for s8 and 0.2 for all others. Canonical correlations below 50 % with respect to the highest representable value are not shown.

culated the boundary element head model. Subsequently, 15028 sources were calculated from the preprocessed EEG with the sLORETA method. The noise covariance matrix was set to the identity matrix. We build a feature vector for each source consisting of the current source value and 3 time delayed values with a time interval of 62.5 ms between them. Furthermore, we assumed that subjects imagined movement positions corresponding to a sine oscillation with a frequency of 0.5 Hz. Finally, we calculated for each source the canonical correlation between the feature vector and the sine oscillation. Here, to avoid any possible existing movement onset effects, we removed the first 2 s of MI data, leading to remaining 18 s of MI data per trial. As the canonical correlation builds a linear model of the independent variables (feature vector), the method described here is in fact the same as the position decoding described in [4].

Results

Tab. 1 shows the maximum absolute canonical correlations of all brain sources for each subject. Fig. 1 visualizes the absolute values of the canonical correlations of all brain sources. White corresponds to a canonical correlation of 0.5 for subject s1, 0.4 for s4 and s9, 0.3 for s8 and 0.2 for all others. Canonical correlations on the supplementary motor area (SMA) with the position of the rhythmic movement imagination are observable for subjects s1, s4, s5, s8. Subject s9 shows canonical correlations on the medial part of the motor cortex. Higher canonical correlations on the hand area of the primary motor cortex (M1) than on the SMA are observable for subjects s2, s6 and s7.

Discussion

We found correlations of brain sources with imagined rhythmic movements. Those correlations were observable on the SMA for 4 out of 9 subjects. However, we used a standard brain anatomy which can have caused inaccuracies and the central correlation pattern of s9 is similar to the ones of s1, s4, s5 and s8. Therefore, it is possible that this pattern has to be attributed to the SMA. The SMA is involved in motor control. Thus, these correlations are plausible from a neurophysiological point of view. Higher canonical correlations on the hand area of M1 than on the SMA were observed for 3 subjects only. Furthermore, they were always lower than 0.21. These findings suggest that in the *time-domain* primarily the SMA, and not M1, provides decodable information about rhythmic movement imaginations. Due to the lack of a control condition (metronome beat without MI), we do not know if these correlations exist also when just listening to a metronome. Indeed, [5] reports in an functional magnetic resonance imaging study an increased activity of the SMA during the perception of a beat. However, that is not conclusive for time-domain correlations. We have shown that rhythmic MI, synchronised to a beat, can be decoded from neurophysiological plausible brain sources. In the future, methods have to be improved to allow the decoding of non-rhythmic MI with sufficient accuracy to control neuroprotheses.

Bibliography

[1] G. R. Müller-Putz, R. Scherer, G. Pfurtscheller, and R. Rupp, "EEG-based neuroprosthesis control: a step towards clinical practice," *Neuroscience Letters*, vol. 382, pp. 169–174, 2005.

[2] S. Waldert, H. Preissl, E. Demandt, C. Braun, N. Birbaumer, A. Aertsen, and C. Mehring, "Hand movement direction decoded from meg and eeg," *The Journal of Neuroscience*, vol. 28, pp. 1000–1008, January 2008.

[3] T. J. Bradberry, R. J. Gentili, and J. L. Contreras-Vidal, "Reconstructing three-dimensional hand movements from noninvasive electroencephalographic signals," *Journal of Neuroscience*, vol. 30, pp. 3432–3437, 2010.

[4] P. Ofner and G. Müller-Putz, "Decoding of velocities and positions of 3d arm movement from eeg," in *Proceedings of the 34th Annual International Conference of the IEEE EMBS*, pp. 6406–6409, 2012.

[5] J. A. Grahn and M. Brett, "Rhythm and beat perception in motor areas of the brain," *Journal of Cognitive Neuroscience*, vol. 19, no. 5, pp. 893–906, 2007.

Secondary Publication III

Movement Target Decoding from EEG and the corresponding Discriminative Sources: a Preliminary Study

Patrick Ofner[1] *Student Member, IEEE,* and Gernot R. Müller-Putz[1] *Member, IEEE*

***Abstract*— Brain-computer interfaces (BCIs) can detect movement imaginations (MI) which can act as a control signal for a neuroprosthesis of a paralyzed person. However, today's non-invasive BCIs can only detect simply qualities of MI, like what body part is subjected to MI. More advanced future non-invasive BCIs should be able to detect many qualities of MI to allow a natural control of a neuroprosthesis. In this preliminary study, we decoded movement targets during a self-paced center-out reaching task, and calculated corresponding spatial patterns in the source space. We were able to decode the movement targets with significant classification accuracy from one out of three subjects during the movement planning phase. This subject showed a distinct spatial pattern over the central motor area.**

I. INTRODUCTION

Tetraplegic persons have lost a substantial amount of movement functions regarding their limbs and torso. If this loss is due to a spinal cord injury (SCI) a remedy for hand movement functions could be the use of a brain-computer interface (BCI) in combination with a neuroprosthesis. The BCI detects the movement intention and the neuroprosthesis executes the movement. Together, these two systems would bridge the gap in the severed spinal cord. For example, Hochberg et al. [1] and Collinger et al. [2] showed remarkably progress in decoding movement intention and translation into robotic movements. Their BCIs (also called brain-machine interfaces) rely on invasive recordings of neuronal activities. However, probably not everyone would be comfortably with invasive recording techniques, and also the longterm use can not be guaranteed yet. Therefore, also non-invasive BCIs based on electroencephalographic (EEG) recordings are researched. Furthermore, experiments can be conducted with less effort and costs. Non-invasive EEG-based BCIs often exploit power changes in sensorimotor rhythms (SMR) accompanying motor imagination (MI) [3]. For example, Pfurtscheller et al. employed foot MI to restore the lateral grasp in a tetraplegic person's right hand [4]. Müller-Putz et. demonstrated the switching between different lateral grasp phases [5]. Recently, [6], [7] restored hand and elbow movement functions. However, SMR-based BCIs detect the process of MI but not the actual MI itself. They can detect that one is imaging a hand movement but not the trajectory of the hand movement. Furthermore, SMR-based BCIs often need to rely on MI of body parts which do not correspond to the body part in control, e.g., foot MI is used to restore hand movement functions. Thus, these BCIs do not decode the actual movement intention. However, the intended movement should be close to the executed movement to allow for a natural and therefore intuitive and easy neuroprosthesis control. An alternative BCI could be based on low-frequency EEG signals which contain movement information about trajectories of executed movements [8], [9]. Recently, our group showed the decoding of imagined restricted movements [10] from EEG. However it is unclear if this decoding can be generalized to unrestricted movement trajectories. Low-frequency signals seem to provide also information about movement direction or movement target, respectively. Here, the user imagines a reach to a target, this imagination would be decoded with a BCI and the neuroprosthesis executes the reach. The movement intention would correspond to the executed movement and a natural neuroprosthesis control could be possible. The previously mentioned trajectory decoding would give the user more control about the neuroprosthesis as target decoding but requires the decoding of more movement information from the brain. Target decoding would need an additional controller which generates the movement trajectory towards the target. However that would at the same time simplify the movement decoding problem as we need to extract less information from the EEG, and may be at this time the only realistic way to decode movement intentions accurately enough to control a neuroprosthesis. Waldert et al. [11] classified self-chosen center-out movements with a joystick; Li et al. [12] classified movements in a delayed saccade-or-reach task; Hammon et al. [13] demonstrated the classification of the target location during a reach; Lew [14] predicted directions in self-paced center-out reaching movements. All of these publications indicate that the planning phase before the movement onset contains decodable information at least in low-frequency EEG signals (delta band), and may be used to decode movement directions/targets before the actual movement onset.

We designed a preliminary study to classify the movement target from the EEG before the movement onset (planning phase). We employed a self-paced center-out reaching paradigm with 4 targets. An ARMEO Spring rehabilitation device was used to measure the position of the hand (to determine the movement onset), and to support the weight of the arm to avoid fatigue. For the first time in this context, we applied a method to find the spatial patterns containing

*This work is supported by the European ICT Programme Project H2020-643955 MoreGrasp. This paper only reflects the authors' views and funding agencies are not liable for any use that may be made of the information contained herein.

[1]Both authors are with the Institute of Knowledge Discovery, Graz University of Technology, Inffeldgasse 13/IV, 8010 Graz, Austria.

Correspondence to Patrick Ofner (patrick.ofner@tugraz.at)

978-1-4244-9270-1/15/$31.00 ©2015 IEEE

discriminative information [15] (as opposed to analyzing each channel individually) and combined it with source imaging. Analyzing discriminative sources is important to show that movement intention has been decoded from brain sources and not from artifacts, and to gain understanding about movement processes in the brain. Notably, we used a paradigm which do not caused eye movements in the planning phase and during the movement phase. Eye movements contain low-frequency components which otherwise could have affected our classification results. Furthermore, we took care that the actual movement intention and not an evoked potential due to the cue presentation was classified.

II. METHODS

A. Subjects

Three subjects participated in this preliminary study, two of them females. Two subjects have already participated in earlier BCI experiments. Their age ranged from 22 to 24, and all of them haven been right-handed. All experimental procedures involving human subjects followed the principles outlined in the Declaration of Helsinki.

B. Paradigm

Subjects were seated in the rehabilitation device ARMEO Spring (Hocoma, Switzerland), see Fig. 2. The ARMEO Spring supported the weight of the subjects' arm and prevented muscle fatigue, it is basically an arm exoskeleton. Furthermore, it allowed us to measure the position of the hand. We employed a self-paced center-out reaching task. Subjects moved their right arm from a resting position — approximately 10 cm in front of the abdomen — to one of 4 targets on a computer screen. The targets were filled green circles positioned at the edges of the computer screen. The paradigm is shown in Fig. 1. At second 0 a target appeared in one of the edges of the computer screen. We instructed the subjects to immediately look at the target. Thus, eye movements happened in a controlled way in the beginning of a trial, and not later during the reaching phase which may have affected the classification. Four to 5 s after the trial start a beep sounded serving as a go cue. This relative long and variable delay period was inserted to ensure that the signals resulting from eye movements and possible evoked potentials due to cue presentation have vanished. We instructed subjects to start the reaching movements 1 to 3 s after the go cue, i.e., subjects executed self-paced movements. When subjects touched a virtual wall in front of the computer screen, the target was reached and turned from green to red. Subjects stopped the reaching movement and moved the arm back to the resting position. The trial ended 3 s after the target was reached. After a trial a break of 3 s followed. We recorded 4 reaching runs, each comprising of 40 trials (10 trials for each target, randomly distributed). Thus, in total we recorded 160 reaching trials. Additionally, we recorded 3 (subject 1), and 4 (subject 2 and 3), respectively, resting state runs, each run comprising of one trial with 60 s. This data were used to estimate the noise covariance matrix in the source imaging process.

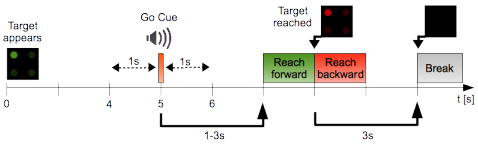

Fig. 1: The trial sequence. Subjects reached the green target on the screen self-paced after the go cue.

Fig. 2: A subject mounted with the electrode cap and the Armeo exoskeleton.

C. Recording

We recorded 68 EEG channels and 3 electrooculography (EOG) channels with 5 g.USBamp biosignal amplifiers (g.tec medical engineering GmbH, Austria). EEG channels covered frontal, central, parietal and temporal areas, EOG channels were placed above the nasion and below the outer canthi of the eyes. Reference was placed on the left mastoid, ground on the right mastoid. We applied an 8-th order Chebyshev band-pass filter from 0.01 Hz to 200 Hz, a Notch filter at 50 Hz, and sampled the signals with 512 Hz. For subsequent source imaging, we measured the electrode positions with ELPOS (Zebris Medical GmbH, Germany). Movement data, i.e., 3D position of the right hand, was recorded using a custom made plugin for the ARMEO Spring software.

D. Preprocessing

We did a principal components analysis (PCA) on the aggregated EEG/EOG data and retained components which explained 99 % of the variance of the data. Subsequently, we filtered the data from 0.3 to 100 Hz (4-th order zero-phase Butterworth filter) and did an independent component analysis (ICA), then we marked components suspected to be muscle, technical or eye movement artifacts. Samples which exceeded a threshold of 5 times the standard deviation of the absolute value, Kurtosis or slope (moving average of absolute value of differentiated signal) were excluded from the PCA and ICA. The time window for calculating the Kurtosis and slope was 0.25 s. Then we removed artifact contaminated components from the raw (unfiltered) but PCA compressed EEG/EOG data. Subsequently, we applied a zero-phase anti-aliasing filter and downsampled to 64 Hz

to reduce the computational effort. Afterwards, we applied a 0.3 – 3 Hz 4-th order zero-phase Butterworth band-pass filter to extract low frequency signals. To remove possible remaining artifacts, we removed samples from the analysis exceeding a threshold of 4.4 times the median absolute deviation (MAD) of an EEG channel. MAD is a robust deviation measure, and the chosen threshold corresponds to 3 times the standard deviation when data are normally distributed. Finally, we referenced the EEG channels using common average reference (CAR).

E. Classification

We computed the classification accuracy within the time window -2 s to 2 s relative to movement onset. Within this window, we classified with a shrinkage linear discriminant analysis (LDA) [16] each time point individually using data from all EEG channels, i.e., only data from the current time point were used for classification. Each target corresponded to a class resulting in a 4 classes classification problem, and therefore we used an one-vs-one classification strategy. This classification strategy required 6 binary LDA classifiers combined with a majority vote to obtain the final class. Classification accuracies were calculated using 5×10 fold cross-validation. We report the accuracy for each time point as the mean value of the test sets' classification accuracies.

To determine the movement onset, we filtered the hand positions with a 6 Hz 4-th order low-pass Butterworth filter and calculated the acceleration. Finally, we defined the movement onset when the acceleration reached 400 $\mathrm{mm/s^2}$. The cutoff frequency and acceleration threshold were found empirically so that movements were detected as early as possible without yielding a high number of false positives.

F. Discriminative Sources

It is not only interesting to see if a classification is possible, it is also interesting to locate the brain sources carrying the discriminative information, i.e., patterns. To reveal the brain sources we combined sources imaging with discriminative spatial patterns [15]. EEG channels in the lower frequency range are usually highly correlated [10] which prohibits a direct interpretation of the LDA classifier weights. The weights found by the classifier must be treated as filters and not as patterns. However, an LDA can be performed by solving a generalized eigenvalue problem which yields a spatial filter matrix which can be inverted to obtain the spatial patterns [15]. A binary LDA classifier yield only one spatial filter with discriminative information, and therefore only one spatial pattern of interest. As we used 6 binary classifiers due to the one-vs-one classification strategy we also got 6 spatial patterns. We took their absolute values and averaged them to obtain the final spatial pattern. This was done for every time point within the time-window.

To encounter the volume conduction in the head and to increase the spatial resolution we applied source imaging using the software Brainstorm [17]. We computed boundary element head models with the Colin27 brain model and subject individual electrode positions. Full noise noise covariance were estimated based on the resting state runs with a shrinkage regularization [18]. Subsequently, we computed 5001 brain sources using standardized low-resolution brain electromagnetic tomography (sLORETA) [19] with source orientations constrained normally to the cortex. Finally, we calculated the patterns as described above using all brain sources. To cope with the high dimensionality compared to the trial number we utilized the shrinkage approach when calculating the spatial patterns.

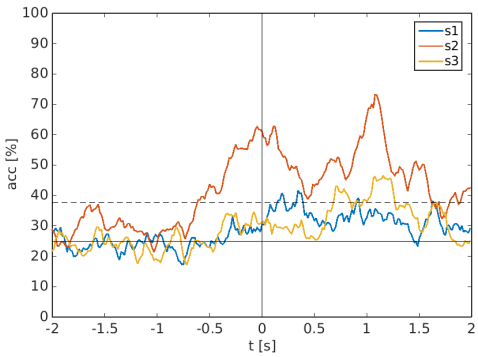

Fig. 3: Subjects' classification accuracies. Time point 0 s corresponds to the movement onset. The dashed line depicts the significance level.

III. RESULTS

A. Classification Accuracies

Fig. 3 shows the classification accuracies for all 3 subjects for each time point, $t = 0$ s corresponds to the movement onset. The significance level (based on the number of trials) is 38 % [20] ($\alpha = 0.05$, Bonferroni corrected for the length of the shown time window). Notably, subject 2 shows relative high classification accuracies before and around the movement onset. Table I shows the maximum classification accuracies reached before and after movement onset and the corresponding times. Only subject 2 reached above chance level accuracies before movement onset. After movement onset all subjects reached a significant classification accuracy. The average times and standard deviations to reach the targets were: 750 ± 147 ms (s1), 742 ± 111 ms (s2), and 729 ± 131 ms (s3).

TABLE I: Subjects' largest classification accuracies reached before and after movement onset.

subjects	pre movement onset	post movement onset
s1	33 % @ -281 ms	42 % @ 344 ms
s2	63 % @ -47 ms	73 % @ 1078 ms
s3	35 % @ -78 ms	47 % @ 1156 ms

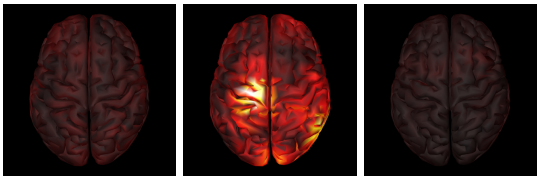

s1 s2 s3

Fig. 4: Patterns showing discriminative information in source space. All patterns have the same scale, white corresponds to the maximum value, black to zero, the units are dimensionless as sLORETA yields standardized brain sources.

B. Discriminative Sources

Fig. 4 shows the subjects' patterns at the time point when the largest pre movement classification accuracy was reached (cf. Table I). Here, we averaged the absolute values of the patterns of the 6 binary classifiers. Only subject s2 shows a distinctive pattern which is located on the left-side of the primary motor cortex and partly on the supplementary motor area (SMA).

IV. DISCUSSION

We demonstrated the classification of targets when executing a self-paced reach. One subject showed a significant classification accuracy before the movement onset (planning phase), and all 3 subjects showed a significant classification accuracy after the movement onset. However, relevant for neuroprosthesis control is the planning phase: the intended target is decoded from the EEG and the neuroprosthesis executes the movement towards the target. In our preliminary study only one of three subjects showed significant classification accuracies in the planning phase. This is different to a comparable study with a 2-class paradigm [12] where 9 of 10 subjects reached a decent classification accuracy. However, an evoked potential due to the cue presentation may have contributed to the extracted signal features which we have prevented with a long and variable delay between target cue and go cue. Also [14] obtained higher classification accuracies in two healthy subjects (83 % and 68 %) in a comparable study but with reaches via a manipulandum instead of natural reaches as in this work. A likely reason could be that in [14] a time window has been used for the classifier input instead of one single time point as in this work. However, we used only a single time point for classification to analyze the classification accuracy over time as accurate as possible. A main contribution of our study is the demonstration of source imaging with spatial patterns when executing reaching tasks. Only the subject who reached significant classification accuracies in the planning phase showed also a distinct pattern. The pattern is located centrally over the motor cortex which is similar to the pattern shown in [11] where subjects moved a joystick in 4 directions, or in a work from our group where we decoded imagined movements trajectories [10]. The advantage of spatial patterns compared to an often performed individual evaluation of channels is that spatial pattern can better deal with noise and show a more accurate picture of the real source distribution. To assess the stability of this pattern we plan to conduct a full study with more participants.

REFERENCES

[1] L. R. Hochberg, D. Bacher, B. Jarosiewicz, N. Y. Masse, J. D. Simeral, J. Vogel, S. Haddadin, J. Liu, S. S. Cash, P. van der Smagt, and J. P. Donoghue, "Reach and grasp by people with tetraplegia using a neurally controlled robotic arm," *Nature*, vol. 485, pp. 372–375, 2012.

[2] J. L. Collinger, B. Wodlinger, J. E. Downey, W. Wang, E. C. Tyler-Kabara, D. J. Weber, A. J. C. McMorland, M. Velliste, M. L. Boninger, and A. B. Schwartz, "High-performance neuroprosthetic control by an individual with tetraplegia," *Lancet*, vol. 381, no. 9866, pp. 557–564, 2013.

[3] G. Pfurtscheller and F. H. L. D. Silva, "Event-related eeg/meg synchronization and desynchronization: basic principles," *Clin Neurophysiol*, vol. 110, no. 11, pp. 1842–1857, 1999.

[4] G. Pfurtscheller, G. R. Müller, J. Pfurtscheller, H. J. Gerner, and R. Rupp, ""Thought"-control of functional electrical stimulation to restore handgrasp in a patient with tetraplegia," *Neurosci Lett*, vol. 351, pp. 33–36, 2003.

[5] G. R. Müller-Putz, R. Scherer, G. Pfurtscheller, and R. Rupp, "EEG-based neuroprosthesis control: a step towards clinical practice," *Neurosci Lett*, vol. 382, pp. 169–174, 2005.

[6] A. Kreilinger, V. Kaiser, M. Rohm, R. Leeb, R. Rupp, and G. Müller-Putz, "Neuroprosthesis control via noninvasive hybrid brain-computer interface," *IEEE Intell Syst*, vol. 28, no. 5, pp. 40–43, 2013.

[7] M. Rohm, M. Schneiders, C. Müller, A. Kreilinger, V. Kaiser, G. R. Müller-Putz, and R. Rupp, "Hybrid brain-computer interfaces and hybrid neuroprostheses for restoration of upper limb functions in individuals with high-level spinal cord injury," *Artif Intell Med*, vol. 59, no. 2, pp. 133–142, 2013.

[8] T. J. Bradberry, R. J. Gentili, and J. L. Contreras-Vidal, "Reconstructing three-dimensional hand movements from noninvasive electroencephalographic signals," *J Neurosci*, vol. 30, pp. 3432–3437, 2010.

[9] P. Ofner and G. R. Müller-Putz, "Decoding of velocities and positions of 3d arm movement from eeg," in *EMBC, 2012 Annual International Conference of the IEEE*, 2012, pp. 6406–6409.

[10] P. Ofner and G. R. Müller-Putz, "Using a noninvasive decoding method to classify rhythmic movement imaginations of the arm in two planes," *IEEE Trans Biomed Eng*, vol. 62, no. 3, pp. 972–981, 2015.

[11] S. Waldert, H. Preissl, E. Demandt, C. Braun, N. Birbaumer, A. Aertsen, and C. Mehring, "Hand movement direction decoded from meg and eeg," *J Neurosci*, vol. 28, no. 4, pp. 1000–1008, 2008.

[12] J. Li, Y. Wang, L. Zhang, and T. P. Jung, "Combining erps and eeg spectral features for decoding intended movement direction," in *EMBC, 2012 Annual International Conference of the IEEE*, 2012.

[13] P. S. Hammon, S. Makeig, H. Poizner, E. Todorov, and V. R. de Sa, "Predicting reaching targets from human eeg," *IEEE Signal Processing Magazine*, vol. 25, no. 1, pp. 69–77, 2008.

[14] E. Y. Lew, R. Chavarriaga, S. Silvoni, and J. D. R. Millan, "Single trial prediction of self-paced reaching directions from eeg signals," *Front Neurosci*, vol. 8, no. 222, 2014.

[15] X. Liao, D. Yao, D. Wu, and C. Li, "Combining spatial filters for the classification of single-trial eeg in a finger movement task," *IEEE Trans Biomed Eng*, vol. 54, no. 5, pp. 821–831, 2007.

[16] R. Peck and J. V. Ness, "The use of shrinkage estimators in linear discriminant analysis," *IEEE Trans Pattern Anal Mach Intell*, vol. 4, no. 5, pp. 530–7, 1982.

[17] F. Tadel, S. Baillet, J. C. Mosher, D. Pantazis, and R. M. Leahy, "Brainstorm: A user-friendly application for meg/eeg analysis," *Comput Intell Neurosci*, 2011.

[18] J. Schäfer and K. Strimmer, "A shrinkage approach to large-scale covariance matrix estimation and implications for functional genomics," *Stat Appl Genet Mol Biol*, vol. 4, no. 1, pp. 1–30, 2005.

[19] R. D. Pascual-Marqui, "Standardized low-resolution brain electromagnetic tomography (sloreta): technical details," *Methods Find Exp Clin Pharmacol*, vol. 24, pp. 5–12, 2002.

[20] G. R. Müller-Putz, R. Scherer, C. Brunner, R. Leeb, and G. Pfurtscheller, "Better than random? a closer look on bci results," *International Journal of Bioelectromagnetism*, vol. 10, no. 1, pp. 52–55, 2008.

Secondary Publication IV

Proceedings of the
7th Graz Brain-Computer Interface Conference 2017 DOI: 10.3217/978-3-85125-533-1-67

VISUAL INPUT AFFECTS THE DECODING OF IMAGINED MOVEMENTS OF THE SAME LIMB

P. Ofner[1], P. Kersch[1], G. R. Müller-Putz[1]

[1]Institute of Neural Engineering, Graz University of Technology, Graz, Austria

E-mail: gernot.mueller@tugraz.at

ABSTRACT: A better understanding how movements are encoded in electroencephalography (EEG) signals is required to develop a more natural control for motor neuroprostheses. We decoded imagined hand close and supination movements from seven healthy subjects and investigated the influence of the visual input. We found that motor imagination of these movements can be decoded from low-frequency time-domain EEG signals with a maximum average classification accuracy of $57.3 \pm 5.0\%$. The simultaneous observation of congruent hand movements increased the classification accuracy to $64.1 \pm 8.3\%$. Furthermore, the sole observation of hand movements yielded discriminable brain patterns ($61.9 \pm 5.5\%$). These findings show that for low-frequency time-domain EEG signals, the type of visual input during classifier training affects the performance and has to be considered in future studies.

INTRODUCTION

Understanding the encoding of movements in the human brain is paramount for the development of a new and more intuitive control of motor neuroprostheses. Our group already restored movement function in persons with spinal cord injury (SCI) with motor neuroprostheses [1, 2, 3, 4] based on functional electrical stimulation (FES) [5, 6]. However, the control of FES via a non-invasive brain-computer interface (BCI) is in general unintuitive and unnatural. The BCI requires subjects to learn the expression of brain patterns which can be unrelated to the actual restored movement (e.g. imagination of foot movement to control the hand). Furthermore, the imagined movements are usually repetitive movements and not single movements. These BCIs are usually based on sensorimotor rhythms (SMR) extracted from electroencephalography (EEG) signals. However, newer research suggests that more details of movements can be decoded from low-frequency EEG signals [7, 8, 9, 10]. Furthermore, our group decoded six single movements (elbow extension/flexion, pronation/supination, hand open/close) of the upper limb from low-frequency time-domain signals [11]. This is of special interest in the context of neuroprosthesis control as, e.g., persons with SCI may then imagine or attempt one of these single movements to control a motor neuroprosthesis more naturally. However, as there are no overt movements causing a change in the sensory feedback, the visual input (here: movement observation) becomes potentially more important and may have an impact on the decoding performance. In fact, a sole observation of another movement is known to interfere with the execution of a movement [12], and affects brain rhythms [13, 14]. Furthermore, the visual system can partly substitute the somatosensory system [15]. This point is of special interest because we speculate that the decoding of movements from EEG may depend on a closed loop between the motor cortex and the spinal cord, i.e. proprioceptive feedback may partly be responsible for the modulation of low-frequency EEG signals which is then decoded with a BCI. In this work, we analysed if the lack of varying sensory feedback during motor imagination (MI) can be partly substituted by visual input which in turn may improve the classification accuracy. We hypothesize that the simultaneous observation of hand movements which correspond to imagined movements improves the classification accuracy. As a control condition, we used abstract visuals.

MATERIALS AND METHODS

Subjects: Seven healthy and right-handed subjects participated in the study. They were aged between 20 and 28 years. Three of them were female. The subjects received payment for their participation.

Paradigm:

The subjects sat in a comfortable chair in front of a horizontal computer screen which was used to give instructions and visual input to the subjects. The right arm was positioned under the computer screen (see Fig. 1). We instructed the subjects to perform kinesthetic motor imagery (MI) [14] of closing the right hand (CLOSE) or rotating the right arm (SUPINATION) while observing a movie showing a congruent realistic or an abstract movement. The realistic visual input (RVI) was pre-recorded from a human arm performing the movements while the abstract visual input (AVI) was an animation of a circle turning into an ellipse (see Fig. 2). The circle narrowed either from the top and bottom corresponding to CLOSE or from the left and right side corresponding to SUPINATION. Additionally to CLOSE and SUPINATION, we recorded a REST condition where we showed a picture (realistic or abstract) instead of a movie. In

Proceedings of the
7th Graz Brain-Computer Interface Conference 2017 DOI: 10.3217/978-3-85125-533-1-67

REST subject were instructed to not perform any MI. However, REST was not further analysed in this work. To disentangle the effect of MI and the observation of visual input, we employed a movement observation condition. In this condition, subjects were instructed to omit any MI while observing the movie (OBS). Thus, we had three types of conditions: CLOSE/SUPINATION/REST (movement condition), AVI/RVI (visual input condition) and MI/OBS (mental task condition) (see Fig. 3). Fig. 4 shows the sequence of one trial. At the beginning of one trial, the subjects were informed on a computer screen whether MI has to be performed synchronously to the upcoming movie or whether the movie should only be observed. When the movie appeared, it immediately started to play for 2 seconds, paused then and finally disappeared at the end of the trial, i.e. every MI or observation lasted 2 seconds. The movie was either an RVI or AVI type and the movement shown was either CLOSE, SUPINATION or REST. The initial frames of the movies were exactly the same (AVI) or indistinguishable (RVI). After the movie stopped playing, a 1.5 s long idle period followed and then the trial ended. Subsequent to one trial, an inter-trial interval with a random duration of 1.5 - 2.5 s followed. We used a block design to record the trials and runs. Each block exclusively comprised 3 AVI or 3 RVI runs and the blocks where arranged as follows: RVI/AVI/AVI/RVI. Before the first RVI and AVI run, respectively, we additionally recorded a training run. This two training runs were used to familiarize the subjects with the paradigm and were not further evaluated. At the beginning, middle and end of a recording, we also recorded runs in which subjects performed eye movements or rested. However, those runs were not further used in this work. Each run comprised 11 trials per CLOSE/SUPINATION class and 5 trials per REST class. Thus, in total we recorded 66 trials (CLOSE/SUPINATION) and 30 trials (REST) for each RVI/AVI and MI/OBS condition.

Figure 1: Subjects observed or performed MI according to real visual input or abstract visual input. The right hand was under the computer screen.

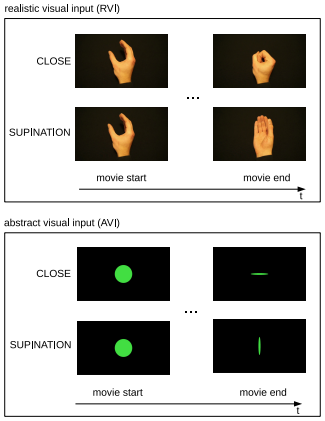

Figure 2: Subjects observed movements or performed MI with real visual input or abstract visual input.

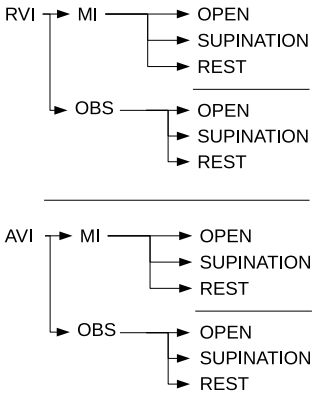

Figure 3: Types of conditions. Subjects perceived real (RVI) or abstract visual input (AVI). They performed MI of CLOSE/SUPINATION/REST or observed (OBS) CLOSE/SUPINATION/REST.

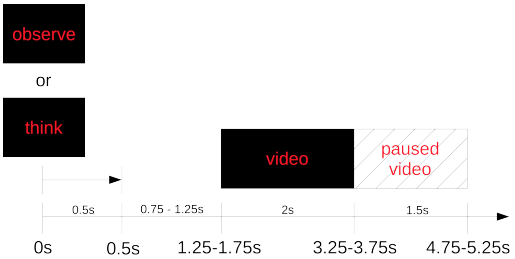

Figure 4: Trial sequence. An instruction was shown at second 0 for 500 ms to inform the subject if a MI has to be performed synchronously to the upcoming movie ("think") or if the movie should only be observed ("observe"). Subsequently, a movie appeared after a random interval and started to play.

Proceedings of the
7th Graz Brain-Computer Interface Conference 2017 DOI: 10.3217/978-3-85125-533-1-67

Recording: We recorded 61 EEG channels covering frontal, central, parietal and temporal areas of the head as well as 3 EOG channels placed above the nasion and the outer canthi of the eyes. Signals were recorded with active electrodes and biosignal amplifiers (g.tec medical engineering GmbH, Austria) with the reference placed on the right mastoid and ground on AFz. We applied an 8th-order Chebyshev bandpass filter from 0.01 Hz to 200 Hz and sampled the signals at 512 Hz. Furthermore, a notch filter at 50 Hz suppressed line noise.

Preprocessing: First, EEG channels were visually inspected and noisy or defective channels were removed. To prepare the data for an independent component analysis (ICA), we band-pass filtered with a zero-lag 4th-order Butterworth filter from 0.3 Hz to 70 Hz. Then we calculated the median absolute deviation (MAD) for each channel using data only from trials (i.e. not from inter-trial intervals) and marked EEG samples as artefact contaminated if they exceeded a threshold of 7.41 times the MAD (corresponding to 5 times the standard deviation for normally distributed data) of the respective channel. All samples which were not marked as artefact contaminated were subjected to an Extended Infomax ICA [16] implemented in EEGLAB [17] (which was applied using the first n principal components explaining 99 % of the variance of the data). ICA components corresponding to eye movements and muscle artefacts were marked as artefact contaminated. The above mentioned sample-based MAD method was solely used to detect transient artefacts which can impair an ICA. However, for the actual classification we used EEGLAB to detect artefact contaminated trials with: (1) amplitudes above/below -80 μV and 80 μV, respectively; (2) trials with abnormal joint probabilities; (3) trials with abnormal kurtosis. The methods (2) and (3) used 4 times the standard deviation of their respective statistic as a threshold to detect artefacts.
Finally, we applied a 0.3 Hz to 3 Hz zero-lag 4th-order Butterworth band-pass filter the original (unfiltered) EEG data to extract low-frequency time-domain features from the EEG, and removed independent components and trials previously marked as artefact contaminated.

Classification: We classified the two classes CLOSE and SUPINATION in each RVI/AVI and MI/OBS condition. We used a shrinkage linear discriminant analysis (sLDA) [18, 19] and a sliding window. In more detail, we used the time lags -200 ms to 200 ms in 100 ms time intervals relative to the center of the sliding window as an input to the sLDA classifier (i.e. 5 time lags). We moved this window over the trials (from -1 s to 3 s in 62.5 ms time steps relative to the start of the movie) and report the classification accuracies associated to the center point of the sliding window. The classification results were validated with a 10x10-fold cross-validation at each classification time step.

Topoplots: To calculate the topoplots, we first interpolated removed channels. Then, we calculated the difference between the average scalp potentials (monopolar) of CLOSE and SUPINATION for each RVI/AVI and MI/OBS condition at each time point within a trial (using a time resolution of 62.5 ms). Afterwards, we took the absolute value of each channel value and time averaged over the movie period of 2 s. Finally, we averaged over subjects.

RESULTS

Classification Accuracies: Fig. 5 shows the classification accuracies of CLOSE vs SUPINATION for all conditions. Classification accuracies were calculated from -1 s to 3 s relative to movie start with a time resolution of 1/16 s. The significance level with respect to a single subject is 64 % ($\alpha = 0.05$, adjusted Wald interval [20, 21], Bonferroni corrected for the time duration in Fig. 5). Five subjects exceeded the significance level between 0 s and 2 s in the RVI-MI condition, 6 in RVI-OBS, 4 subjects in AVI-MI, and no subject in AVI-OBS. RVI yielded higher classification accuracies than AVI, and MI yielded higher classification accuracies than OBS, c.f. Table 1. We conducted a two-way repeated measure ANOVA with 2 factors - RVI/AVI (visual input) and MI/OBS (mental task) - and compared the classification accuracies at the time point of maximal average classification accuracy. The visual input main effect was significant ($F(1,6) = 8.25$, $p = 0.03$), i.e. the classification accuracy increase between AVI and RVI was significant. The mental task main effect ($F(1,6) = 0.79$, $p = 0.41$) and the interaction effect ($F(1,6) = 0.04$, $p = 0.84$) were not significant. The sphericity assumption was tested with Mauchly's test and was not violated ($p = 0.57$).

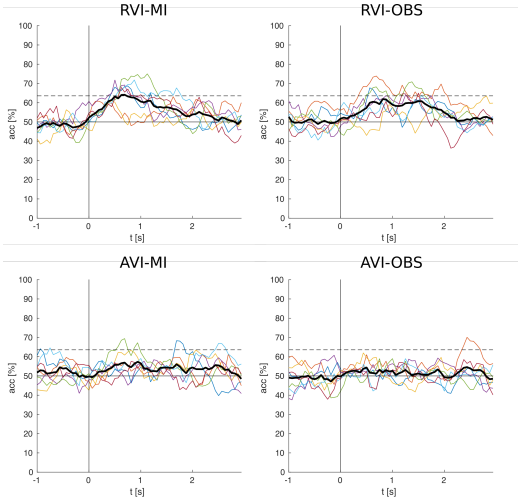

Figure 5: Classification accuracies for RVI/AVI and MI/OBS conditions. Shown are the individual subjects' accuracies and the grand average in bold. At second 0 the movie started to play for 2 seconds. The horizontal solid line is the chance level, the dashed line is the significance level on a single subject basis.

Proceedings of the
7th Graz Brain-Computer Interface Conference 2017 DOI: 10.3217/978-3-85125-533-1-67

Table 1: Maximum average classification accuracies with standard deviations and times relative to the movie start

	RVI-MI	RVI-OBS	AVI-MI	AVI-OBS
max acc [%]	64.1	61.9	57.3	54.4
std dev [%]	8.3	5.5	5.0	4.3
time [t]	0.69	0.81	0.94	0.50

We also analysed the classification accuracy of MI vs OBS with RVI. For this purpose, we aggregated CLOSE and SUPINATION trials in the RVI-MI and RVI-OBS conditions and classified these two conditions, see Fig. 6. The significance level with respect to a single subject is 60 %.

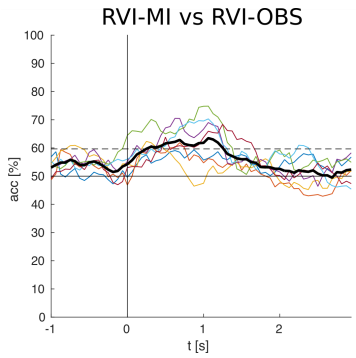

Figure 6: Classification accuracy of MI vs OBS with RVI. Shown are the individual subjects' accuracies, the grand average in bold, the chance level (horizontal solid line), and the significance level (dashed line).

Topoplots: Fig. 7 shows the topoplots where a prominent central pattern is observable for motor imagery during real visual input (RVI-MI).

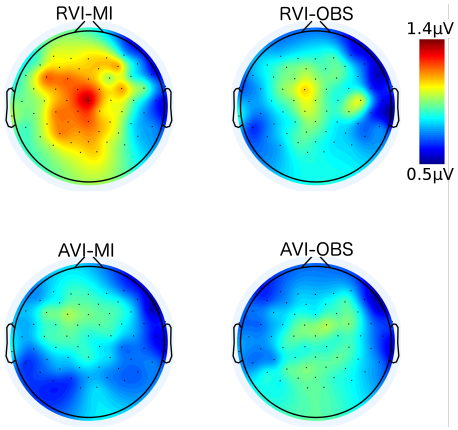

Figure 7: Topoplots. Shown are subject averaged absolute differences between the CLOSE and SUPINATION scalp potential maps. All plots have the same scale (blue is the minimum, red the maximum).

DISCUSSION

We showed the classification of two MIs from the same upper limb based on low-frequency time-domain EEG signals. Importantly, the MIs were not repetitive as in classical SMR-based BCIs but single ones, which are closer to ordinary movements. Furthermore, the MIs corresponded closely to movements which currently could be restored with a motor neuroprosthesis [6]. Some subjects reached a significant classification accuracy when observing abstract visual input. This indicates that the analysed imagined movements can be decoded even in the absence of any realistic visual input. This is in line with [22, 23], where imagined hand movements were decoded from the frequency-domain of EEG. Furthermore, consistent with our initial hypothesis, the results show that the classification accuracy can be increased when serving realistic visual input. Perhaps by substituting the somatosensory feedback at the somatosensory cortex with forwarded input from the visual system as in [15]. However, in our experiment there was no dedicated phase to incorporate the observed hand in ones own body schema.

In a practical setup, we cannot simply present realistic visual input to improve the classification accuracy because that would require knowledge about the indented movement before it was classified. The idea is rather to bootstrap the classification, i.e. presenting realistic visual input in the initial training of the classifier when no feedback is provided yet (open-loop). If the classifier performance is on an acceptable performance level, the subject can then be trained with actual feedback (closed-loop). A principle which has been applied in invasive studies [24, 25] with a robotic arm. However, their the idea was rather to obtain kinematic data for decoder calibration than observing human movements. A robotic arm is different to a human arm, however the boundary between abstract and realistic visual feedback is probably not sharp but continuous and the robotic arm may have been perceived similar to an human arm. Further studies could investigate if the presentation of a human hand is advantageous to a robotic arm in the open-loop classifier training. However, in the context of motor neuroprostheses, movement function is restored without using a robotic arm and this question does not arise.

Most surprisingly, the sole observation of hand movements yielded classification accuracies comparable to MI (c.f. RVI-MI and RVI-OBS). Movement observation has been reported to modulate brain rhythms [13, 14] (with respect to a no-movement condition). In this work, we show for the first time (to the best of our knowledge) that the observation of different movements of the same limb can be decoded from low-frequency time-domain EEG signals. In the context of motor neuroprosthesis control,

Proceedings of the
7th Graz Brain-Computer Interface Conference 2017 DOI: 10.3217/978-3-85125-533-1-67

this raises the question if the discriminability in RVI-MI is solely due to the simultaneously observed movement. The classification accuracies in AVI-MI indicate that a classification is basically possible, regardless of the visual input. Furthermore, the results show that MI and movement observation are discriminable during real visual input. However, it can not be answered in this study whether the classification accuracy *increase* is (1) solely due to movement observation or (2) whether the neural correlate of MI is modulated by the movement observation in a way which increases the discriminable information or (3) a combination of both. Nevertheless, the open-loop/closed-loop training approach may still work even when the increase of classification accuracy is solely due to the movement observation. Thus, the impact of this finding on the open-loop/closed-loop training has to be investigated in forthcoming studies. If the observation of movements has activated the mirror neuron system which in turn facilitated the classification is debatable. Mirror neurons fire only when observing meaningful movements. However, in our study no interaction of the movement with the environment was given, i.e. the observed movements were non-goal-directed and should not have activated the mirror neuron system.

The amount of discriminative information in the 4 different conditions is also reflected in the topoplots. The RVI-MI topoplot shows the largest amplitude differences between CLOSE and SUPINATION, followed by RVI-OBS and then the two AVI conditions. The observed RVI patterns are widespread. However, central motor areas are pronounced the most, showing that the discriminative information is indeed encoded in brain signals. Interesting is that RVI-MI has a more amplified pattern than RVI-OBS but similar classification accuracies. This may be due to a more stable pattern during the video sequence (topoplots are averaged over the whole movie period as opposed to the classification accuracies). This indicates that the discriminative information is encoded differently between MI and movement observation.

CONCLUSION

We show the classification of two imagined movements of the same upper limb and show that the classification accuracy can be increased if the movement is simultaneously observed in a video. Furthermore, we show that also the sole observation of movement videos yields discriminable brain patterns.

ACKNOWLEDGEMENTS

This work is supported by the European ICT Programme Project H2020-643955 "MoreGrasp" and the ERC Consolidator Grant ERC-681231 "Feel Your Reach".

REFERENCES

[1] G. R. Müller-Putz, R. Scherer, G. Pfurtscheller, and R. Rupp, "EEG-based neuroprosthesis control: a step towards clinical practice," *Neurosci Lett*, vol. 382, pp. 169–174, 2005.

[2] G. Pfurtscheller, G. R. Müller, J. Pfurtscheller, H. J. Gerner, and R. Rupp, ""Thought"-control of functional electrical stimulation to restore handgrasp in a patient with tetraplegia," *Neurosci Lett*, vol. 351, pp. 33–36, 2003.

[3] A. Kreilinger, V. Kaiser, M. Rohm, R. Leeb, R. Rupp, and G. Müller-Putz, "Neuroprosthesis control via noninvasive hybrid brain-computer interface," *IEEE Intell Syst*, vol. 28, no. 5, pp. 40–43, 2013.

[4] M. Rohm, M. Schneiders, C. Müller, A. Kreilinger, V. Kaiser, G. R. Müller-Putz, and R. Rupp, "Hybrid brain-computer interfaces and hybrid neuroprostheses for restoration of upper limb functions in individuals with high-level spinal cord injury," *Artif Intell Med*, vol. 59, no. 2, pp. 133–142, 2013.

[5] R. Rupp and H. J. Gerner, "Neuroprosthetics of the upper extremity - clinical application in spinal cord injury and challenges for the future," *Acta Neurochir. Suppl.*, vol. 97, no. Pt 1, pp. 419–426, 2007.

[6] R. Rupp, M. Rohm, M. Schneiders, A. Kreilinger, and G. Muller-Putz, "Functional rehabilitation of the paralyzed upper extremity after spinal cord injury by noninvasive hybrid neuroprostheses," *Proceedings of the IEEE*, vol. 103, pp. 954–968, June 2015.

[7] T. J. Bradberry, R. J. Gentili, and J. L. Contreras-Vidal, "Reconstructing three-dimensional hand movements from noninvasive electroencephalographic signals," *J Neurosci*, vol. 30, pp. 3432–3437, 2010.

[8] P. Ofner and G. R. Müller-Putz, "Decoding of velocities and positions of 3d arm movement from eeg," in *EMBC, 2012 Annual International Conference of the IEEE*, pp. 6406–6409, 2012.

[9] Y. Gu, K. Dremstrup, and D. Farina, "Single-trial discrimination of type and speed of wrist movements from eeg recordings," *Clin Neurophysiol*, vol. 120, no. 8, pp. 1596–1600, 2009.

[10] M. Jochumsen, I. K. Niazi, D. Taylor, D. Farina, and K. Dremstrup, "Detecting and classifying movement-related cortical potentials associated with hand movements in healthy subjects and stroke patients from single-electrode, single-trial eeg," *J. Neural Eng.*, vol. 12, no. 5, p. 056013, 2015.

[11] P. Ofner, A. Schwarz, J. Pereira, and G. R. M, "Movements of the same upper limb can be classified from low-frequency time-domain eeg signals," in *6th International BCI Meeting, Asilomar*, 2016.

Proceedings of the
7th Graz Brain-Computer Interface Conference 2017 DOI: 10.3217/978-3-85125-533-1-67

[12] J. M. Kilner, Y. Paulignan, and S. J. Blakemore, "An interference effect of observed biological movement on action," *Current Biology*, vol. 13, pp. 522–525, 2003.

[13] S. Cochin, C. Barthelemy, B. Lejeune, S. Roux, and J. Martineau, "Perception of motion and qeeg activity in human adults," *Electroencephalogr Clin Neurophysiol*, vol. 107, pp. 287–295, 1998.

[14] C. Neuper, R. Scherer, M. Reiner, and G. Pfurtscheller, "Imagery of motor actions: differential effects of kinesthetic versus visual-motor mode of imagery on single-trial eeg," *Brain Research Cognitive Brain Research*, vol. 25, pp. 668–677, 2005.

[15] S. Shokur, J. E. O'Doherty, J. A. Winans, H. Bleuler, M. A. Lebedev, and M. A. L. Nicolelis, "Expanding the primate body schema in sensorimotor cortex by virtual touches of an avatar," *PNAS*, vol. 110, no. 37, pp. 15121–15126, 2013.

[16] T. W. Lee, M. Girolami, and T. J. Sejnowski, "Independent component analysis using an extended infomax algorithm for mixed sub-gaussian and supergaussian sources," *Neural Comput*, vol. 11, no. 2, pp. 417–441, 1999.

[17] A. Delorme and S. Makeig, "Eeglab: an open source toolbox for analysis of single-trial eeg dynamics including independent component analysis," *J Neurosci Methods*, vol. 134, no. 1, pp. 9–21, 2004.

[18] B. Blankertz, S. Lemm, M. Treder, S. Haufe, and K.-R. Müller, "Single-trial analysis and classification of erp components - a tutorial," *Neuroimage*, vol. 56, no. 2, pp. 814–825, 2011.

[19] R. Peck and J. V. Ness, "The use of shrinkage estimators in linear discriminant analysis," *IEEE Trans Pattern Anal Mach Intell*, vol. 4, no. 5, pp. 530–7, 1982.

[20] G. R. Müller-Putz, R. Scherer, C. Brunner, R. Leeb, and G. Pfurtscheller, "Better than random? a closer look on bci results," *International Journal of Bioelectromagnetism*, vol. 10, no. 1, pp. 52–55, 2008.

[21] M. Billinger, I. Daly, V. Kaiser, J. Jin, B. Z. Allison, and G. R. Müller-Putz, *Towards Practical Brain-Computer Interfaces*, ch. Is it significant? Guidelines for reporting BCI performance, pp. 333–354. Springer, Berlin Heidelberg, 2012.

[22] A. Vučković and F. Sepulveda, "Delta band contribution in cue based single trial classification of real and imaginary wrist movements," *Med Biol Eng Comput*, vol. 46, no. 6, pp. 529–539, 2008.

[23] A. Vučković and F. Sepulveda, "A two-stage four-class bci based on imaginary movements of the left and the right wrist," *Med Eng Phys*, vol. 34, no. 7, pp. 964–971, 2012.

[24] L. R. Hochberg, D. Bacher, B. Jarosiewicz, N. Y. Masse, J. D. Simeral, J. Vogel, S. Haddadin, J. Liu, S. S. Cash, P. van der Smagt, and J. P. Donoghue, "Reach and grasp by people with tetraplegia using a neurally controlled robotic arm," *Nature*, vol. 485, pp. 372–375, 2012.

[25] J. L. Collinger, B. Wodlinger, J. E. Downey, W. Wang, E. C. Tyler-Kabara, D. J. Weber, A. J. C. McMorland, M. Velliste, M. L. Boninger, and A. B. Schwartz, "High-performance neuroprosthetic control by an individual with tetraplegia," *Lancet*, vol. 381, no. 9866, pp. 557–564, 2013.